MODELLING OF ENERGY GENERATION FROM OPEN NON-EQUILIBRIUM STEADY STATE THERMODYNAMIC SYSTEMS

PATRICK WANYONYI MUNIALO

A thesis submitted to the Department of Mechanical and Industrial Engineering in partial fulfilment for the requirements for the award of the degree of Doctor of Philosophy in Mechanical Engineering of Masinde Muliro University of Science and Technology

NOVEMBER, 2023

DECLARATION

This thesis is my original work prepared with no other than the indicated sources and has not been presented for a degree or any other award in any other university or any other institution.

Signature: _____ Date: _____

Patrick Wanyonyi Munialo

MIE/H/01-55698/2016

CERTIFICATION

We the undersigned certify that we have read and hereby recommend for acceptance by Masinde Muliro University of Science and Technology, a thesis entitled "**Modelling of Energy Generation from Open Non-Equilibrium Steady State Thermodynamic Systems"**

Signature: _____ Date: _____

Prof. Chrispus K. Ndiema.(Post Humous)

Department of Mechanical and Industrial Engineering

Masinde Muliro University of Science and Technology

Signature: _____ Date: _____

Dr. James O. Owuor

Department of Electrical and Communication Engineering

Masinde Muliro University of Science and Technology

Signature: _____ Date: _____

Dr. Peter T. Cherop

Department of Mechanical and Industrial Engineering

Masinde Muliro University of Science and Technology

DEDICATION

To my wife Christine, my son Yisrael, to my brothers, sisters, my parents, in-laws and friends.

ACKNOWLEDGEMENT

The entire session of thesis completion has been a great experience providing us with great insight into learning various modelling concepts, engineering concepts and bene-fits of team work. As rightly said, for the successful completion of any project, an effective and timely guidance is the most important asset. This thesis would not have been materialized without the co-operation of many of the people involved. I would like to appreciate and thank my supervisors that is the late Prof. Chrispus. Ndiema who was instrumental from the onset of proposal writing and development of the initial thesis draft may his soul rest in peace. I wish to thank Prof. Christopher. Enweremadu, who took over from Prof. Ndiema, I enjoyed his counsel, even though for a brief moment. I thank Drs James. Owuor and Peter Cherop for their timely and enthusiastic support for making it possible for me to complete this thesis. I sincerely appreciate their support. I wish to thank Seth Makokha, a lecturer in the department of electrical and communications engineering, for devoting his valuable time to this thesis and assistance throughout my study. My sincere thanks to my wife Christine, she encouraged me, and helped me with love, patience and understanding throughout my study. For my son Yisrael Samuel thanks for understanding since I denied you valuable play time during the study period. Thanks, are also due to my extended family for their encouragement and prayers. Last but definitely not least I want to express my highest praise and love to my Lord Jesus Christ. I always felt that He has always accompanied me and helped me during my thesis work. May the Lord be pleased with my work and the glory is His.

ABSTRACT

Affordable and sustainable energy system is a critical ingredient that supports life. The overall objective of this study was to model electrical energy generation from open non equilibrium steady state thermodynamic systems. The specific objectives were to build two physical open thermodynamic Monopole Energizer Machines (MEM) and determine their Electrical Characteristics, to undertake comparative analysis of electrical characteristics of ceramic and neodymium magnet-based MEMs, to develop a predictive mathematical model for open non equilibrium steady state thermodynamic systems under study, and to perform steady state analysis of the systems. The MEM has been observed to produce electrical power without a cogent explanation of its apparent violation of classical electrical machine theory. It has also been observed that the MEM exhibits characteristics typical to open non equilibrium steady state thermodynamic systems (NESS). The model developed was anchored on system theory which draws similarities from those of heat pumps, photo electric systems which are all open NESS systems. The model was also partly anchored on switched reluctance machine theory. The switched reluctance machine has some physical and electrical similarities to the MEM. Two physical models were built, one using ceramic magnets and the other using neodymium magnets. The model using ceramic magnets was a replication of the original MEM, and the other was a reconstruction of the original model but using neodymium magnets. Seven sets of experiments were undertaken for each physical model, with different levels of magnetic loading. Data from the models were then used to analytically determine electrical characteristics of the machines under study. The study showed that contrary to known coefficients of performance for most energy generating machines, which range from 33% to 40%, the coefficients of performance of the two sets of machines under study ranged from 96% to 170% depending on the design and level of magnetic loading. A validation of the model was carried out using regression analysis and a good fit was observed. A steady state analysis of the system confirmed the observed stable operation exhibited by the physical models. The study further established that the power output profile for Neodymium Magnet based MEM was superior to that of Ceramic Magnet based MEM. The findings from this study provides insight into an innovate method of power generation that could provide a significant improvement in efficacy of energy transfer.

TABLE OF CONTENTS

LIST OF TABLES

LIST OF FIGURES

LIST OF ABBREVIATIONS AND ACRONYMS

AC	Alternating Current
AFM	Artificial Force Molecule
ATP	Adenosine Triphosphate
BC	Boost Converter
C	Speed of light
CCS	Carbon Capture and Storage
CVT	Continuously Variable Transmission
DC	Direct Current
(D_W)	Diameter of the wheel
Expi	Experimental value,
G	Boltzmann Gibbs Distribution
G_C	Model constant associated with number of ceramic magnets
G_N	Model constant associated with number of Neodymium magnets
GEET	Global Environment Energy Technology
FES	Flywheel Energy Storage
HP	Horse Power
J_e	Energy current density
J_Q	Thermodynamic flow
K	Heat conductivity
K_C	Model constant associated with Voltage output for original design
K_N	Model constant associated with voltage output for replication design
KERS	Kinetic Energy Recovery System
K_{Type}	Constant associated with magnetic type
KW	Kilowatts
L_C	Model constant associated with Load current for original design
L_N	Model constant associated with Load current for replication design
IEA	International Energy Agency
N	Number of observations
N_C	Number of Ceramic Magnets
(N_M)	Number of magnets per wheel

N_N	Number of Neodymium Magnets
FT	Fluctuation Theorem
NEAS	Non Equilibrium Aging State
NESS	Non Equilibrium Steady State
NETS	Non Equilibrium Transient State
MEM(s)	Monopole Energizer Machine(s)
MPPT	Maximum Power Point Tracking
M_{type}	Type of Magnet
Predi	Predicted value of the model
P	Pressure of fluid
PV	Photovoltaic
Q	Quantity of heat
R_C	Rate of Charging
Re	Reynolds Number
RE	Regenerative Energy
R_p	Rate of pulse Production
RMSE	Root Mean Square Error
SRM	Switch Reluctance Machine(Motor)
(S_W)	Speed of the wheel
T	Absolute Temperature
T_c	Temperature at point c on a plate
Toes	Tons of oil equivalent
TPES	Total Primary Energy Supply
T_h	Temperature at point h on a plate
τ_k	Coupling constant
U	Internal Energy
UPS	Uninterruptible Power Supply
USA	United States of America

LIST OF SYMBOLS

EF	Modelling efficiency
e	The elementary charge (1.6×10^{-19}Coulombs).
$h_1, h_2, h_3 \; and \; h_4$	Steady state enthalpies of the working fluid at the Respective states
$h_1(t), h_2(t), h_3(t))$ $and \; h_4(t)$	Time function enthalpies of the working fluid at the respective states
i_o	Initial current
I	Current
i_{pk}	Peak current
I_{in}	Time independent input current
l_{out}	Time independent load current
I_{in} (t)	Time function input current
I_{out} (t)	Time function load current
L	Inductor
L	Length of conductor in meters
M	Mass in Kg
m	Mass flow rate of the working fluid,
n_k	Mole number density of component k
η	Viscosity of the fluid
η_q	Quantum efficiency
η	Efficiency
λ	Value or set of values that defines the state of thermodynamics
λ(t)	Control parameter defining a time evolution of a given protocol
e	Total energy density
$M_k n_k$	Mass per unit volume of component K.
V_k	Velocity of component K.

ρ	Density of fluid.
ψ	Potential
δ_u	Change in internal energy
δ_s	Change in entropy
δ_Q	Element quantity of heat
δ_w	Element quantity of work
$\Delta T = T_n - T_{n-1}$	Temperature gradient
R	Load resistor
S	Entropy
T	Absolute temperature
T_{on}	Continuos conduction mode1
τ_k	Coupling constant
U	Internal energy
V	Velocity
V_D	Voltage drop across diode (D_m)
V_{in}	Time independent input voltage
V_{out}	Time independent output voltage
V_{in} (t)	Time function input voltage
V_{out} (t)	Time function output voltage
V_T	Voltage through a transistor
Q_H	Steady state heat transfer in condenser
	or high temperature reservoir
Q_L	Steady state heat transfer in the evaporator
	or low temperature reservoir
Q_H(t)	Time function heat transfer in the condenser
	or to high temperature reservoir
$Q_L(t)$	Time function heat transfer in the Evaporator or low

	temperature reservoir
R^2	Coefficient of determination
W_{in}	Steady state work input
W_{in} (t)	Time function work input
$\Phi(t)$	Is the time-dependent incident photon flux at a given time
Φ	Is the steady state incident photon flux at a given time
W	Quantity of work
γ, .	Collection efficiency

DEFINITION OF SIGNIFICANT TERMS

Bohren Experiment:

The Bohren experiment, also known as the two-slit or Young's double- slit experiment, demonstrates the wave-particle duality of light and matter. It involves shining light or particles through two narrow slits onto a screen. When only one slit is open, the pattern on the screen corresponds to the shape of the slit. However, when both slits are open, an interference pattern emerges, displaying alternating bright and dark fringes. The Bohren experiment has profound implications for quantum mechanics and our understanding of reality. It highlights the wave-particle duality, where particles can exhibit wave-like properties and interference effects. This experiment has led to further investigations into the nature of quantum phenomena and has been pivotal in the development of quantum physics as a scientific discipline.

Boost Converter:

A boost converter, also known as a step-up converter, is a type of DC-DC (direct current to direct current) converter used to increase the voltage level of a DC power source. It is a switching power supply circuit that provides a higher output voltage than the input voltage.

Coherent structures:

Coherent structures refer to organized patterns or structures that emerge in fluid flow or other dynamic systems. These structures exhibit a high degree of organization and stability and can persist over time. They are often characterized by well-defined boundaries or regions of concentrated energy.

Dissipative structures:

Dissipative structures are self-organizing patterns or structures that emerge and persist in far-from-equilibrium systems. These structures are characterized by the continuous flow of energy and matter through the system, and they are able to maintain their stability and organization by dissipating or releasing excess energy.

Dry micro battery:

A dry micro battery, also known as a solid-state micro battery or thin-film micro battery, is a miniature power source that provides electrical energy in a compact and solid-state form. Unlike traditional batteries that use liquid or gel electrolytes, dry micro batteries employ solid-state electrolytes, which offer several advantages such as improved safety, higher energy density, and longer lifespan.

Duty cycle:

Duty cycle refers to the ratio of time a system or device is ON (active) compared to the total time of a complete cycle. It is commonly expressed as a percentage or a fraction.

Equilibrium system:

An equilibrium system refers to a state in which opposing forces or processes within a system balance each other out, resulting in a stable and unchanging condition. In an equilibrium system, there is no net change or tendency for change to occur over time.

Monopole Energizer Machine:

Devices and technologies used for charging batteries, such as battery chargers, power supplies, and energy harvesting systems. These devices typically operate based on established

principles of electrical engineering and utilize techniques such as constant current or constant voltage charging to efficiently charge batteries.

Non equilibrium steady state system;

A non-equilibrium steady state system refers to a system that is maintained far from thermodynamic equilibrium but exhibits a steady or stationary behavior over time. In contrast to equilibrium systems, which are balanced and have no net flow of energy or matter, non-equilibrium systems constantly exchange energy, matter, or information with their surroundings, leading to an ongoing flow or flux within the system.

Non equilibrium system:

A non-equilibrium system refers to a system that is not in a state of thermodynamic equilibrium. In such systems, there are ongoing processes or interactions that result in a continuous flow of energy, matter, or information, leading to a lack of balance or steady state.

Open thermodynamic Energy System:

This is a system that can exchange both energy and matter with its surroundings. This means that energy and/or matter can flow into or out of the system, allowing for interactions and exchanges with the environment.

Proto type:

A prototype is an early version or model of a product, system, or concept that is created to test and evaluate its design, functionality, and feasibility. It is typically developed during the initial stages of a project to validate ideas, gather feedback,

and identify potential improvements before moving forward with full-scale production or implementation.

Self-organized patterns:

Self-organized patterns refer to the spontaneous emergence of ordered structures or behaviors in a system without the need for external control or design. These patterns arise from the interactions and dynamics of the system's components or elements, often exhibiting collective or cooperative behavior.

Switch Reluctance Machine:

A Switched Reluctance Machine (SRM) is a type of electric machine used for converting electrical energy into mechanical energy or vice versa. It is a form of a synchronous machine that operates based on the principle of magnetic reluctance.

Switch Reluctance Motor:

A Switched Reluctance Motor (SRM) is a type of electric motor that operates based on the principle of magnetic reluctance. It is also known as a Variable Reluctance Motor (VRM). The SRM is characterized by its simple construction and the absence of permanent magnets or field windings on the rotor.

Systems Theory:

Systems theory is an interdisciplinary framework that examines the behavior and interactions of complex systems. It provides a holistic approach to understanding the structure, behavior, and dynamics of systems, regardless of their specific domain or discipline.

Time function system:

A time function refers to a mathematical function that represents how a quantity varies with time. It describes the

behavior of a variable or signal over a specific time interval. Time functions can take various forms, such as continuous functions (e.g., sine wave, exponential decay) or discrete functions (e.g., discrete-time sequences).

Time invariant system

A time-invariant system is a concept in systems theory that describes a system whose behavior or characteristics do not change over time. The system's response to inputs remains constant or unchanged regardless of when the inputs are applied. A time-invariant system possesses the property of time invariance, which means that a shift or delay in the input signal results in a corresponding shift or delay in the output signal, without altering the system's overall behavior.

Wet Micro battery:

A wet micro battery, also known as a microfluidic battery or flow battery, is a type of energy storage device that combines concepts from microfluidics and battery technology. It is designed to provide power in micro scale applications where small size, high energy density, and rechargeability are required. Unlike traditional solid-state batteries, wet micro batteries use liquid electrolytes or flowing electrolyte solutions to store and release energy. They typically consist of two electrodes immersed in separate electrolyte solutions, and the energy is stored in the form of chemical reactants dissolved in the electrolyte.

CHAPTER ONE:
INTRODUCTION

1. Introduction

1.1 Background Information of the Study

This chapter introduces the research area. The major areas of focus in this chapter are historical overview of the study, global, regional and local challenges of energy sector information on energy types and sources. The other areas of focus are problem statement, objectives of the study, scope, justification, limitations of the study and system theory on which this study is anchored

1.1.1 Historical Background of the Study

Energy has been the main anchorage and lead drive in facilitation of goods and services to support man kind and societies in general. This phenomenon has been in existence since before industrial revolution. The evolution of energy is historically believed to have started before 200 BC by the Chinese community who utilized coal for heating and cooking. Global Energy development is characterized by three stages, namely fire wood, coal and oil and gas. Firewood stage was characterized by low energy uptake; industrial revolution was associated with coal, which is also known as second phase of energy evolution. During this stage there was growth and expansion in utilization of steam in steam engines, growth in electrical and metallurgical industries. The third stage was that of petroleum and natural gas industrial evolution. This stage sprung up in the twentieth century and facilitated accelerated growth of internal combustion engines, production of various types of machinery and equipment, including cars, tracks, ships, planes, tractors etc. Firewood stage period was before the 18th Century (Xiaoren *et al.*, 2008).

Table 1-1: Global Primary Energy Consumption (Dudley, 2019).

Energy source	Million Tonnes	Percentage
Oil	4,331.3	32.94
Coal	3,839.9	29.21
Natural Gas	3,135.2	23.85
Nuclear Energy	583.1	4.44
Hydro-electric power	892.9	6.79
Renewable Energy	364.9	2.78
Total	13,147.3	100.00

The figures of energy consumption were captured as early as 1860, and since then the figures have been on upward trend, increasing from 500 million tons by then to nine billion of tons of oil per annum.

According to Rangan *et al.* (2012) petroleum, coal, natural gas, nuclear energy and renewables have grown at 38%, 26%, 23%, 7% and 2% respectively. Fossil fuel was the largest energy consumption globally at the end of 20^{th} century, (Xiaoren *et al.*, 2008). According to Dudley (2019) the Global Primary Energy Consumption in 2016 was distributed as shown in Table 1-1

A number of investigations undertaken indicate that, there have been great milestones made due to fossil fuels. Apart from great achievements attained through utilization of fossil fuels and generally non renewables, we have also witnessed shortcomings like Global collateral damage such as massive pollution on water sources and air , emissions' such as Carbon dioxide (CO_2) emission , global warming, climate change due to fossil fuel and non-renewable'(Liu *et al.*, 2002)**.** It is estimated that fossil fuels may be exhausted between 2050s and 2200,(Dangerman and Schellnhuber, 2013; Liu *et al.*, 2002). However, nuclear wastes, safety and nuclear proliferation will restrict the development of nuclear energy (Carrington and Stephenson, 2018).

1.1.2 Global Challenges of Energy Sector

The urgent need to shift towards environmentally friendly and carbon-neutral energy sources is a significant obstacle that the global energy industry must address. As a consequence of the climate change phenomenon, a considerable number of countries have made pledges to decrease their carbon emissions, promoting a transition away from the consumption of fossil fuels. Obstacles that must be overcome in the context of the worldwide energy transition include the development of efficient energy storage technologies, the successful integration of renewable energy sources into existing infrastructures, and the formation of international collaborations to combat climate (Yusaf *et al.*, 2022) change Consequences of geopolitical tensions and economic instability on the global energy markets include supply chain disruptions and price fluctuations.

1.1.3 Regional challenges of energy sector

A multitude of determinants contribute to the divergent energy challenges encountered in various regions, encompassing climatic fluctuations, economic state, and political instabilities. A considerable proportion of the population in a number of developing countries encounters obstacles when attempting to obtain affordable and reliable energy resources (Liu *et al.*, 2002). Potential obstacles to the effective integration of renewable energy sources may arise from disparities in technological capability and regional energy infrastructure. Potentially influencing the dependability and accessibility of energy resources are geopolitical factors and regional conflicts (Garimella *et al*. 2022). To safeguard energy security in the region, it is critical that neighbouring countries work together to resolve common energy challenges.

1.1.4 Local Challenges of Energy Sector

Kenya's energy sector is currently facing unique and significant obstacles. Although significant progress has been achieved by the government in improving electricity accessibility, concerns continue to revolve around the dependability of the power grid (Pakulska and Poniatowska-Jaksch, 2022) The energy sector in Kenya is significantly more vulnerable to variations in precipitation patterns caused by climate change. This is primarily due to the sector's heavy reliance on hydropower as its principal electricity source. The principal aims encompass the augmentation of energy storage capacity, the encouragement of energy supply diversification, and the fortification of the overall system. In order to secure private investment, it is imperative to contemplate the long-term financial viability of energy initiatives and address any regulatory uncertainty (Wambui *et al.*, 2022). Kenya's commitment to increasing its geothermal capacity signifies a significant advancement towards a more environmentally sustainable energy path. Nonetheless, in order to overcome infrastructure constraints and ensure equitable energy access for all segments of the population, persistent efforts are required.

1.1.5 Facts and Figures on Conventional and Alternative Energy Systems

Classification of energy globally is generalized into Conventional energy systems which include oil, coal, natural gas, uranium and biofuels as energy inputs. Conventional energy sources are characterized by problematic operating systems that come along with their shortcomings. The second type is less problematic

alternative energy sources. Associated technologies with conventional energy sources are coal gasification, cracking, refining and CO_2 separation as technologies (Dangerman and Schellnhuber, 2013). According to Dangerman and Schellnhuber (2013) the alternative energy system comprises solar, wind, geothermal and hydro energy; among its associated technologies. Figure 1.1 shows global energy supply per region. The figures show that Africa had the lowest energy consumption compared with the rest of the world. It was also observed that the region with the highest per capita consumption was North America. North America had 217 GJ/head), followed by CIS (150 GJ/head) and the Middle East (140 GJ/head).

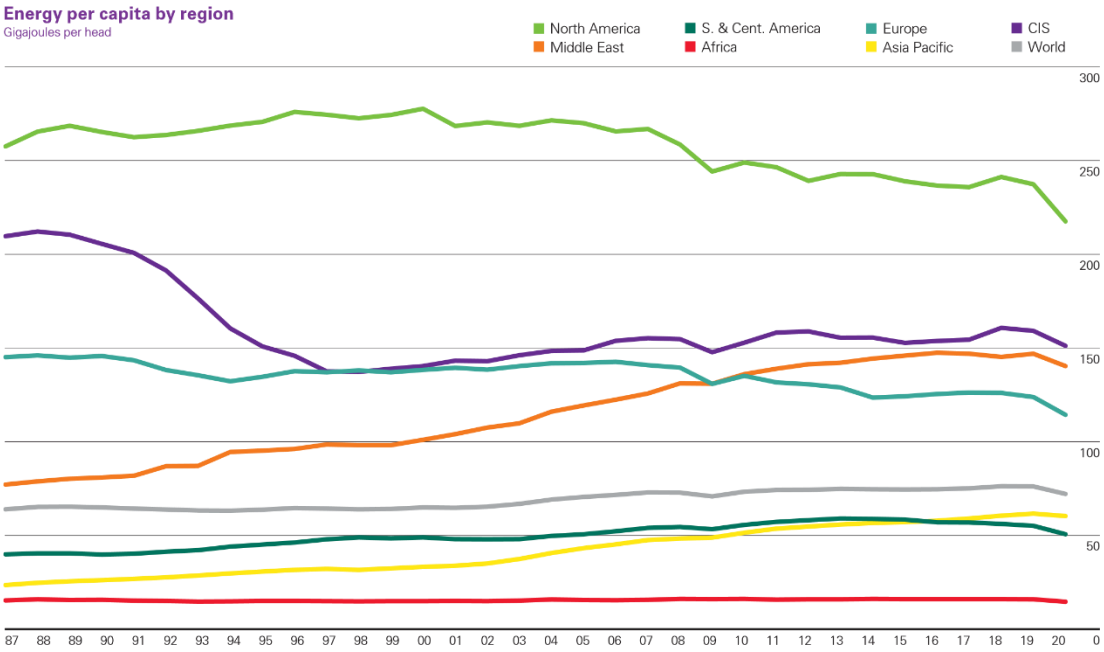

Figure 1-1: Energy Per Capita by Region (Energy, 2021).

The energy demand per capita has been on decline globally even as the global population increases. For instance in 2020 , about 63.7% of the global population lived in countries where average energy demand per capita was less than 100 GJ/head, a significant decrease from 81% in 2019, as energy demand per capita in China increased to 101 GJ/head from 99 GJ/head in 2019. The share of the global population consuming less than 75 GJ/head increased from 57% in 2019 to 60.6% in 2020. Figure 1-2 shows Energy distribution across the countries.

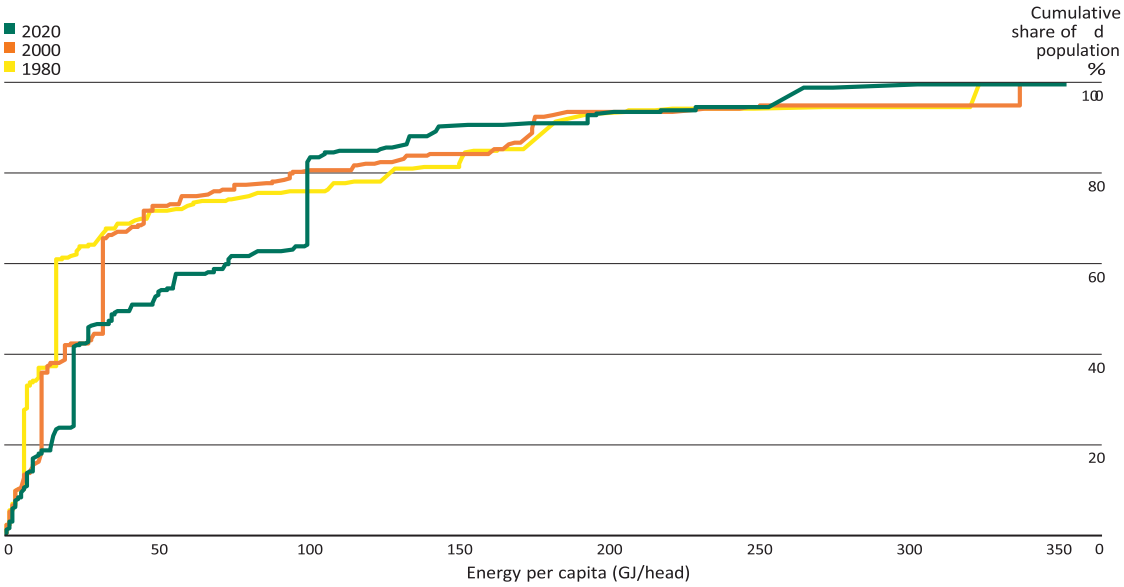

Figure 1-2: Energy Distribution Across the Countries (Energy, 2021).

The conventional energy sources have had their prices fluctuating over the years. The occurrences have consistently affected price of commodities world all over negatively. depicts this picture

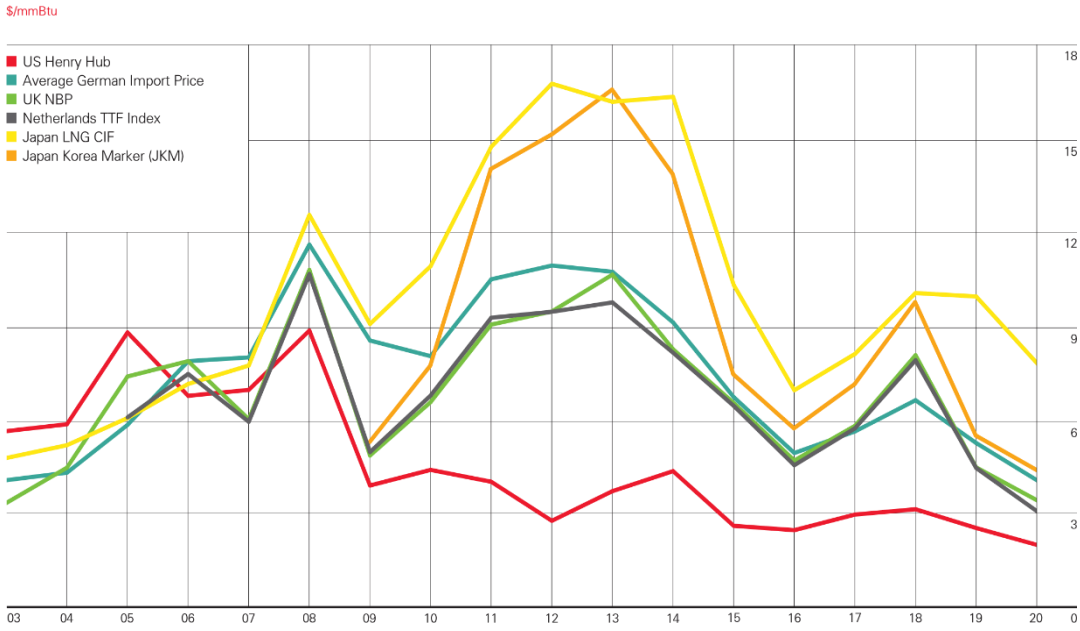

Figure 1-3: Global Fuel Prices in US Dollars Per MM BTU (Energy, 2021).

1.1.6 Contemporary Context of the Study

This study is underpinned on understanding of open non equilibrium steady state thermodynamic system for energy generation. Understanding this system is fundamental in achieving high co-efficiencies in energy generation.

Steady state non-equilibrium is a situation in which there is no time dependence but in which a quantity of the conserved variable is flowing, driven by injection at one boundary and subtraction at another. The recent findings have indicated that open NESS thermodynamics system can exhibit both time independent and time function aspects. Since the dynamics of the system are dissipative there will usually be an injection of energy current within the system, sometimes a transformation between different forms of energy and then the subtraction of the energy to maintain the steady state. Work done in this section has dwelled largely on application and almost nothing on power generation from open NESS thermodynamic system (Green *et al.*, 2019; Liu *et al.*, 2002; Xiangxiong Zhang and Shu, 2010).

Recent studies carried out on performance of current power generation systems indicated that their co-efficiencies and efficiencies were less than 100%. Part of these studies are those done on performance of thermal power plant from 2008 to 2012,(Bamisaye and Adeoye, 2016), making Nuclear cheap,(Nordhaus, 2014), Geothermal Power Plant Cycles thermal efficiency,(Bilyk *et al.*, 2016) the researchers established that the efficiencies of the above power systems were found to be less than 100%,they ranged between 7.58% and 33%..It was also established that none of these studies were done in the context of open non equilibrium steady state thermodynamics. A number of replications studies and operations done fall in open non- equilibrium thermodynamic systems. It was further established that none of the studies undertaken were in the context of open thermodynamics NESS (McDonald *et al.*, 2013). This observation showed that there was knowledge deficit in this area hence need for further investigation to narrow the gap.

In summary, the current world energy system is replete with fossil fuels, collateral damage and associated with high level pollutants need to be replaced with a more sustainable energy systems,(Khan *et al.*, 2009; Warf and Arias, 2008; Xiangxiong Zhang and Shu, 2010). The utilization of NESS open thermodynamics systems is critical for seeking alternative solution for the current wasteful energy systems marred with high levels of in efficiencies and collateral damage to the environment (Agardy *et al.*, 2003; C. V. Baxter *et al.*, 2005; M. Baxter and King, 1993; Bridgewater *et al.*, 2004; Cieszczyk *et al.*, 2009; Kodama *et al.*, 2007; Ma, 2006; Svoboda *et al.*, 2006).

1.1.7 Monopole Energizer Machine model (MEM)

Monopole energizer machine exhibits peculiar behavior unlike other electrical generating machines. This machine appears to give more output than input. The behavior of MEM motivated the study of electrical characteristics of MEM in the context of open NESS thermodynamic system. This system was thought to exhibit the behavior of open thermodynamic system which allow the transfer of matter a cross its boundaries. One of the significances of this study was to properly locate it in proper thermodynamic setting and frame work. This was deemed possible by building a physical system and collect data through undertaking experimental runs, which will then be analyzed and render relevant explanation and conclusion. This system showed the potential of generating more energy than the output. This striking behavior is what informed the study on modeling of energy generation from open NESS thermodynamic system using MEM.

1.2 Statement of the Problem

Key challenges facing energy sector are expensive inefficiency and wasteful energy systems associated with fossil fuels, petroleum products and gas, coal and oil are major energy sources globally. These energy sources are associated with low efficiencies, pollution which impacts on the environment, hence causing collateral damage. The problem of the underlying study is to generate energy at high coefficient and efficient which is not or is less problematic to the environment. This is contrary to current nonrenewable energy systems which are characterized by large amounts of input materials, high generation costs and related problematic systems which are inefficient and injurious to the environment globally. These aspects remain a global concern. Literature has asserted that there is minimal undertaking in terms of investigation regarding energy generation from open NESS thermodynamics systems. The purpose of this research was to undertake a study on energy generation from NESS open thermodynamic system. The study focused on both physical modeling and predictive mathematical modeling of energy generation from open non equilibrium steady state thermodynamic systems. By undertaking modeling on non-equilibrium steady state, open thermodynamic system will enhance better understanding and operationalization of the energy system under study. The study focused on modeling of energy generation system from open NESS thermodynamic system.

Secondly, the study has taken cognizance of the fact that there is no coherent and sound scientific theory to explain the functioning of MEM and properly locating it in scientific frame work. Arguments contrary to accommodation of MEM in scientific framework have been advanced by some authors who have doubted the functioning and operation of MEM and similar inventions. Even though some authors have argued that Monopole Energizer Machines are possible and that they could be used to create perpetual motion machines, the augment advanced fall below threshold in meeting the acceptable scientific standard to support the claim. These happenings seem to be inconsistent with energy conservational laws. Such concerns need to be addressed by undertaking disciplined research to address the gaps. Therefore, the second purpose of this investigation is to locate systems like MEM in proper scientific context, in terms of operational principle, theory and practice. In summary the aim of this study was therefore to answer the key questions and concerning energy generation systems with high inefficiencies, expensive in terms of costs and collateral damage to the environment. Therefore, modeling of energy generation from open NESS thermodynamic system was deemed to give a solution to the underlying problem.

1.3 Objectives of the Study

1.3.1 General Objective

Modeling of energy generation from open non equilibrium steady state thermodynamic Systems

1.3.2 Specific Objectives

The specific objectives of this study were:

1. To build two physical open thermodynamic monopole energizer machines and determine their electrical characteristics**.**
2. To undertake comparative analysis of electrical characteristics of ceramic and neodymium magnets-based monopole energizer machines
3. To develop a predictive mathematical model for open non-Equilibriums steady state for monopole energizer machine.
4. To perform steady state analysis of monopole energizer machine

1.4 Justification of the Study

Transformation of the current energy mix requires a paradigm shift to our energy generation systems. This is critical in ensuring sustainability and affordability of our energy generation systems. Affordability and sustainable energy systems will ensure easily accessible in sufficient quantities commensurate to the needs at low cost and without damage to the environment. The critical area for improvement and paying attention is scaling up efficient and coefficient of performance in energy generation systems. This will go a long way in fostering flexibility, affordability and accommodative energy supply system. (This scenario demonstrates that a sustainable future requires a transformation from today's energy systems to those with: (i) radical improvements in energy efficiency, especially in end use, and (ii) greater shares of renewable energies and advanced energy systems with carbon capture and storage (CCS) for both fossil fuels and renewables including biomass.

One of the research gaps identified was lack of scientific proof that MEM cannot be located in scientific setting or frame work, there has been little or scanty information in locating the working of monopole Energizer machine in scientific setting and frame work. This system is an open system because it exchanges both matter and energy with the environment. The model operates under non-equilibrium state because voltage and current does not remain uniform at any point in time making the system operate at different states back and forth. Steady state applies to our model in the sense that each pulse of energy driven to the storage battery was consistently equal to the succeeding pulse and follows in step at constant period so that the general flow appears to be steady

MEM, is a time function system that can also exhibit time independent aspects just like a heat pump and Photoelectric systems, based on this behavior the system satisfies the condition for it to be classified as an open Non-Equilibrium Steady State Thermodynamic System.

1.5 Scope of the Study

In this research, two monopole energizers, open non equilibrium steady state thermodynamic systems were physically constructed and ran to collect data for two models. The models were constructed from two types of magnets, namely ceramic magnets and neodymium magnets. The monopole machine constructed using

ceramic magnets was called the original design, whereas that build from neodymium magnets was referred to as replication design.

1.6 Significance of the Study

The study will provide invaluable prepositions for the theory, police and practice of engineering thermodynamics. There is no modeling and simulation software targeting energy generation by using monopole energizer machine, this study will provide a basis for establishing this software.

Monopole energizer machine is of a peculiar type, it has been doubted on how it should be classified in scientific framework, it has been also exhibited characteristics that are near perpetual machines which are impossible as per the third corollary of the first law of thermodynamics. In this context this research comes in handy to contribute to the body of knowledge, first by modeling of energy generation system from open NESS thermodynamic system, secondly by giving a scientific explanation on peculiarity of MEM which seem not understood in scientific setting.

This study will provide valuable information to institutions and individuals that will enrich their understanding and application in their practice and development in the area of energy and engineering thermodynamics. This study will provide invaluable policy prepositions in energy sector, especially the policy guiding the development, modeling and design of energy systems, especially the ones associated with monopole energizer machines.

1.7 Conceptual Framework

System theory or general systems theory, is an interdisciplinary approach to understanding complex systems in natural, social, and technological realms. It seeks to explore the general principles and patterns that apply to a wide variety of systems, regardless of their specific nature. The foundation of system theory lies in the idea that complex entities can be seen as composed of interconnected and interdependent parts or elements, which interact with each other to form a whole that is greater than the sum of its parts. These parts are called subsystems. System theory is concerned with the structure, behavior, and properties of these systems and their interactions (Datta *et al.*, 2022; Warf and Arias, 2008).

This study is anchored on system theory which draws its similarities from heat pump system and photoelectric system. The study adapts the building of the physical model and the development of predictive mathematical model for open NESS thermodynamic system. The conceptual framework for the study is shown in Figure 1-4

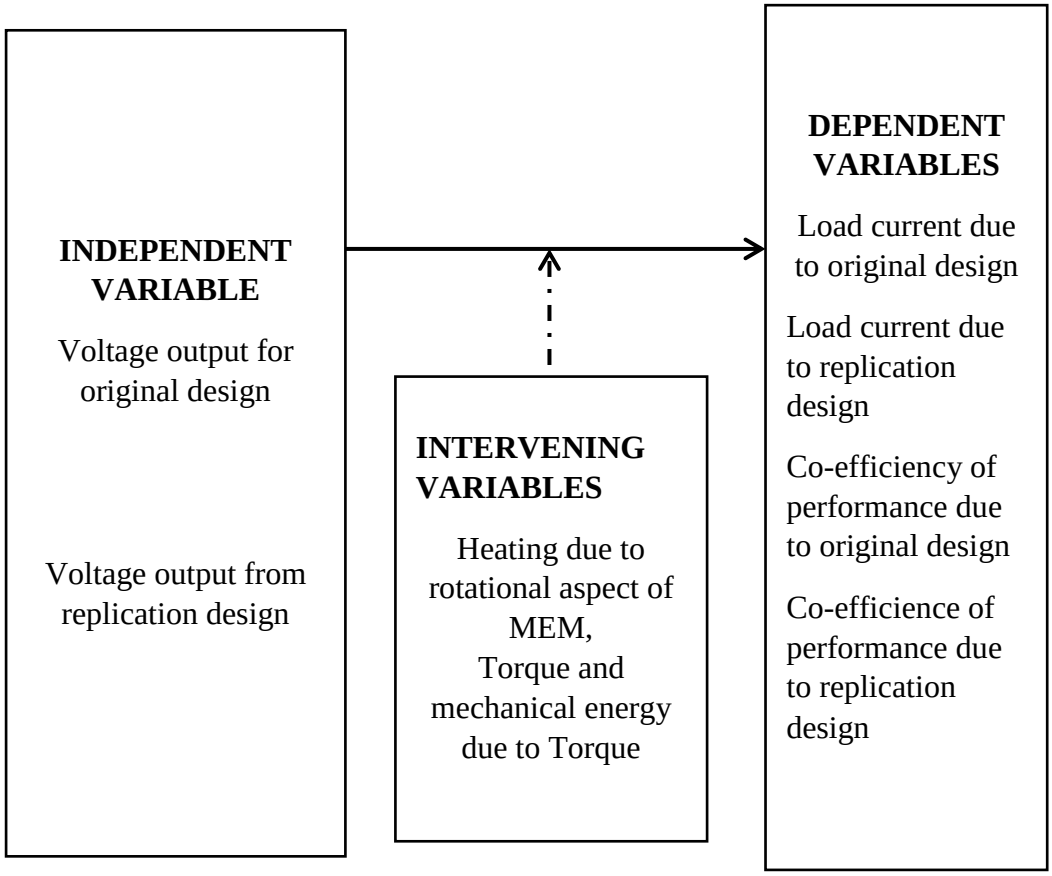

Figure 1-4: Conceptual Framework

The focus of this study was on Monopole Energizer Machine system open NESS thermodynamic system. This system can be utilized to generate energy with high output and high efficiencies. The model was used to demonstrate the relationship between energy output and energy input of thermodynamic non-equilibrium steady state system. The model under consideration has the voltage output as independent variable, since this is the determining and the controlling variable. This model has the load current, output power, co-efficiencies involved (average coefficient, peak coefficient, instantaneous coefficient and coefficient related to magnetic loadings). The model has the following as intervening variables,-Heating due to rotational aspect of MEM, Torque and mechanical energy due to Torque (Datta *et al.*, 2022; Warf and Arias, 2008).

Heating can affect a mono pole energizer machine in a few ways. First, it can cause the components of the machine to expand, which can put stress on the wires and other parts. This can lead to premature wear and tear on the machine. Second, heating can also cause the insulation on the wires to degrade, which can increase the risk of electrical shock. Third, heating can also reduce the efficiency of the machine. This is because the heat can cause the resistance of the wires to increase, which reduces the amount of current that can flow through the machine. The effects of heating on a mono pole energizer machine were mitigated by keeping the machine in a cool environment and well-ventilated environment or room. The MEM was not put close to any heat source.

Mono pole energizer machines use mechanical energy to generate electricity. The mechanical energy is typically provided by a motor, which converts the rotational energy of the motor into electrical energy. The amount of mechanical energy that is required to power a mono pole energizer machine depends on the power output of the machine. The higher the power output, the more mechanical energy is required can affect a mono pole energizer machine: To minimize the effects of mechanical energy on a mono pole energizer machine, stability evaluation of the machine was undertaken

First, torque can affect the amount of current that can be generated by the machine. The more torque that is applied to the machine, the more current that can be generated. Second, torque can affect the efficiency of the machine. A machine that

is subjected to excessive torque may be less efficient, meaning that it will generate less electricity for a given amount of torque. Thirdly, torque can affect the lifespan of the machine. A machine that is subjected to excessive torque may wear out prematurely. To minimize the effects of torque on a mono pole energizer machine, matching the machine design and amount of torque the machine will be subjected to.

1.8 Outline of the Thesis

In chapter one background of the study is introduced, followed by problem statement objectives of the study. The chapter has also discussed justification of the study, scope of the study and, conceptual frame work. Chapter two presents literature review related to engineering thermodynamics, equilibrium systems, non-equilibrium system, energy generation from open NESS thermodynamic system. Other areas discussed in literature review are modeling, monopole energizer system, SRM, BC, lead acid batteries and research gaps.

Chapter three materials and methods are discussed, followed by discussion and analysis of results in chapter. Chapter five discusses the development of predictive mathematical model. In chapter sis summary, conclusions and recommendations are discussed.

CHAPTER TWO:
LITERATURE REVIEW

2. Literature Review

2.1 Introduction

Practice of engineering principles can be traced to Adam Smith and James Watt. Adam Smith published the book called wealth of nations in the year 1776.The book was associated with application of steam. Seven years earlier James Watt (1736–1819) had obtained a patent for his version of the steam engine. Both men worked at the University of Glasgow. Yet, in Adam Smith's great work the only use for coal was in providing heat for workers. The machines of the eighteenth century were driven by wind, water and animals. Nearly 2000 years had passed since Hero of Alexandria made a sphere spin with the force of steam; but still fire's power to generate motion and drive machines remained hidden. Adam Smith (1723–1790) did not see in coal this hidden wealth of nations (Plasson *et al.*, 2007).The steam engine revealed a new possibility. Wind, water and animals converted one form of motion to another.

Besides the above, the steam engine was fundamentally different: it converted heat to mechanical motion. Its enormous impact heralded the industrial revolution and gave birth to a new science: thermodynamics. Unlike the science of Newtonian mechanics, which had its origins in theories of motion of heavenly bodies, thermodynamics was born out of a more practical interest: that is generating motion from study of heat and its ability to generate motion; merged with larger energy subject and it inter conversion from one form to another. With time, it evolved into a theory that describes transformations of states of matter in general motion generated by heat being a consequence of particular transformations. Thermodynamics is founded on essentially two fundamental laws, one concerning energy and the other entropy (Plasson *et al.*, 2007)

2.2 Engineering Thermodynamics

2.2.1 Anchorage of Engineering Thermodynamics

According to Koder *et al.* (2002), the engineering thermodynamics is anchored upon two fundamental laws. The first and second laws of thermodynamics, i.e. both laws need to be local for purposes of compatibility with the principle of relativity, and

validity regardless of the observer's state of motion. Non local laws of energy conservation or entropy production are in admissible because the notion of simultaneity is relative. The first law of thermodynamics states that; when a closed system goes through a cycle, the net work done on the environment is directly proportional to the net heat from the environment or surroundings and vice versa (Rodger *et al.*, 2016). The disapproval of this law lies on the fact that neither it nor any of its consequences have been contradicted by experience. This law is anchored on three corollaries. The first is non-flow energy equations thus: -

$$\sum_1^2(\partial Q + \partial w) = U_2 - U_1 \text{ or} Q_{12} + W_{12} = (U_2 - U_1) \text{ ..... (2-1)}$$

and second corollary is based on the fact that internal energy of an isolated system remains unchanged and the third corollary is based on the fact that, it is impossible to have perpetual motion machine of the first kind (Rodger *et al.*, 2016).

On other hand the second law of thermodynamics states thus it is not possible to have a system which will operate in a cycle, extract heat from reservoir and do an equivalent amount of work on the surroundings. This Law is anchored on 8 corollaries. It was postulated, that it is not possible to build a system which will operationally function in a cycle and cause the transfer of heat from a cooler to a hotter body without work being done on the system by the surrounding. The second law states thus it is not possible to build an engine to function operationally between only two heat reservoirs which will have a higher efficiency than a reversible engine operating between the same two reservoirs. The third and fourth states that all reversible engines operating between the same two reservoirs have the same efficiency and a scale of temperature can be defined which is independent of any thermodynamic substance and which provides an absolute zero of temperature respectively (Rodger *et al.*, 2016). The first Law of thermodynamics' corollary states that the internal energy of a closed system remains unchanged if the system is isolated from its surroundings (Rodger *et al.*, 2016) According to Ibanez and Uranga (2012) systems which obtain extra energy from the vacuum cannot be isolated from their active surrounding (vacuum) because the vacuum energy exists at all points in the universe. The second Law of Thermodynamics assumes a flat space time in the relativistic sense and so it cannot be valid in curved space time, Prigogine Nobel Lecture 1977 (Kondepudi, 2008).

2.2.2 Limitations of the Laws of Engineering Thermodynamics

Limitations of laws of thermodynamics are built on the fact that in closed systems there is exchange of energy but not mass across the boundary, however since mass can be related to energy as given by $E=MC^2$ (E is energy, M is mass and C is the speed of light), it can be argued that it is impossible to have a system allowing energy transfer without mass transfer. This has invalided to some degree the application of classical thermodynamic theory to a system in which mass is effectively conserved. According to Rodger *et al.* (2016), it is worth noting some possible restrictions upon the generality of the laws of thermodynamics. It has been observed that it may not be permissible to apply the first law to the whole universe to suggest its total energy is constant. A similar extrapolation of the second law is sometimes made which is questionable (Kondepudi, 2008). This is because thermodynamic principle applies to a finite system. The extrapolation of application of these laws to the whole universe which is infinite raises concern.

Since all real processes are irreversible, the entropy of the "universe" must increase whenever a change occurs within them. This has led to the broad generalization that the entropy of the universe as a whole is increasing. But, the second, like the first, is an expression of the observed behavior of finite system and it is not certain that the universe can be regarded as finite. Thermodynamic laws cannot apply to microscopic systems because their properties are too small to measure for example temperature, pressure and number of moles. Therefore thermodynamic laws apply only to macroscopic systems (Rodger *et al.*, 2016)

2.2.3 Areas Deviating from the Laws of Thermodynamics

According to Evans and Searles (2002) there are four recognized areas that are known to violate thermodynamics; second law. The violating areas are, -Fluctuation theorem, Bohren experiment, rarefied media and strong gradients. Under fluctuation theorem, it has been established that several fluctuation theorems indicated in literature are known to depend on non-equilibrium systems many of which in particular, fit in the category of production of entropy. The entropy production here defined bears some resemblance with the work that is exerted by the external non-conservative forces that act upon the system. Several related theoretical results have followed as well as experiments (Rodger *et al.*, 2016).

According to Rodger *et al.* (2016), Bohren experiment also deviate from the second law of thermodynamics. It stipulates that an element can indeed absorb more light energy than the energy of light incident to it (Abraham *et al.*, 2002; Bohren, 1983; Das, 2004; Felfli *et al.*, 2005; McDonald *et al.*, 2013) The literature has further identified diverse challenges to thermodynamics' second law. The challenges identified in this investigation are Magneto Calorific Effect, (Bauwens *et al.*, 2008; Berry and Geim, 1997; Lutes and Maxwell, 1955)

According to Sheehan *et al.* (2012) Superconducting Loop, and Epicatalytic Thermal Diode and Torsion Oscillator. These challenges span from classical and quantum mechanical regimes, range from nanosomic to planetary in size, and operate from just above zero to more than 3,000K. They make use of ideal and non-ideal gases, plasmas, semiconductors, superconductors, Nano-, micro- and mesoscopic electrical circuits, chemical catalysts and biologically-inspired structures. (Lumley et al., 2011; Sheehan et al., 2012). Even though the superconductors are found to be excellent dial magnets, without including magnetic flux from their interiors which is found to be bulky, the outer layers are shallowly penetrated by surface-parallel fields, which are also found to decaying exponentially in strength with a characteristic penetration depth. The combination of the Magnetocaloric Effect with reversible transition renders the Coherent Magneto calorific Effect (CMCE). Keefe CMCE Engine, (Lumley *et al.*, 2011; Sheehan *et al.*, 2012)

This is the key new insight underlying Keefe's second law challenge. Inherently, this is a quantum mechanical process that relies on the superconductor's long-range order parameter (wavefunction) .The other illustrations of magneto calorific effect, include a simple thermodynamic process in which a small superconducting sample is cycled through field-temperature (H-T) space and performs network solely at the expense of heat from a heat bath(Lumley *et al.*, 2011), we use Keefe's nomenclature (Cápek and Sheehan, 2005; Nikulov, 2001; Sheehan *et al.*, 2012; Shih *et al.*, 2016)

2.3 Equilibrium Systems and Non Equilibrium Systems

The discussion in this section is centered on equilibrium systems and non-equilibrium systems.

2.3.1 Equilibrium Systems

Experience has shown that if a physical system is isolated, it states that specified by macroscopic variables such as pressure, temperature and chemical composition, evolves irreversibly towards a time-invariant state in which we see no further physical or chemical change in the system. State of thermodynamic equilibrium is characterized by uniform temperature throughout the system and other physical features. The state of equilibrium is also characterized by several other physical features. The evolution of a state towards the state of equilibrium is due to irreversible processes. At equilibrium, these processes vanish. Thus, a non-equilibrium state can be characterized as a state in which irreversible processes drive the system to the state of equilibrium (Rodger *et al.*, 2016; Vilariño-Güell *et al.*, 2011)

In some situations, especially with chemical systems, the rate at which the state is transforming due to irreversible processes may be extremely slow, and the isolated system might appear as if it had reached its state of equilibrium. Nevertheless, with appropriate specification of the chemical reactions, the non-equilibrium nature of the state can be identified. A system in equilibrium experiences no changes when it is isolated from its surroundings. It is in mechanical equilibrium if the pressure remains constant. There are also many complicated types of equilibrium. Thus, equilibrium systems have one uniform temperature and for these systems there exist state functions of energy and entropy(Idogwu *et al.*, 2019; Vilariño-Güell *et al.*, 2011)

2.3.2 Non-Equilibrium Steady State Systems (NESS)

Non-equilibrium steady state (NESS) is a case of where a system maintains a stable and time independent average behavior a way from thermodynamic equilibrium position. As compared to equilibrium states where there is no net flow of fluxes of particles, energy or matter, non-equilibrium steady states are characterized by continuous flow of mater or particles. Despite of the ongoing processes sustained flow of energy or matter fluxes enables the system to maintain a steady state

condition. These steady states often arise due to the presence of external driving forces or energy inputs that continuously perturb the system away from equilibrium (Sieberer *et al.*, 2015) . In a NESS, the system fails to reach thermodynamic equilibrium, even though it sustains a stable average behavior over time. This implies that there is a sustained continuous exchange of particles, matter or energy fluxes between the surroundings and the system.

The sustained flow of energy or particles through the system is a consequence of the ongoing processes within it and the external driving forces. This can be conceptualized by considering a system subjected to constant energy input which continuously perturbs it, hence pushing it away from equilibrium. The system responds to perturbation effect by adjusting its internal dynamics. This results into a balanced state where the external driving force effects are counteracted by internal processes. For example, consider a system under constant rate addition of energy. The energy is then absorbed by the system which in turn redistributes the energy internally and the process is then allowed to reach a steady state condition where energy input and energy loss are balanced (Raimondi *et al.*, 2022; Sieberer *et al.*, 2015). Examples of Non-equilibrium steady states systems or processes are electrical circuits with current flows, social systems with information flows, chemical reactions far from equilibrium, biological systems with metabolism etc. These systems may exhibit interesting phenomena such as self-organization, pattern formation, and complex dynamics (Abuissa *et al.*, 2005; Van Kampen, 1992)

2.3.3 Characterization of NESS

In general, an equilibrium steady state (NESS) system can be characterized using an efficiency metric that relates the desired output to the energy input. This concept can be applied broadly to different types of NESS systems, including photoelectric, thermoelectric, and piezoelectric systems. The specific efficiency metric will depend on the nature of the NESS system and the energy conversion mechanism involved. For example, in a photoelectric system, the efficiency metric could be the photoelectric efficiency. In a thermoelectric system, it could be the thermoelectric efficiency, and in a piezoelectric system, it could be the piezoelectric efficiency. The general principle remains the same regardless of the energy output that is of interest in the given NESS system. This could be electrical energy, mechanical work, heat transfer, or any other desired form of energy output. The energy source or driving

force that sustains the non-equilibrium steady state of the system. This could be incident light, temperature difference, mechanical stress/strain, or any other form of input energy. The efficiency metric (η) is then defined as the ratio of the desired energy output (Eout) to the energy input (Ein or Win) in the given NESS system (Pekarek *et al.*, 2019; Xue *et al.*, 2022)

$$\eta = \frac{E_{out}}{E_{in}} \; or \; \eta = \frac{E_{out}}{W_{in}} \qquad \text{.....(2-2)}$$

NESS, is characterized by external driving forces which causes perturbations and the system response. The external driving forces are temperature and concentration gradients, mechanical perturbations and electric or magnetic fields, whereas the system response comprises of the forces exhibited by energy or particle fluxes within the system (Xuexiang Zhang *et al.*, 2022).This behavior stops the settlement of the system into a thermodynamic equilibrium state. The Non-equilibrium steady states condition can often lead to emergent phenomena and self-organization ranging from formation of dissipative structures, dynamic instabilities and emergence of spatial patterns (Yang *et al.*, 2015; Z. Zhang *et al.*, 2016)

The continuous flow of energy or particles can lead to the formation of spatial or temporal patterns, dynamic instabilities, or the emergence of dissipative structures. These features arise due to the complex interplay between the external driving forces and the system's internal dynamics (Xuexiang Zhang *et al.*, 2022). Similarly, in a biological system which has a maintained particle flow, like nutrient uptake and waste expulsions the continuous sustainability of supply and removal of particles is due to external driving forces. To sustain a steady state distribution of particles or matter, its internal mechanisms like metabolism or transport or both are adjusted (Xuexiang Zhang *et al.*, 2022)

Considering a case of a chemical reaction taking place in a closed container, consider a further consideration where the reactants are continuously removed or added, the reaction can proceed and arrive at non equilibrium steady state. In this reaction matrix the sustainability and compensation for product formation and reaction is due to fuel provision by input reactants. Another example is in a system where the temperature gradient is a driving force, energy flux is sustained due to heat flow from hotter to cold region. This phenomenon leads to a sustained energy flux. A non-equilibrium steady state is sustained by heat energy influx. The process

is also observed to have a stable temperature profile even as the heat flux continues to flow through it (Faraday, 1839; Z. Zhang *et al.*, 2016).

2.3.4 Formation of Dissipative Structures for NESS

Formation of dissipative structures is a phenomenon that arises due to non-equilibrium steady states. These are self -organized patterns or coherent structures, that happen, appear and persist in systems which are driven away from equilibrium. These systems continuously exchange matter and energy or particles with their surroundings. This concept was pioneered by the physicist Ilya Prigogine in 1977, who won the Nobel Prize in Chemistry for his work on non-equilibrium thermodynamics. Dissipative structures indicate a deviation from the equilibrium paradigm, where stable patterns and structures tend to appear spontaneously as a result of energy dissipation (Raimondi *et al.*, 2022; Z. Zhang *et al.*, 2016) The formation of these systems are associated with the presence of non-linearities and feedback mechanisms within the system. Non-linearities show that small variations or perturbations or both in the system can cause effects that are not proportionate, which can lead to magnified feedback. Examples of these systems are the Belousov-Zhabotinsky reaction, a chemical oscillatory reaction. In this reaction, the system undergoes a series of color changes as chemical species oscillate in concentration. These oscillations arise due to the interplay between autocatalytic reactions and inhibitory reactions, which create a dynamic feedback loop. The continuous exchange of reactants and products with the environment sustains these oscillations and gives rise to a dissipative structure (Abuissa *et al.*, 2005; Xuexiang Zhang *et al.*, 2022).

Another example is the Rayleigh-Bénard convection, which takes place in a fluid layer heated from the bottom. As the temperature gradient between the layer increases, the system transitions from a stable conductive state to a convective state which is characterized by the formation of cellular patterns. The heat input at the bottom of the system drives fluid motion and generates convection cells, which dissipate heat and maintain the non-equilibrium steady state. The formation of dissipative structures can also happen in biological systems. For example, in the development of organisms, intricate patterns emerge due to the interplay of genetic regulation, cell-cell signaling, and diffusion processes. These patterns include the formation of fingers in developing limbs, branching patterns in blood vessels, or the

spatial organization of tissues and organs. The specific system under investigation will determine the mechanism used for dissipative structure formation. Precise mechanisms underlying the formation of dissipative structures depend on the specific system under study. Even though the following factors: - feedback loops, energy or matter fluxes are known to influence dissipative structures formation, the ability of the system to dissipate energy and the presence of nonlinear interactions characterize the formation of dissipative structures (Perkinson *et al.*, 2019; Ried *et al.*, 2007).

Studying these systems can assist in grasping the emergence of behaviors that are complex in nature and at the same time assist in understanding how complex, organized behavior can emerge from basic components driven far from equilibrium. It shows the rich dynamics and self-organization potential of non-equilibrium systems, revealing more knowledge and understanding on the functioning of natural systems and motivating the innovation of new approaches in new materials, technologies, and engineering approaches.

2.3.5 Classification of NESS

It is possible to distinguish at least three different types of non-equilibrium states:

In Non- Equilibrium Transient State (NETS), the system is initially prepared in an equilibrium state and later driven out of equilibrium by switching on an external perturbation. The system quickly returns to a new equilibrium state once the external perturbation stops changing. Non-Equilibrium Steady State (NESS), the system is driven by external forces (either time dependent or non-conservative) in a stationary non equilibrium state where its properties do not change with time. The steady state is an irreversible non equilibrium process that cannot be described by the Boltzmann-Gibbs distribution, where the average heat that is dissipated by the system (equal to the entropy production of the bath) is positive (Kondepudi, 2008).

Non-Equilibrium Aging State (NEAS) is a situation whereby the system is initially prepared in a non-equilibrium state and put in contact with the sources. The system is then left to evolve alone but fails to reach thermal equilibrium in observable or laboratory time scales. In this case the system is in a non-stationary slowly relaxing non equilibrium state called aging state and characterized by a very small entropy production of the sources. In the aging state two-times correlations decay slower as

the system becomes older. Two-time correlation functions depend on both times and not just on their difference (Kondepudi, 2008).

There are many examples of non-equilibrium states, first there is a classic example of a NESS where an electrical circuit is made out of a battery and a resistance. The current flows through the resistance and the chemical energy stored in the battery is dissipated to the environment in the form of heat; the average dissipated power, P_{dis} = V I, is identical to the power supplied by the battery. Another example is a sheared fluid between two plates or cover slips and one of them is moved relative to the other at a constant velocity v. To sustain such state a mechanical power that is equal to $\left(\frac{p}{\eta v^2}\right)$has to be exerted upon the moving plate where η is the viscosity of the fluid. The mechanical work produced is then dissipated in the form of heat through the viscous friction between contiguous fluid layers (Kondepudi, 2008).

Another example of NESS is chemical reactions in metabolic pathways that is sustained by activated carrier molecules such as Adenosine Triphosphate (ATP). In such case, hydrolysis of ATP is strongly coupled to specific oxidative reactions. For example, ionic channels use ATP hydrolysis to transport protons against the electromotive force. A classic example of NETS is the case of a protein in its initial native state that is mechanically pulled (e.g. using AFM) by exerting force at the ends of the molecule. The protein is initially folded and in thermal equilibrium with the surrounding aqueous solvent. By mechanically stretching the protein is pulled away from equilibrium into a transient state until it finally settles into the unfolded and extended new equilibrium state. Another example of (Non equilibrium Transient State) NETS is a bead immersed in water and trapped in an optical well generated by a focused laser beam. When the trap is moved to a new position (e.g. by moving the laser beams) the bead is driven into a NETS. After some time the bead reaches again equilibrium at the new position of the trap (Rodger *et al.*, 2016).

In another experiment the trap is suddenly put in motion at a speed v so the bead is transiently driven away from its equilibrium average position until it settles into a NESS characterized by the speed of the trap. This results in the average position of the bead lagging behind the position of the center of the trap. The classic example of a NEAS is a liquid cooled below its glass transition temperature. The liquid

solidifies into an amorphous slowly relaxing state characterized by huge relaxation times and anomalous low frequency response (Kondepudi, 2008).

Other systems are colloids that can be prepared in a NEAS by the sudden reduction or increase of the volume fraction of the colloidal particles or by putting the system under a strain or stress. The classes of non-equilibrium states previously described do not make distinctions whether the system is macroscopic or small. In small systems, however, it is common to speak about the control parameter to emphasize the importance of the constraints imposed by the bath that are externally controlled and do not fluctuate. The control parameter (λ) represents a value (in general, a set of values) that defines the state of the bath. Its value determines the equilibrium properties of the system, e.g. the equation of state. In macroscopic systems it is unnecessary to discern which value is externally controlled because fluctuations are small and all equilibrium ensembles give the same equivalent thermodynamic description, i.e. the same equation of state. Differences arise only when including fluctuations in the description. The non-equilibrium behavior of small systems is then strongly dependent on the protocol used to drive them out of equilibrium. The protocol is generally defined by the time evolution of the control parameter $\lambda(t)$. As a consequence, the characterization of the protocol $\lambda(t)$ is an essential step to unambiguously define the non-equilibrium state (Kondepudi, 2008).

2.4 Energy Generation from Open NESS Thermodynamic System

2.4.1 Energy Generation from NESS

A system in a non-equilibrium steady state can be used to harness electrical energy. The sustained flow of energy or particles in such a system can be harnessed and converted into electrical power through various mechanisms. One common example is a thermoelectric generator. This system harnesses electrical energy by taking advantage of a temperature difference in a non-equilibrium system to convert heat energy directly into electrical energy. The temperature gradient across the system drives the flow of charge carriers (e.g., electrons) from the hot side to the cold side through a thermoelectric material, leading to the generation of an electric potential. This potential difference can be harnessed and used to power electronic devices (Z. Zhang *et al.*, 2016; Zheng *et al.*, 2018)

Another example is a photoelectric cell or solar cell. In a non-equilibrium state, such as when exposed to sunlight, certain materials exhibit the photoelectric effect. When photons (light particles) strike the surface of the material, they excite electrons, causing them to move and create an electric current. This current is collected and utilized as electrical energy (Z. Zhang *et al.*, 2016; Zheng *et al.*, 2018). Additionally, non-equilibrium systems that involve chemical reactions can also be employed to generate electrical energy. Fuel cells are a prime example. These devices use the electrochemical reactions of fuel and oxidant to produce electricity. Fuel, such as hydrogen, reacts with an oxidant, typically oxygen, in an electrochemical cell, releasing energy in the form of an electric current. The reaction is sustained by continuously supplying the fuel and oxidant to the system (Abuissa *et al.*, 2005; Xue *et al.*, 2022).Other forms of non-equilibrium systems, such as piezoelectric materials or electromagnetic induction setups, can also be used to generate electrical energy. In brief, NESS is a source of energy that can be converted into electrical energy through various mechanisms (Abuissa *et al.*, 2005; Cortés *et al.*, 2022).

2.4.2 NESS Open Thermodynamic Energy Systems

A heat pump is an example of a non-equilibrium steady state system. In a heat pump, the system operates by continuously transferring heat from a low-temperature reservoir to a high-temperature reservoir. This process requires the input of energy or work to drive the heat transfer against the temperature gradient. This system sustains a non-equilibrium steady state by continuously extracting heat from the low-temperature source and delivering it to the high-temperature destination. In this case continuous heat transfer and the stable temperature difference between low and high temperature reservoirs is sustained by steady state operations. This system also ensures stability of NESS by maintaining a constant supply of a working fluid like refrigerants, which absorbs heat from the low-temperature source, undergo a thermodynamic cycle, and consequently releasing the heat to the reservoir at high-temperature. The energy input to the heat pump is used to drive the cycle and facilitate the heat transfer (Al-Zareer *et al.*, 2019; Sun *et al.*, 2019).

The NESS in a heat pump arises as a result of continuous input of heat or work, which consequently perturbs the system away from thermal equilibrium. Minus continuous input of heat energy, the heat transfer process ceases, and the temperature gradient between the two reservoirs reduces to zero hence, a thermal

equilibrium state is attained. Therefore, a heat pump is an example of a non-equilibrium steady state system, where the sustained flow of energy or work allows for the continuous transfer of heat from a low-temperature source to a high-temperature destination (Braatz *et al.*, 2022; Sun *et al.*, 2019).

2.4.3 NESS as Time Independent and Time Dependent Systems

This section aims at demonstrating that a system in a non-equilibrium steady state can be time-independent while its energy output is a function of time. This is done by considering the characteristics of a non-equilibrium steady state and the behavior of the energy output over time. In a non-equilibrium steady state, the system maintains a stable average behavior over time, despite the ongoing processes and energy fluxes within the system. This means that the macroscopic properties of the system, such as temperature, concentration, or pressure, do not vary significantly over time (Green *et al.*, 2010; Wheeler, 2019). However, even though the system is time-independent in terms of its macroscopic properties, the energy output generated by the system can vary with time. This variation arises due to the continuous influx or removal of energy or particles from the system, which sustains the non-equilibrium steady state (Z. Liu *et al*., 2022; Xie *et al.*, 2022).

Considering a thermoelectric, the temperature difference that drives the energy generation can be constant, resulting in a time-independent system in terms of temperature gradient and other macroscopic properties. However, the energy output generated by the thermoelectric generator can vary with time if, for example, the external heat source supplying the temperature gradient fluctuates. Similarly, in a solar cell, the sunlight intensity may vary over time due to factors such as clouds or changes in the position of the sun. As a result, the energy output of the solar cell will fluctuate accordingly, even though the system itself remains time-independent in terms of its average behavior and other macroscopic properties (Z. Liu *et al*., 2022; Xie *et al.*, 2022). In summary, a non-equilibrium steady state can exhibit time-independent macroscopic properties while simultaneously having an energy output that varies with time. The time variation in the energy output arises from the continuous influx or removal of energy or particles that sustain the non-equilibrium steady state.

2.5 Modeling

2.5.1 Mathematical Modeling

A model is defined as an imitation or approximate representation of a prototype (i.e. concept, system or process) that is used to study, plan, design, or control the proto type. The construction of mathematical model to represent some system in the real world is known as simulation (Cardoza *et al.*, 2004).

A model is an abstraction of reality or representation or a real object or simulation. In other words, a model represents a simplified version of something. Mathematical model uses mathematical language to describe the behavior of a system. It is a representation of the essential aspects of an existing system (or a system to be constructed), which presents knowledge of that system in usable form,(Stevenson and Cole, 1999)

2.5.2 Modeling Time Independent and Time Function of Ness Systems

In mathematical modeling of a heat pump and demonstrating that it is a non-equilibrium steady state system, thermodynamic principles and equations are applied. Consider a simplified model for a heat pump operating in a Carnot refrigeration cycle, commonly used to describe the operation of a heat pump. It consists of four processes: two isothermal processes and two adiabatic processes. The working fluid in the heat pump undergoes these processes to transfer heat from a low-temperature reservoir (source) to a high-temperature reservoir (sink) (Ali and Anwar, 2021; Braatz *et al.*, 2022). Heat pump process consists of compression process: from state 1 to state 2, increasing its pressure and temperature. This process requires the input of mechanical work, represented by W_{in}. Secondly, high-Temperature Heat Rejection Process: where working fluid is cooled at constant high temperature (T_H) in the condenser, releasing heat to the high-temperature reservoir. The amount of heat released is represented by Q_H. Thirdly the expansion Process: where the working fluid undergoes expansion from state 3 to state 4, reducing its pressure and temperature. This process occurs adiabatically, meaning no heat is transferred to or from the system and finally Low-Temperature Heat Absorption Process: The working fluid is heated at a constant low temperature (T_L) in the evaporator, absorbing heat from the low-temperature reservoir. The amount of heat absorbed is represented by Q_L.

The equations describing time independent heat pump operation are:

Heat Transfer in the Condenser: $\boldsymbol{Q_H = m(h_2 - h_1)}$ **…….(2-3)**

Heat Transfer in the Evaporator: $\boldsymbol{Q_L = m(h_4 - h_3)}$**…… …..(2-4)**

Work Input: $\boldsymbol{W_{in} = m(h_2 - h_3)}$**……..……. (2-5)**

Where:

Q_H is the heat transfer to the high-temperature reservoir,

Q_L is the heat transfer from the low-temperature reservoir,

W_{in} is the work input to the system,

m is the mass flow rate of the working fluid,

h_1, h_2, h_3 and h_4 are the enthalpies of the working fluid at the respective states.

In a non-equilibrium steady state system, the heat pump continuously operates, transferring heat from the low-temperature reservoir to the high-temperature reservoir. This continuous operation, which requires work input W_{in}_ is imperative in maintaining the pressure difference and drive the heat transfer against the temperature gradient. So long us the energy input (work input) and energy output (heat) are balanced, the system remains in steady state. Any variations from the steady state would result in changes in the system properties, such as temperature and pressure, until a new steady state is achieved. Therefore, heat pump mathematical model, with arrange of equations describing heat transfer and work input, demonstrates that it is a non-equilibrium steady state system. The continuous operation and the need for external energy input to maintain the heat transfer against the temperature gradient characterize its non-equilibrium nature. Similarly, in the case of time dependent process, we consider extending the mathematical model of a heat pump to include time dependence; we can introduce the concept of time-varying heat transfer rates and work input. Let's modify the equations to incorporate the time-dependent aspects (Monthus, 2019; Tseng *et al.*, 2020)

Time-Dependent Heat Transfer in the Condenser:

$\boldsymbol{Q_H(t) = m(h_2 - h_1)t}$**……..(2-6)**

Time dependent Heat Transfer in the Evaporator:

$$\boldsymbol{Q_l(t) = m(h_4 - h_3)t} \text{..... (2-7)}$$

Time-Dependent Work Input:

$$\boldsymbol{W_{in}(t) = m(h_2 - h_3)t} \text{.....} \quad \textbf{(2-8)}$$

Where:

Q_H (t) and Q_L (t) is the time-dependent heat transfer to the high-temperature reservoir and heat transfer from the low-temperature reservoir respectively.,

W_{in}(t) is the time-dependent work input to the system,

h_1 (t) and h_2 (t) are the enthalpies of the working fluids at the evaporator inlet and at condenser outlet at time t, respectively

h_3 (t) and h_4 (t) are the enthalpies of the working fluid at the evaporator outlet and inlet at time t. respectively.

Other examples of models exhibiting both aspects of time dependent and time independent of NESS open thermodynamic systems are Photoelectric systems(Al-Zareer *et al.*, 2019; Braatz *et al.*, 2022; Sun *et al.*, 2019) and thermos electric and piezo electric systems.

In the time-independent case, a steady-state condition is assumed, and taking Φ, to represents the number of photons incident on the solar cell per unit area per unit time. Taking ηq, to represent Quantum Efficiency (the probability of absorbing a photon and generating an electron-hole pair. And taking γ,to represent collection efficiency (represents the probability that the generated electron-hole pairs are collected as charge carriers). Let the external circuit be modeled as an ideal load resistor, denoted by R, connected to the solar cell. Using these parameters, we can express the steady-state current output of the solar cell as:

$$\boldsymbol{I_{ss} = \Phi * \eta q * \gamma * e} \text{.....} \textbf{(2-9)}$$

Where:

I_{ss} is the steady-state current output,

e is the elementary charge (1.6 × 〖10〗^(-19) Coulombs).

In coming up with time-varying Model: In the time-varying case, we consider fluctuations in the incident light intensity, which affect the energy output of the solar cell over time. We incorporate these variations by introducing a time-dependent parameter for the incident photon flux, Φ(t). The time-varying current output of the solar cell can be modeled as:

$$\boldsymbol{I_{ss}(t) = \Phi(t) * \eta q * \gamma * e} \text{ ……..(2-10)}$$

where:

I(t) is the time-varying current output,

Φ(t) is the time-dependent incident photon flux at a given time t.

2.5.3 The Effect of Time Dependence on NESS Models

In a non-equilibrium steady state, the system continuously receives energy or work input to drive the heat transfer process. This external input perturbs the system, allowing it to maintain a steady state despite ongoing processes. The time dependence arises from the dynamic nature of the heat pump operation, as it responds to varying conditions, changes in temperature gradients, and other factors (Chen *et al.*, 2021; Saikia *et al.*, 2020; Zhu *et al.*, 2018). Therefore, even with time-dependent aspects, a heat pump remains a non-equilibrium steady state system because it requires continuous energy input to sustain the heat transfer process against the temperature gradient. The system's ability to continuously operate away from thermodynamic equilibrium distinguishes it as a non-equilibrium system, regardless of the time-dependent variations in its performance.

The time-dependent behavior of a heat pump, such as variations in heat transfer rates, work input, and system parameters, is a characteristic feature of its operation. These variations are essential for the heat pump to adapt to changing environmental conditions and maintain its non-equilibrium steady state. This principle equally apply to other systems like photosynthetic, thermoelectric and piezoelectric time independent and time dependent NESS open thermodynamic systems (Kerner *et al.*, 2021; Zhu *et al.*, 2018).

2.6 Comparison and Contrast Between Mem and Motors in Operations

A motor is defined as an electrical machine that converts electrical energy to kinetic energy, whereas a generator is defined as an electrical machine that converts kinetic

energy to electrical energy. All electric motors are governed by the laws of electromagnetism. Lenz-law governs energy conservation in electrical machines. Lenz law is a function of current. Power output of the motor is also directly proportion to motor speed, whereas the efficiency of the motor is directly proportional its size. Monopole Energize Machine is an open non equilibrium steady state thermodynamic system. It has both characteristics of motor and generator as it converts electrical energy to kinetic energy and vice versa (Valone, 2007)

These characteristics is analogous to solid state energizer which will neither behave like a motor nor a generator also likened to operation of a transformer which basically involves current and voltages as some major electrical characteristics. The concept of Monopole Energizer can be accomplished without using current, but mechanical motion and this is referred to as solid state Energizer (LINDEMANN and MURAKAMI, 2012).

Monopole Energizer Machine survives on very low amount of current. Due to this, MEM was modeled after SRM as the current passes through the rotor and stator windings of the motor, and due to Lenz law, the current establishes magnetic fields in the two fields. Interaction between the two fields creates relative motion (poles/ like or unlike)(Chiaramonti *et al.*, 2007; Felfli *et al.*, 2005).

2.7 Switched Reluctance Machine and Monopole Energizer Machine

2.7.1 Features and Basics of Switched Reluctance Machine

SRM is a type of synchronous machine. It uses few poles, not expensive, it is simple structured steeper motor, it has no commutators. The phase windings are independent, electrically commutated, electrically isolated, has a solid laminated rotor,(Anwar and Rashid, 2007). SRM commutation is achieved electronically. The optimal drive waveform is not a pure sinusoidal, due to the nonlinear torque relative to rotor displacement and the highly position-dependent inductance of the stator phase winding(Majid, 2009). The stator windings on diametrically opposite poles are connected in series to form one phase of the motor. By varying the number of phases, the number of stator poles and the number of rotor poles, many different SRM geometries can be realized (Shang *et al.*, 2000).When a stator phase is energized, the most adjacent rotor pole-pair is attracted towards the energized stator in order to minimize the reluctance of the magnetic path. Therefore, by energizing

consecutive phases in succession, it is possible to develop constant torque in either direction of rotation. SRM éliminâtes permanent magnets (PMs), bushes and commutators (Bien *et al.*, 1993).

2.7.2 Operational Characteristics of Switched Reluctance Machine

SRM has wound field coils as in a DC motor for the stator windings. The rotor, however, has no magnets or coils attached. It is made of soft magnetic material. When power is delivered to the stator windings, the rotor magnetic reluctance creates a force that attempts to align the rotor with the powered windings. SRM has the following limitations, first it must always be electronically commutated and thus cannot be directly connected to a DC bus or an AC line. Secondly its salient structure causes strong non-linear magnetic characteristics, complicating its analysis and control, and thirdly it shows strong torque ripple and noisy effects (Krishman 2001). If the stator does not have windings, the switching of power from winding to winding may be difficult to arrange in a fashion that is properly timed to the movement of the rotor. Brushes could be used, but this would eliminate most of the advantages of the design. The reluctance of the magnetic circuit decreases as the rotor aligns with the stator pole (Çetin and Özmen, 2003). SRM is also known as Variable Inductance Motor (Bass *et al.*, 1997). The inductance of the rotor to stator flux path varies with the position of the rotor as shown in Figure 2-1. Hence, modern high power electronic switch system is required, which also offers advantages in terms of control and power shaping (Bien *et al.*, 1993).

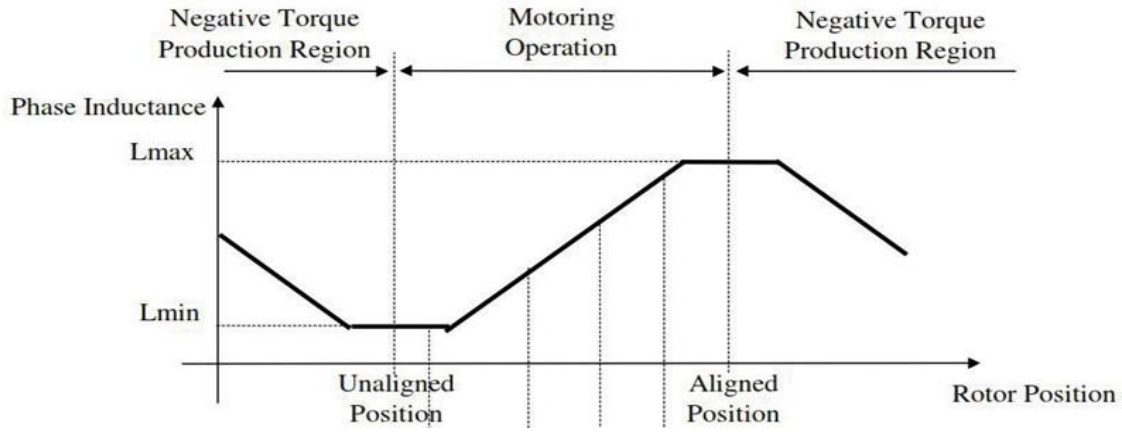

Figure 2-1: Inductance vs. rotor position (Miller1993).

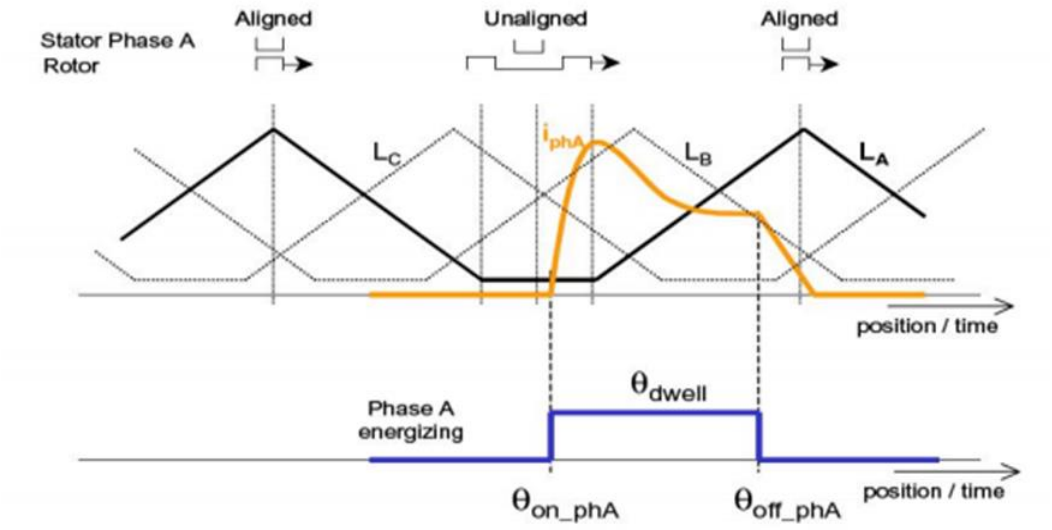

Figure 2-2: Phase Energizing (Miller1993).

2.7.3 Comparison and Contrast Between MEM and SRM

In both machines that is SRM and MEM, the torque constant is given by the slope of the inductance vs. rotor position characteristics. It is understood that the inductance of a stator winding is a function of both the rotor position and current, thus making it nonlinear. Because of its nonlinear nature, a simple equivalent circuit development for this motor is not possible. Torque and speed control are achieved with converter control (Hashemi *et al.*, 2019). Both machines require a controllable converter for their operation and cannot be operated directly from a three-phase line supply hence the motor drive is an inherently variable speed motor drive system (Hashemi *et al.*, 2019).

2.7.4 Boost Converter(BC)

The boost converter consists of an inductor, a semi-conductor, a switch (MOSFET), diode, a capacitor, a source of periodic force wave which can be a 555 timer or even a dedicated SMPSIC, like the famous MC34063AIC. The circuit below is used to demonstrate the making of a boost converter. Before the circuit is closed the output capacitor is charged to the input voltage minus one diode drop. When the circuit is closed by turning the switch on the signal source goes high, turning on MOSFET. This causes all the current to be diverted to the MOSFET through the inductor. The output capacitor stays charged since it cannot discharge through the reverse biased diode. The power source is not immediately short-circuited and the inductor makes the current ramp up relatively slowly. Also, the magnetic field builds up in the

inductor causing the polarity of voltage applied to be positive on the side of the diode. When MOSFET is turned off, the current to the inductor is stopped abruptly (Sriphan *et al.*, 2018a).

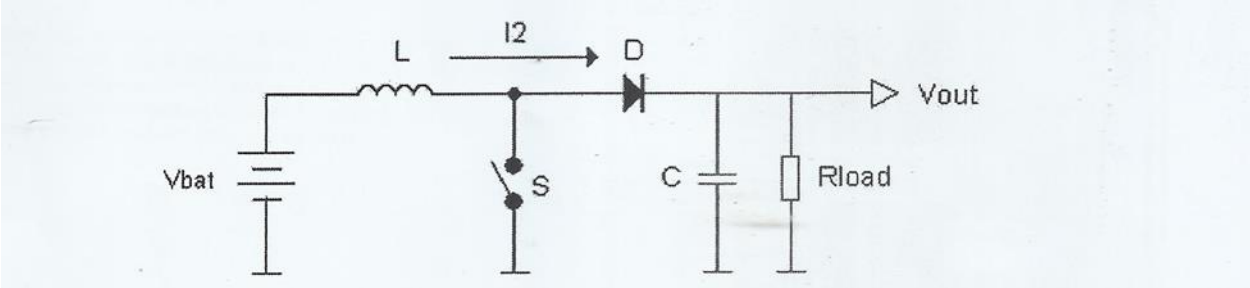

Figure 2-3: Boost Converter Circuit (Miller, 1993).

2.7.5 Comparison and Contrast between MEM and BC

The nature of the inductor is to maintain smooth current flow. It does not like sudden turning off the current or sudden change of the current. It responds to this by generating a large voltage with a possible polarity of the voltage originally supplied to it by using the energy stored in the magnetic field to maintain that current flow. Both MEM and BC can be used to boost DC voltage to the required level and hence save on weight and space that would have been occupied by having large numbers of battery banks (Miller1993). Another problem is that battery voltage may become too low to power the circuit being supplied. Both MEM and BC may be used to solve this problem by boosting the low output batteries to useful levels again by using MEMs and BCs the life of the battery or batteries can be extended. Based on these similarities it was justified to model the Monopole Energizer Machine output parameters after the boost converter.

2.8 Modeling of Monopole Energizer Machine

Based on the outgoing facts above, it is clear that the functioning of motors and even their basic operations and structure are very distinct from Monopole Energizer Machine and hence there is nothing to be borrowed from motors of all types except SRM in terms of modelling, design and operations of input parameters.

2.9 Charging Curve for Lead Acid Baterry, Dry Battery and Wet Battery

This section focused on the general behavior of charging voltage profile for lead acid battery. Figure 2-4 shows charging curves for both current and voltage. Figure

2-5 shows the charging curve for micro – battery charger (Dry battery) for voltage and current, whereas

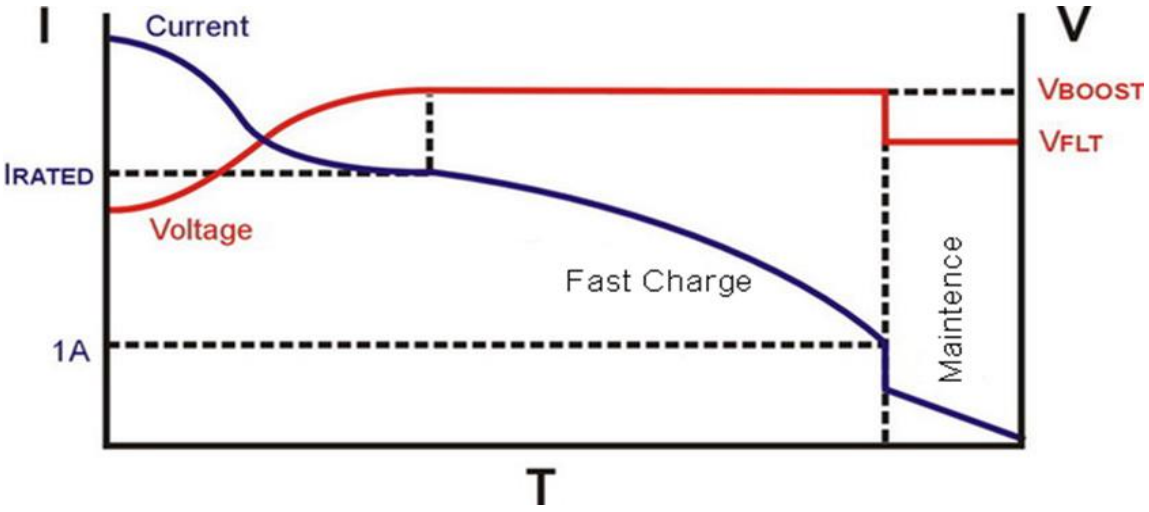

Figure 2-4: Charging curve for Lead-Acid Battery Charger.

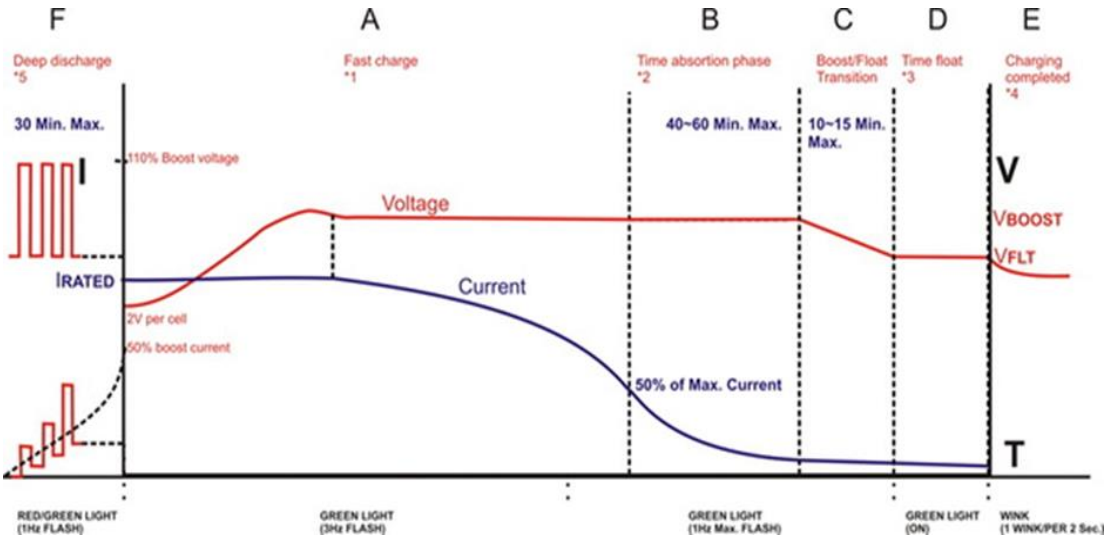

Figure 2-5: Charging Curve for Micro Battery Charger (Dry Battery).

The batteries were presumed to demonstrate ideal and standard behavior of ordinary batteries during charging and discharging. Figure 2-6 shows charging curve for micro-Battery charger (Wet – Battery) for both voltage and current.

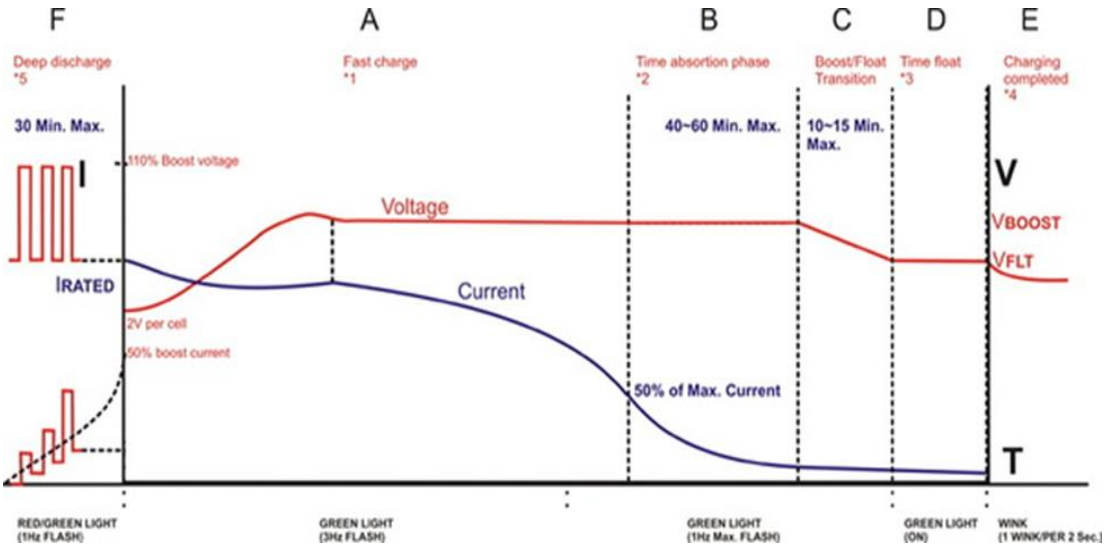

Figure 2-6: Charging Curve for Micro Battery Charger (Wet Battery).

There is no significant different between figures Figure 2-5, and Figure 2-6,Figure 2.5 is a dry battery and 2.6 is a wet battery. The two batteries were included in the discussion to set a basis for comparison with the results of Monopole Energizer Machine.

2.10 Research Gaps

A number of studies done in this area indicate that there is scanty literature on energy generation from open NESS thermodynamic system. It has been argued that Monopole Energizer Machines are possible, but there is need to be cautious before arriving at radical conclusion or deduction. It has been said that there is no conclusive scientific evidence to support the existence of Monopole Energizer Machines. The authors assert that the laws of thermodynamics do not rule them out, that is there are high chances of fitting these types of systems in proper scientific setting. This implied that there was knowledge deficit in this area hence need for further investigation to narrow the gap. Secondly there was need to locate MEMs in scientific context, theory and practice (LINDEMANN and MURAKAMI, 2012; McDonald *et al.*, 2013). There has been little research undertaken on Modeling of Energy generation from open NESS thermodynamic system using both time function and time independent aspects. These concerns coupled with gaps identified in Bedini Monopole Energizer Machines, Newman's Energy Machines, hence there was need to enhance knowledge to the body of knowledge in this area. (Crutchfield *et al.*, 2016; Gallavotti and Cohen, 1995)

Thirdly there has been lack of coherent explanation on the areas deviating from thermodynamic laws and selective applications of perpetual motion machine principle in relation to source charge problem in power systems. Whereas investigation on power generation from NESS open thermodynamic system has been scantly researched with thermoelectric generator and photoelectric solar cells none has been done with Monopole Energizer Machine. Development of predictive mathematical model using MEM has not been done especially with the focus on SRM and hence this investigation is important in generating information and knowledge in this area.

Similar studies on non-energy production applications of non-equilibrium steady state thermodynamics were carried by several authors (Kassebaum *et al.*, 2014; Landon, 2015; Murakami *et al.*, 2010) others. From the foregoing literature and observation all the studies were carried out in the context of non-equilibrium steady state thermodynamics were for non-energy generation applications. To the best of my knowledge no studies have applied non-equilibrium steady state thermodynamics knowledge for energy generation especially the generation of energy from non-stationary irreversible open non equilibrium steady state thermodynamic system. Some inventions and replications (Moore *et al.*, 2006) have shown strong possibilities of the use of open non- equilibrium steady state thermodynamics and lend themselves to further research. (Aharonov and Bohm, 1961; Büscher and Sumpf, 2015; Siviero *et al.*, 2011). This research seeks to advance these suggestions

CHAPTER THREE:
MATERIALS AND METHODS

3. Materials and Methods

3.1 Introduction

In this section two Monopole Machines are build. These Machines are then used to run and collect data. This chapter was divided into four sections.

3.2 Equipment for Research

The equipment for research was monopole energizer machine. This equipment was built and located at MMUST, where the experimental was ran. The details of construction materials, circuit design and running of the experiments is discussed below.

3.3 Construction of Experimental Equipment

3.3.1 Components and Materials of Construction of Monopole Energizer Machine

In construction of Monopole energizer Machine, the following materials and components were required.

Table 3-1: List of Quantities for Monopole Energizer Model Construction

No.	Item	Units of measurement	Quantity
1	12” diameter non-magnetic wheel (wood, plastic, Aluminum Alloy	Number	3
2	Ceramic Magnets of size 2 x 3/8 inches and Neodymium magnets	Number	16
3	R60 gas welding magnets	Number	4
4	Super glue 300grams	Grams	1
5	Bearing ½ inch	Number	4
6	4Ah, 12V Batteries	Number	2

Other materials required were Wooden Props, Wooden Base. Nails, Glue, tools required are Hammer, saw, drill, assorted Drill Bits.

Table 3-2: List of Electronic Components for Mono Pole Energizer Construction

No.	Item	Units of measurement	Quantity
1	2N3055 NPN transistor	Number	8
2	1N4001 Diode	Number	6
3	1N4007 Diode	Number	6
4	Neon Bulb NE-2	Number	6
5	7Ah, 12V Lead Acid Motorcycle Battery	Number	2
6	680 Ω	Number	8
7	1KΩ variable resistor	Number	4
8	1 m thickness electrical cable	Kg	0.5

Figure 3-1: Photograph of Monopole Energizer Machine Used in The Study

3.3.2 Construction of Monopole Energizer Machine and Experimental Set Up

In the experimental set up, the original design was assembled by the sets of Ceramic magnets, whereas the replication design was assembled by Neodymium magnets. The Monopole Energizer Machine was assembled by using the components outlined above. These parts were assembled according to the schemes well known in the art

of electric circuit construction. The wheel was non-magnetic and was supported on either side by non-magnetic (wood, Aluminium alloys, plastic etc.) props. The magnets were glued to the wheel circumferentially in such a way that the north poles face away from the wheel Centre.

Bifilar coil was wound to a ratio of 1:1 on a plastic spool whose centre was filled with soft steel R60 gas welding rods. The rods were cut to the length of the plastic spool and served as magnetic core of the bifilar coil. The model built was 30 cm diameter which could also accommodate up to 16 magnets at ago. In these experiments two sets of magnets that is Neodymium and Ceramic magnets were used. The Figure 3-2 shows the Monopole Energizer Machine generator test rig used in this investigation. According to Figure 3-2, most of the test-rig's components were mounted on the base (1) with a covering of a safety guard. When the rotating wheel (2) that contained magnetic bars mounted on it rotated, the stationary coil (3) generated electricity. The rectifier (4) then converted the generated ac power into dc using control signal from the control circuit (5). The output dc power then was regulated by the regulating circuit (6) that provided suitable output voltage level for the battery (7). It is noted that one of the batteries was used as the electric source or primary source and the other was used as the energy storage or secondary source. The figure below shows bifillercoil, coil core, the rotor and battery. All these components are part of the Monopole Energizer Machine. A brief explanation for each is explained below

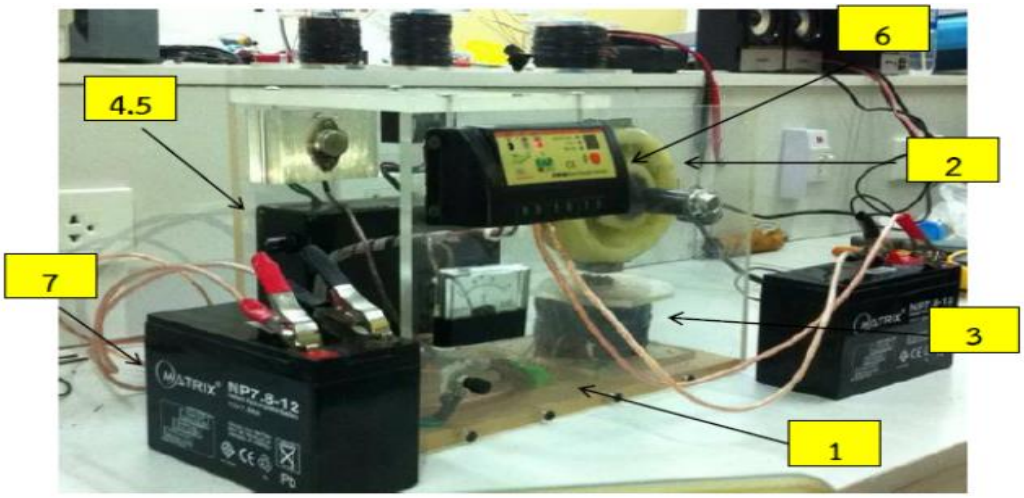

Figure 3-2: Constructed Monopole Energizer Machine Used for This Research

3.3.3 Bifiller Coil, Coil Core, The Rotor and Battery

Bifilar coil, as indicated in figure 3.3 is one of the main parts of for producing electromagnet when connected to Monopole Energizer Machine Circuit. This winding is usually used in making of a few types of winding for transformer. (Ahn *et al.*, 2006).There are two types of windings on the spool together, one is trigger coil and the other one is power coil. The coil core is a metal rod that is stuffed in the middle of the coil winding as shown in the figure 3.4. Normally, it is stuffed with welding rods. Suitable materials are those which do not retain any magnetism when the magnet is taken away from them. In this experiment it was ensured that suitable core was used, that is, the one that attracted to both core ends that is north end and south end. Figure 3.4 shows coil core.

It is worth noting that anything round and non-magnetic can be used as a rotor (J. C. Bedini, 2003). For example, skate board wheels, with a little grinding or machining of the rubber to accommodate the magnets can make a good 3 or 4 pole rotors. Basically, smaller diameter, 3 or 4 pole rotors run at higher RPM and draw less current like 6 pole rotors. This may be an important Consideration in keeping the current draw down, below the critical battery C20 rate, on the smaller batteries (Sauer and Wenzl, 2008). In addition, precaution was taken in wrapping some kind of heavy-duty strapping tape with the little strings imbedded in it.

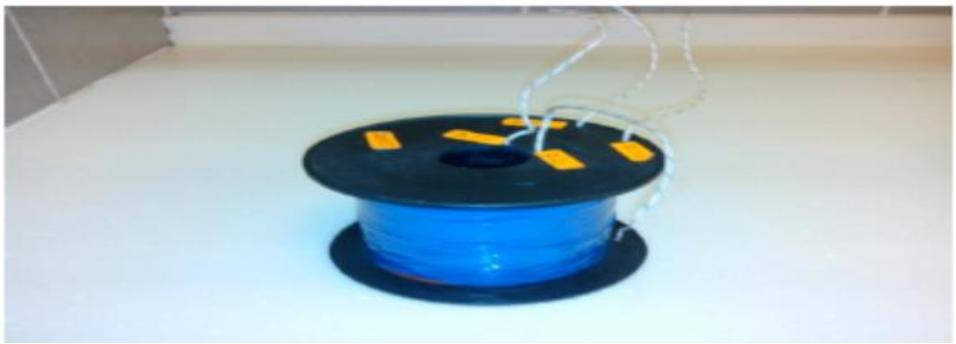

Figure 3-3: Bifilar Coil for Bedini SSG (Fakhrurrazey et al., 2014).

Figure 3-4: Coil Core (Fakhrurrazey *et al.*, 2014).

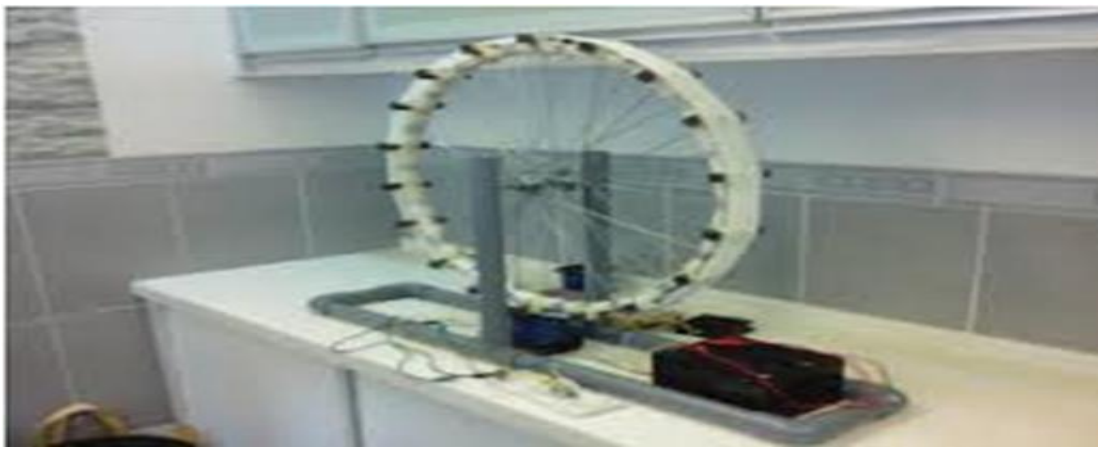

Figure 3-5: Photograph of Prototype of Original Monopole Energizer (Fakhrurrazey et al., 2014).

A battery is one of the most important tools that have to be considered in building Monopole Energizer Machine. In this project, a lead acid battery was chosen and was used for charging and discharging. Both charging and discharging were performed simultaneously. Lead acid battery was important in determining (COP) by discharging battery with load and recharge the charging battery.

In this experiment the battery was charged to full capacity of 15 volts. Normally, Lead-acid batteries are rated for a 20-hour discharge. The current that discharges the battery from fully charged volts to fully discharge is called the C20 rate. In this

process about 13.3 to 13.8 mill amps current is used to full discharge of around 11.5 volts in 20 hours.

Figure 3-6: Photograph of a Typical Lead Acid Battery (Fakhrurrazey *et al.*, 2014).

3.3.4 Types of Magnets, Original and Replication Design

Figure 3-7 and Figure 3-8 show the two sets of magnets used in these experiments. Figure 3-9 shows the mounting of both original design and replication with relevant design circuits. Ideally the magnet width should be equal to or greater than the coil core. Rectangular magnets give an improved performance over simple discs in order for the magnetic field to sweep across the entire face of the coil or close to it (Zimm *et al.*, 2006). The distance between each magnet was not less than 1.5 to 2 size of magnet widths. This was done to avoid interactivity of the scalar south poles.

Figure 3-7: Photograph of Typical Ceramic Magnet (Fakhrurrazey *et al.*, 2014)

Figure 3-8: Photograph of Typical Set of Neodymium Magnets

The original design Monopole Energizer Machine has advantage over the replication design in terms of simple design, and application for larger power generator (Felfli *et al.*, 2005) which is part of the focus for this thesis.

Figure 3-9: Monopole Energizer Machine Based on the Original Design (Fakhrurrazey et al., 2014).

3.4 Experimental Set Up

3.4.1 Monopole Energizer Machine Circuit Diagram

Figure 3-10 shows the circuit design for monopole energizer machine and its circuit diagram.

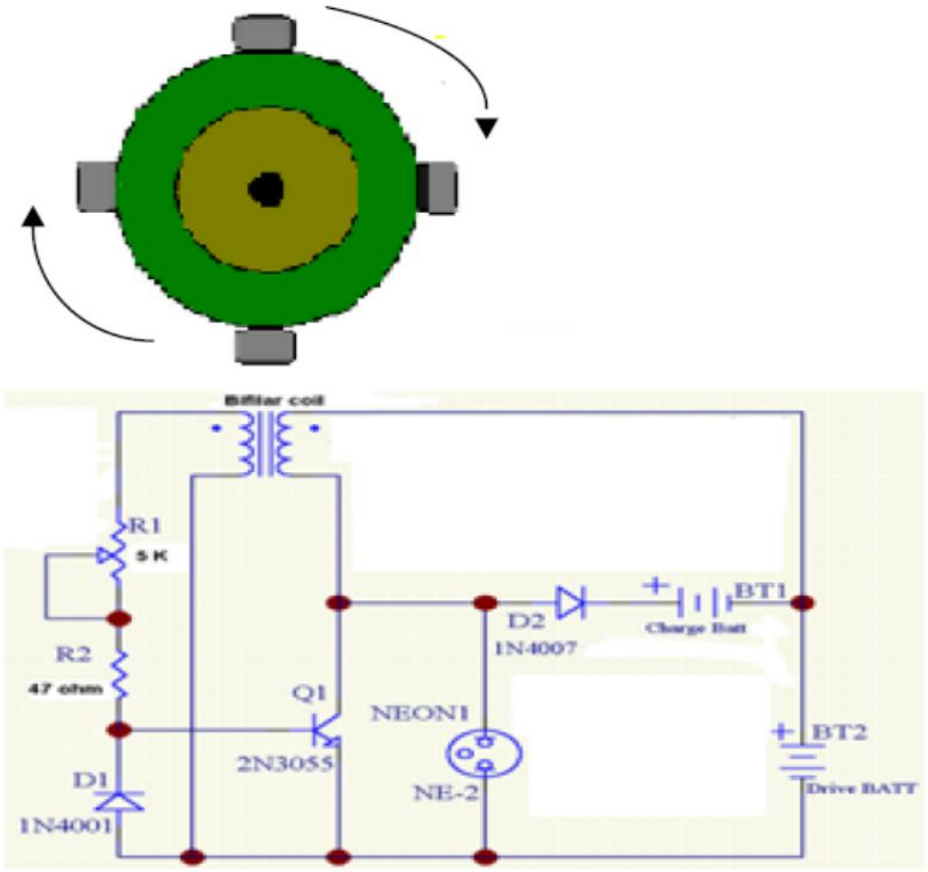

Figure 3-10: Schematic Circuit of Monopole Energizer Machine (Fakhrurrazey *et al.*, 2014).

3.4.2 Running of the Experiment of Monopole Energizer Machine

The switch was closed and wheel was given a gentle push in one direction to get it spinning because the machine was not self-starting. When the magnets approached the coil, it induced a current in the trigger coil that went through the 1N4001diode, the resistor and potentiometer. When the magnet was directly above the core the induced current stopped. Then when the magnet had passed the core, it induced a current in the opposite direction that flows through the base of the transistor and out through the emitter. This turned on the transistor and current was then free to flow from the positive of the primary battery through the primary coil and back to the negative of the battery. Once the magnet had past the coil, it no longer induced a current in the trigger coil and so the transistor turned off. The coils magnetic field then collapsed created a high potential spike in the primary coil that went through the charging battery (J. Bedini, 2003)(J. Bedini, 2003)(J. Bedini, 2003)(J. Bedini, 2003)(J. Bedini, 2003)(J. Bedini, 2003)(J. C. Bedini, 2003).

3.4.3 Sizing of the Model

The size of this model was guided only by its relevance to parameter measurement and not necessarily to adaptation to a particular useful application.

3.4.4 Input and Output Parameters of the Model

In this model the input parameters were source voltage and input current. The output parameters were battery output voltage, battery load current and the temperature of battery electrolyte. The design of the variations in the design of the monopole energizer was considered. Parameters of said variation included varying the number of magnets used (number of poles), varying the type of magnets used (magnetic flux density) and changing the wheel (permeability) and varying the size of battery being charged (capacity).. In this experiment input and output parameters measured directly were current, voltage and temperature.

The input and output parameter computed from data generated were input and output instantaneous power, input and output average power, instantaneous coefficient, average co-efficient, rate of charging and rate of discharging batteries and coefficient of performance.

3.5 Experimental Procedure

3.5.1 Monopole Energizer Machine with Ceramic and Neodymium Magnets Experiments

Several sets of experiments with magnets ranging from 4, 6, 8, to 16 in number were assembled and for each set of experiment the type and set of magnets, the input and output components of voltage, current and time were tabulated. The input and output parameters recorded were voltage (V), current (I) and time. The results were recorded for each set and type of magnets during each experimental run in Table 3-3. The efficiency of the model was calculated as a ratio of Energy output ($E_O = V_oI_ot_o$) to Energy input ($E_{i=}V_iI_it_i$)) , where $V_oI_ot_o$ and $V_iI_it_i$ are components of output and input voltage, current and time respectively. Calculation of coefficient of performance (COP) was based on energy accumulated in the battery with respect to energy from the source. COP was calculated for each table and an average was determined. The experiments were run for a period of between 4hours and 9 hours depending on the time it would take for the battery to be fully charged.

3.5.2 Recording of Results

Voltage and Current measurements of primary and secondary batteries was done in time intervals of 5 minutes. Similar measurements were performed for a varied number of magnets e.g., 4,6 up to 16. Input quantities were primary battery temperature, voltage and current, output quantities were secondary battery Load current, temperature, voltage. Temperature measurements were taken using an infrared Thermometer. The results of this experiment were recorded as indicated in Table 3-3. The recording of results was done for Energizer model with Ceramic and Neodymium magnets separately.

Table 3-3: Results of Monopole Energizer Model

Time (Minutes)	Input voltage (V)	Input Current (A)	Input Temp (^{0}C)	Output voltage (V)	Output current (A)	Output Temp (^{0}C)
Start charging (0)						
5						
10						

3.5.3 Purpose of experimental results

Experimental laboratory research aimed at determining the rate of charging, rate of generation of output current, power, voltage, of MEM on the basis of increasing output quantities in relation to time accumulation or increase. The mathematical model developed predicted the output quantities in relation to the number of magnetic loadings on Monopole Energizer Machine. The COP at different levels of magnetic loadings for both original and replication designs was also determined. In chapter four experimental and data analysis were done for the physical model. Data was also generated for development of mathematical model

3.5.4 Data analysis

Results were presented by tabulation, graphs and power calculation. P = V.I, Energy = Power x Time = *VIt*. In this experiment 1-ohm resistor was used (thin wire wound on a nail) to discharge the secondary battery in order to establish capacity of charge. Confirmation of the state of charge (capacity of charge) was carried out for each set of magnets.

3.6 Overview of Mathematical Modeling of Mem

In developing mathematical model the following steps were followed: According to Cheng *et al.* (2015), steps of model development are :

i. Definition of the problem that is prototype identification and statement of the modelling problem.
ii. Construction of the model that is selects the criteria to guide the decision and establish objectives.
iii. Formulation of a model to establish the relationship between influential factors and the objectives to be achieved.
iv. Solution of the model equation.
v. Model validation, sensitivity analysis, verification adjustment and use.
vi. Finally, Implementations of the alternative and Limitations of the model.

The scope of this research was to determine electrical characteristics of monopole energizer machine for both ceramic and neodymium magnets. The key parameters studied and analysed were voltage, current, power, coefficient of performance (COP), charging and discharging rates of secondary and primary batteries respectively. The input and output parameters were experimentally determined for a range of a given data for both designs of Monopole Energizer machines.

The Predictive models are useful and under certain conditions they lead to real insight into process or problem and hence the reason why this approach was adapted. The experimental data as outlined in materials and method in Chapter three, were used to determine and develop predictive mathematical model for MEM. This section outlines the steps taken in developing predictive mathematical model. Model solution and analysis is undertaken in chapter seven and eight. This section outlines the steps adopted in the development of predictive mathematical modelling of MEM. The section is organized in seven sections focusing on: -

a) Stages of Model development
b) Modelling of electrical characteristics of monopole energizer machine (MEM) of original Design based on experimental data.
c) Modelling of electrical characteristics of monopole energizer machine (MEM) of replication design based on experimental data
d) Model validation and sensitivity analysis,

e) Implementation of alternative use

f) Verification of mathematical model,

g) Weaknesses of the model,

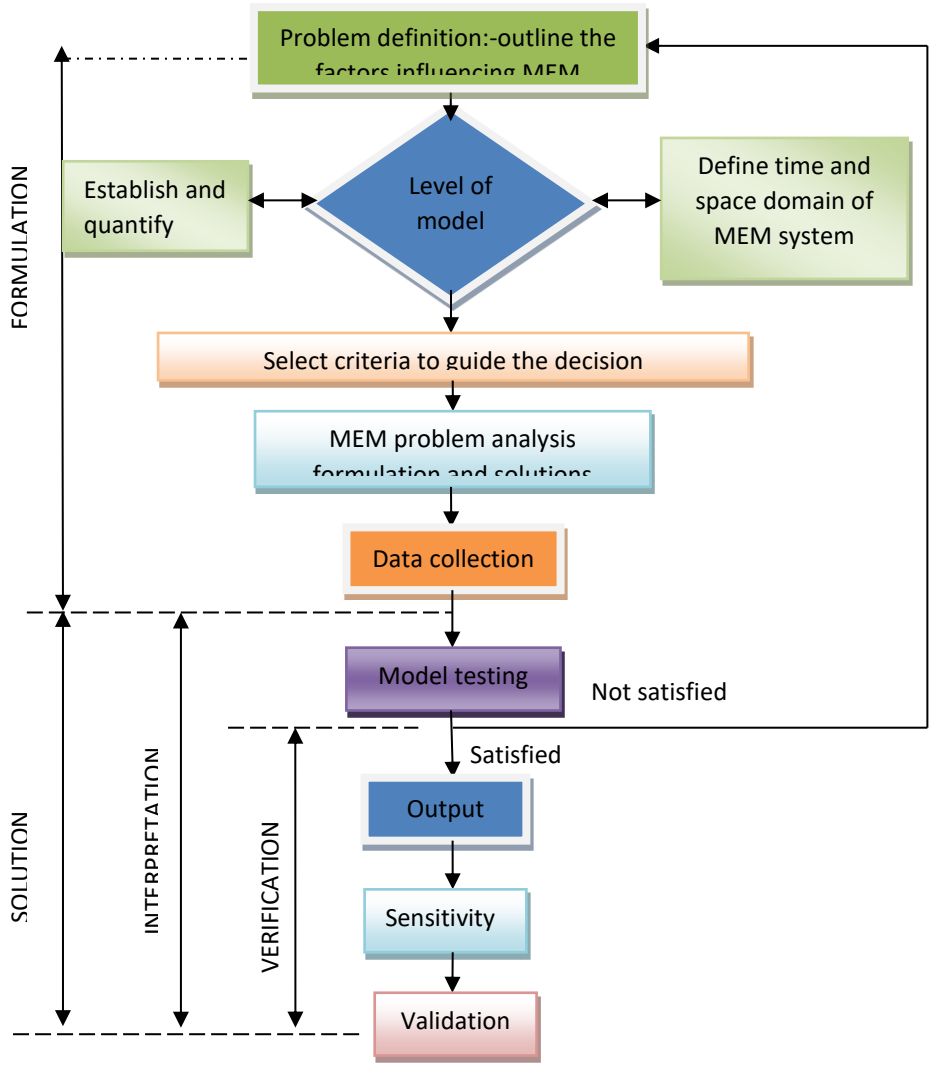

Figure 3-11: Stages of Modelling (Cardoza *et al.*, 2004)

3.7 Stages of Model Development

This stage entails establishing the model purpose, a preliminary modeling strategy, and identification of possible equations to define the problem.

3.7.1 Identification of Proto Type and Modelling Problem

For this research, the prototype is the Monopole Energizer Machine system and the modelling problem is the determination of predictive mathematical equation(s) to determine time independent and time varying function of NESS open thermodynamic system (MEM) under consideration. The independent variable in this model was voltage output, which was taken as the critical and controlling

variable. The second variable considered for modelling was load current even though it was a dependent variable, but yet critical in completing the modelling function. Hence the model focused on output voltage and load current for both MEM designs. The other variables were, power output, power input and various co-efficient of performance were dependent variable. The model focused on developing predictive equations of the following functions: -

1. Prediction of time function voltage output for MEM for original design
2. Prediction of steady state voltage output for MEM for original design
3. Prediction of time function load current for MEM for original design
4. Prediction of steady state load current for MEM for original design
5. Prediction of time function voltage output for MEM for Replication design
6. Prediction of steady state voltage output for MEM for Replication design
7. Prediction of time function load current for MEM for Replication design
8. Prediction of steady state load current for MEM for Replication design

3.7.2 Construction of the Model

In chapter 5 of this thesis the predictive mathematical Model for MEMs is developed, tested, verified and validated.

3.7.3 Model Formulation

Based on literature, features and characteristics of SRM, and conventional electrical motors in comparison to MEM input equations were formulated. Likewise, after undertaking analytical comparative analysis between boost converter and MEM, output mode equations were developed. The proceeding sections under gives details on formulation of the equations. Sections 3.7 and 3.8 development of model equation for input and output parameters is done. Section 3.9 solution of the model

3.8 Model Formulation for Input Parameters

In this section the analysis and derivation of voltage equations and Torque production equation are formulated.

3.8.1 Switch Reluctance Machine

$$V = iR + \frac{d\lambda}{dt} \quad \text{---------- (3-1)}$$

$$\frac{d\lambda}{dt} = \frac{d}{dt}\boldsymbol{i} + \frac{di}{dt}\boldsymbol{\theta} \quad \textbf{---------- (3-2)}$$

$$\boldsymbol{V = iR + \frac{d(Li)}{dt}} \text{---------- } \text{---------- (3-3)}$$

$$\boldsymbol{V = iR + L\frac{d}{dt} + i\frac{dL}{dt}} \text{---------- (3-4)}$$

$$\boldsymbol{V = iR + L\frac{di}{dt} + i\frac{dL}{d\emptyset} \times \frac{d\emptyset}{dt}} \text{---------- (3-5)}$$

$$\boldsymbol{V = iR + L\frac{di}{dt} + i\omega\frac{dL}{d\emptyset}} \text{----------(3-6)}$$

Where

λ Is flux linkage

iR is ohmic drop

$L\frac{di}{dt}$ Is emf due to incremental inductance

$i\omega\frac{dL}{d}$ Self-induced emf, e (or self emf)

$$\boldsymbol{V = iR + L\frac{di}{dt} + e} \text{---------- (3-7)}$$

Self-induced emf, is proportional to current, speed and the rate of change of inductance with rotor angle.

If flat topped current is assumed $L\frac{di}{dt} = 0$ on the other hand if the inductance is constant, self emf is zero. So the first term $L\frac{di}{dt}$ absorbs all applied voltage.

$$\boldsymbol{Vi = iR + L\frac{di}{dt} + i^2\omega\frac{dL}{d\emptyset}} \text{---------- (3-8)}$$

The dynamic mathematical model of an SRM is composed of a set of electrical equations for each phase and the equations of the mechanical system (Krishnan 2001).Considering the voltage, and inductance per phase we have; the voltage equation phase given by :-

$$\boldsymbol{V = R_s i + \frac{d\lambda(\phi,i)}{dt}} \text{----------(3-9)}$$

where R_s is the resistance per phase and λ is the flux linkage per phase and it is given by

$$\boldsymbol{\lambda = L(\phi, i)I} \text{ y } \text{---------- (3-10)}$$

where

L is the inductance per phase dependent on the rotor position and phase current.

Substituting the Equation (3.2) in Equation (3.1), the voltage equation becomes

$$V = R_s i + L(\phi, i)\frac{di}{dt} + \frac{dL(\phi,i)}{d\theta} i\omega_m \text{----------} \quad (3\text{-}11)$$

Where

ω_m is angular velocity

The instantaneous induced emf is obtained as

$$e = \frac{dL(\phi,i)}{d\theta} i\omega_m = i\omega_m K_b \text{----------} \quad (3\text{-}12)$$

where$K_b$may be constructed as an emf constant and is given by

$$K_b = \frac{dL(\phi,i)}{d\theta} \text{----------} \quad (3\text{-}13)$$

Torque Production equations of SRM

$$\textbf{Energy stored in the magnetic circuit} = \frac{1}{2}Li^2 \text{----------} \quad (3\text{-}14)$$

Rate of change of energy stored in the magnetic circuit =

$$\frac{d}{dt}\left[\frac{1}{2}Li^2\right] \text{----------} \quad (3\text{-}15)$$

$$= \frac{1}{2}L.2i\frac{di}{dt} + \frac{1}{2}i^2\frac{dL}{dt} \text{----------} \quad (3\text{-}16)$$

$$= \mathbf{Li}\frac{\mathbf{di}}{\mathbf{dt}} + \frac{\mathbf{1}}{\mathbf{2}}\mathbf{i}^2\frac{\mathbf{dL}}{\mathbf{d}} \times \frac{\mathbf{d}}{\mathbf{dt}} \text{----------} \quad (3\text{-}17)$$

$$\frac{dW_{mag}}{dt} = Li\frac{di}{dt} + \frac{1}{2}i^2\omega\frac{dL}{d\emptyset} \text{----------} \quad (3\text{-}18)$$

Mechanical energy transferred = electrical energy input + i^2R + rate of change of energy stored in the magnetic circuit.

$$\textbf{Mechanical energy transferred} = Vi + i^2R + \frac{dW_{mag}}{dt} \text{----------} \quad (3\text{-}19)$$

$$= \mathbf{i}^2\mathbf{R} + \mathbf{Li}\frac{\mathbf{di}}{\mathbf{dt}} + \mathbf{i}^2\boldsymbol{\omega}\frac{\mathbf{dL}}{\mathbf{d}\emptyset} + \mathbf{i}^2\mathbf{R} + \mathbf{Li}\frac{\mathbf{di}}{\mathbf{dt}} + \frac{\mathbf{1}}{\mathbf{2}}\mathbf{i}^2\boldsymbol{\omega}\frac{\mathbf{dL}}{\mathbf{d}\emptyset} \text{----------} \quad (3\text{-}20)$$

$$P_m = \omega T \text{----------} \quad (3\text{-}21)$$

$$P_m = \frac{1}{2} i^2 \omega \frac{dL}{d\emptyset} \text{----------(3-22)}$$

$$T = \frac{1}{2} i^2 \frac{dL}{d\emptyset} \text{----------(3-23)}$$

This equation can also be written as Torque equations per phase as shown under The torque per phase is given by

$$T_e(\theta, i) = \frac{1}{2} i^2 \frac{dL(\theta,i)}{d\theta} \text{----------(3-24)}$$

Under the simplifying assumption of magnetic linearity, the torque equation becomes

$$T_{total}(\theta, i) = \sum_{phases} \frac{1}{2} i^2 \frac{dL(\theta,i)}{d\theta} \text{---------- (3-25)}$$

Which on substitution into the mechanical equation results in the following

$$T_{total} - T_l = J_m \frac{d\omega_m}{dt} + B_m \omega_m \text{----------(3-26)}$$

Where

T_l is load torque,

J_m is moment of inertia and

B_m is the friction coefficient.

φ is the flux linked by the winding.

Because of the double salience construction of the SR motor and the magnetic saturation effects, the flux linked in an SRM phase varies as a function of rotor position θ and the phase current.

The SRM can be described by convex function .This function is the co-energy $W(I, \theta)$. In a similar manner, the function energy $W(\varphi, \theta)$, whose variables are the fluxes of n phases $(\varphi_1, \varphi_2, \dots \varphi_n)$ and the rotor position, θ, it also permits to describe the SRM. Whatever the vectors φ and I are, the function of co-energy,

Consider the following energy inequality equation

$$\overline{W}(I, \theta) + W(\varphi, \theta) \geq \varphi_1 I \text{----------(3-27)}$$

The partial derivative of the energy function in relation to the rotor position gives the machine torque T:

$$\boldsymbol{T(\varphi_1, \ldots \varphi_n, \emptyset) = \frac{\partial W}{\partial \emptyset}(\varphi_1, \ldots \varphi_n, \emptyset)} \quad \text{----} \quad \text{----------.----------(3-28)}$$

When one energizer one phase, the torque appears so that the rotor evolves in the direction where the inductance increase. Therefore, the torque will be in direction of the nearest aligned position (Bassily *et al.*, 1995; Jazdzynski and Majchrowicz, 2013; Vujicic and Vukosavic, 2000).

3.8.2 Design of MEM Equivalent Circuit for Input Parameters

The equivalent circuit for Monopole Energizer Machine (MEM) consists of same components as the SRM circuit, that is, it has Resistance, Inductance and back emf, in addition to these parameters on SRM Circuit, it has a base-emitter Junction or a diode. The equivalent circuit for MEM model for input parameters is shown in Figure 3-12.

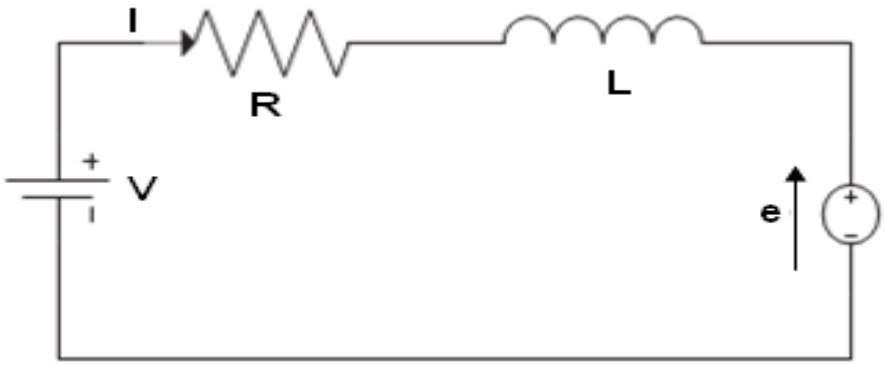

Figure 3-12: The equivalent Circuit for SRM.

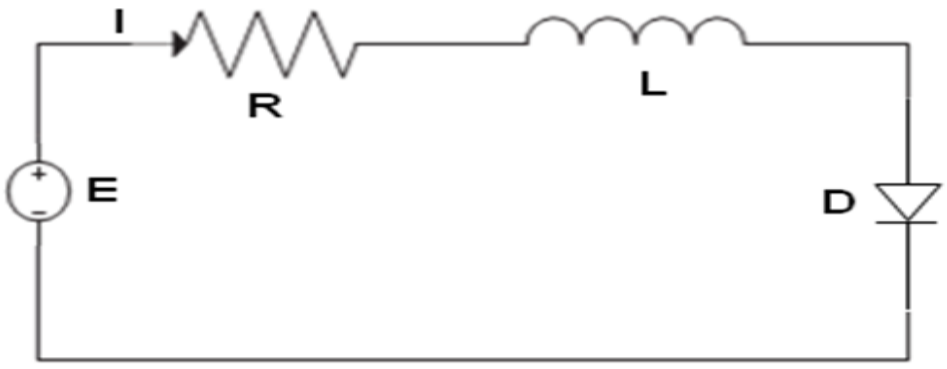

Figure 3-13: Monopole Energizer Machine Input Equivalent Circuit

In modelling of the MEM input parameters, the linear analytical model of the SRM can be described by three differential equations, which can be classified as the voltage equation or electromagnetic equations, the motional equation or torque production and the electromagnetic torque equation or electromagnetic torque

production (Gommans *et al.*, 2001). The derivation of differential equations is shown in Equation (3-29). From circuit in Figure 3-13, the model equation describing the Monopole Energizer Machine is derived as under ;

$$\mathbf{e(t) = I(t)R + L\emptyset\frac{dI}{dt} + V_D} \text{---------- (3-29)}$$

e(t) is the voltage source.

R is the Resistance.

L(∅) is the trigger coil inductance

V_D is the diode voltage drop

Back emf $e_b = I\omega\frac{dL}{d\emptyset}$, but in the case of MEM current I is very small and hence back emf is negligible. In model formulation of MEM it was assumed that the effects of magnetic saturation, fringing flux around the pole corners were ignored and further leakage flux and the mutual coupling of phases were not considered (Bassily *et al.*, 1995; Jazdzynski and Majchrowicz, 2013; Vujicic and Vukosavic, 2000)

3.9 Model Formulation for Output Parameters

In this section, model formulation for output parameters is undertaken**.**

3.9.1 Development of Circuit for Output Parameters of MEM

Boost converters are used in systems which involve power transmission from wind and solar power generators. They absorb energy and then inject this energy into batteries or other loads. In modelling of output parameters of MEM after Boost Converter, an equivalent circuit was developed as shown in the figure below. As outlined earlier, both MEM and BC have a commonality of stepping up DC voltage The BC methodology of stepping up voltage is based on magnification of input voltage. There is need establishment of principle of operation in the case of MEM so as to step up the voltage and current and related parameters (Sriphan *et al.*, 2018b)

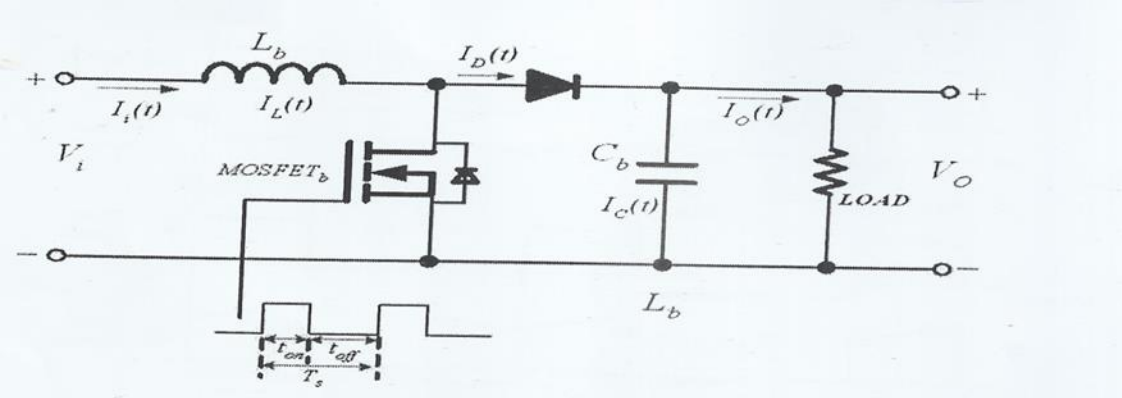

Figure 3-14: Representation of the Electrical Equivalent Circuit of the DC-DC Boost Converter.

It is against this background that MEM equivalent circuit was modelled after BC.BC has four components, inductor, diode, output capacitor and electronic switch Figure 3-14, is a representation of the circuit of the DC-DC Boost Converter. A converter switching cycle is necessary to achieve energy absorption followed by energy injection. When the switching frequency is constant, any alteration of the ON/ OFF duration is known as pulse width modulation switching. The converter is controlled by two steps , absorption and injection ,which is governed by the relative switching period According to (Fakhrurrazey *et al.*, 2014; Sriphan *et al.*, 2018a) the control of the converter operates in two separate modes namely, continuous conduction mode (here referred to mode 1) and discontinuous conduction mode (here referred to mode 2) The working of the two modes are discussed below:-

Mode1 which is the first mode begins when switch $\mathbf{S_1}$is switched on at time$t = t_{on}$as shown in Figure 3-15. During this mode current input rises and flows through switch $\mathbf{S_l}$ and inductor L. The energy during Mode 1 phase is stored in the inductor's magnetic flux. (Fakhrurrazey *et al.*, 2014; Sriphan *et al.*, 2018a).

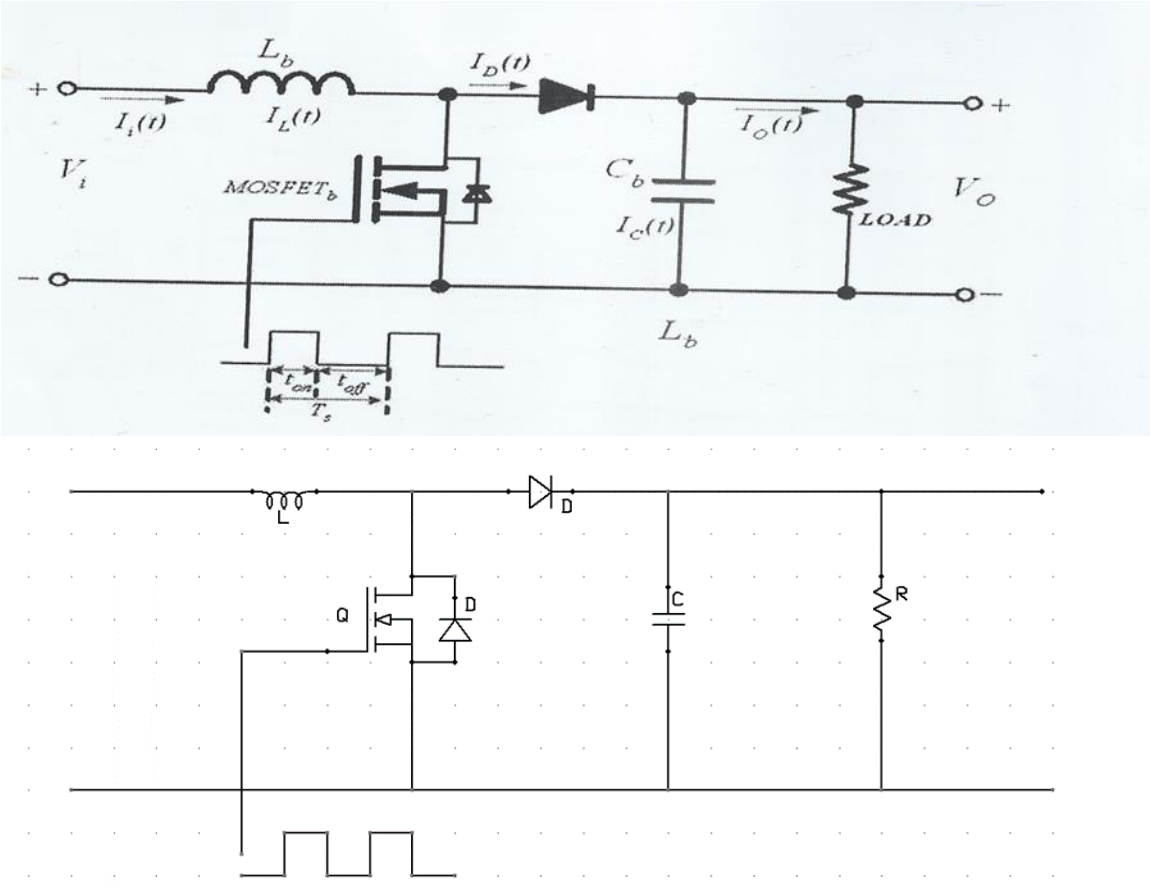

Figure 3-15: The Equivalent Circuit of The Boost Converter During Ton in Mode 1

Mode 2 commences when the switch S_1 is switched off at $t = t_{off}$. The input current instead of passing through S1 is diverted through L, D, C and Load as observed in Figure 3-16. The consequence of this is that the inductor current drops until the next cycle takes place and the switch S_1 is again switched on. The energy stored in the inductor is transferred to the load and hence the output voltage is greater than the input voltage. Figure 3-17 shows the waveform of the Boost Converter in a continuous conduction mode.

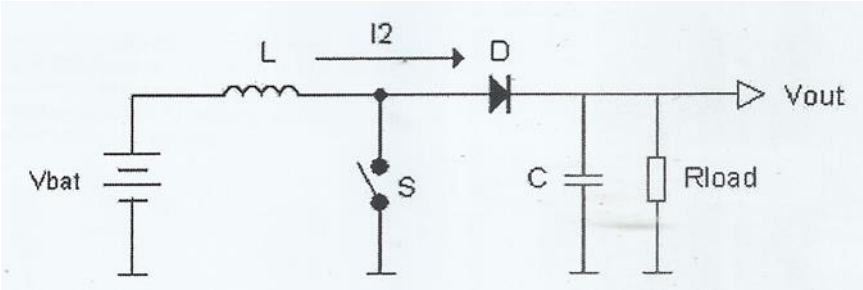

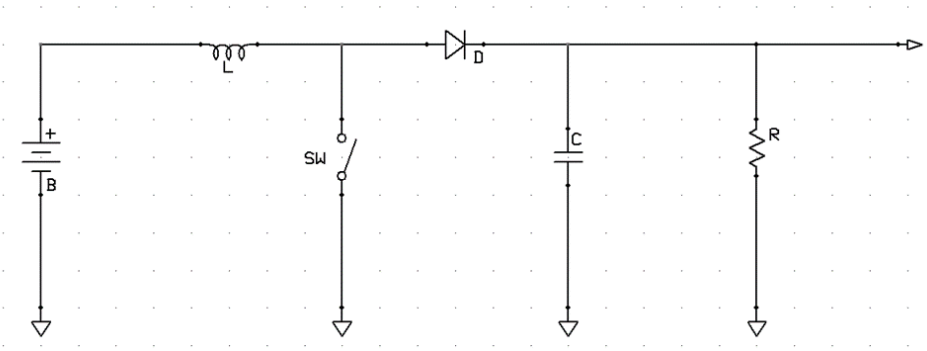

Figure 3-16: The Equivalent Circuit of The Boost Converter During Toff in Mode 2

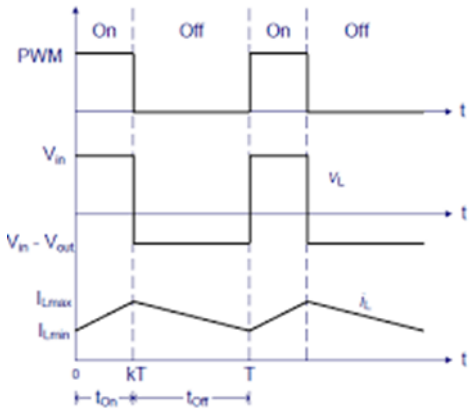

Figure 3-17: The Wave Forms of the Boost Converter in Continuous Conduction Mode

3.9.2 Development of Model Equations for Output Parameters

In deriving and developing the model equations for Boost Converter reference is made to the two functions of Boost Converter that is Mode 1

The voltage –current relation for the inductor L is:

$$\mathbf{i = \frac{1}{L}\int_o^t V.\,dt + i_o \text{ or } V = L\frac{di}{dt}} \text{---------- (3-30)}$$

Where L is the Inductor

V is the Voltage

I is the current

i_o is the initial current

For a constant rectangular pulse the current is given by:

$$\mathbf{i} = \frac{\mathbf{Vt}}{\mathbf{L}} + \mathbf{i_o} \text{ ---------- (3-31)}$$

As indicated above, the model equations in the case of Mode 1, that is considering a case of when switch S1 is ON. During this case the current flows continuously and hence the peak current equation is given by

For Equation for Continuous-Conduction Mode, taking

i_{pk} as the peak current

V_{in}as the input Voltage

$V_T$as Voltage through a transistor

T_{on} Implying that the switch s_1 is closed hence implying continuous conduction mode1

Therefore, the peak current (i_{pk}) through an inductor is given by

$$\boldsymbol{i_{pk} = \left[\frac{V_{in}-V_T}{L}\right] T_{on} + i_o} \text{ ---------- (3-32)}$$

$$\boldsymbol{i_{pk} - i_o = \left[\frac{V_{in}-V_T}{L}\right] T_{on}} \text{ ----------(3-33)}$$

This is a case of Mode I, whereby the transistor is on.

Taking $i_{pk} - i_o$ as net current through the inductor and symbolizing$i_{pk} - i_o$ withΔ_i, we have

$$\Delta_\mathbf{i} = \left[\frac{\mathbf{V_{in}-V_T}}{\mathbf{L}}\right] \mathbf{T_{on}} \text{ ---------- (3-34)}$$

Also indicated above is the model equations in the case of Mode 2 that is considering a case of when switch S_1 is switched OFF. During this case the current does not flow continuously and hence the initial current equation and in the circuit is given by Equation for Discontinuous Conduction mode and when the transistor is switched off

Taking (Fakhrurrazey *et al.*, 2014; Sriphan *et al.*, 2018a)

$$\mathbf{i_o} = \mathbf{i_{pk}} - \left(\frac{\mathbf{V_{out}-V_{in}+V_D}}{\mathbf{L}}\right) \mathbf{T_{off}} \text{ ---------- (3-35)}$$

Or

$$\mathbf{i_{pk} - i_o = \Delta_i = \left(\frac{V_{out} - V_{in} + V_D}{L}\right) T_{off}}$$ ---------- **(3-36)**

V_{out} as the output Voltage

V_D as the voltage drop across the diode (D_m)

During the discontinuous

Here

V_D is the voltage drop across the diode D_m

V_T is the voltage drop across the transistor S_1.

3.10 Solution to The Model Equations.

This section focused on developing solution to model equations. The solution to model equations is divided into two:- solution equation for input parameters and solution equation of output parameters. Both input and output solution equations are further divided into two: - Time function equation and time independent equations.

3.10.1 Time Function Solution for Input Parameters

Below are input –time function equations as modelled from SRM for MEM input parameters

Input Voltage

$$\boldsymbol{v_{in}(t) = i(t)R + L\phi\frac{di}{dt} + i\omega\frac{dL}{d\phi} + V_D}$$ ---------- **(3-37)**

Input current:-

$$\mathbf{v_{in}(t) - L\phi\frac{di}{dt} - V_D = i\left\{R + \omega\frac{dL}{d\phi}\right\} - V_D}$$ ---------- **(3-38)**

$$\mathbf{i\left\{(t)R + \omega\frac{dL}{d\phi}\right\} = v_{in}(t) - L\phi\frac{di}{dt} - V_D}$$ **……..…(3-39)**

$$\mathbf{i = \left[\frac{V_{in}(t) - L\phi\frac{di}{dt} - V_D}{\left\{R + \omega\frac{dL}{d\phi}\right\}}\right]}$$ ---------- **(3-40)**

Torque Equation

$$\mathbf{T_{total} - T_{load} = J_m\frac{d\omega_m}{dt} + B_m\omega_m}$$ ---------- **(3-41)**

Out of these input parameters equations both time function and time independent solution equations were developed as under; -

3.10.2 Time Independent Solution for Input Parameters

From the above equations time independent functions were developed as under

Input Voltage

$$v_{in} = i\omega \frac{dL}{d\phi} + V_D$$ ---------- **(3-42)**

Input current:-

$$v_{in} - V_D = i\left\{R + \omega \frac{dL}{d\phi}\right\}$$ ---------- **(3-43)**

Input current:-

$$v_{in} - V_D = i\left\{R + \omega \frac{dL}{d\phi}\right\}$$ ---------- **(3-44)**

$$i = \left[\frac{V_{in} - V_D}{\left\{R + \omega \frac{dL}{d\phi}\right\}}\right]$$ ---------- **(3-45)**

Torque Equation

$$T_{total} - T_{load} = B_m \omega_m$$ ------ ---------- **(3-46)**

3.10.3 Time Function Solution for Out Put Parameters

Recalling development on continuous conduction mode 1 and equation on discontinuous conduction mode 2 respectively.

We can solve for V_{out} by equating Δ_i components in continuous conduction mode (mode 1) and Δ_i in discontinuous 2conduction mode (mode2)

Hence

Taking $V_D - Diode\ drop$ and $V_T - Transistor\ drop$

$$\frac{T_{on}}{T} = \Delta \qquad \frac{T_{off}}{T} = 1 - \Delta \qquad \frac{T_{on}}{T_{on} + T_{off}} = \Delta$$ ---------- **(3-47)**

$$T = T_{on} + T_{off}$$ ---------- **(3-48)**

$$\left(\frac{V_{in} - V_T}{L}\right) T_{on} = \left(\frac{V_{out} - V_{in} + V_D}{L}\right) T_{off}$$ ----------**(3-49)**

$$(V_{in} - V_T) \times \Delta = (V_{out} + V_D)(1 - \Delta)$$ ----------(3-50)

$$V_{in}T_{on} - V_T T_{on} = V_{out}T_{off} - V_{in}T_{off} + V_D T_{off}$$ ----------(3-51)

$$V_{in}T_{on} + V_{in}T_{off} - V_T T_{on} = V_{out}T_{off} + V_D T_{off}$$ ----------(3-52)

$$V_{in}(T_{on} + T_{off}) - V_T T_{on} = V_{out}T_{off} + V_D T_{off}$$ ---------- (3-53)

$$V_{in} - V_T \frac{T_{on}}{T} = V_{out} \frac{T_{off}}{T} + V_D \frac{T_{off}}{T}$$ ---------- (3-54)

$$V_{in} - V_T \Delta = [V_{out} + V_D][I - \Delta]$$ ----------(3-55)

$$V_{out}(1 - \Delta) = V_{in} - V_T \Delta - V_D(1 - \Delta)$$ ---------- 3.55

$$V_{out}(1 - \Delta) = V_{in} - V_T - V_D(1 - \Delta)$$ ---------- (3-56)

$$V_{out} == \left(\frac{V_{in} - V_T \Delta}{(1 - \Delta)}\right) - V_D$$ ----------(3-57)

Hence representing duty cycle by K, we have

$$K = \Delta = 1 - \frac{V_{in}}{V_{out}}$$ ----------(3-58)

Therefore, output voltage is given us

$$v_{out}(t) = \frac{1}{1-k} v_{in(t)}$$ ----------(3-59)

3.10.4 Time Independent Solution for Output Parameters

$$v_{out} = \frac{1}{1-k} v_{in}$$ ---------- (3-59)

where the output voltage is shown byv_{out}, the duty cycle is k, and the input voltage is represented by v_{in} (Phurahong *et al.*, 2019; Sriphan *et al.*, 2018a)

The inductance value must be carefully calculated if the converter is to be operated in continuous conduction mode, since it is necessary for the conductor current i_L to flow constantly it must never be allowed to drop to zero.

$$L_{min} = \frac{R(1-k)^2 k}{2f}$$ ---------- (3-60)

Where

L_{min} represents the minimum inductance value,

k denotes the duty cycle,

output resistance is given by *R*, and

f denotes the switching frequency for the switch S_1.

The required output capacitance for any selected output voltage ripple can be calculated using the equation (Sriphan *et al.*, 2018a)

$$\boldsymbol{c_{min} = \frac{k}{RfV_r}} \text{----------} \textbf{(3-61)}$$

In which

c_{min} is used to indicate the minimum capacitance,

the duty cycle is shown by *k*,

R denotes the output resistance,

f is the switching frequency for switch S1,

an output voltage ripple factor is represented by V_r(12). $V_r$is thus given by the equation 3.65

$$\boldsymbol{V_r = \frac{\Delta V_{out}}{V_{out}}} \text{----------} \textbf{(3-62)}$$

So, it is clear that the output voltage is related directly to the duty cycle. The main challenge when designing a converter is the sort of inductor to be used. From above equations, it can be seen that the inductance is inversely proportional to the ripple current. So, to reduce the ripple, a larger inductor should be used. In the MEM, inductor current i_L is never allowed to flow continuously but manifests as impulses thus is nearly insignificant, moreover there is no output resistance in its design (Sriphan *et al.*, 2018a).

3.11 Model Validation And Sensitivity Analysis

The tools used for testing and validating predictive mathematical model were:-

3.11.1 Coefficient of Determination

This model is denoted by R^2, and is according to Şen (2008)

$$R^2 = \frac{\left(\sum_{i=1}^{N} \text{Exp}_i \ \text{Pred}_i\right)^2}{\sum_{i=1}^{N} \text{Exp}^2 \sum_{i=1}^{N} \text{Pred}^2} \quad \text{.....(3-63)}$$

Exp_i = Experimental value

$Pred_i$ = Predicted value of the model

N = Number of observations

In other words, R^2 indicates how well the regression model fits the data.

R^2 ranges from 0 to 1, with the value 0 indicating that the regression model does not explain any of the variability in the dependent variable and the value 1 indicating that the regression model explains all of the variability in the dependent variable R^2 can be interpreted as the percentage of the variance in the dependent variable that is explained by the independent variable(s). R^2 is a widely used measure of goodness of fit in regression analysis. It is easy to interpret and can be used to compare the fit of different regression models.

In summary**,** R^2 varies from 0 to 1; the closer the value is to 1, the better is the relationship between the experimental and predicted values.

3.11.2 Modelling Efficiency(EF)

Modelling efficiency (EF) is a performance metric that is commonly used to evaluate the accuracy of models that simulate or predict processes. The EF was first proposed by Lahsasni *et al.* (2004)and is a dimensionless statistic that ranges from -∞ to 1, with 1 indicating perfect model performance and values less than zero indicating poor performance. The EF takes into account both the bias and the variability of the simulated values relative to the observed values. A perfect model (EF = 1) has a simulated time series that is identical to the observed time series, both in terms of mean and variance. A model with an EF of zero has no predictive skill and is no better than a model that simply predicts the mean observed value for each time step. A negative EF indicates that the model performs worse than the mean observed value.

The modeling efficiency tool, according to Lahsasni *et al.* (2004) is given by the equation3.65 :-

$$EF = \frac{\sum_{i=1}^{N}\left(\mathrm{Exp}_i - \mathrm{Exp}_{i\,mean}\right)^2 - \sum_{i=1}^{N}\left(\mathrm{Pred}_i - \mathrm{Exp}_i\right)^2}{\sum_{i=1}^{N}\left(\mathrm{Exp}_i - \mathrm{Exp}_{i\,mean}\right)^2} \quad \text{.....(3-64)}$$

where,

$\boldsymbol{Exp}_i$ = Experimental value,

Expi mean = Experimental mean value

Predi = Predicted value,

N = Number of observations

EF varies from 0 to 1. The best fit comes when EF tends to 1.

Efficiency is a measure of how effectively a magnet motor is converting electrical energy into mechanical energy. A higher efficiency indicates that the motor is operating more efficiently, which can result in less energy loss and greater power output.

3.11.3 Root Mean Square Error (RMSE)

Root Mean Square Error (RMSE) is a commonly used metric for measuring the accuracy of a model's predictions. RMSE measures the difference between the predicted values and the actual observed values, with lower values indicating better model performance. (Allen, 2015).

The formula for RMSE is

$$\textbf{: } \boldsymbol{RMSE} = \sqrt{\left(\frac{\mathbf{1}}{\boldsymbol{N}}\left(\sum_{\mathbf{1}}^{\boldsymbol{N}}(\boldsymbol{Predi} - \boldsymbol{Expi})^2\right)\right)^{\mathbf{2}}} \quad ----------(3\text{-}65)$$

Where,

Exp_i = Experimental value,

$Pred_i$ = Predicted value of the model

N = Number of observations,

RMSE should tend to zero for a good fit between the experimental and predicted values. A lower RMSE indicates better model performance, while a higher RMSE suggests that the model's predictions are less accurate.

3.12 Methodology to Perform Steady State Analysis

In this analysis, MATLAB was employed in developing MEM equations and undertaking steady state analysis

3.13 Ethical Considerations

Proper procedure was followed to get information required. This research used information derived from two US patent numbers 5,794,601 and 6,545,444. The former expired and so can be referred to without the express permission of the inventor. The latter is still valid but the inventor has allowed it to be used for non-commercial purposes. In areas where we have quoted information, the source or author was indicated and acknowledged. References are available

CHAPTER FOUR:
ANALYSIS AND DISCUSSION OF RESULTS

4. Analysis and Discussion of Results

4.1 Introduction

This section focused on discussion and analysis of results obtained from experimental runs

4.2 Characteristics of Electrical Input and Output of Mem with Original Design Experiments

Under this section the Voltage electrical characteristics of MEM are presented. The subsequent sections below present the experimental results and the findings of the investigation.

4.2.1 Characteristics of Voltage Input and Output of MEM Experiments With Four, Six and Eight Ceramic Magnets

Figure 4-1 and Figure 4-2 shows the results of voltage profiles with time during charging of secondary battery and discharging of primary battery. The results showed that for four ceramic magnets, it took 460 minutes for the battery to be fully charged, the output voltage profile showed that the output voltage increased from 7.0 volts to 15 volts within seven hours and 40 minutes. The battery charged on average rate of 1.04 volts per hour. Equation 4.8, shows voltage output equation, the graph was found to be linear and point 0.01509 was found to be the gradient, point 7.0816 was the constant of the equation. The input voltage profile indicated that the input voltage discharged steadily from 13.50 volts to 13.29 volts in seven hours and forty minutes. The voltage was discharged at the rate of 0.025 volts per hour. Equation 4.1 shows voltage input equation. Point -0.0004 is the gradient, whereas 13.512 was the constant of the equation. Table 4-1 shows Voltage input equations for original experimental design at different levels of magnetic loadings. Equations 4.2 and 4.9 gives general equation for input voltage and output voltage at 6 magnetic loading level respectively.

It was further established that for six ceramic magnets the input voltage decreased steadily from 13.50 volts to 13.29 volts within seven hours and twenty-five minutes. The voltage was discharged at the rate of 0.028 volts per hour. Point -0.0005 is the gradient, whereas 13.509 is the constant of the equation for the six ceramic magnets

and t is the time interval in minutes. Figure 4.1shows output voltage versus time graphs at a magnetic loading of 4, 6 and 8 for ceramic design MEM.

Similarly, the results showed that at a ceramic magnetic loading of six, the output voltage profile showed that output voltage increased from 7 volts to 15volts within seven hours and 25 minutes. The voltage increased at rate of 1.08 volts per hour. Point 0.0171 is the gradient, and 6.7542 is the constant of the equation or x (t) intercept on vertical axis.

Table 4-1: Voltage Input Equations for Original Experimental Design

Item No.	**No of magnets the wheel**	**Voltage input equations**	
1	4	$V = -0.0006t + 13.527$	4.1
2	6	$V = -0.0005t + 13.509$	4.2
3	8	$V = -0.0004t + 13.526$	4.3
4	10	$V = -0.0008t + 13.5$	4.4
5	12	$V = -0.007t + 13.518$	4.5
6	14	$V = -0.0007t + 13.513$	4.6
7	16	$V = -0.0007t + 13.525$	.4.7

The above equations were generated by excel after inputting the data.

These equations guided the graphs of voltage input verses time across all levels of magnetic loadings. Table 4-2 below also shows the voltage output equations for original design Monopole Energizer Machines across all levels of magnetic loadings.. Similarly, these equations guided the output graph for the voltage a cross all levels of magnetic loading.

Table 4-2: Voltage Output Equations for Original Experimental Design

Item No.	No of ceramic magnets On the wheel	Voltage output equations	
1	4	$V = 10^{-6}t^2 + 0.01509t + 7.1067$	4.8
2	6	$V = 10^{-5}t^2 + 0.0275t + 6.7542$	4.9
3	8	$V = -5 \times 10^{-5}t^2 + 0.0407t + 6.5603$	4.10
4	10	$V = -0.0255t + 6.7172$	4.11
5	12	$V = -0.024t + 6.8952$	4.12
6	14	$V = -0.0264t + 5.8884$	4.13
7	16	$V = -0.0299t + 7.2437$	4.14

.

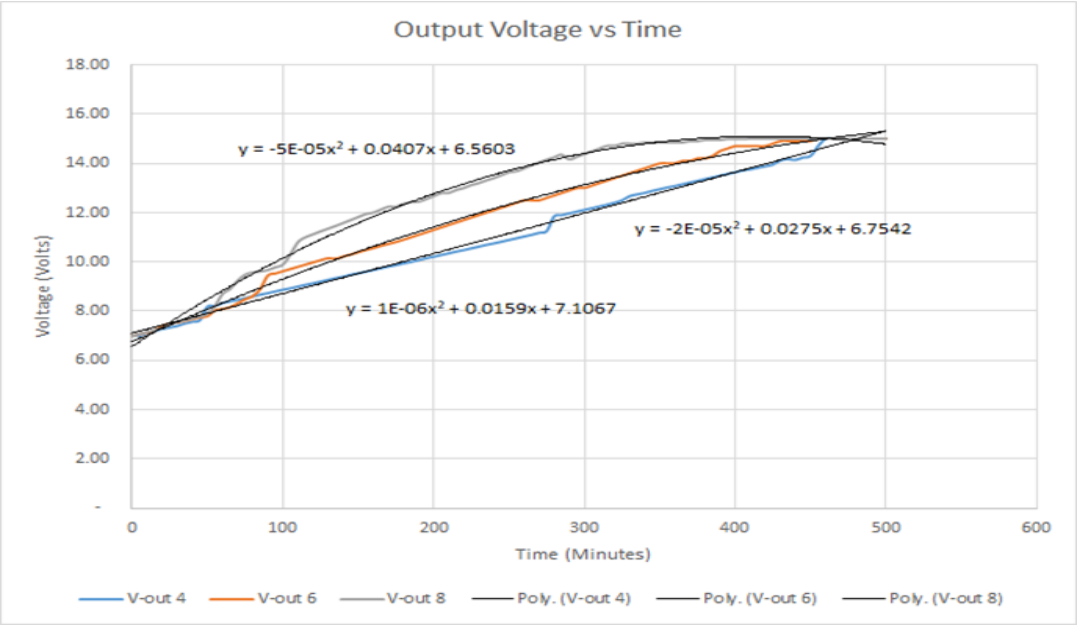

Figure 4-1: Output Voltage Versus Time Graphs For 4, 6 and 8 Ceramic Magnets.

The gradient will inform on electrical characteristics under consideration. Negative slope will indicate downward trend, whereas positive gradient will show upward trend. This trend will assist the designer of MEM. For eight ceramic magnets, it was deduced that output voltage increased from 7volts to 15 volts within six hours and 50 minutes. The voltage increased at rate of 1.18 volts per hour. Equation 4.10 shows voltage output characteristics at a magnetic loading of 8, whereas equation 4.3 shows voltage input characteristics at a magnetic loading of 8.

The profile for input voltage at a magnetic loading of 8 indicated that the input voltage discharged at the rate of 0.031 volts per hour. In this equation, point. -0.0004 was the gradient, whereas 13.526 is the constant of the equation. Figure 4-2 shows the graphical presentation for voltage versus time for input voltage at a magnetic loading of 4, 6 and 8 of original design MEM.

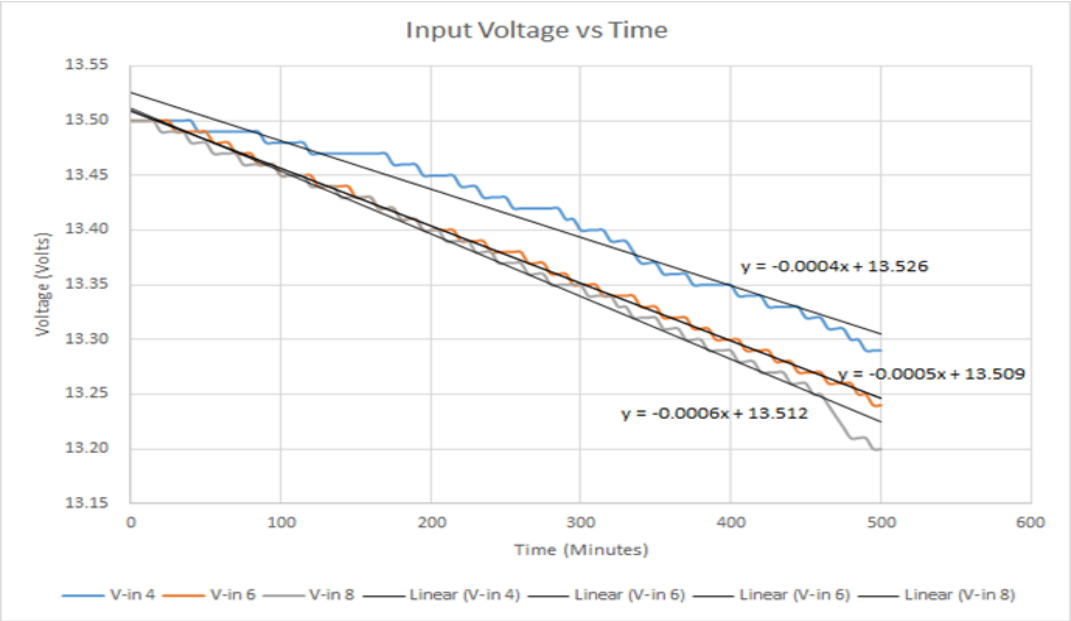

Figure 4-2: Input Voltage Versus Time Graphs for 4, 6 and 8 Ceramic Magnet.

At the magnetic loading of 4,6 and 8, it was deduced that the voltage output. Increased with magnetic loading whereas the voltage input decreased marginally. With the level of magnetic loadings. This behavior was consistent across the three levels of magnetic loadings for both input and output voltages

4.2.2 Performance Comparison of Ceramic Model Charging and Discharging Rates

Charging rate is taken as the rate at which the battery gains voltage with time during the charging process. Discharging rate is taken as the rate at which the battery drops in voltage with time during the discharging process. The charging rate and discharging rate vary with magnetic loading. Figure 4-3 shows the charging and discharging rate of original design. The results show that the charging rate was higher and faster than the discharging rate the results also showed that the charging rate increased fairly steeply with the increase of number of magnets

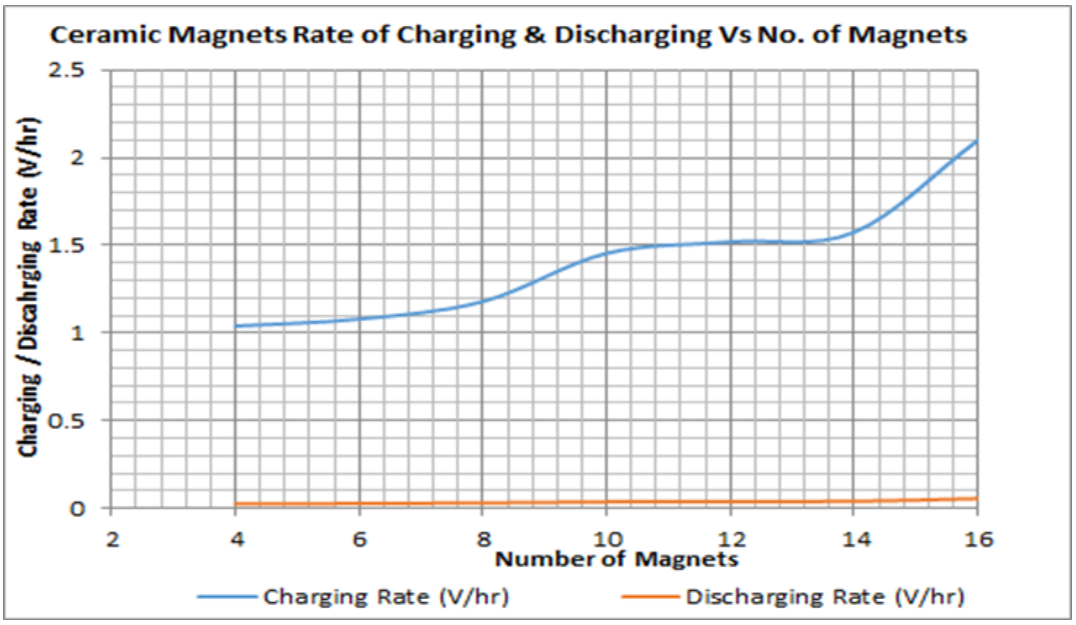

Figure 4-3: Comparison of Charging and Discharging Rate for Ceramic Magnets Monopole Energizer Model

4.2.3 Characteristic of Voltage Input and Output of MEM Original Design Experiments With Over 8 Magnets.

Furthermore, it was observed that the rate of charging increased with increase in magnetic loadings of original design. This was deduced by the rate at which a plateau curve was achieved. The time of achieving plateau curve was shortened as the number of magnetic loadings increased. Figure 4-4 below depicts the output voltage characteristic of Monopole Energizer Machine at a magnetic loading level of 10 and 12 respectively.

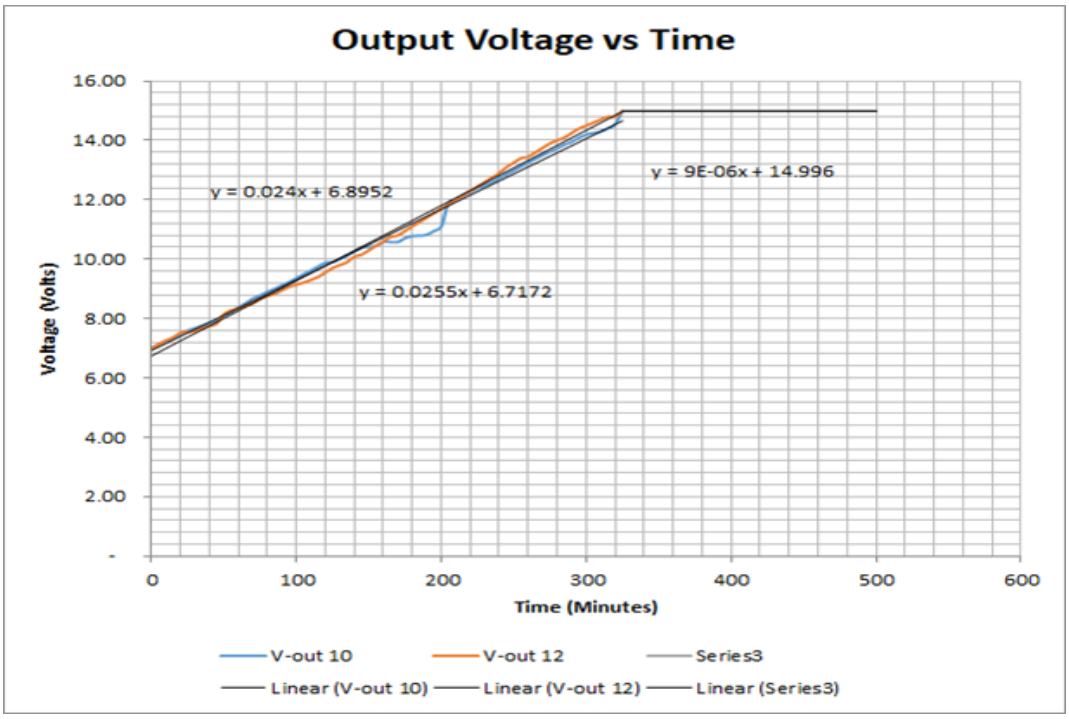

Figure 4-4: Instantaneous Voltage Output Versus Time Graph for 10 and 12 Ceramic Magnets.

In addition, analysis of results was done for voltage input behavior in relation to magnetic loading level of 10 and 12. It was further observed and deduced that the input voltage verses time graph had a negative gradient. Figure 4-4 shows graphical presentation of ceramic magnets of voltage input for 10 and 12 ceramic magnets experimental results. It was observed that the discharge rate of Monopole Energizer Machine showed marginal and irregular trend of decreasing with increase in Magnetic Loading level. The slope at a magnetic loading level of 10 was greater than that of at a magnetic loading level of 12. This implied that the voltage input continued to drop with the level of magnetic loading.

Equations 4,4 and 4.5 shows voltage input equations at magnetic loading of 10 and 12 respectively. On top of this equation 4,11 and 4.12 shows output equations at ceramic magnetic loadings of 10 and 12 respectively.

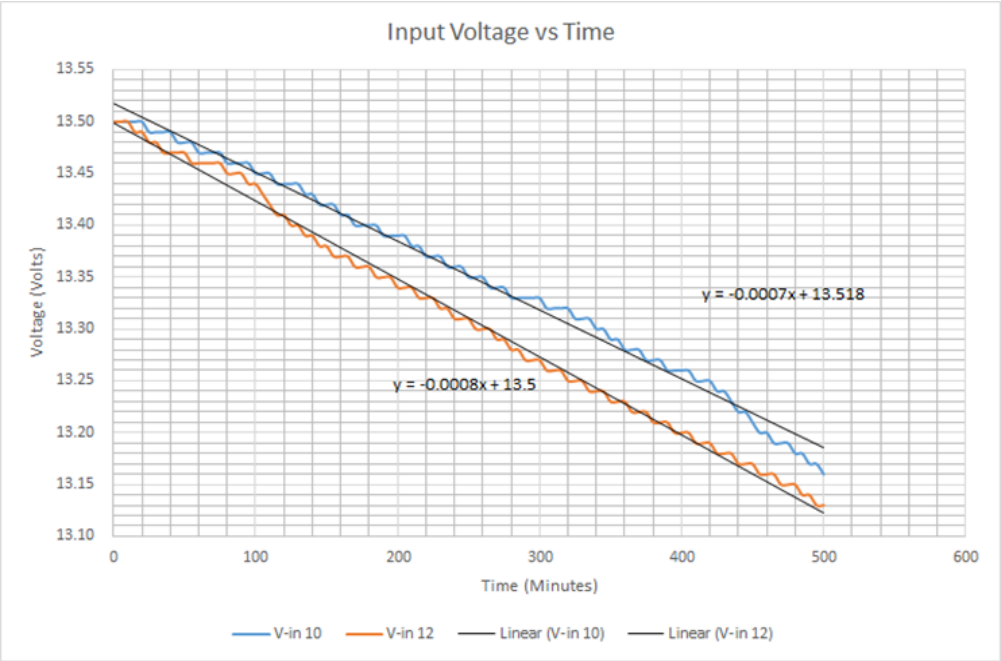

Figure 4-5: Instantaneous Voltage Input Versus Time Graph for 10 and 12 Ceramic Magnets.

It was further established that voltage output increased with time, and it was always greater than input. Figure 4-6 shows the instantaneous voltage output for 14 and 16 ceramic magnets whereas Figure 4-5 shows the instantaneous voltage input at a magnetic loading of 14 and 16 ceramic magnets.

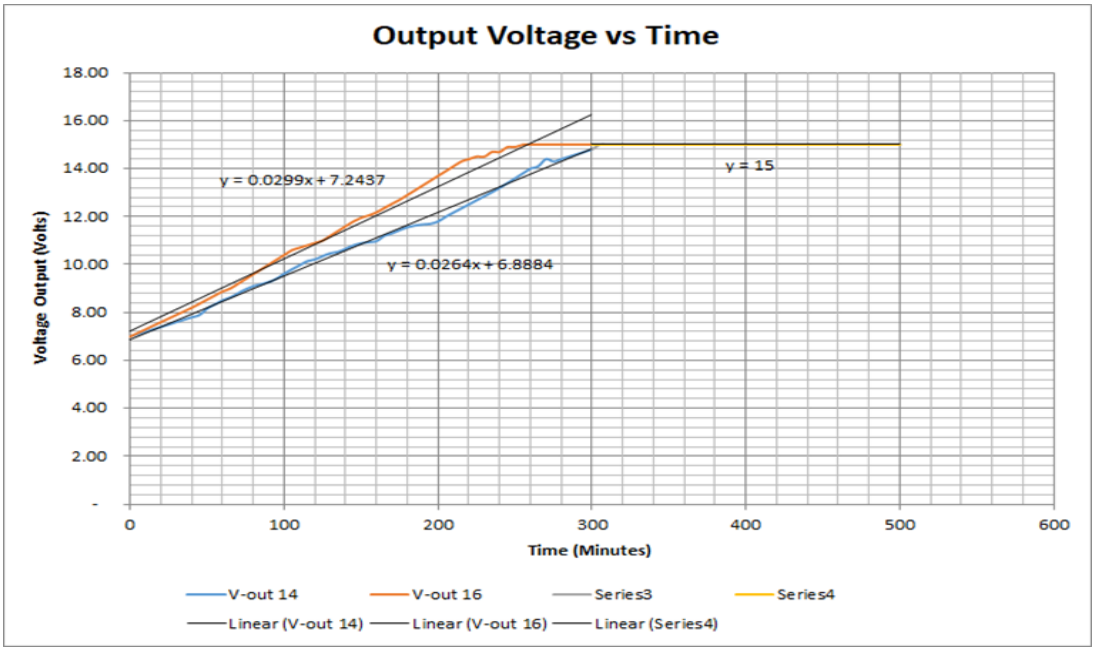

Figure 4-6: Instantaneous Voltage Output Versus Time Graph for 14 and 16 Ceramic Magnets.

Similar behavior was observed for both input and output voltage at a magnetic loading level of 14 and 16. In the case of output voltage the graph had a positive gradient and the time taken to reach a plateau phase was shorter than what was observed at the magnetic loading level of 10 and 12. Similar trend was observed for the case of input voltage. The input voltage continued reducing with the level of magnetic loading, its slope became less steep than the case of magnetic loading of 10 and 12. Figure 4-7 shows Instantaneous voltage input versus time graph for 14 and 16 ceramic magnets.

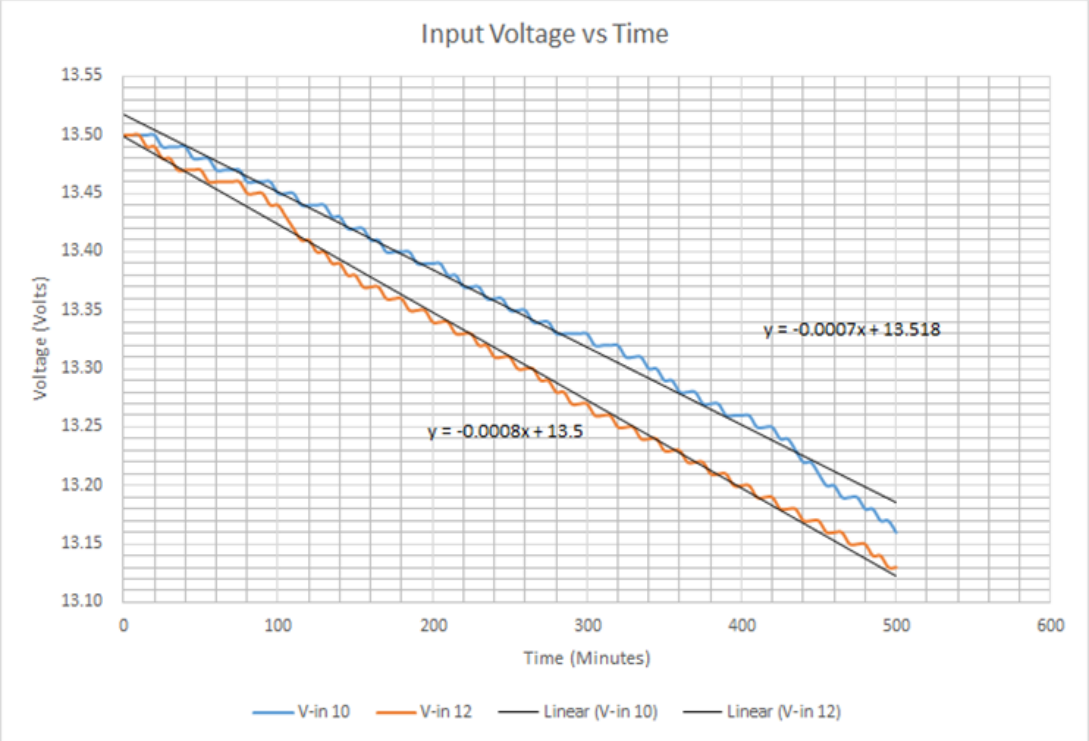

Figure 4-7: Instantaneous Voltage Input Versus Time Graph for 14 and 16 Ceramic Magnets.

At the magnetic loading of 10.12.14, and 16 it was further established that the voltage output increased with magnetic loading whereas the voltage input decreased marginally with the level of magnetic loadings. These behaviors were consistent across all the levels of magnetic loading under experimentation. Equations 4.6 and 4.7 shows the general equations for voltage input at magnetic loadings of 14 and 16. Besides that equation 4,13 and 4.14 shows the voltage output equations at magnetic loadings of 14 and 16 respectively.

4.3 Current Characteristics Of Monopole Energizer Model Experiments With Ceramic Magnets

In this section, the electrical behavior of Monopole Energizer Machine mounted with ceramic magnets is discussed. The following sections presents the analysis of the current characteristics.

4.3.1 Characteristic of Current of MEM Experiments with Four, Six and Eight Ceramic Magnets.

Figure 4-8 shows the current profile for 4, 6 and 8 ceramic magnets MEM. From the figures depicting the behavior of electrical characteristics of monopole energizer model It was observed, that the current output was higher than the current input. It was further established that the current fluctuations were too small for both input and load current values of the current.

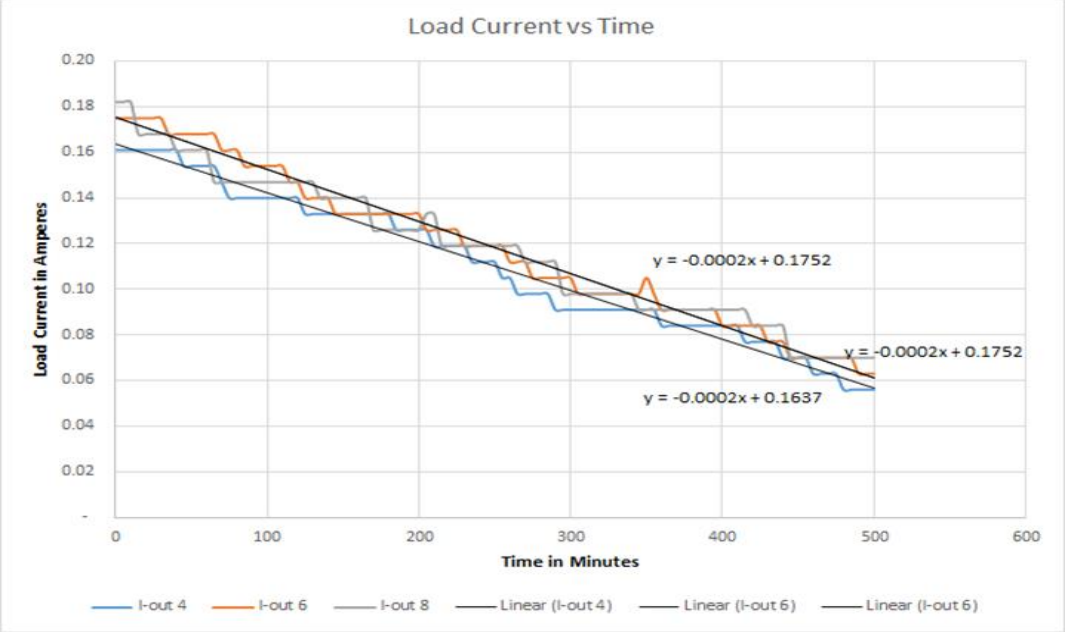

Figure 4-8: Load Current Versus Time Graphs For 4, 6 and 8 Ceramic Magnets.

Table 4-3 shows the equations governing the generation graphs for input current profiles.

Table 4-3: Input Current Equations for Original Design

Item No.	No of magnets)	Current input equations	
1	4	$I = -10^{-7}t^2 - 3 \times 10^{-5}t + 0.1091$	4.15
2	6	$I = -10^{-7}X^2 - 3 \times 10^{-5} + 0.1139.$	4.16
3	8	$I = -6 \times 10^{-8}t^2 - 7 \times 10^{-5}t + 0.1186 - -$ $-$	4.17
4	10	$I = -8 \times 10^{-5}t^2 + 0.1081.$	4.18
5	12	$I = -8 \times 10^{-5}t + 0.1102$	4.19
6	14	$I = -8 \times 10^{-5}t + 0.1074$	4..20
7	16	$I = -7 \times 10^{-5}t - 0.1086t.$	4.21

In undertaking current profile analysis, it was established that current profile for four ceramic magnets showed that the output current decreased at the rate of 0.0128 amps within seven hour and forty minutes. Equation 4.22 shows load current characteristics at magnetic loading of 4. The load current reduced at the rate of 0.0128 amps per hour. The profile for input current showed that the input current decreased from 0.11 amps to 0.068 amps within 7 hours and 40 minutes. The current decreased at the rate of 0.0055 amps per hour. Equation 4.15 shows the general equation for input current Table 4-4 shows profile equations governing the load current behaviors at different levels of magnetic loadings.

Table 4-4: Load Current Equations for Original Design

Item No.	No of ceramic magnets On the wheel	Load Current equations
1	4	$I = -0.0002t + 0.1637.$ 4.22
2	6	$I = -0.0002t + 0.1752 - - - -$ $- -$ 4.23
3	8	$I = -0.0002t + 0.1752$ 4.24
4	10	$Y = I = -0.0002t + 0.1751$----------4.25
5	12	$I = -0.0002t + 0.1871$ 4.26
6	14	$I = 0.0002t + 0.1871$ 4.27
7	16	$I - 0.0002t + 0.1909$ 4.28

On top of the above results, it was noted that during 445 minutes experimental runs using six ceramic magnets, it was observed that output current decreased from 0.175amps to 0.070 Amps. The general equation for the load current behavior is as shown by equation 4.23. The load current decreased at the rate of 0.0142 amps per hour. For the case of six ceramic magnets monopole energizer, it was further deduced that the input current decreased from 0.116 Amps to 0.076Amps within 7 hours and 25 minutes. The input current as depicted by equation 4,16 at magnetic loading of 6, showed a decrease at the rate of 0.0054 AS^{-1} per hour. Figure 4.8 shows Load Current versus Time graphs for 4, 6 and 8 ceramic magnets. It was also observed that for eight ceramic magnets the output current decreased from 0.189 Amps to 0.091 Amps within 410 minutes. Equation 4.24 shows the general load current equation at magnetic loading of 8. It was further deduced that the load current reduced at the rate of 0.014 amperes per hour. Similarly, equation 4.17 shows the input electrical current characteristic behavior at magnetic loading of 8. Similarly, it was also indicated that the input current decreased from 0.0.119Amps to 0.0.078 Amps within 410 minutes. The current decreased at the rate of 0.0097

Amps per hour. Figure 4-9 shows the current behavior of 4,6 and 8 for original design using 4,6 and 8 ceramic magnets.

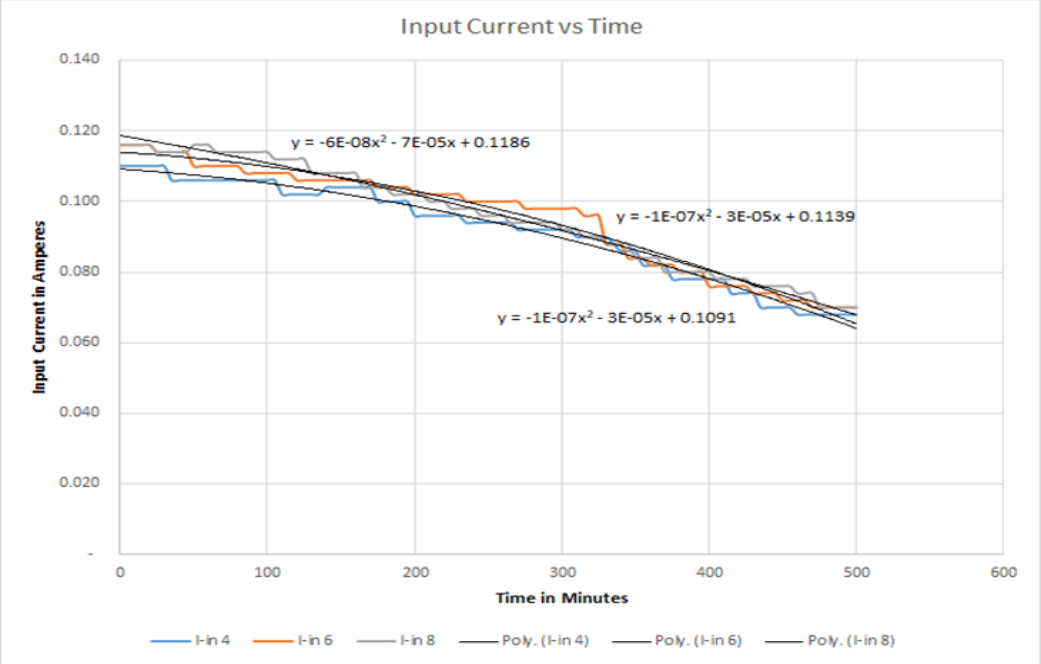

Figure 4-9: Input Current Versus Time Graphs For 4, 6 and 8 Ceramic Magnets.

Moreover, analysis showed that both load and input current profile had a negative slope a cross the three levels of magnetic loading that is level 4,6 and 8. It was further deduced that both load and input current marginally increased with magnetic loading. It was further observed that both input and load current profiles had a negative slope. The magnitude of the slope increased with magnetic loading. Table 4-5 represents the input and load current reduction rate during the process of charging the battery by MEM.

Table 4-5: Input and Load Current Reduction Rates Per Hour

Item No.	Number of Ceramic magnets on the wheel	Input current reduction rate per hour in amperes	Output current Reduction rate per hour in amperes
1	4	0.0055	0.0128
2	6	0.0054	0.0142
3	8	0.0097	0.014
4	10	0.0075	0.013
5	12	0.0086	0.015
6	140	0.091	0.014
7	16	0.096	0.016

4.3.2 Characteristic of Current Input And Output of Monopole Energizer Model Experiments With More Than 8 Magnetic Loadings of Original Design

Figure 4-10 shows the load current behavior for ten and twelve Ceramic Magnets original design MEM. The graph showed that the trend of increasing magnitude of negative slope continued increasing with the level of magnetic loading. This observation is in consistent with what was observed for magnetic loading of 4,6 and 8 where the load current marginally increased with magnetic loading but maintained a negative slope.

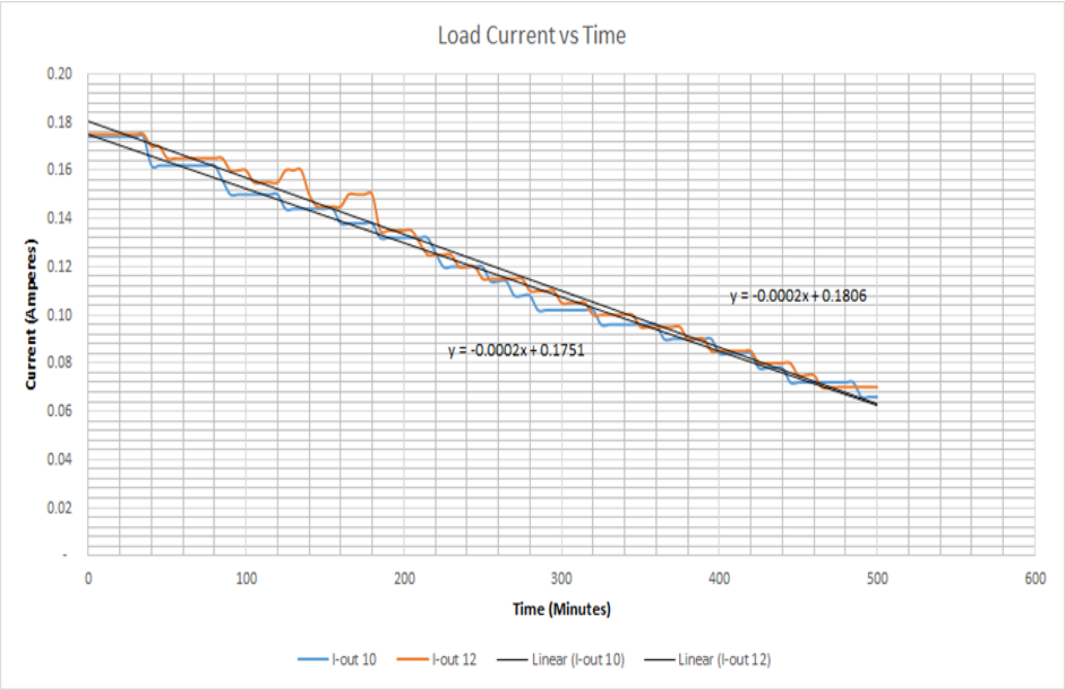

Figure 4-10: Instantaneous Load Current Versus Time Graph for 10 and 12 Ceramic Magnets Experiments.

Figure 4-11 likewise shows the input current behavior for ten and twelve Ceramic Magnets original design of Monopole Energizer Machine. From the figures it was established that the current output for 10 ceramic model decreased from 0.17amps to 0.10 amps in 330 minutes. It was also observed that at the magnetic loading of 10 and 12 the negative slope for load current was marginally greater than that of input current at the same level of magnetic loading.

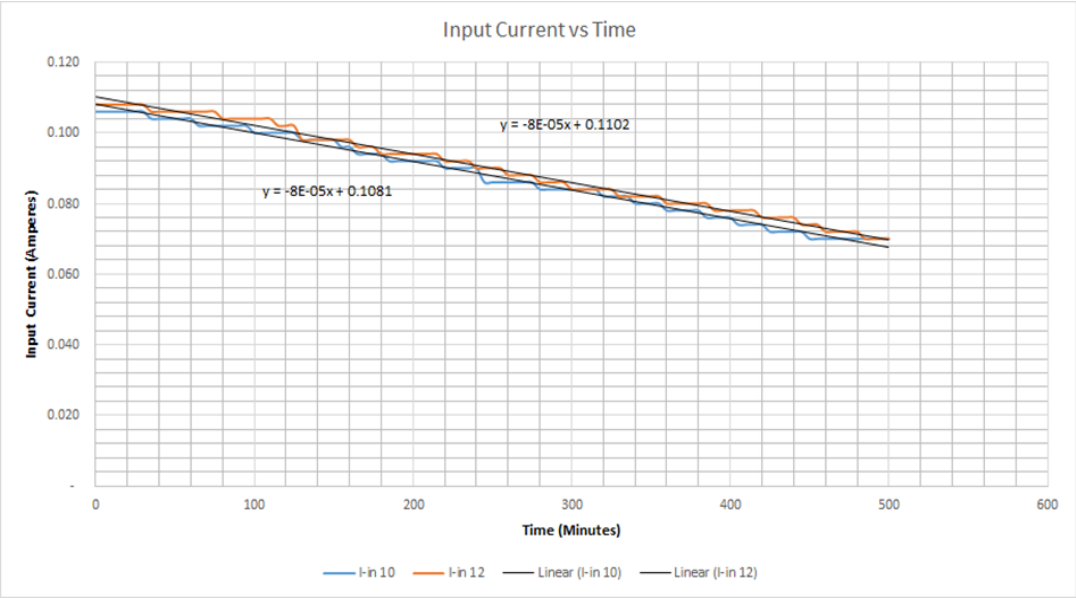

Figure 4-11: Instantaneous Input Current Versus Time Graph for 10 and 12 Ceramic Magnets Experiments.

Notably both load and input current increased with magnetic loading even though both profiles maintained a negative slope. Input current rate of reduction ranged between 0.0055 amperes for four magnetic loadings to 0.096 for 16 magnetic loadings. The rate of reduction in amperes for loading current ranged from 0.0128 amperes at magnetic loading of 4 to 0.016amperes at a magnetic loading of 16. These behavior of current input and output with the level of magnetic loadings on Monopole Energizer Machine is depicted by Figure 4-12

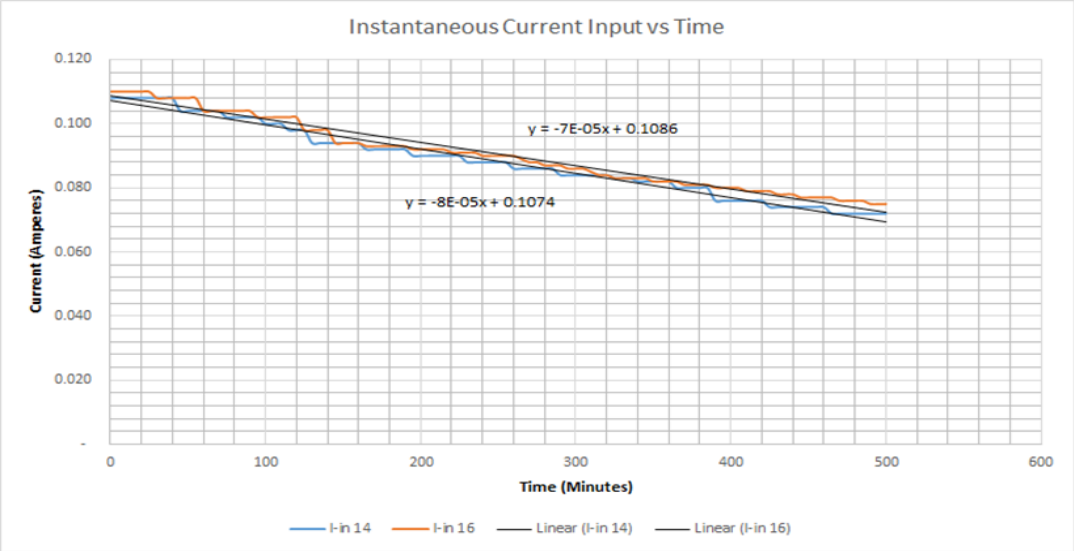

Figure 4-12:Instantaneous Input Current Versus Time Graph for 14 and 16 Ceramic Magnets Energizer Model.

In addition, the results showed that both load and input current profile had a negative slope a cross all levels of magnetic loadings. Both load current and input current increased marginally with magnetic loadings a cross all levels even though the increase in load current was marginally greater than that of input current across all levels of magnetic loadings. Moreover, it was noted that the negative slope magnitude increased with magnetic loading, but it was marginally more for the load current than input current across all magnetic loading levels.

4.4 Characteristics Of Electrical Power Of Mem With Ceramic Magnets

In this section, the electrical current behavior of Monopole Energizer Machine mounted with ceramic magnets is discussed. The power quantity was derived from current and voltage characteristics.

4.4.1 Characteristic of Power Input and Output Of Monopole Energizer Experiments With Four, Six And Eight Magnets

Table 4-6 shows the power input profile equations that were used to generate respective graphs. It was generally observed that the input power profile graphs were characterized by negative slope hence negative gradient. This implied that the power input decreased with the level of magnetic loading.

Table 4-6: Power Input Equations

Item No.	No of ceramic magnets On the wheel	Power input equations	
1	4	$P = -2 \times 10^{-6}t^2 + 0.0004t + 14745$	4.29
2	6	$P = -2 \times 10^{-6}t^2 - 0.005t + 1.5398\ldots$	4.30
3	8	$P = -8 \times 10^{-6}t^2 + 0.001t + 1.6018$	4.31
4	10	$P = -8 \times 10^{-6}t^2 + 0.033t + 1.2213$	4.32.
5	12	$P = -7 \times 10^{-6} + 0.0028t + 1.2167$	4.33
6	14	$P = -0.0011t + 1.4654 \ldots\ldots\ldots\ldots\ldots\ldots$	4.34
7	16	$P = -0.0011t + 1.4847 \ldots\ldots\ldots\ldots\ldots\ldots\ldots$	4.35 ...

At a magnetic loading of 4, it was established that, within 460 minutes the power output increased from 0.95 to 1.13. The rate of power increase was found to be 0.023 watts per hour. The results also indicated that the power input decreased from 1.49 Watts to 0.9 watts. The rate of power decrease was found to be 0.077 watts per hour. The temperature remained fairly constant at 25^{o}C during the experimental runs. Table 4-7 shows the power output profile equations that were used to generate respective graphs. Hence output power profile graphs were characterized by upward trajectory. This implied that power output increased with magnetic loading, up to the limit where it assumed the bell curve shape.

Table 4-7: Power Output Equations

Item No.	**No of ceramic magnets On the wheel**	**Power output equations**	
1	4	$P = -3 \times 10^{-6}t^2 + 0.001t + 1.1724$	…4.36.
2	6	$P = -5 \times 10^{-6}t^2 + 0.002t + 1.2505$	4.37
3	8	$P = -8 \times 10^{-6}t^2 + 0.0035t + 1.2106$	4.38
4	10	$P = -7 \times 10^{-6}t^2 + 0.0028t + 1.2167$	4.39
5	12	$P = -8 \times 10^{-6}t^2 + 0.033t + 1.2213$	4.40
6	14	$P = -9 \times 10^{-6}t^2 + 0.0041t + 1.2618$	4.41
7	16	$P = -10^{-5}t^2 + 0.0049t + 1.3531$	4.42

Furthermore, it was established that at a magnetic loading of 6 the power output increased at the rate of 0.342 watts per hour. It was likewise deduced that within 445 minutes power input decreased from 1.57 watts to 1 watt. The power input reduced at the rate 0.077 watts per hour. Figure 4-13 shows the Instantaneous Power output versus Time graphs for 4, 6 and 8 ceramic magnets.

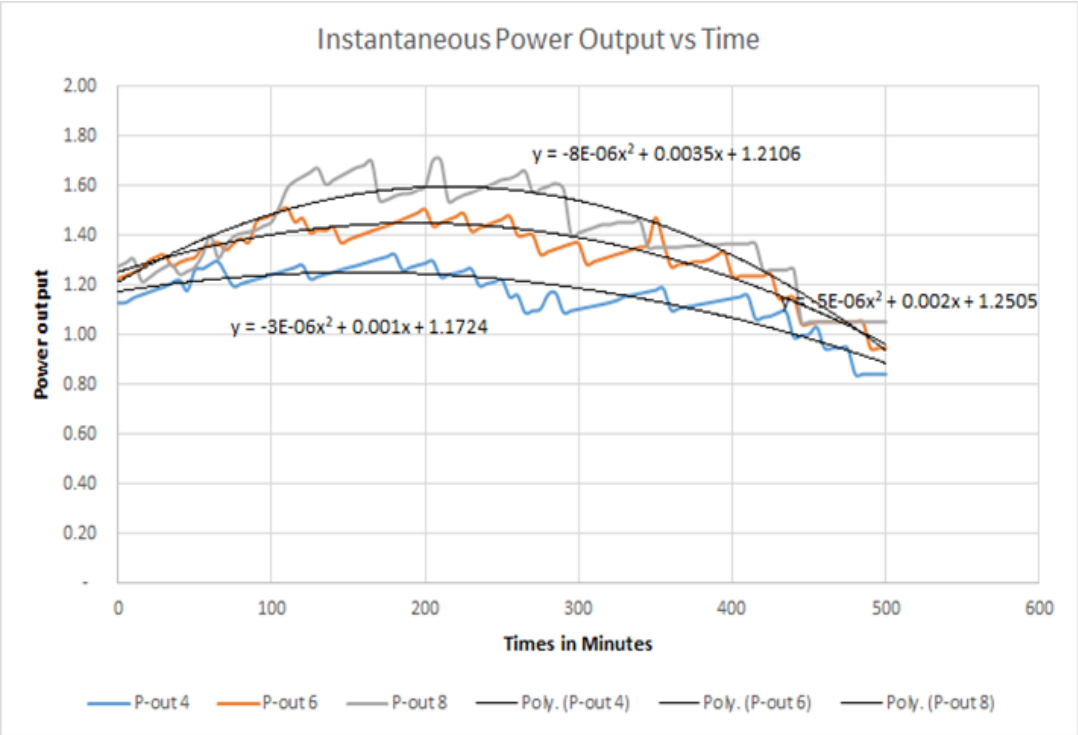

Figure 4-13: Instantaneous Power Output Versus Time Graphs for 4, 6 and 8 Ceramic Magnets.

For eight ceramic magnets, the power output increased from 1.32Watts to1.37 Watts within 410 minutes. The power output increased at the rate of 0.0074 Watts per hour. Likewise, the power input decreased from 1.57 Watts to 1.06 Watts within 410 minutes. The power input decreased at the rate of 0.0544 watts per hour. Furthermore, it was established that at a magnetic loading of 4, 6 and 8 , the general equations for input power were equations 4.29,4.30 and 4.31 respectively as indicated in table 4.6..Likewise the general equation for power output as shown in table 4.7 were s 4.36,4.37 and 4.38 at the magnetic loadings of 4, 6 and 8 respectively.

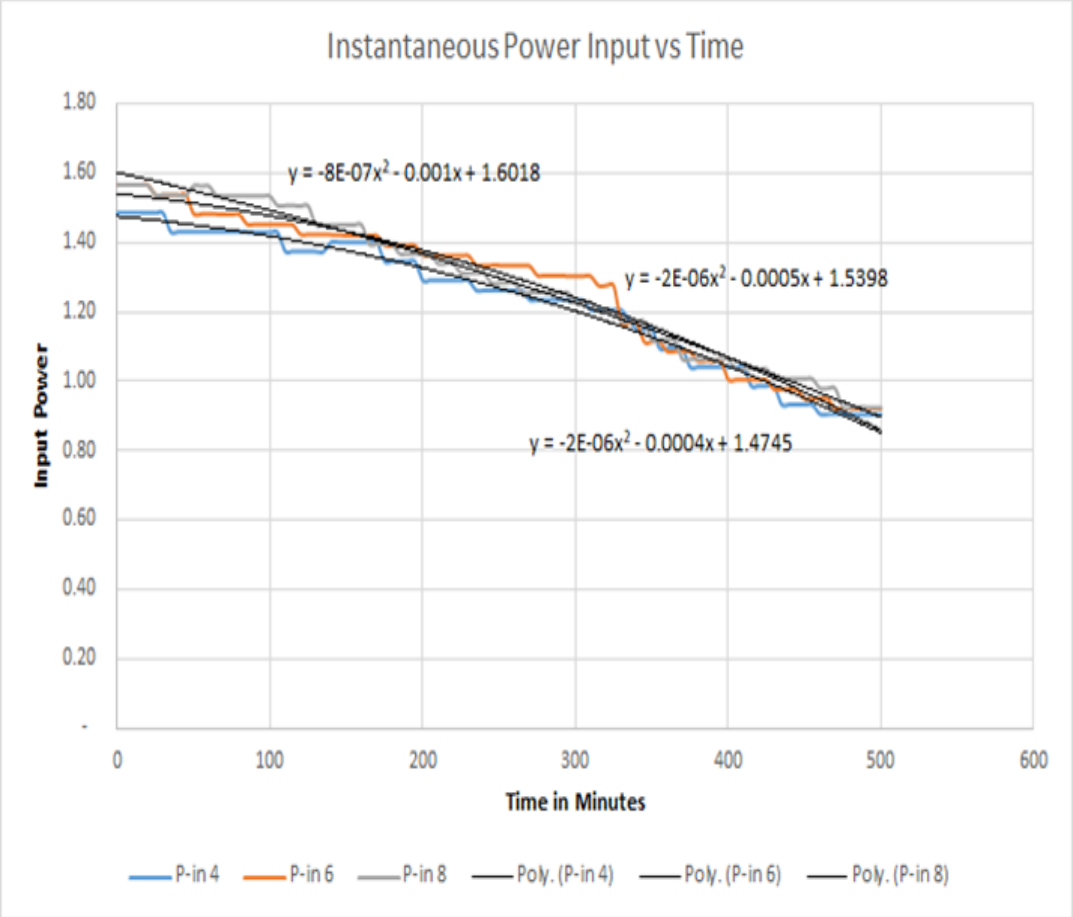

Figure 4-14: Instantaneous Power Input Versus Time Graphs for 4, 6 and 8 Ceramic Magnets

In addition, more analysis was undertaken on the behavior of input power reduction rate and output power increase rate, at different levels of ceramic magnetic loadings.

Table 4-8 below shows input power reduction rate and output power increase rate per hour

Table 4-8: Input Power Reduction Rate and Output Power Increase Rate Per Hour

Item No.	Number of Neodymium magnets on the wheel	Input Power reduction rate per hour in watts	Output Power Increase rate per hour in watts
1	4	0.077	0.023

2	6	0.077	0.342
3	8	0.0544	0.074
4	10	0.0673	0.04
5	12	0.0705	0.095
6	14	0.067	0.069
7	16	0.085	0.168

Besides this, analysis for power output and power input showed that across the three levels of magnetic loadings, the magnitude of the input and output power profiles increased with magnetic loading, even though power output maintained a positive slope whereas the input power graphs maintained a negative slope. This implies that the power output increased with magnetic loadings across the three levels of magnetic loading, this was vice versa in the case of power input profiles. This implication was due to reduced effect of Lenz law with magnetic loading.

4.4.2 Characteristic of Power Input and Output of Monopole Energizer Model with Over Eight Ceramic Magnets

Figure 4.15 shows instantaneous power output versus time graph for 10 and 12 ceramic magnets Monopole energizer model. From Figure 4.15 the power output increased at the rate of 0.04 and 0.095 watts per hour for 10 and 12 magnetic loadings respectively

The analysis showed that for ten and twelve magnetic loadings, it was observed that input power reduced at the rate of 0.0673 and 0.0705 per hour for magnetic loadings of 10 and 12 respectively

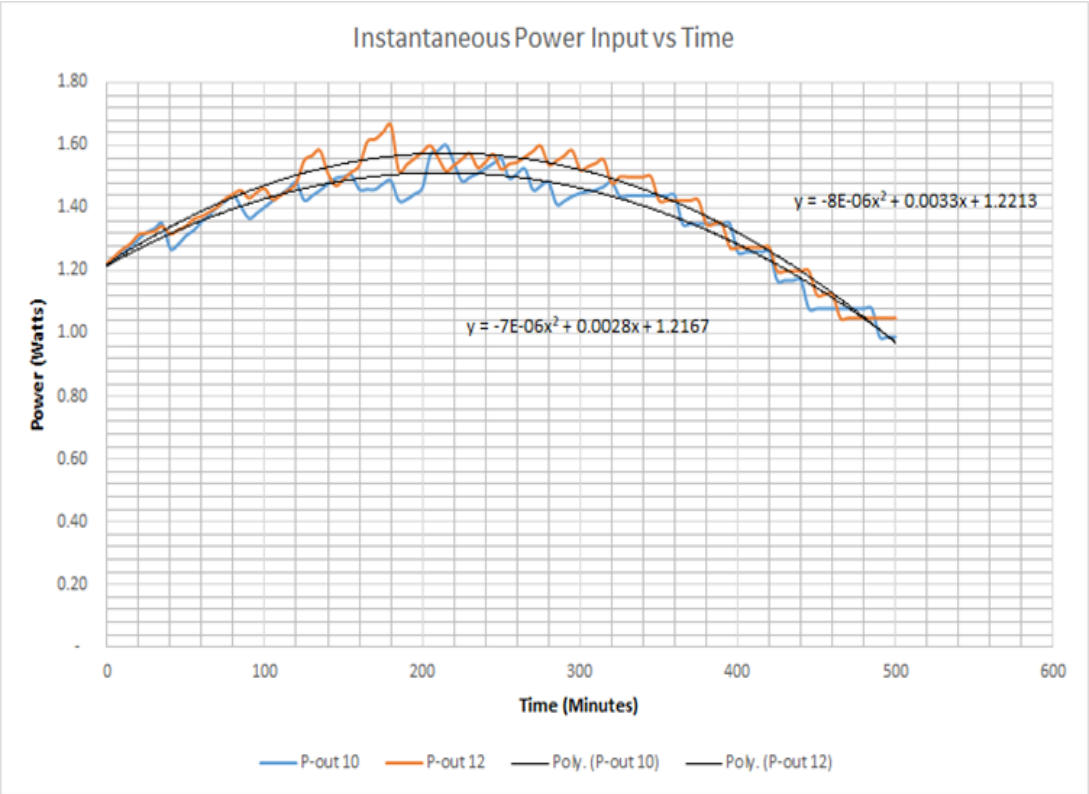

Figure 4-15: Instantaneous Power Output Versus Time Graph for 10 and 12 Ceramic Magnets Monopole Energizer Model.

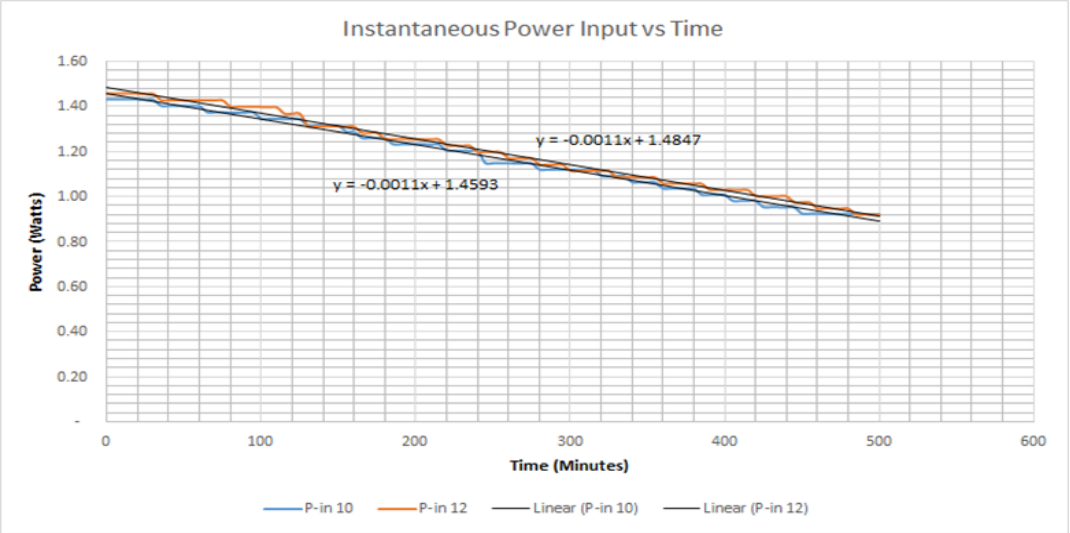

Figure 4-16: Instantaneous Power Input Versus Time Graph for 10 and 12 Ceramic Magnets Monopole Energizer Model.

Notably output power increased at the rate of 0.069 watts per hour and 0.168 watts per hour for 14 and 16 magnetic loadings respectively. Figure 4-17 shows power

output behavior for 14 and 16 magnetic loading. The power curves took a bell shape formation

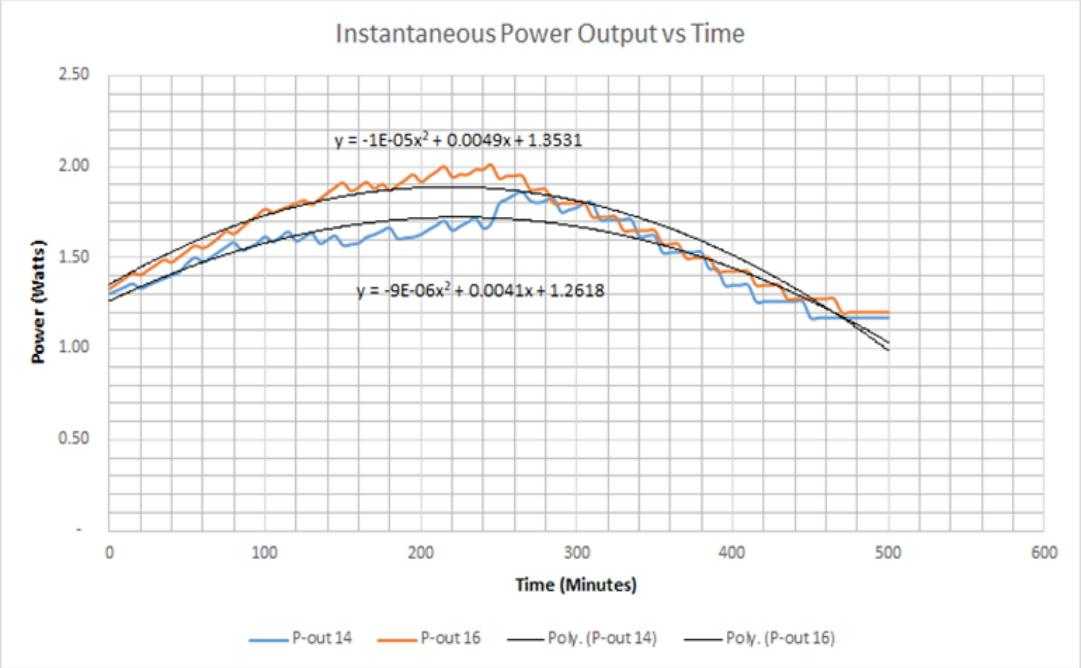

Figure 4-17: Instantaneous Power Output Versus Time Graph For 14 and 16 Ceramic Magnets Energizer Model.

Figure 4-18 shows power input behavior for 14 and 16 magnetic loading. The input power profile showed a negative slope. The power input continued decreasing with increase in magnetic loading.

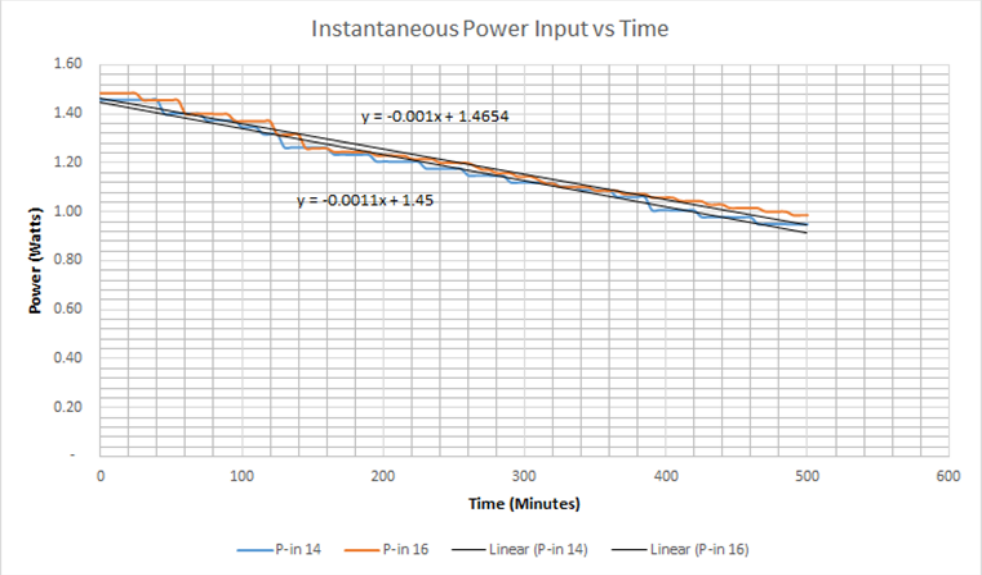

Figure 4-18: Instantaneous Power Input Versus Time Graph for 14 and 16 Ceramic Magnets Energizer Model.

The analysis for power output and power input showed that across the three levels of magnetic loadings, the magnitude of the input and output power profiles increased with magnetic loading, even though power output maintained a positive slope whereas the input power graphs maintained a negative slope. This implies that the power output increased with magnetic loadings across the three levels of magnetic loading, this was vice versa in the case of power input profiles.

4.5 Comparison of Input and Output Paramaters for Original Design

It was generally established that the output voltages were higher than input voltages. The rate of voltage output increased with magnetic loadings across the board. The output voltage graph was linear and had a positive gradient. The observation made from the graph, which was drawn from the experimental data showed that the voltage output curves were linear from the onset of the experimental run and after sometimes they attained a flat curve. The rate of attaining flat curve increased with magnetic loading.

4.5.1 Voltage Comparison Characteristics

Figure 4-19 shows Comparison of input voltage and output voltage for 4, 6 and 8 ceramic magnets of monopole energizer model.

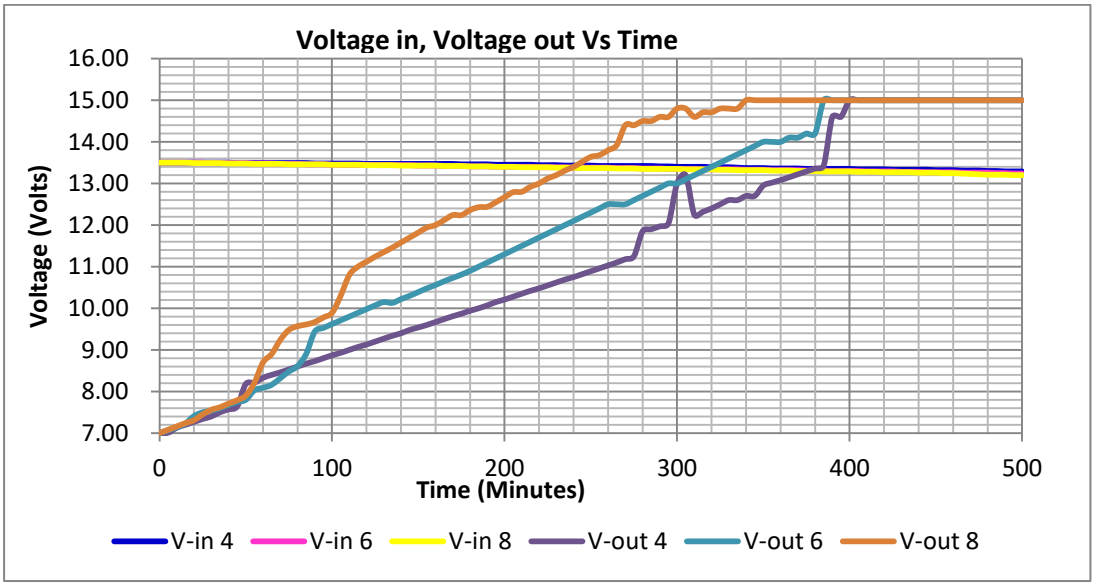

Figure 4-19: Comparison of input voltage and output voltage verses time for 4, 6 and 8 ceramic magnets of monopole energizer model.

The general steepness of the slope for voltage output increased with magnetic loadings. It was generally observed that as the output voltage rate increased with magnetic loadings, the input voltage decreased marginally with magnetic loading.Figure 4-20 shows comparison of input voltage and output voltage for 10 and 12 ceramic magnets of monopole energizer model.

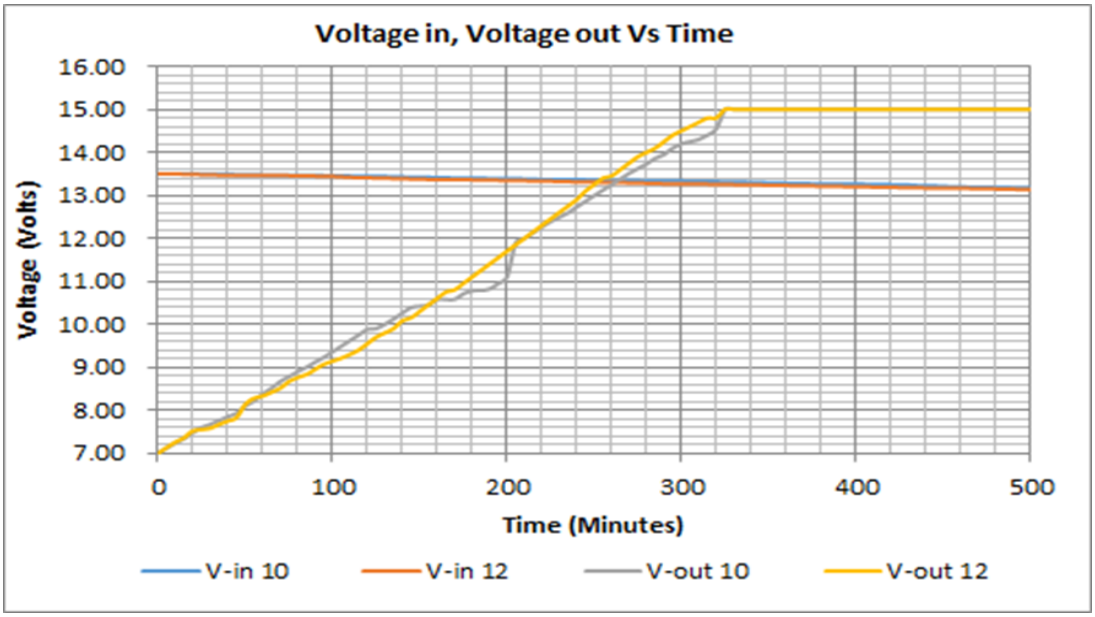

Figure 4-20: Comparison of Input Voltage and Output Voltage for 10 and 12 Ceramic Magnets of Monopole Energizer Model.

Taking a case at hand for original MEM magnetic loading at the flat level or plateau level was attained after 400 minutes, while in the case of 6 monopole energizer ceramic model it took 380 minutes to attain a plateau level, similarly in the case of eight ceramic magnet monopole energizer model it took about 340 minutes to flatten. This behavior was consistent even at a higher level of magnetic loading.

Similar trend was observed whereby the voltage output took an upward trajectory as Magnetic loading increased. The input voltage reduced marginally also with increased Magnetic loading. In the case of 16 ceramic magnets Monopole Energizer Model, it took 260 minutes only to flatten Figure 4-21 gives a voltage profile in relation to different loadings of ceramic magnets on Monopole Energizer Models.In the case of

input voltage, the voltage figures remained fairly constant. The voltage figures were about 13.5 regardless of the loading of ceramic magnets on monopole energizer model. It was further observed that the output- input ratio for voltage profiles were greater than one. Figure 4-21 shows the Comparison of input voltage and output voltage for 14 and 16 ceramic magnets of monopole energizer model.

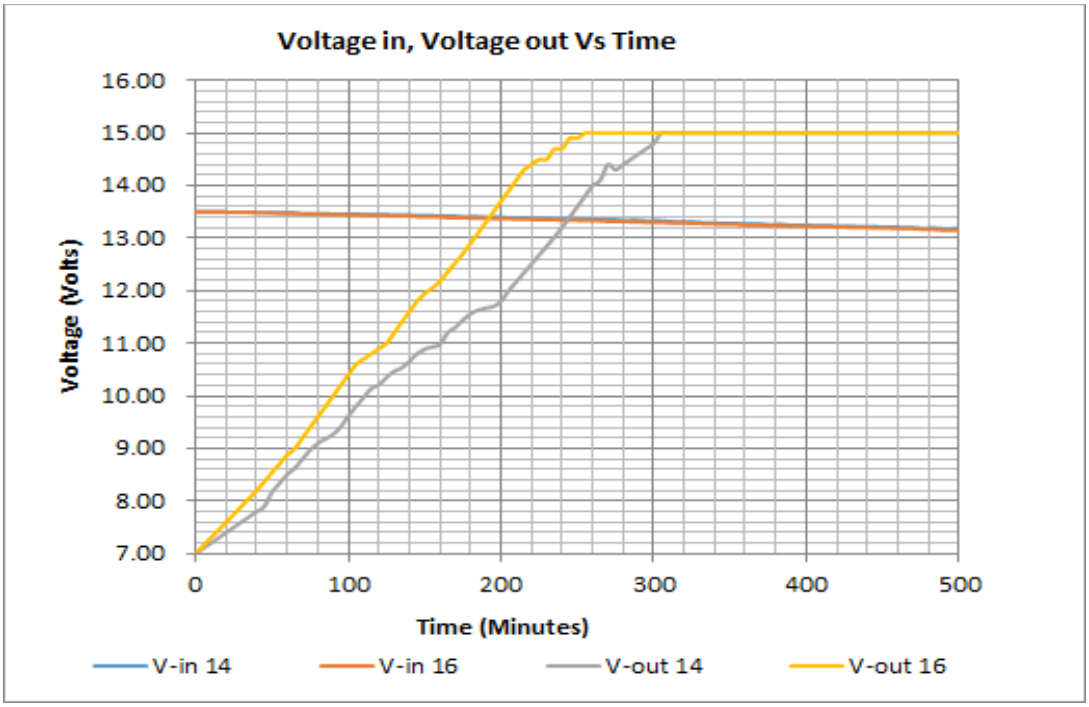

Figure 4-21: Comparison of Input Voltage and Output Voltage For 14 and 16 Ceramic Magnets of Monopole Energizer Model.

Similar observation was made with current profiles. Generally, the loading currents profiles were found to be higher than the input current profiles. Both loading and input currents had a negative slope. The initial loading and input current increased with increase in loading of Monopole Energizer Models with ceramic magnets. Figure 4-22 shows comparison of input current and load current for 4, 6 and 8 ceramic magnets of monopole energizer model.

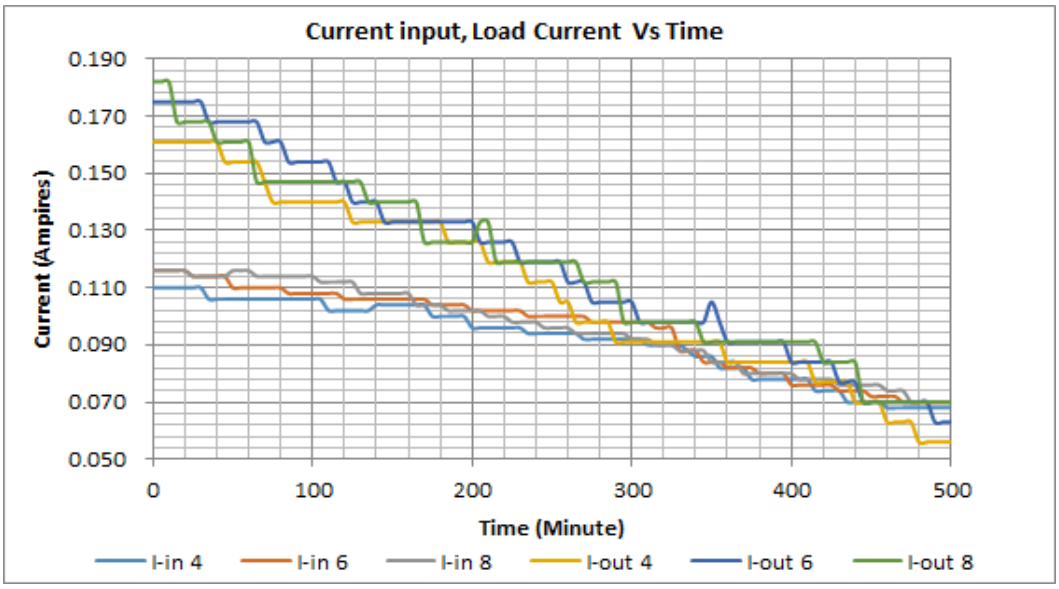

Figure 4-22: Comparison of Input Current and Load Current for 4, 6 and 8 Ceramic Magnets of Monopole Energizer Model.

Furthermore, regardless of the level of magnetic loadings, loading and input currents reduced linearly with time, even though loading currents profile graphs were marginally steeper than input current profile graphs. The rate of reducing current was greater for loading current than input current. Figure 4-23 shows Comparison of input current and Load current for 10 and 12 ceramic magnets of monopole energizer model.

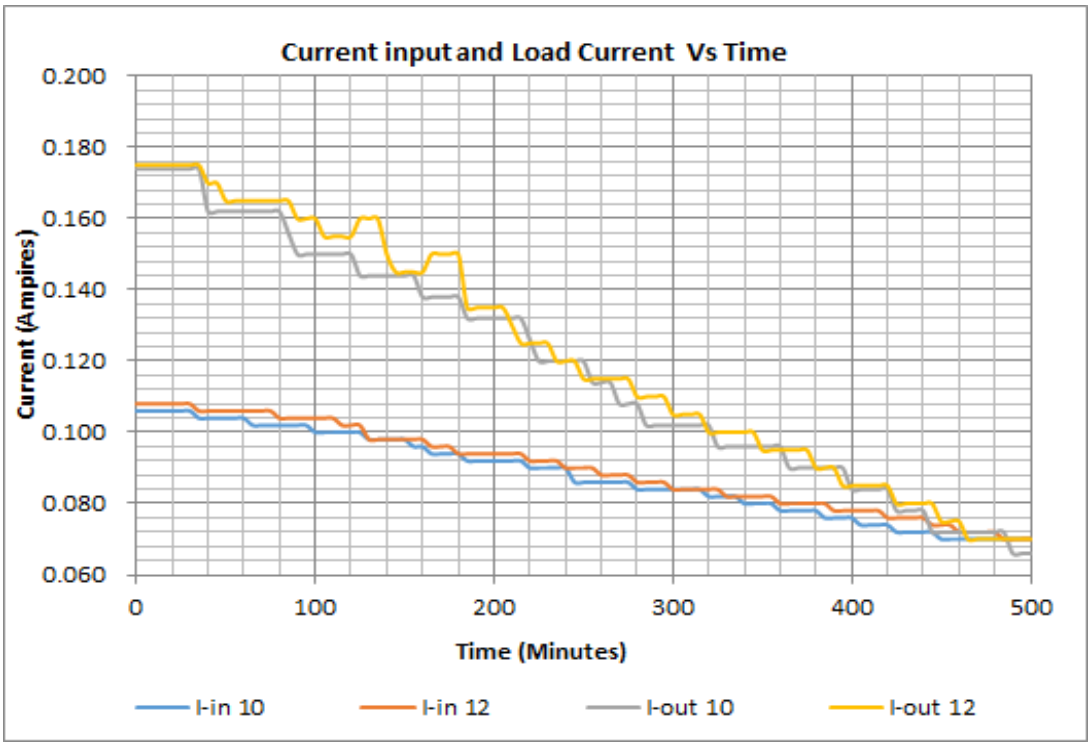

Figure 4-23: Comparison of Input Current and Load Current for 10 and 12 Ceramic Magnets of Monopole Energizer Model.

Furthermore, the magnetic loading of 14 and 16 the load current and input current behavior was consistent with the previous depiction. The load currents were observed to be marginally higher in magnitude than input currents. Similar observations were made for input and output power profiles. Figure 4-24 gives comparison profile behavior at a magnetic loading of 14 and 16 for load and input currents.

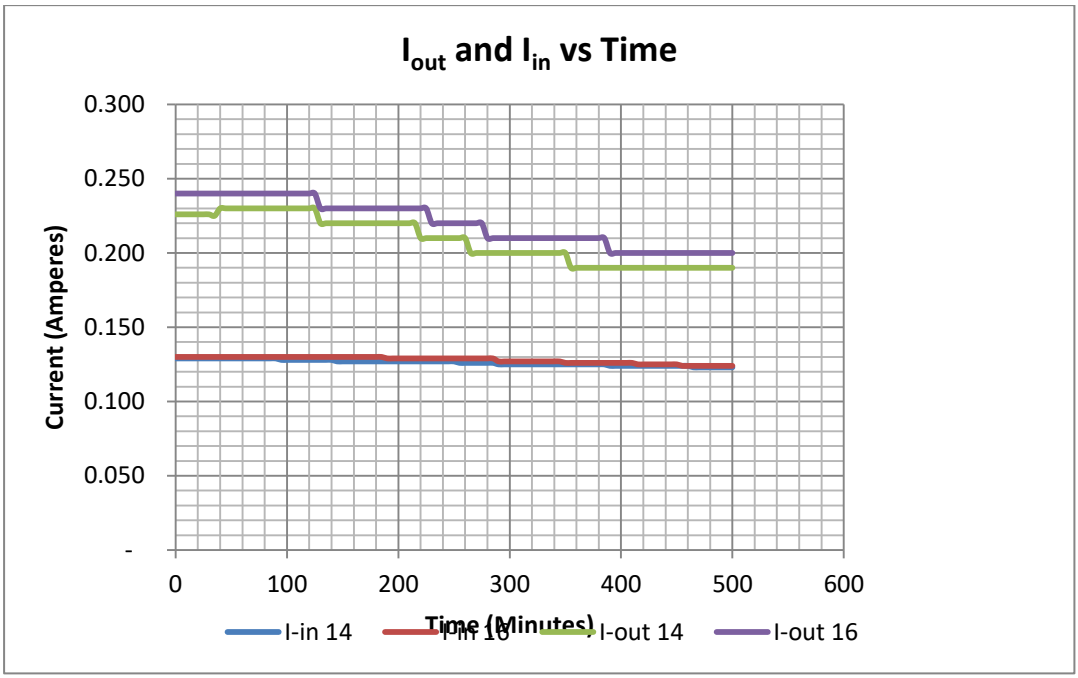

Figure 4-24: Comparison of Input Current and Load Current for 14 and 16 Ceramic Magnets of Monopole Energizer Model.

4.6 Comparison Of Coefficiences at Different Levels of Magnetic Loadingd for Original Design

This section presents the analysis of the Instantaneous-efficiencies, peak co-efficiencies and Average efficiencies based on data from experimental investigation. In computing the co-efficiencies of monopole energizer model for original design using ceramic magnets, the emphasis was put on power output compared with power input. The co- efficiencies of monopole energizer model fitted with various numbers of ceramic magnets ranging from 4 magnets to 16 magnets was computed. The co-efficiency was computed as the ratio of energy output to energy input. Thus, Coe efficiency was computed as

$$n = \frac{Energy\ output}{Energy\ input} = \frac{V_O I_O t_O}{V_i I_i t_i} = \frac{E_o}{E_i}$$

Where;

ηis the efficiency,

E_O is energy output,

$E_i$is energy input,

v_o voltage output,

I_O current output,

t_o time associated with input parameters.

V_i voltage input,

I_i current input,

t_i time associated with output parameters.

Using the above formula of monopole energizer model mounted with various magnets, the co-efficiency was computed. coefficient of performance was based on energy accumulation in the battery being charged with respect to the charging Battery.

Figure 4-24 shows the effect of number of magnets on coefficient of performance.Table 4-9 shows that coefficient of performance increased with increase in number of ceramic magnets. The COP with 4 ceramic magnets was 0.96 or 96% whereas COP with 16 Ceramic magnets was 1.35 or 135%.

Table 4-9: Effect of Number of Ceramic Magnets on COP of Original Design

No of Ceramic magnets	Average COP	Input Joules Calculation				Output Joules Calculation			
		Avg Input Current (Amps)	Avg Input Voltage	Charge Time in Sec	Input Joules	Av Load Current (Amps)	Avg Output Voltage	Discharge Time in Sec	Output Joules
4	0.96	0.097	13.44	24000	31288.32	0.12	10.41	24000	29980.8
6	1.05	0.102	13.42	23100	31620.204	0.13	11.01	23100	33063.03
8	1.07	0.105	13.42	19800	27900.18	0.13	11.64	19800	29961.36
10	1.15	0.095	13.42	19500	24860.55	0.135	10.85	19500	28562.625
12	1.25	0.097	13.38	18300	23750.838	0.14	10.85	18300	27797.7
14	1.28	0.095	13.42	18000	22948.2	0.15	10.92	18000	29484
16	1.35	0.099	13.42	15300	20327.274	0.16	11.17	15300	27344.16

4.6.1 Comparison of Coefficiencies of Original Designs tt Magnetic Loadings of 4,6 And8

When the graph of instantaneous co-efficiency of four ceramic magnet monopole energizer models was plotted against time it, showed the typical bell curve. This is characteristic behavior of the power curve. The instantaneous co-efficiency ranged from 78.2% to 93% and this happened from the start of the experiments to 495 minutes respectively. The graph also showed that the highest co-efficiency recorded was 117.45 % after 435 minutes. It was further showed that for six ceramic magnets model the instantaneous co-efficiency ranged from 81.35% and 102.66 % at 0 minutes and 500 minutes respectively. The peak instantaneous co-efficiency reached was 117.45 % after 350 minutes. Figure 4-25 shows instantaneous co-efficiency versus time graph for 4, 6 and 8 ceramic magnets energizer model.

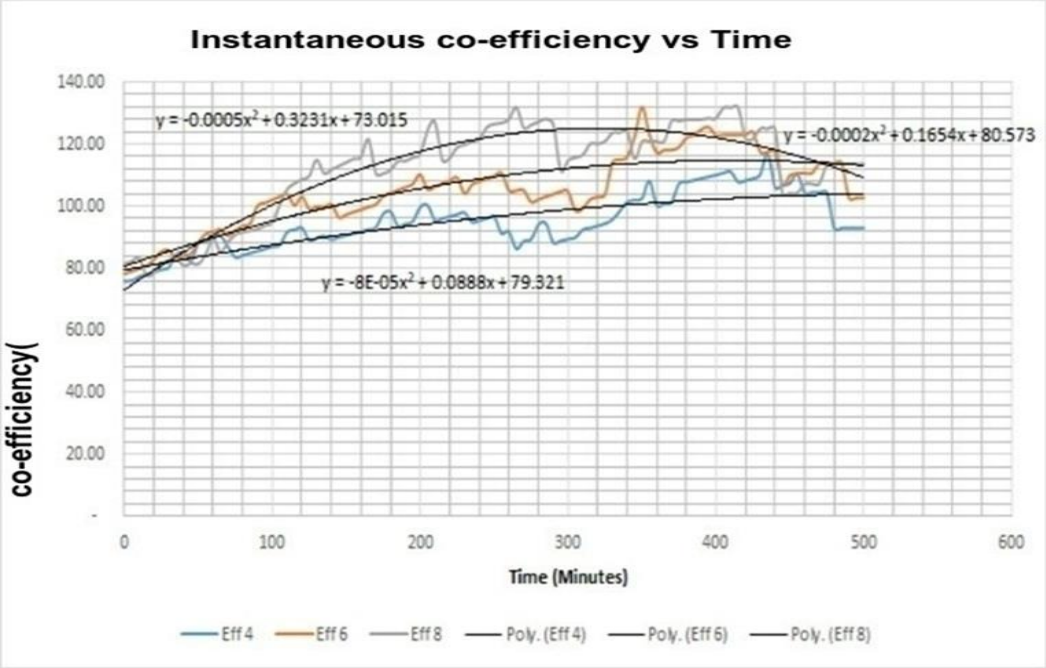

Figure 4-25: Instantaneous Co-efficiency Versus Time Graph for 4, 6 and 8 Ceramic Magnets Energizer Model.

The investigation showed that with eight ceramic magnet model monopole energizer model showed that the co- efficiencies ranged from 81.35 to 113.64 % after 0 minutes and 500 minutes respectively. The highest co-efficiency reached was 135.9 % after 265 minutes. Table 4-10 shows the range of instantaneous co-efficiencies at different levels of magnetic loadings and the time range at which it occurs.

Table 4-10: Range and Time Range of Instantaneous Efficiency for Original Design

Item No.	No. of Magnets	Range of Instantaneous Co-efficiency	Time range at which it occurs between 0 minutes and xx minutes
1	4	78% to 93%	0 and 500
2	6	81.35% to 102.66%	0 and 500
3	8	81.35% to 113.64%	0 and 500
4	10	108.22%to121.67%	0 and 495
5	12	108.22%to114.2%	0 and 495
6	14	89.5% to 221.67%	0 and 500
7	16	108.22% to 111.2%	0 and 495

4.6.2 Comparison of Coefficiencies of Original Designs At Magnetic Loadings of Over 8 Ceramic Magnets

The experiments further established that for ten ceramic magnets monopole energizer model it was established that the highest co-efficiency recorded was 139.02% at 360 minutes. The instantaneous co-efficiency ranged between 108.22 % and 114.24 % at 0 minutes and 495 minutes. Similarly, in the case of twelve ceramic magnets monopole energizer model the instantaneous co-efficiencies ranged between 108.22% and 114.24 and they occurred after 0 minutes and 500 minutes respectively. Figure 4-26 shows the instantaneous efficiencies for original designs of 8 Ceramic magnets loading.

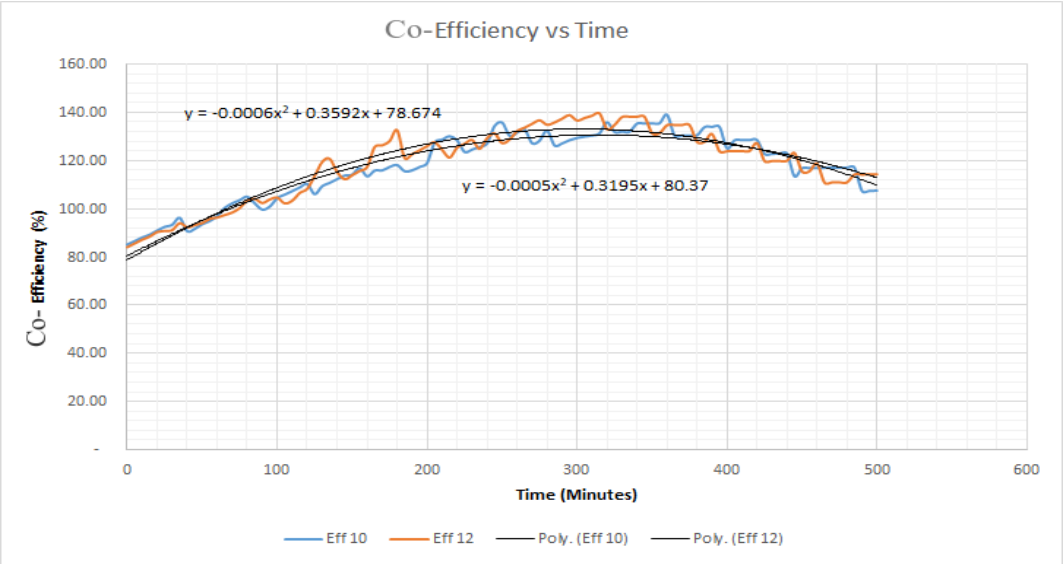

Figure 4-26: Instantaneous Co-efficiency Versus Time Graph for 10 and 12 Ceramic Magnets Energizer Model.

Further analysis was done for co-efficiencies of performance at a magnetic loading of 14 and 16 ceramic magnet MEM design. Figure 4-27 shows the results instantaneous co-efficiencies of performance for original designs of14 and 16 Ceramic magnets loading.

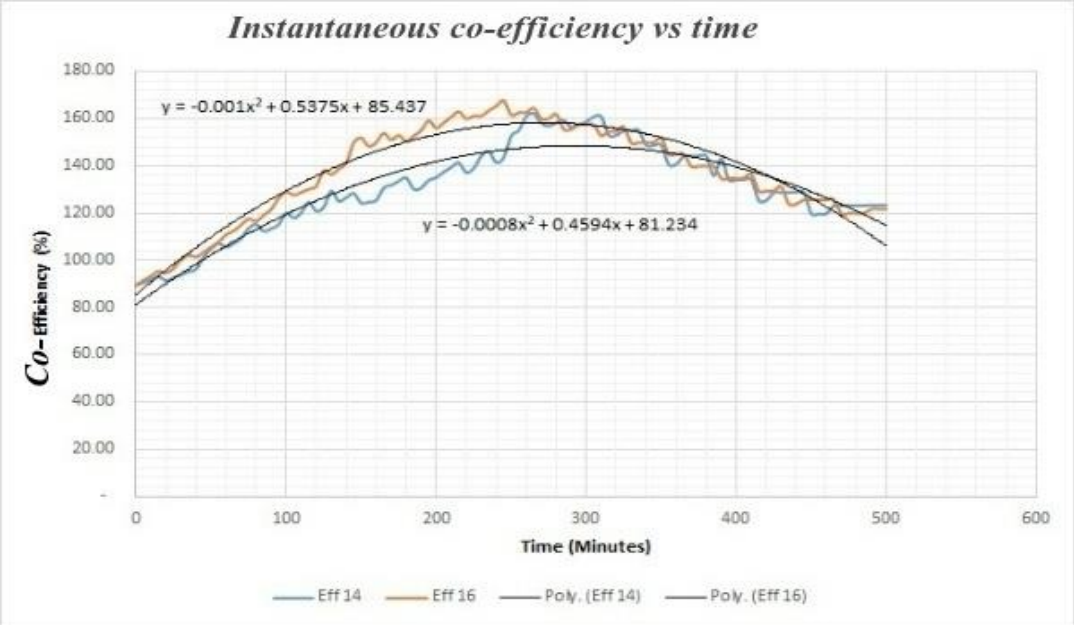

Figure 4-27: Instantaneous Co-efficiency Versus Time Graph For14 and 16 Ceramic Magnets Energizer Model.

It was concluded that peak co-efficiencies increased with the increase of the number of ceramic magnets. The lowest co-efficiency recorded was with four ceramic magnets and was 117.5% and it was after 435 minutes of running the experiment. Whereas the highest peak Co-efficiency was recorded with 16 ceramic magnets and it was recorded after 240 minutes. This investigation further showed that the instantaneous co-efficiencies increased with the increase in number of ceramic magnets. It was shown that the peak co-efficiency for 16 ceramic magnets was highest that is 165.29% and it only took 240 minutes whereas the peak co-efficiency for 4 ceramic magnets was lowest and it took 435 minutes to reach the pick that is 195 minutes higher than the case of 16 ceramic magnets. Table 4-11 shows the variation of peak co-efficiencies with the number of magnets with time.

Table 4-11: Original Design Variation of Peak Efficiencies with Time in Minutes

Number of ceramic magnets fixed on the monopole energizer model wheel.	**Peak Coe-efficiency Recorded in percentage**	**Time taken in minutes to reach it**
4	117.45	435
6	131.98	350
8	135.9	265
10	139.02	360
12	148.57	310
14	162.5	260
16	165.29	240

The graphs of co-efficiencies of monopole energizer model fitted with varying numbers of ceramic magnets were also plotted.

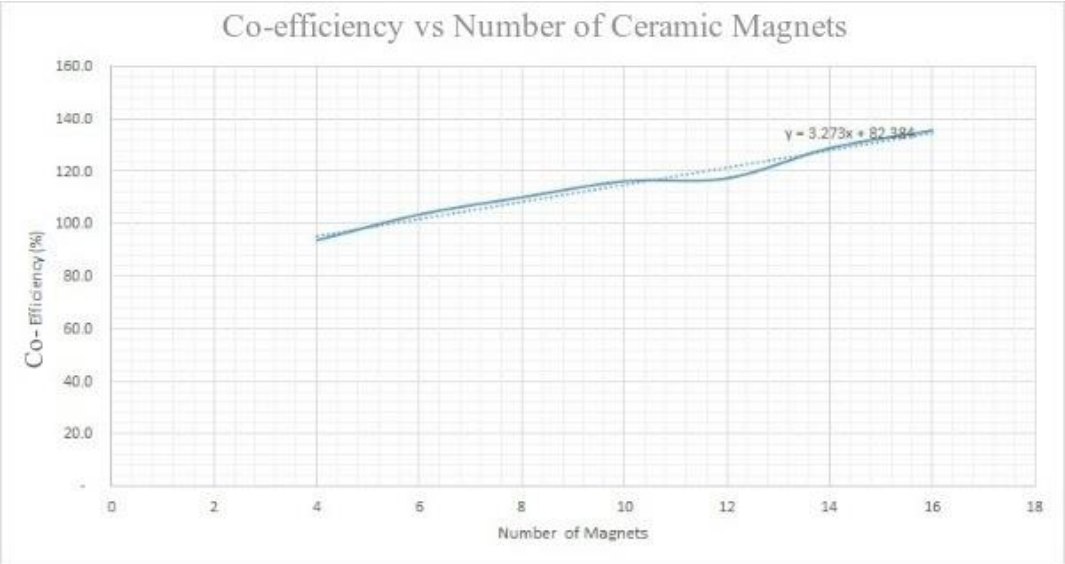

Figure 4-28: Average Co- Efficiency Variation with the Number of Ceramic Magnets Fixed on Monopole Energizer Model.

From Figure 4-28 it was observed that the efficiency of monopole energizer model increased with increasing number of magnets mounted on energizer model wheel. From the experiments it was established that the Coe-efficiency increased linearly. The analysis of results of peak co-efficient revealed that it also increased with magnetic loading as shown below. Figure 4-29: Peak Co-efficiency Versus Number of Ceramic Magnets for Monopole Energizer Model

also showed that the average co- efficiency of the monopole energizer model increased linearly from 93.8% when four ceramic magnets were used to 135.6% compared to when 16 ceramic magnets were used.

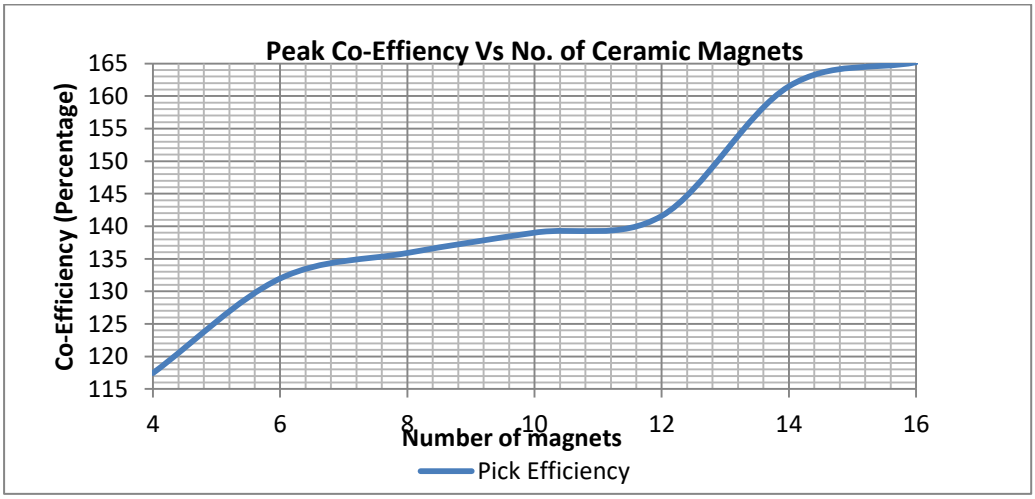

Figure 4-29: Peak Co-efficiency Versus Number of Ceramic Magnets for Monopole Energizer Model

Table 4-12: Coefficient of Performance of MEM Based on Original Design.

No of Ceramic magnets fixed on the model wheel	Input Power Calculation			Output Power Calculation				Average COP
	Average Input Current (Amps)	Average Input Voltage	Input Power (Watts)	Average Load Current	Average Output Voltage	Discharge Time in Seconds	Output Power (Watts)	
4	0.1031	13.473	1.39	0.1385	9.064	14,700	1.26	**0.90**
6	0.1075	13.445	1.45	0.1473	9.689	14,700	1.43	**0.99**
8	0.1088	13.441	1.46	0.1442	10.566	14,700	1.52	**1.04**
10	0.0984	13.436	1.32	0.1481	9.795	14,700	1.45	**1.10**
12	0.1004	13.407	1.35	0.1527	9.796	14,700	1.50	**1.11**
14	0.0978	13.442	1.32	0.1577	10.094	14,700	1.59	**1.21**
16	0.0996	13.425	1.34	0.1622	11.015	14,700	1.79	**1.34**

4.7 Characteristic Of Voltage Input And Output Of Mem Experiments With Neodymium Magnets

In this section presentation of the findings of Monopole Energizer with Neodymium magnets is presented. The focus is on voltage input and output characteristics. The experimental results are presented graphically, by tables and discussions in the preceding sections

4.7.1 Characteristics of Voltage Input And Output of Monopole Energizer Model Experiments With Four, Six and Eight Neodymium Magnets

In analysing input and output characteristics of voltage MEM, a number of input and output equations at different levels of magnetic loadings were generated. The investigation showed that for the four Neodymium magnet replication design monopole energizer model, it took 385 minutes to fully charge the secondary battery. Within the same timeline the secondary battery charged at the rate of 1.25 volts per hour.

The output voltage increased from 7 volts to 15 volts within the same time interval, implying that it took 385 minutes to charge the battery from 7 volts to 15 volts. The

general equation for the output voltage at magnetic loading of four is equation 4.50 as indicated in Table 4.14.The analysis of the results also showed that the input voltage discharged from 13.50 volts to 13.29 volts. The primary battery discharged at the rate of 0.033 volts per hour. Equation 4.43 in table 4.13 shows the general equation for the input voltage at a magnetic loading of 4.

Table 4-13below shows a range of input equations at different level of magnetic loading. These equations were used to generate graphs for input voltage for MEM replication design at different levels of magnetic loading.

For six Neodymium magnets monopole energizer model, the output voltage increased steadily from 7 volts to 15 volts within 335 minutes. The secondary battery was charged at the rate of 1.43 volts per hour. The general equation for the output voltage at a magnetic loading of 6 is equation 4.51 as shown in table 4.14.

Table 4-13: Voltage Input Equations for Replication Experimental Design

Item No.	**Number of Magnets (Ceramic magnets) On the wheel**	**Voltage input equations**	
1	4	$V = 0.0004t + 7.013.526.$	4.43
2	6	$V = -0.0005t + 13.509$	4.44
3	8	$V = -0.006t + 13.512.$	4.45
4	10	$V = -0.0007t + 13.58.$	4.46
5	12	$V = -0.0007t + 13.525.$	4.47
6	14	$V = -0.0004X + 13.527$	4.48
7	16	$V = -0.0004t + 13.527.$----------	4.49

Furthermore, loading of six showed that he input voltage discharged from 13.50 to 13.29 within 335 minutes. The primary battery was discharged at the rate of 0.038volts per hour. The general equation for the input voltage at a magnetic loading of 6 is equation 4.43 as shown in table 4.13.

Table 4-14: Voltage Output Equations for Replication Experimental Design

Item No.	No of Neodymium Magnets	Voltage output equations	
1	4	$V = 10^{-9}t^4 - 0.0004t^2 - 0.0011t + 71.1872.$	4.50
2	6	$V = 10^{-10}t^4 - 3 \times 10^{-7}t^3 + 0.0002t^2 + 0.0029t + 7.3476$	4.51.
3	8	$V = 3 \times 10^{-10}t^4 + 5 \times 10^{-10}t^3 + 0.0002t^2 - 0.013t + 7.337$	4.52
4	10	$V = -9 \times 10^{-10}t^4 + 10^{-6}t^3 + 0.0006t^2 + 0.1186t + 6.4171.$	4.53
5	12	$V = -10^{-9}t^4$ +2× $10^{-6}t^3 + 0.0007t^2$+0.1302t + 6.5709	4.54
6	14	$V = 10^{-9}t^4 + 2 \times 10^{-6}t^3 + 0.0007t^2$ +0.1302t + 6.5709	4.55
7	16	$V = 10^{-9}t^4 + 2 \times 10^{-6}t^3 + 0.0006t^2$ +0.1186t + 6.4171	4.56

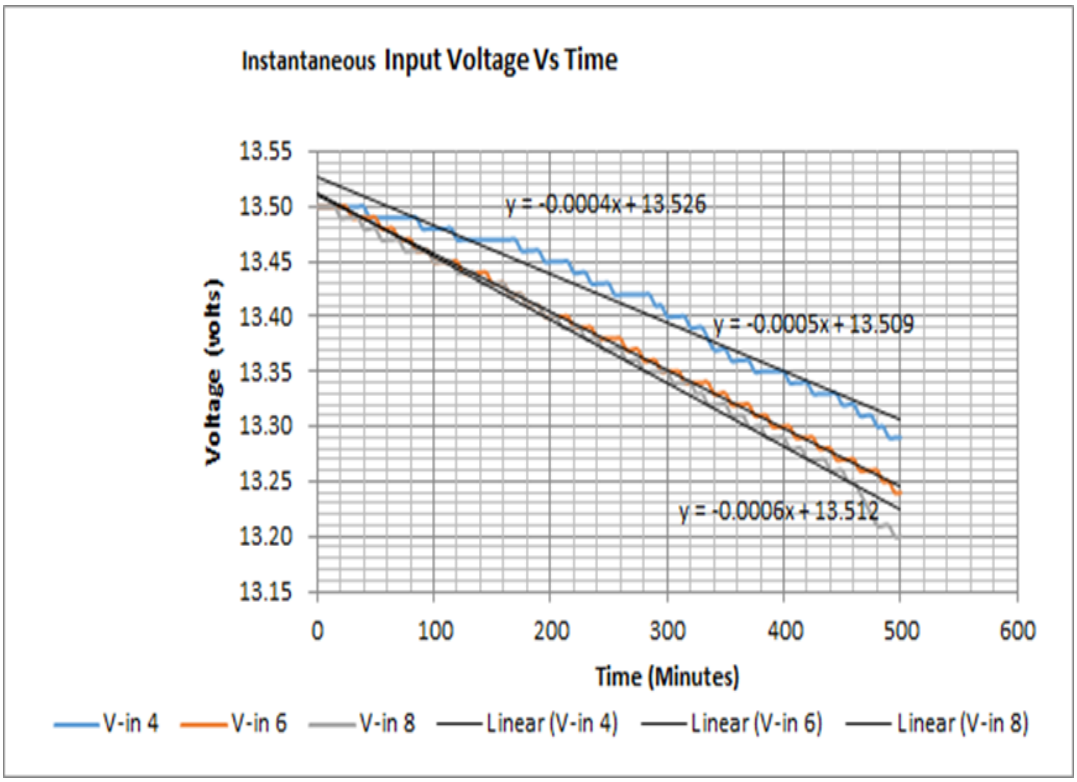

Figure 4-30: Instantaneous Input Voltage Versus Time for 4, 6 And 8 Neodymium Magnets Monopole Energizer Model.

The primary battery was discharged at the rate of 0.049 volts per hour. Equation 4.45 in table 4.13 shows general equation for the input voltage at a magnetic loading of 8.Figure 4-31 shows the voltage Profiles of output voltage at a magnetic loading of 4, 6 and 8 Neodymium magnets of MEM Model after experimentation.

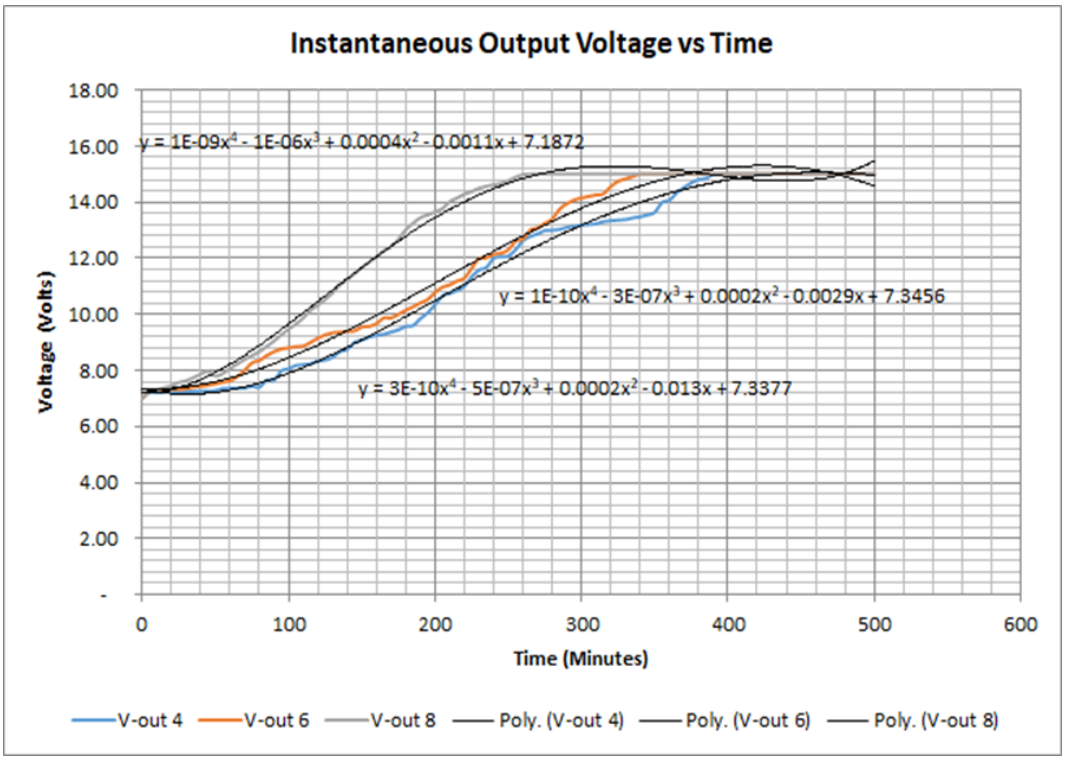

Figure 4-31: Instantaneous Output Voltage Versus Time for 4, 6 and 8 Neodymium Magnets Monopole Energizer Model.

Just like the case of original design, it was observed that the rate of charging increased with increase in magnetic loadings in replication design. This is shown by the time taken to arrive at the plateau curve. The time of achieving plateau curve was shortened as the number of magnetic loadings increase.

Table 4-15: Charging and Discharging Rate in Volts Per Hour of Replication Design

Item No.	No of Neodymium Magnets on the wheel	Charging Rate in Volts/ Hour	Time Taken to full charge in minutes	Discharging Rate in Volts / Hour	Time taken to discharge in minutes
1	4	1.25	385	0.033	385
2	6	1.43	335	0.038	355
3	8	1.9	225	0.049	225
4	10	3.85	215	0.056	215
5	12	4.57	205	0.0585	205
6	14	3.85	205	0.11	205
7	16	4.57	125	0.12	125

It was observed that both discharge and charging rate of Monopole Energizer Machine increased with increase in Magnetic Loadings. It was generally observed that voltage output had a positive gradient unlike voltage input which had a negative gradient. It was further established that voltage output was always greater than input voltage.Figure 4-32 shows the Neodymium Magnets monopole energizer model rate of charging and discharging

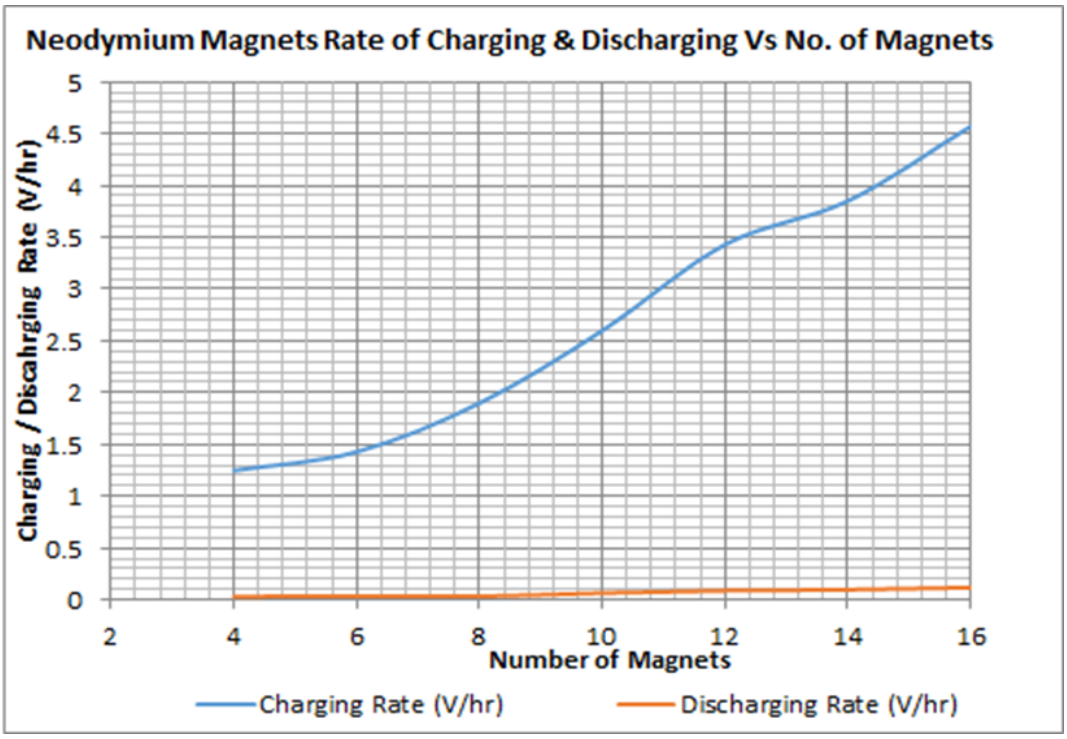

Figure 4-32: Neodymium Magnets Monopole Energizer Model Rate of Charging and Discharging.

It was generally observed that output voltages increased as the magnetic loading at the magnetic loading level of 4,6 and 8 Neodymium magnets monopole energizer model. It was also deduced that the voltage input decreased marginally with the level of magnetic loadings. This behavior was in agreement across the three levels of magnetic loadings for both input and output voltages.

4.7.2 Characteristic Of Voltage Input and Output Of Monopole Energizer Experiments With Over Eight Neodymium Magnets

From experimental analysis, it was deduced that at a magnetic loading level of replication design, the output voltage increased steadily from 7 volts to 15 volts within 215 minutes. The secondary battery charged at the rate of 3.85 volts per hour. Figure 4-33 below shows instantaneous output Voltage for 10 and 12 Neodymium magnets monopole energizer model. Equations 4.53 and 4.54 in table 4.14 shows general voltage output equations at a magnetic loading of 10 and 12 respectively.

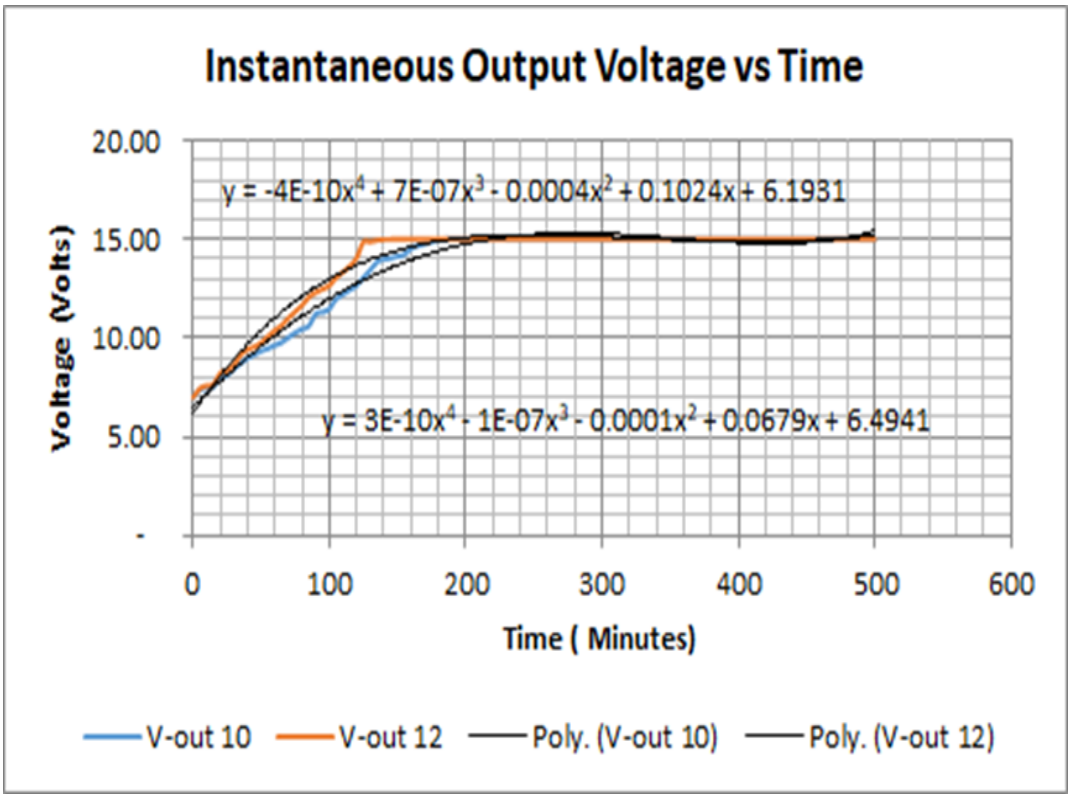

Figure 4-33: Instantaneous Output Voltage for 10 and 12 Neodymium Magnets Monopole Energizer Model.

At 12 magnetic loading replication design, output voltage increased at the rate of 4.57 volts per hour for 205 minutes. The general equation at this level is denoted by Eq. 4.54 in Table 4.14. The primary battery was discharged at the rate of 0.038volts per hour. The general equation for the input voltage at a magnetic loading of 6 is equation 4.43 as shown in table 4.13.

Furthermore, loading of six showed that he input voltage discharged from 13.50 to 13.29 within 335 minutes. The primary battery was discharged at the rate of 0.038volts per hour. The general equation for the input voltage at a magnetic loading of 6 is equation 4.43 as shown in table 4.13.

Table 4-14, from this table , notably equations 4.55 and 4.56 shows the general equations at a magnetic loadings of 14 and 16 for output voltage replication design. The primary battery discharged from 13.5 to 13.29 volts. Figure 4-34 below demonstrates the behavior of voltage output against the magnetic loadings of 10

and 12. . Equations 4.46 and 4.47 in table 4.13 indicates general voltage input equations at a magnetic loading of 10 and 12 respectively

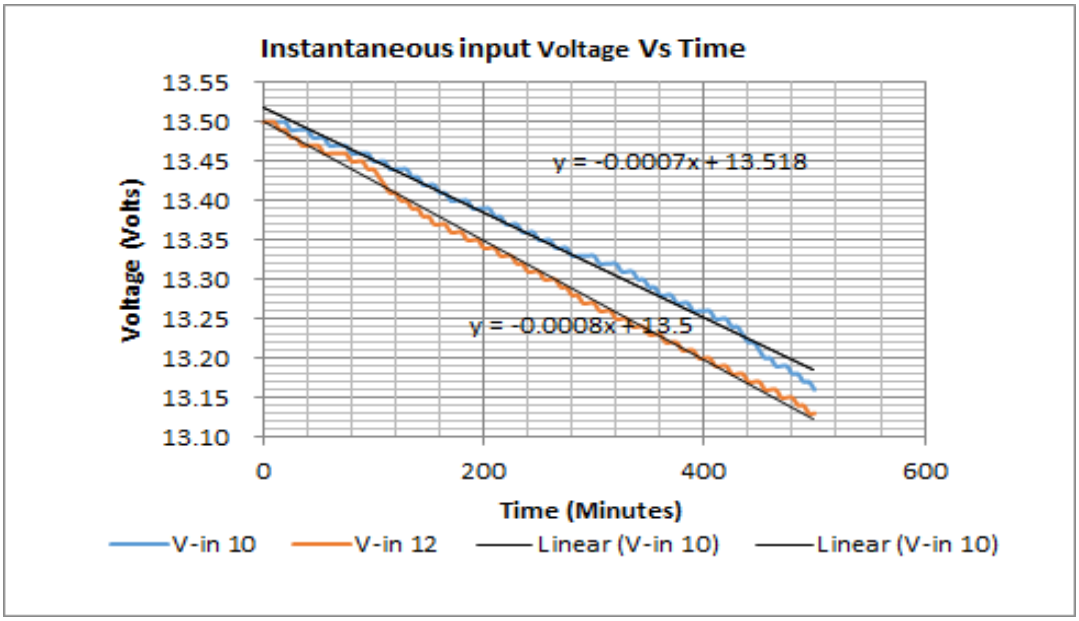

Figure 4-34: Instantaneous Input Voltage for 10 and 12 Neodymium Magnets Monopole Energizer Model.

Similar trend was observed at magnetic loadings of 14 and 16 where the plateau curve was approached in a much shorter time as compared to the magnetic loadings of 10 and 12 in the case of voltage output. This was inconsistent with the assertion that the charging rate of replication design increased with magnetic loading.

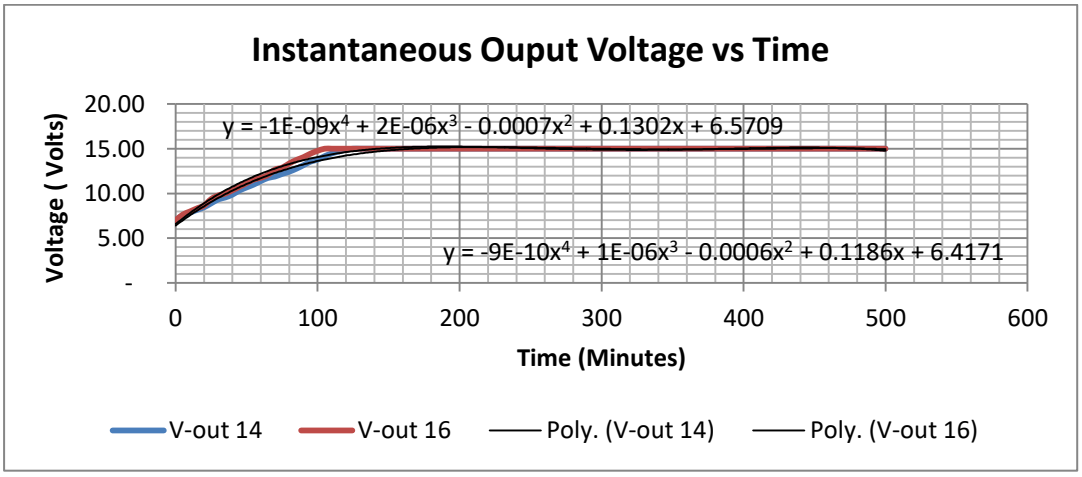

Figure 4-35: Instantaneous Output Voltage for 14 and 16 Neodymium Magnets Monopole Energizer Model.

In the case of input voltage behavior, it was observed that the graph had a negative gradient which decreased with magnetic loading. Figure 4-36 demonstrates this behavior at the magnetic loading of 10 and 12.

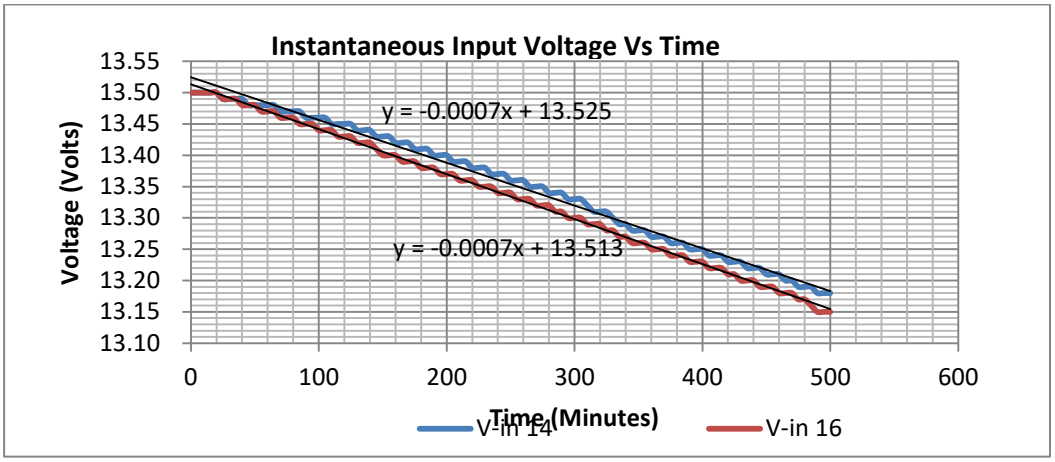

Figure 4-36: Instantaneous Input Voltage for 14 and 16 Neodymium Magnets Monopole Energizer Model.

From the analysis of results, it has been deduced that at the magnetic loading level of 10.12.14, and 16 the voltage output increased with magnetic loading whereas the voltage input decreased marginally with the level of magnetic loadings. This behavior is in agreement with what was observed at the magnetic loading of 4,6 and 8 hence the conclusion that this behavior was consistent across all the levels of magnetic loading under experimentation.

Furthermore, loading of six showed that he input voltage discharged from 13.50 to 13.29 within 335 minutes. The primary battery was discharged at the rate of 0.038volts per hour. The general equation for the input voltage at a magnetic loading of 6 is equation 4.43 as shown in table 4.13.

Table 4-14 , equations 4.55 and 4.56 shows general equations for output voltage at a magnetic loading of 14 and 16 respectively. Likewise, equations 4.48 and 4.49 in Table 4-13shows general equations for input voltage at a magnetic loading of 14 and 16

4.8 Characteristic Of Electrical Current Of Monopole Energizer Model Experiments With Neodymium Magnets

In this section, the electrical behavior of Monopole Energizer Machine mounted for Replication design with Neodymium magnets is discussed.

4.8.1 Characteristic of Current Input and Output of Monopole Energizer Model Experiments With Four, Six And Eight Neodymium Magnets

Further analysis with current profiles for MEM replication design showed that at a level of four magnetic loadings it was deduced that within 385 minutes the load current decreased from 0.14 amps to 0.11 amps. The current decreased at the rate of -0.0047 amps per hour. Equation 4.64 in table 4.17 shows the general equation for load current at a magnetic loading of 4.Notably it was observed that input current decreased from 0.115amps to 0.112 amps within the same time interval. Equation 4.57 in table 4.16 shows the general equation for input current at a magnetic loading of 4.The input current decreased at the rate of 0.00047 Amps per hour. Table 4-16 shows input Current equations for replication Design. These equations assisted in coming up with graphical presentations for input current graphs.

Table 4-16: Input Current Equations for Replication Design

Item No.	No of Neodymium magnetsOn the wheel	Current input equations	
1	4	$I = -10^{-5}t + 0.1189$	4.57
2	6	$I = -5 \times 10^{-6}t + 0.1157$	4.58
3	8	$I = -7 \times 10^{-6}t + 0.1149$	4.59
4	10	$I = -2 \times 10^{-5}t + 0.1233$	4.60.
5	12	$I = -2 \times 10^{-5}t + 0.1267.$	4.61
6	14	$I = -1 \times 10^{-5}t + 0.1295$.	4.62
7	16	$I = -1 \times 10^{-5}t + 0.1314$	.4.63

In the case of 6 Neodymium magnet monopole energizer model, it was deduced that the load current decreased from 0.15 amps to 0.13 amps within 335 minutes. The current decreased at the rate of 0.0036 amps per hour. The general equation for load current was Eq. 4.65 in Table 4-17.

Table 4-17: Output Current Equations for Replication Design

Item No.	No of Neodymium magnets On the wheel	Current output equations	
1	4	$I = -7 \times 10^{-5}t + 0.1753$	4.64
2	6	$I = -3 \times 10^{-5}t + 0.1536$	4.65
3	8	$I = -7 \times 10^{-5}t + 0.1456.$	4.66
4	10	$I = -9 \times 10^{-5}t + 0.1998$	4.67
5	12	$I = 0.0001t + 0.189$	4.68
6	14	$I = -1 \times 10^{-4}t + 0.2136$	4.69
7	16	$I = -1 \times 10^{-4}t + 0.2262$	4.70

It was further deduced that both load and input current had a negative slope. Table 4-18:Input and Load Current Reduction Rate Per Hour for Replication Design shows the characteristic behavior of input and load current profiles.

Table 4-18:Input and Load Current Reduction Rate Per Hour for Replication Design

Item No.	No of Neodymium magnets on the wheel	Input current reduction rate per hour in amperes	Load current reduction rate per hour in amperes
1	4	0.0047	0.0047
2	6	0.0072	0.0036
3	8	0.0097	0.0071
4	10	0.0014	0.0172
5	12	0.0043	0.0172
6	14	0.0029	0.024
7	16	0.0034	0.034

It was also observed that input current decreased from 0.116amps to 0.112 amps within the same time interval. The input current decreased at the rate of 0.00072 Amps per hour.

The general equation in the case of 6 neodymium magnets was Eq. 4.58 of Table 4-16. Figure 4.37 shows instantaneous load current versus time for 4, 6 and 8 Neodymium magnets monopole energizer models.

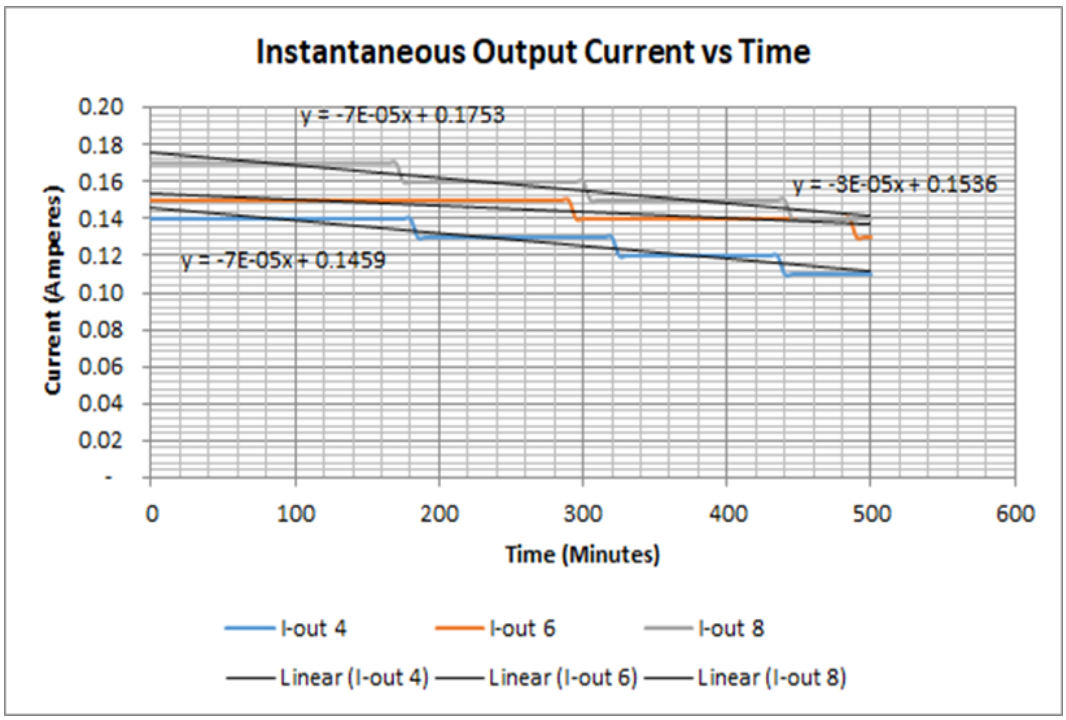

Figure 4-37: Instantaneous Load Current Versus Time for 4, 6 and 8 Neodymium Magnets Monopole Energizer Models.

For eight neodymium magnets, after experimental runs and analysis the following deductions were made on completion of the experimental runs. It was further deduced that the load current decreased from 0.17 amps to 0.14 amps within 225 minutes. The current decreased at the rate of 0.0071 amps per hour. The general equation for load current equation was equation 4.66 in Table 4-17.

It was further observed that input current decreased from 0.119 amps to 0.113 amps within the same time interval. The general equation for input current equation was equation 4.59 Table 4-16. Figure 4-38 shows the load current and input current behavior respectively at the magnetic loadings of 4,6 and 8

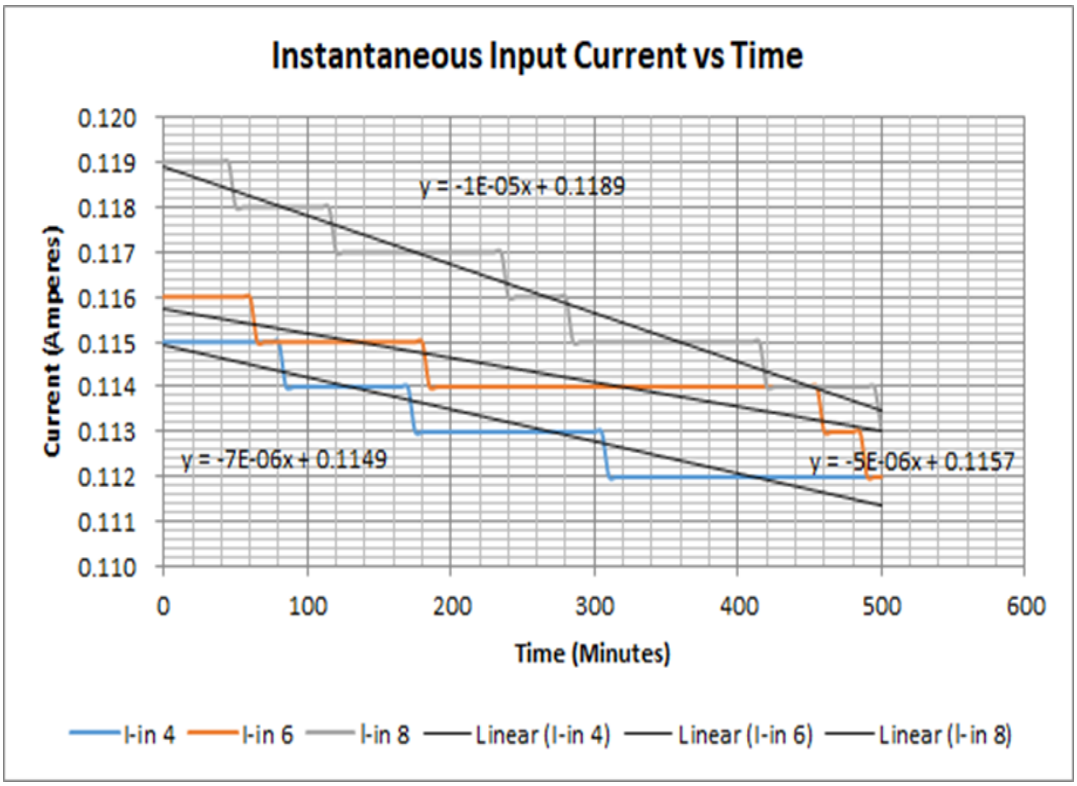

Figure 4-38: Instantaneous Input Current Versus Time for 4, 6 And 8 Neodymium Magnets Monopole Energizer Models.

The input and load current analysis of results of replication design at magnetic loading of 4, 6 and 8 showed that both load and input current profile had a negative slope a cross the three levels of magnetic loading. It was further deduced that both load and input current marginally increased with magnetic loading. It was further observed that both input and load current profiles had a negative slope. The magnitude of the slope increased with magnetic loading.

4.8.2 Characteristic of Current Input and Output of Monopole Energizer Model Experiments With Over Eight Neodymium Magnets

The results at a magnetic loading of 10 and 12 MEM replication design showed that load current at a magnetic loading of 10 decreased from 0.17 amps to 0.10 amps in 330 minutes. The load current reduction rate for 10 and12 magnetic loadings was 0.0172 and 0.0172 amperes per hour respectively. Figure 4.39 shows instantaneous Output current for 10 and 12 Neodymium magnets monopole energizer model.

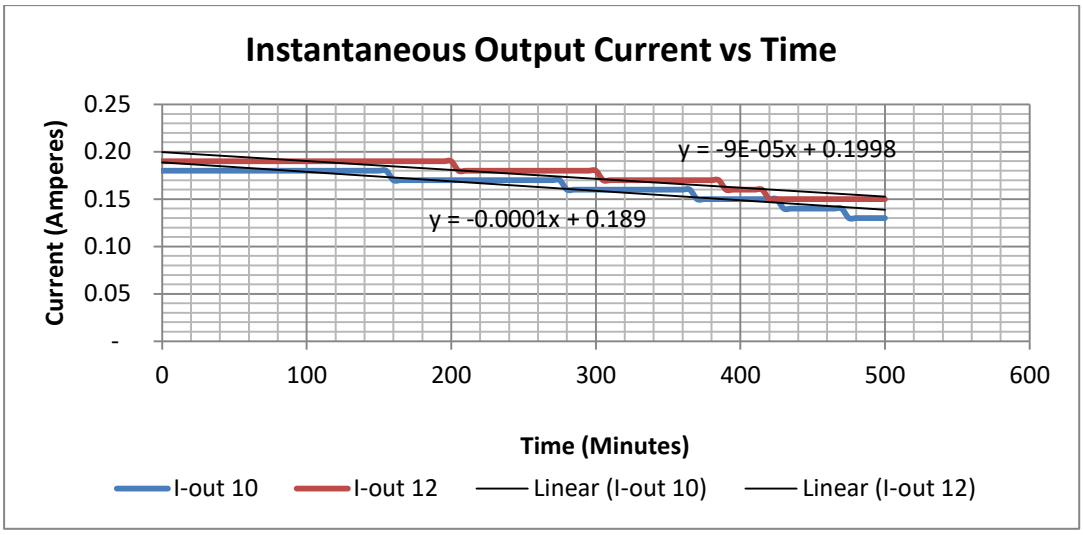

Figure 4-39: Instantaneous Output Current for 10 and 12 Neodymium Magnets Monopole Energizer Model.

It was observed that the input and load currents reduction rate increased with magnetic loading whereas the loading current increased marginally with magnetic loading. Input current rate of reduction was 0.0014 amps per hour and 0.0043 amps per hour for 10 and 12 magnetic loadings respectively. Figure 4.40 shows instantaneous input current for 10 and 12 Neodymium magnets monopole energizer model.

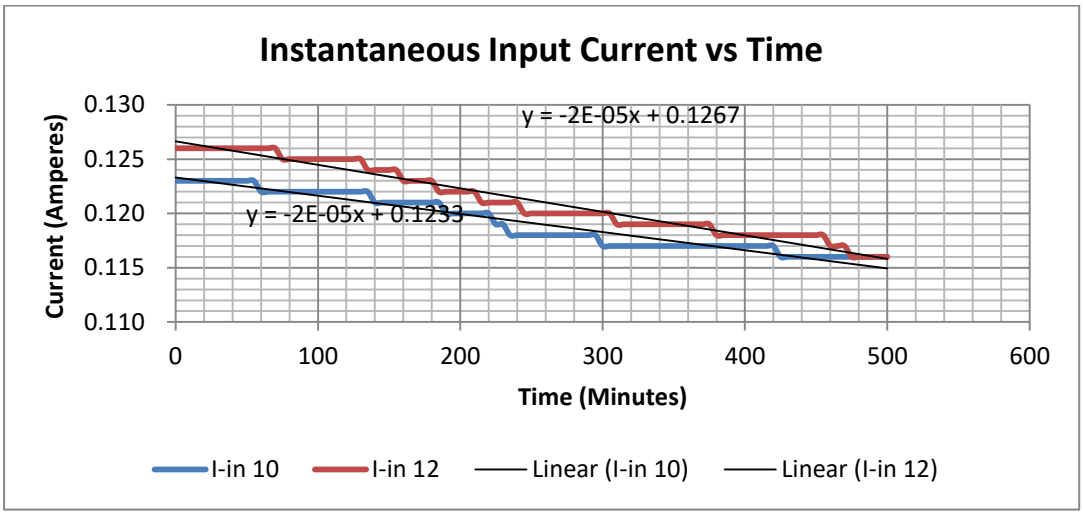

Figure 4-40: Instantaneous Input Current for 10 And 12 Neodymium Magnets Monopole Energizer Model.

The general equations for load current equation at magnetic loadings of 10 and 12 was equation 4.67 and equation 4.68 in Table 4-17 respectively. Whereas the

general equations for input current equation at magnetic loadings of 10 and 12 was equation 4.60 and equation 4.61 in table 4.16 respectively.

In the case of 14 and 6 magnetic loadings input current reduction rate was 0.0029 and 0.0034 amps per hour respectively. The current profile for 14 Neodymium magnets Energizer model showed that the output current increased from 0.21 amps to 0.16 amps in 205 minutes. Figure 4.41 show instantaneous output current for 14 and 16 Neodymium magnets monopole energizer model.

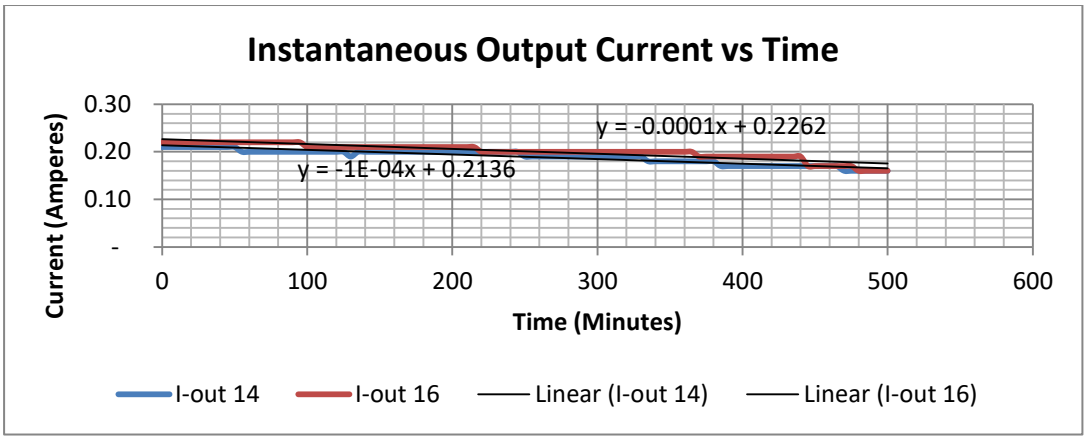

Figure 4-41: Instantaneous Output Current for 14 and 16 Neodymium Magnets Monopole Energizer Model.

The output current increased at the rate of 0.024 Amps per hour. Within the same time interval, the input current decreased at the rate of 0.0029 Amps per hour. In 125 minutes, the input current decreased from 0.129 Amps to 0.123 Amps.

The profile for 16 Neodymium magnets monopole energizer model showed that the output current decreased from 0.22 Amps to 0.16Amps in 125 minutes. Figures 4.41 and 4.42 shows the profile for the current output and input for 14 and 16 Neodymium magnets energizer model.

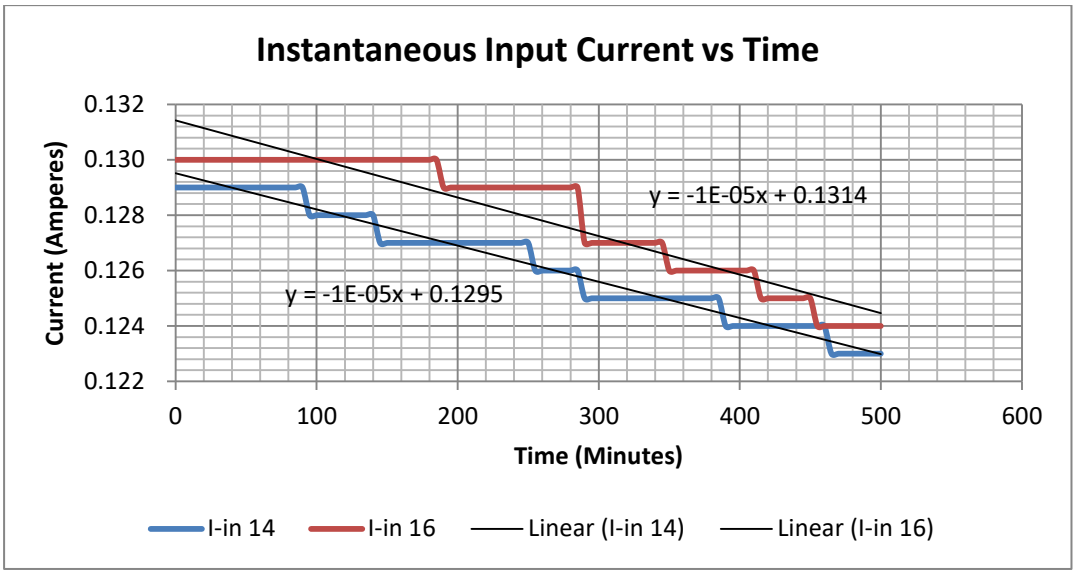

Figure 4-42: Instantaneous Input Current for 14 and 16 Neodymium Magnets Monopole Energizer Model.

Equations 4.69 and 4.70 in table 4.17 shows general equations for output voltage at a magnetic loading of 14 and 16 respectively. Likewise, equations 4.62 and 4.63 in table 4.16 shows general equations for input voltage at a magnetic loading of 14 and 16.

4.9 Characteristic Of Electrical Powermem Experiments With Neodymium Magnets

In this section, the electrical power behavior of Monopole Energizer Machine replication design with different magnetic loading is discussed.

4.9.1 Characteristic Of Power Input And Output Of Monopole Energizer Model Experiments With Four, Six And Eight Neodymium Magnets

The output power graphs were characterized by upward trajectory contrary to input power behavior which was characterized by downward sloping trajectory. Table 4-19shows input power rate and output power rate per hour

Table 4-19: Input Power Reduction Rate and Output Power Increase Rate Per Hour

Item No.	No of Neodymium magnets on the wheel	Input Power reduction rate per hour in watts	Output Power Increase rate per hour in watts
1	4	0.0093	0.182
2	6	0.0125	0.161
3	8	0.0235	0.214
4	10	0.0455	0.22
5	12	0.073	0.395
6	14	0.073	0.44
7	16	0.074	0.491

At the magnetic loading level of four it was deduced that, in 385 minutes power output increased from 0.98 watts to 1.95 watts. The rate of power increase was 0.182 watts per hour. Equation 4.76 in table 4.21 shows the general equation for power output at magnetic loading of 4. The power input decreased from 1.55 watts per hour to 1.49 watts per hour. The power input decreased at the rate of 0.0093 watts per hour. Equation 4.71 in Table 4-20 shows the general equation for power input at magnetic loading of 4. The temperature remained fairly constant at 25^0C during the experimental runs. Table 4-20 shows Power input equations for replication design at different levels of magnetic loading.

Table 4-20: Power Input Equations

Item No.	No of Neodymium magnets On the wheel	Power input equations
1	4	$P = -10^{-14}t^4 + 6 \times 10^{-10}t^3 - 3 \times 10^{-7}t^2 - 0.0001t + 1.5555$ 4.71
	6	$P = -8 \times 10^{-10}t^3 + 7 \times 10^{-7}t^2 - 0.0003t + 1.5724$ 4.72
3	8	$P = 0.0002t + 1.606.$ 4.73
4	10	$P = 10^{-7}t^2 + 0.0004t + 1.6729$ 4.74

5	12	$P = -2 \times 10^{-11}t^4 + 2 \times 10^{-8}t^3 - 6 \times 10^{-6}t^2 + 0.0002t + 1.6972$	4.75

For six Neodymium magnets monopole energizer model it was further deduced that the power output increased from 1.05 watts per hour to 1.95 watts per hour. The power output increased at the rate of 0.161 watts per hour for 335 minutes. Equation 4.77 in table 4.21 shows the general equation for power output at magnetic loading of 6.It was established that the power input decreased from 1.57 watts per hour to 1.50 watts per hour in 335 minutes. This implied that the power decreased at the rate of 0.0125 watts per hour. Table 4-21 shows Power output equations for replication design at different levels of magnetic loading. Equation 4.72 in table 4.20 shows the general equation for power input at magnetic loading of 6.

Table 4-21: Power Output Equations

Item No.	No of Neodymium magnets on the wheel	Power output equations	
1	4	$P = 3 \times 10^{-9}t^3 - 2 \times 10^{-6}t^2 + 0.0027t + 0.9099$	4.76
2	6	$p = 3 \times 10^{-11}t^4 - 6 \times 10^{-8}\,t^3 + 2 \times 10^{-5}t^2 - -5 \times 10^{-5}t + 1.0888$	4.77
3	8	$p = -7 \times 10^{-13}t^5 + 10^{-9}\,t^4 - 6 \times 10^{-7}t^3 + 0.0001t^2 + 0.0039t + 1.2767$	4.78
4	10	$P = 4 \times 10^{-8}t^3 - 4 \times 10^{-5}t^2 + 0.014t + 1.1393.$	4.79
5	12	$P = 6 \times 10^{-8}t^3 - 6 \times 10^{-5}t^2 + 0.018t + 1.2108$	4.80
6	14	$-10^{-10}t^4 + 2 \times 10^{-7}t^3 - 9 \times 10^{-5}t^2 + 0.0213t + 1.3976.$	4.81
7	16	$-4 \times 10^{-10}t^4 + 4 \times 10^{-7}t^3 - 0.0002t^2 + 0.0294t + 1.447$	4.82

Figure 4-43 shows Instantaneous Output Power For 4, 6 And 8 Neodymium Magnets Monopole Energizer Model.

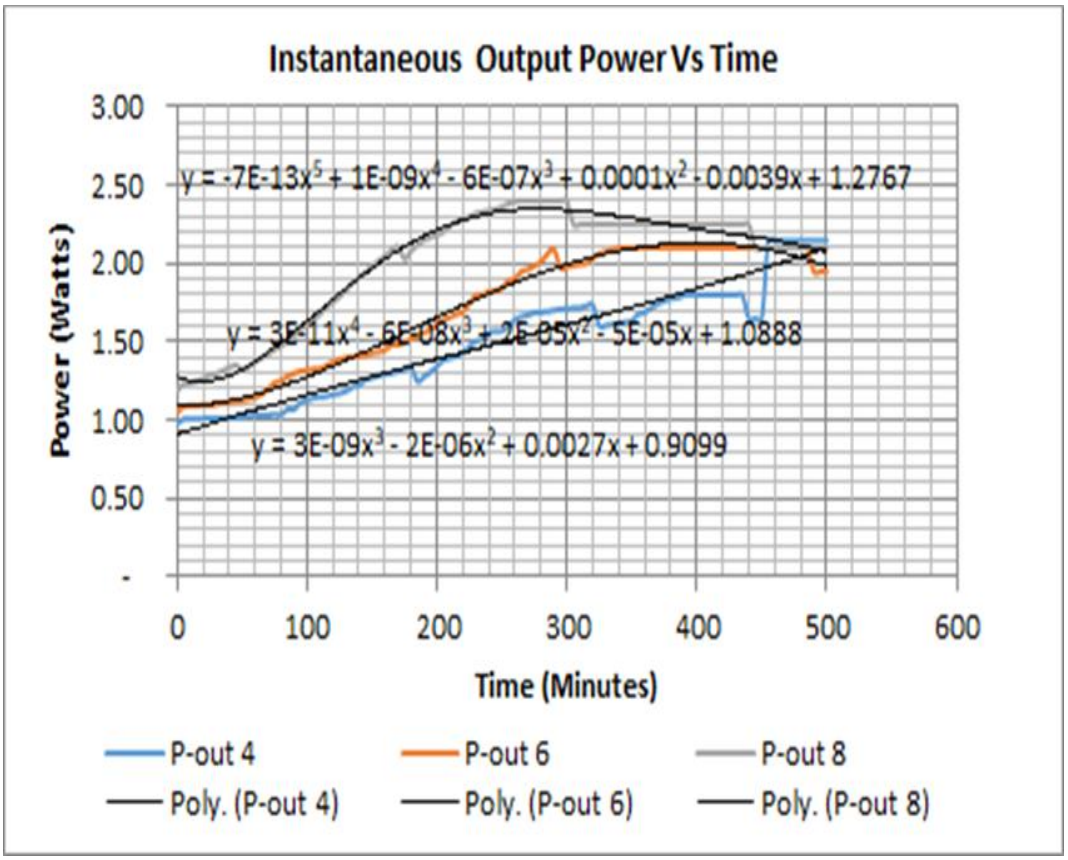

Figure 4-43: Instantaneous Output Power For 4, 6 And 8 Neodymium Magnets Monopole Energizer Model.

The profile for eight Neodymium MEMS further indicated that power output increased from 1.19 watts per hour to 2.10 watts per hour for 255 minutes. This implied that power increased at the rate of 0.214 watts per hour. Equation 4.78 in

Table 4-21 shows the general equation for power output at magnetic loading of 8. The input power profile showed that power decreased from 1.61 watts per hour to 1.52 watts per hour for 255 minutes. The power decelerated at 0.0235 watts per hour. Equation 4.73 in Table 4-20 shows the general equation for power input at magnetic loading of 8. Figure 4.44 shows the power profiles for input behavior for 4,6 and 8 Neodymium magnets.

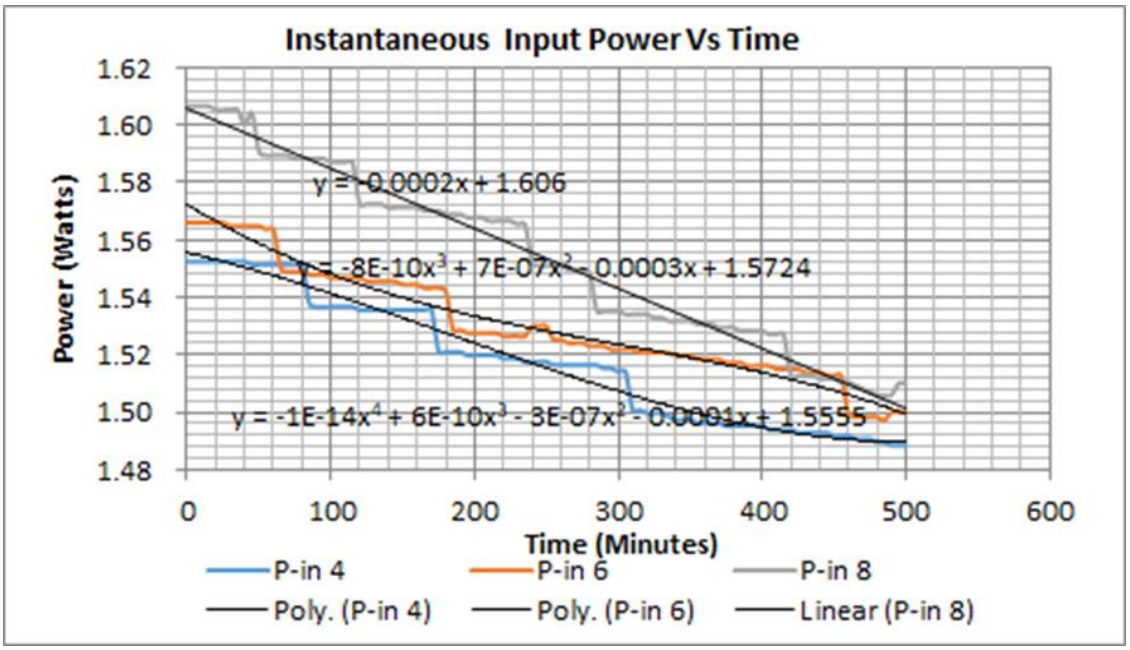

Figure 4-44: Instantaneous Input Power For 4, 6 and 8 Neodymium Magnets Monopole Energizer Model.

4.9.2 Characteristic of power input and output of monopole energizer experiments for over eight Neodymium Magnets

Besides the above results, it was noted that power output and input was done at a magnetic loading of 10 and 12. Figure 4-45 demonstrates the behavior of power input during experimental runs for 10 and 12 monopole Neodymium magnets design.

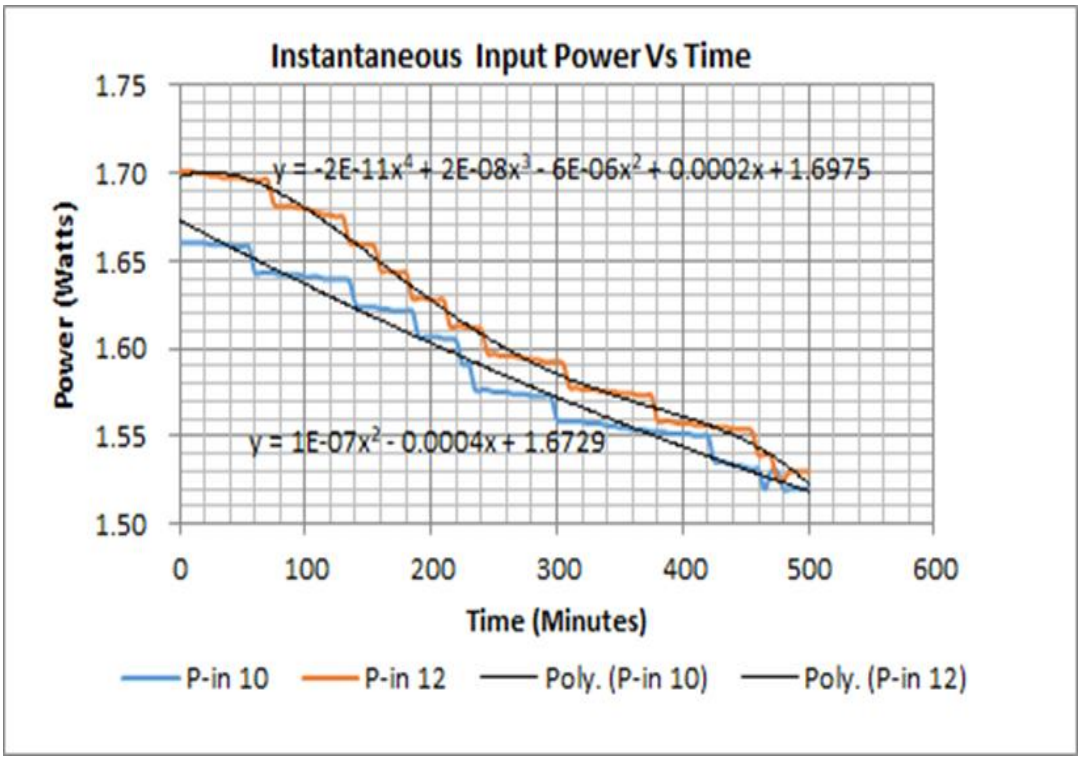

Figure 4-45: Instantaneous Input Power For 10 And 12 Neodymium Magnets Monopole Energizer Model.

Besides the above results, it was noted that for ten and twelve magnetic the that input power reduced at the rate of 0.0455 and 0.073 per hour for magnetic loadings of 10 and 12 respectively. The output power increased at the rate of 0.22 and 0.393 watts per hour for magnetic loadings of 10 and 12 respectively. Equation 4.74 and 4.75 in Table 4-20 shows the general equation for power input at magnetic loading of 10 and 12 respectively. Whereas Equation 4.79 and 4.80 in table 4.21 shows the general equation for power output at magnetic loading of 10 and 12.

In the case of 14 and 16 magnetic loadings, it was observed that input power reduced at the rate of 0.073 and 0.074 watts per hour respectively. It was further observed that output power increased at the rate of 0.44 watts per hour and 0.491 watts per hour for 14 and 16 magnetic loadings respectively. Equation 4.80 and 4.81 in

Table 4-21 shows the general equation for power output at magnetic loading of 14 and 16. Figures 4-46 shows power output behavior for 14 and 16 magnetic loading, the power curves took a bell shape formation

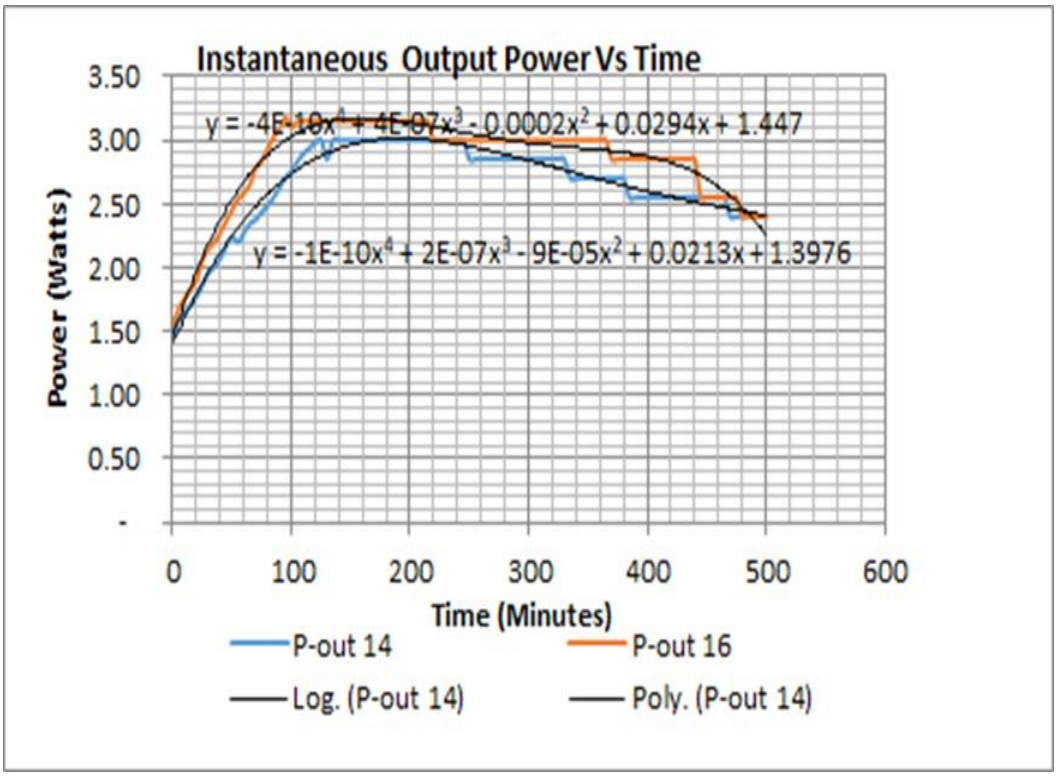

Figure 4-46: Instantaneous Output Power For 14 and 16 Neodymium Magnets Monopole Energizer Model.

4.10 Comparison Of Input and Output Parameters for Replication Design

4.10.1 Voltage Comparison Characteristics

Just like the case of original designs with Ceramic magnets, it was established that there was consistency in behavior of replication Neodymium designs electrical input and output characteristics. It was established that voltage profiles at different levels of loading the input voltages decreased linearly at the loading of 4,6 and 8 Neodymium magnets, the profile showed linear increment in the three cases, however the rate of increase for the case of 8 magnets loading was higher than the four and six magnets loading. Figure 4.47 shows comparison of Instantaneous input and output voltages versus time for 4, 6 and 8 Neodymium magnets monopole energizer models. The output voltage had a positive gradient which increased with magnetic loading.

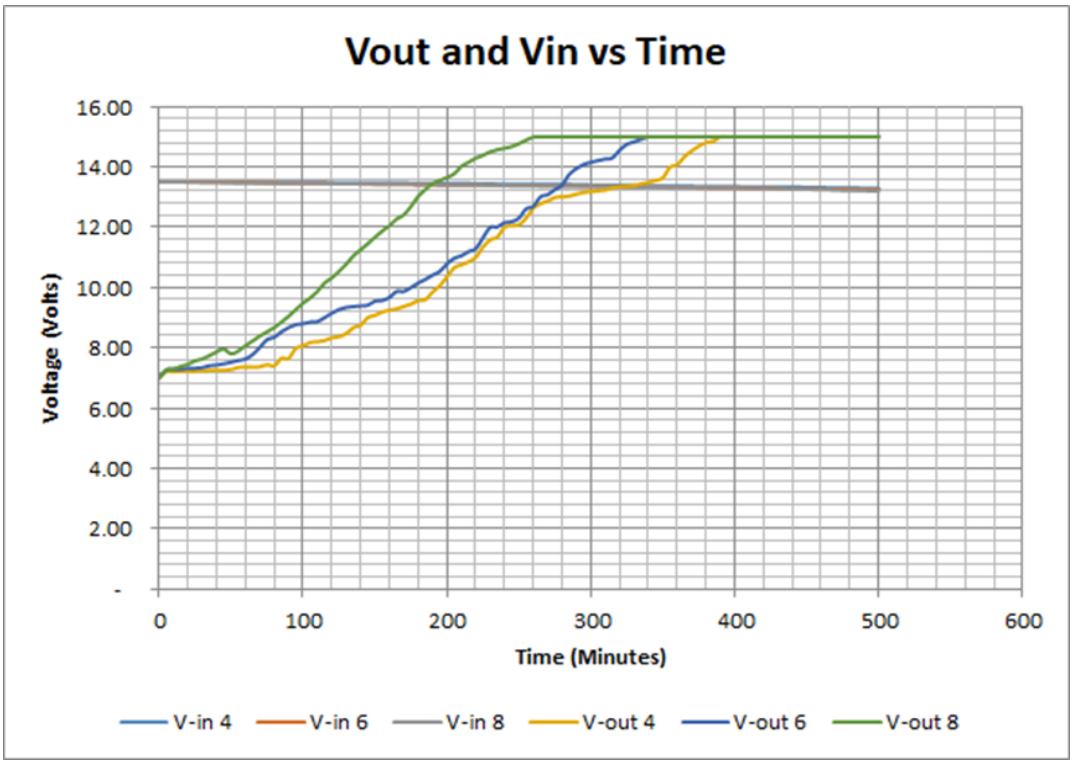

Figure 4-47: Comparison of Instantaneous Input and Output Voltages Versus Time For 4, 6 and 8 Neodymium Magnets Monopole Energizer Models.

The rate of input voltage decreased with magnetic loadings across the board and it had had a negative slope. The input voltage never flattened across the board but it continued dropping even as the magnetic loadings increased.

It was generally observed that when input voltages and output voltages were compared, the output voltages were found to be higher and were increasing linearly. For example, taking the case of replication designs with 4, 6 and 8 neodymium magnets, the output voltage charging rates were found to be 1.25 volts per hour, 1.43 volts per hour and 1.9 volts per hour respectively. When these were compared with discharging rates of primary battery or taking it as input voltage was found to be 0.033 volts per hour,0.038 volts per hour and 0.049 volts per hour for 4,6and 8 Neodymium magnets replication designs respectively. When output and input voltages charging and discharging rates were compared, it was established that the output charging rates for 4,6 and 8 replication designs were 4.3.3.50 and 3.88 times the input charging rates respectively.

The observation made from the graph, showed that the voltage output graphs were linear from the onset of the experimental run and after sometimes they attained a flat

level. It was further observed that the graphs become steeper and reached a flat margin with the increase in number of Neodymium magnets. In the case of input voltage, the voltage values remained fairly constant. It was further observed that the output –input ratio for voltage profiles were greater than one.

In undertaking the analysis of replication design, it was deduced that it took 385 and 335 minutes to attain a plateau level for 4 and 6 magnetic loading respectively. For eight magnetic loading it took 255 minutes to attain the flat level. This behavior remained consistent even at a high magnetic loading. Figures 4.48 shows the comparison behavior of input and output voltage for magnetic loadings at 10 and 12 whereas

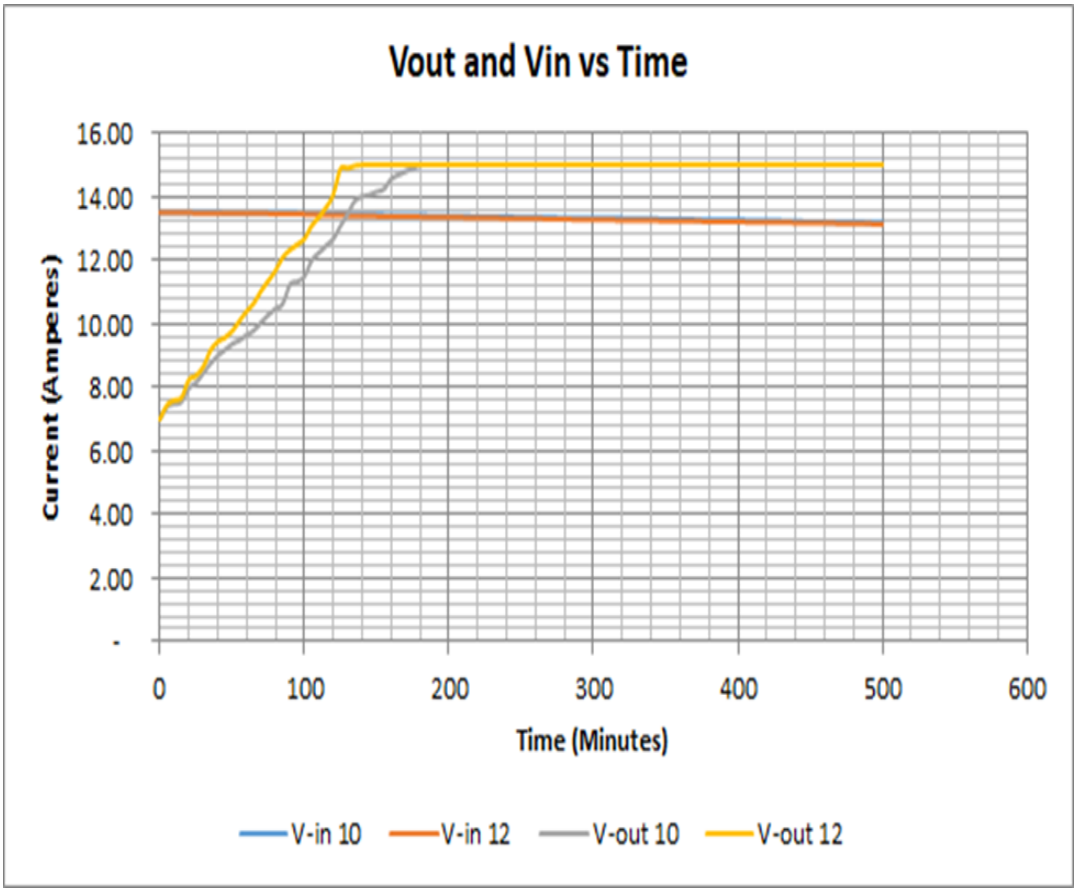

Figure 4-48: Comparison of Instantaneous Input and Output Voltages Versus Time for 10 and 12 Neodymium Magnets Monopole Energizer Models.

The rate of attaining plateau level shortened with the increase in magnetic loading. In case of magnetic loading of 10 and 12 it took 215 and 205 minutes to attain the plateau level respectively. At a higher magnetic loading the time to attain plateau

level continued shortening. In the case of 14 magnetic loading level, it took about 140 minutes whereas in the case of 16 magnetic loading level it about 100 minutes to attain a plateau level. In the case of input voltage, the voltage values remained fairly constant. The voltage values were about 13.5 regardless of the loading of neodymium on monopole energizer model. It was further observed that the output – input ratio for voltage profiles was greater than one. Figure 4.49 shows comparison characteristics of input and out voltage characteristics at the magnetic loading of 14 and 16

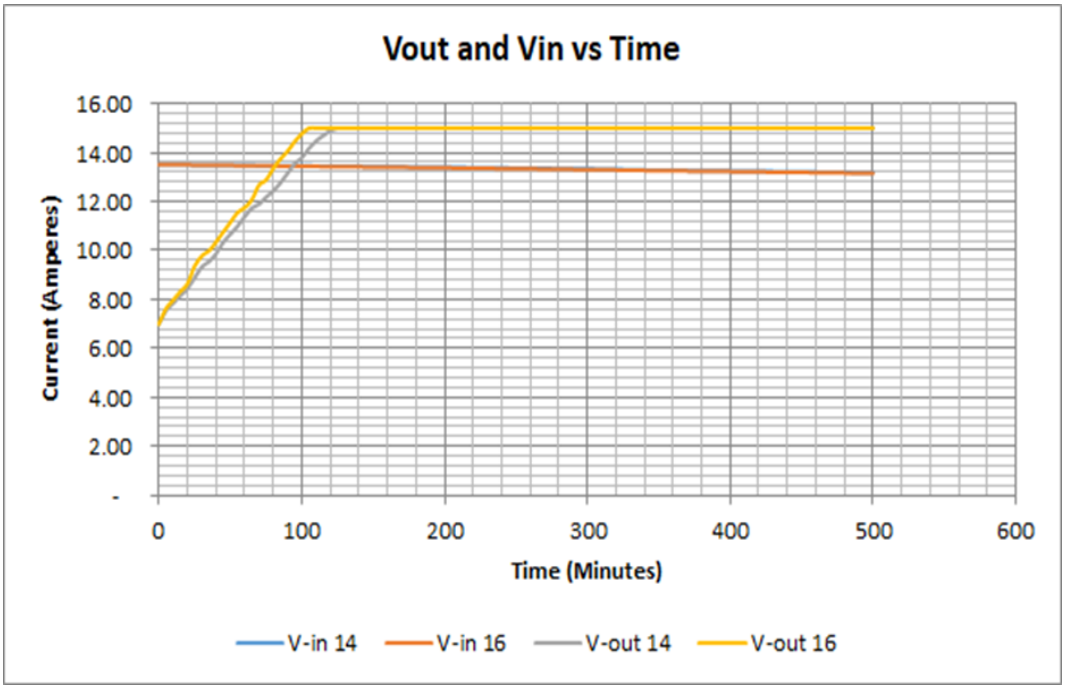

Figure 4-49: Comparison of Instantaneous Input and Output Voltages Versus Time for 14 and 16 Neodymium Magnets Monopole Energizer Models.

4.10.2 Current Comparison Characteristics

Figure 4-50 shows comparison characteristics of load and input current at the magnetic loadings of 4,6 and 8. Similar observation was made with current profiles. Generally, the loading currents profiles were found to be marginally higher than the input current profiles. Both load and input currents marginally increased with increase in loading of monopole energizer models with neodymium magnets as well. The loading current figures were marginally higher than current figures in all cases both loading currents and input currents had a negative slope, implying that both loading and input currents reduced linearly with time, even though loading currents profile graphs were steeper than input current profile graphs.

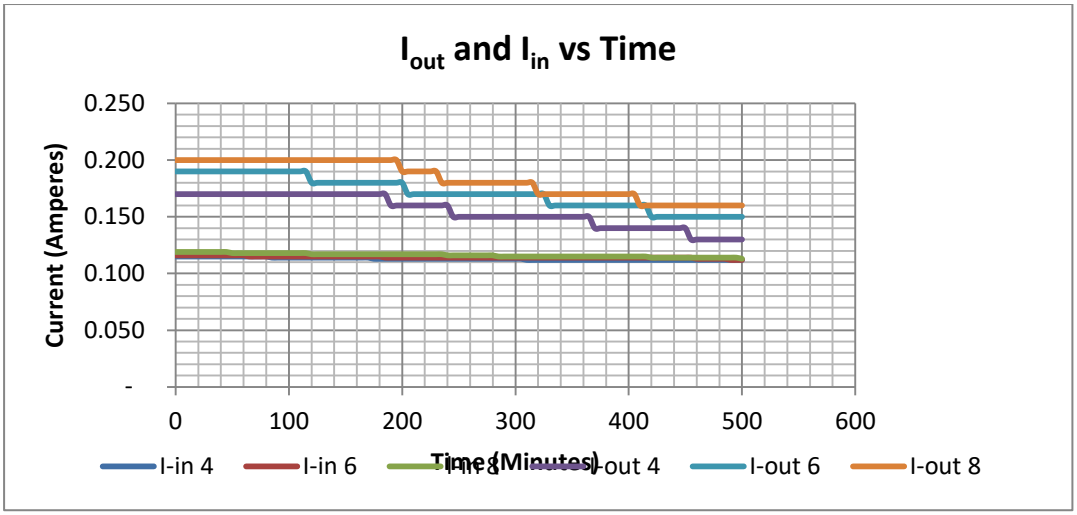

Figure 4-50: Comparison of Instantaneous Input and Load Current Currents Versus Time for 4, 6 and 8 Neodymium Magnets Monopole Energizer Models.

Similar observations were made for input and output power profiles. It was noted that the output power profile figures were found to be higher than those of the input power profile figures. This implied that the co-efficiency of the system in relation to output - input power ratio was greater than one or greater than 100%.

4.10.3 Comparison of Coefficiecies Of Performance At Magnetic Loadings of 4,6 And 8

In computing the co-efficiencies of monopole energizer model using Neodymium magnets, the emphasis was put on power or energy output compared with energy input. The co-efficiencies of monopole energizer model fitted with various numbers of Neodymium magnets ranging from 4 magnets to 16 magnets were computed. The co-efficiency was computed as the ratio of energy output to energy input.. Thus, co-efficiency was computed as

$$\boldsymbol{n = \frac{Energy\ output}{Energy\ input} = \frac{V_O I_O t_O}{V_i I_i t_i} = \frac{E_o}{E_i}} \quad \text{(4-1)}$$

Where

$\eta$is the efficiency,

$E_0$is energy output,

E_i is energy input,

v_o voltage output,

I_0current output,

t_o time associated with output parameters.

V_i voltage input,

I_i current input,

t_i time associated with input parameters

Using the above formula of monopole energizer models fitted with various magnets co-efficiencies were computed. The graph of co-efficiencies of monopole energizer model fitted with varying numbers of Neodymium magnets was plotted. The graph showing the variation of co-efficiencies with the number of Neodymium magnets is also shown below on Figure 4.51. co-efficient of performance was based on energy accumulation in the battery being charged with respect to the charging Batteries.

In the case of replication design, the COP for 4 Neodymium magnet monopole energizer model was 1.01 or 101%, whereas that of 16 Neodymium magnet monopole energizer model was 1.412 or 141.2%. Table4.23 illustrate these results.

Table 4-22: Effect of Number of Neodymium Magnets on COP of Replication Design

Level of Neodymium magnetic loading	Average COP	Input Joules Calculation				Output Joules Calculation			
		Average Input Current (A)	Average Input Voltage	Charge Time in Secs	Input Joules	Average Load Current (A)	Average Output, V	Discharge Time in Sec	Output Joules
4	1.01	0.114	13.42	23400	35458.722	0.13	10.50	23400	35799.192
6	1.09	0.115	13.42	2040	3148.332	0.16	10.49	2040	3423.936
8	1.19	0.117	13.43	16200	25455.222	0.17	10.98	16200	30238.92
10	1.24	0.122	13.45	11100	18213.99	0.18	11.31	11100	22597.38
12	1.244	0.125	13.45	8400	14122.5	0.19	11.01	8400	17571.96
14	1.31	0.129	13.47	7500	13032.225	0.20	11.34	7500	17010
16	1.412	0.130	13.47	6600	11557.26	0.22	11.24	6600	16320.48

When the profile of instantaneous co-efficiency of 4, 6 and 8 neodymium magnets monopole energizer models were plotted against time, it was established that the graphs showed the bell graph. This is the typical behavior of the power graph.

When the graph of four ceramic magnets monopole energizer was plotted, the graph showed that the instantaneous co-efficiency ranged between 63.12% at the starting of experimental run to 144.44% at the end of experimental run after 490 minutes. This was also the highest instantaneous co-efficiency recorded in the case of 4 neodymium magnet model. In the case of 6 neodymium magnet the highest co-efficiency recorded was 140.26% at 485 minutes. Similarly, the co-efficiency recorded from the onset of experiment was 67.05% and the co-efficiency reached at the end of experimental run was 130% after 490 minutes. In the case of 8 neodymium magnets the instantaneous co-efficiency ranged from 74.07% at the initialization of the experiment to 139.07% at the end of experimental run that is after 490 minutes. The highest instantaneous co-efficiency recorded was 156.33% after 285, 290, 295 and 300 minutes respectively. Figure 4.51show the behavior of instantaneous co-efficiencies 4, 6, and 8 neodymium monopole energizer models.

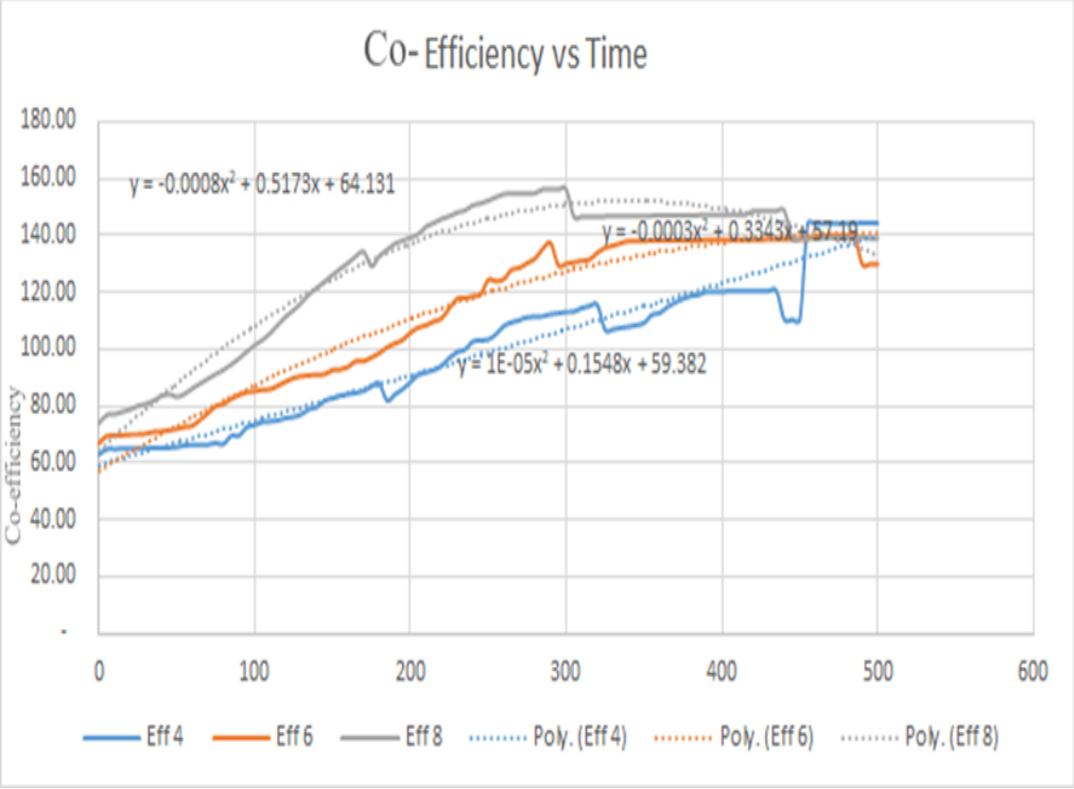

Figure 4-51: Instantaneous Co-efficiency Versus Time For 4, 6 and 8 Neodymium Magnets Monopole Energizer Model.

Table 4-23: Range and Time Range of Instantaneous Efficiency for Replication Design

Item No.	No. of Magnets	Range of Instantaneous Efficiency (%)	Time range at which it occurs (between 0 minutes and xx minutes
1	4	63.12 - 144.4	0 and 490
2	6	67.05 – 130	0 and 490
3	8	74.07 - 139.07	0 and 490
4	10	75.88- 128.29	0 and 500
5	12	78.19 -147.07	0 and 485
6	14	84 - 148.04	0 and 490
7	16	87.75- 147.19	0 and 490

4.10.4 Comparison of Coefficiecies of Performance at Magnetic Loadings of Over 8

The experiments further established that for ten ceramic magnets monopole energizer model it was established that the highest co-efficiency recorded was 162% at 270 and 275 minutes respectively. Whereas in the case of twelve Neodymium magnets monopole energizer model the instantaneous co-efficiencies ranged between 78.19% corresponding to zero time and 147.07 % corresponding to end point of the experimental run after 485 minutes. Figure 4-52 gives more information on instantaneous co-efficiencies for ten and twelve magnetic loadings.

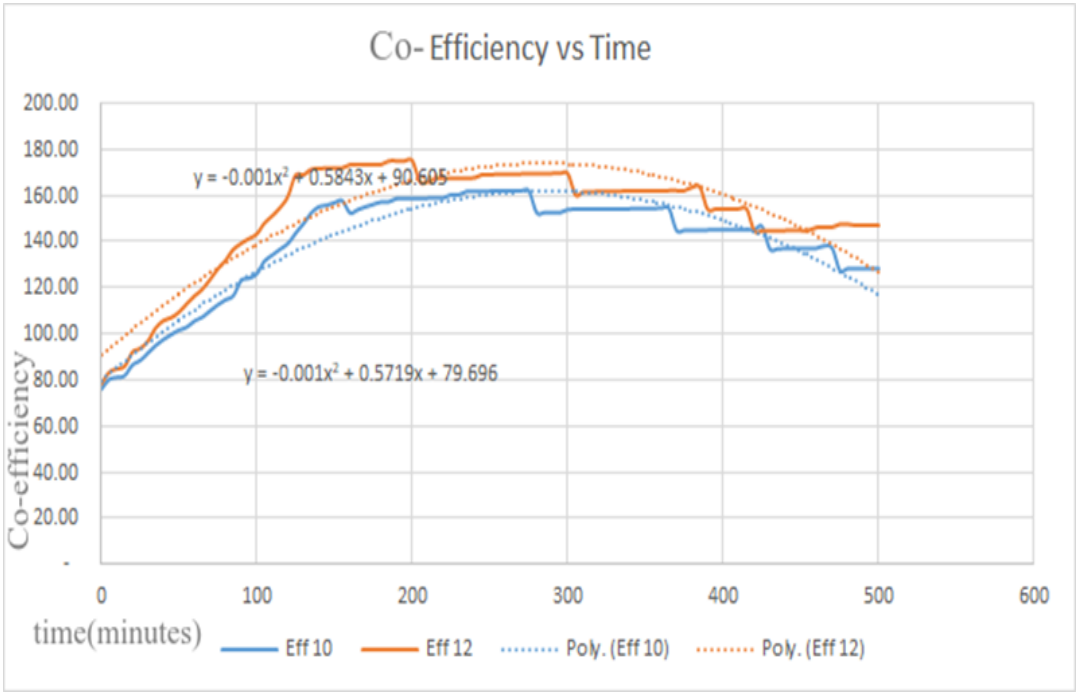

Figure 4-52: Instantaneous Co-efficiency Versus Time for 10 and 12 Neodymium Magnets Monopole Energizer Model.

The experiments further established that for the case of 14 neodymium magnet monopole energizer models, the instantaneous co-efficiencies ranged from 84 at the initialization of experiment ran and 148.04% after 490 minutes at the end of the run. Figure 4-53gives instantaneous co-efficiencies for 14 and 16 neodymium magnetic loadings.

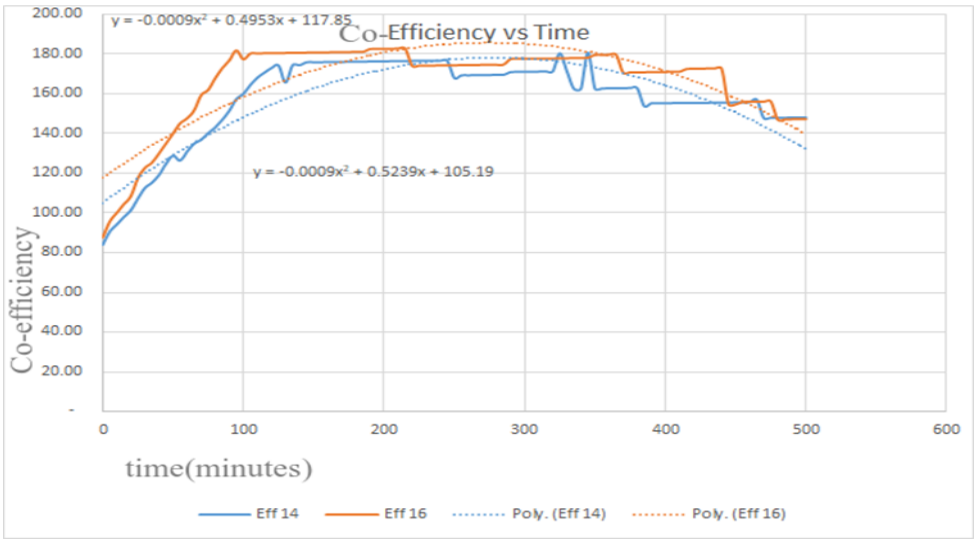

Figure 4-53: Instantaneous Co-efficiency For 14 And 16 Neodymium Magnets Monopole Energizer Model.

Table 4-24: Replication Design Variation of Peak Co-efficiencies with Time in Minutes

Level of Neodymium magnetic loading.	Peak co-efficiency Recorded	Time taken in minutes to reach it
4	144.44	490
6	140.26	485
8	156.33	285,290,295 and 300
10	162	270 and 275
12	175.12	200
14	162.5	260
16	182.27	210 and 215

When the graph of peak co-efficiencies of various Neodymium magnets was plotted against time, it was further concluded that peak co-efficiencies increased with the increase in the number of Neodymium magnets.The lowest co-efficiencies recorded were for 4 and 6 neodymium magnets and at 144.44 % at 490 minutes and at 140.26% at 485 minutes respectively. The highest peak co-efficiency recorded was182.77% after 210 and 215 minutes of experimental run. The peak co-efficiency recorded was for 16 Neodymium magnets monopole energizer model.

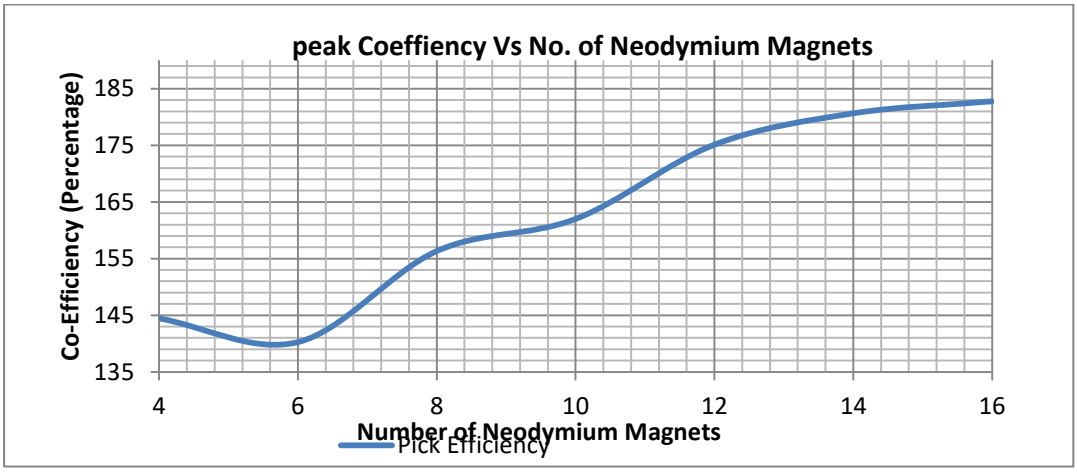

Figure 4-54: Peak Co-efficiency Vs Number of Neodymium Magnets for Monopole Energizer Model.

The graph of co-efficiencies of monopole energizer model fitted with varying numbers of Neodymium magnets was plotted. The graph showing the variation of co-efficiencies with the number of neodymium magnets is also illustrated by Figure 4-55. From this figure, it was observed that the co efficiency of Monopole Energizer Model increased with increasing number of magnets fixed on the rotor. From the experiments it was established that the co-efficiency increased linearly. The graphs show that the average co-efficiency increased linearly from 98.8% when 4 neodymium magnets were used to 167.9% compared to when 16 Neodymium magnets were used. The figure below shows the profile of average co-efficiency of monopole energizer model with Neodymium magnets.

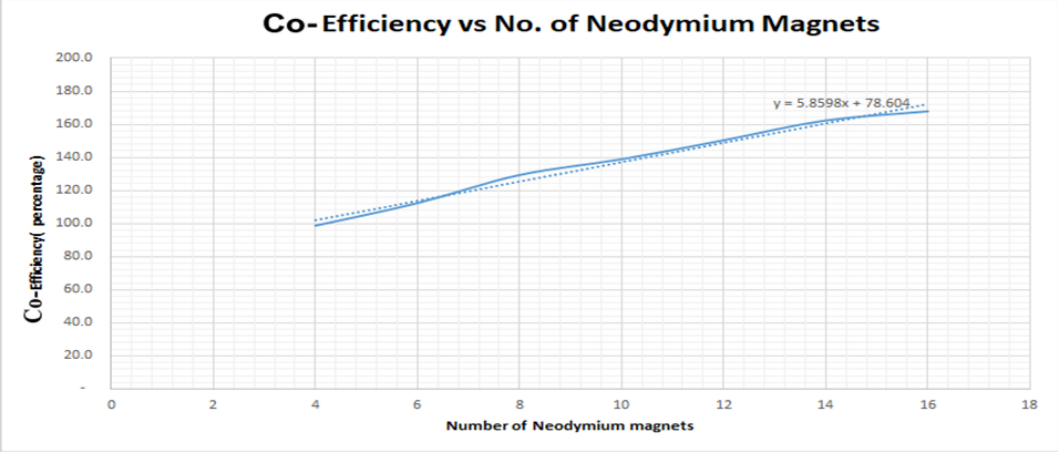

Figure 4-55: Average Efficiency Vs Number of Neodymium Magnets for Monopole Energizer model

4.11 Comparative Analysis of Two MEM

In this section the comparison between monopole energizer model for ceramic and neodymium magnets electrical characteristics was done. The performance parameters compared were based on evaluation of performance between the two design models Parameters compared here were mainly input and output voltages, input and load currents, input and output power and various coefficient of performance under considerations.

4.11.1 Comparison Of Charging Rates And Charging Ratios Of Ceramic Mem Design And Neodymium Mem Design

Analysis on charging and discharging rates was undertaken on Neodymium and ceramic MEM designs. It was observed that in both cases the charging rates of the

two designs increased with magnetic loadings. When the charging rates for Neodymium magnets MEM design and ceramic magnet MEM design were compared it was established that the rate of changing for neodymium magnets design was higher than that of ceramic magnets MEM designs. From table 4.26 it was established that the rate of charging of replication design MEM design was 1.2,1.32,1.61,2.65 and 3 times that of ceramic MEM design at magnetic loadings of 4,6,8,10 and 12 magnetic loadings respectively. This investigation further established that the charging rate of replication design was 3.44 and 2.2 times that of ceramic design at the level of magnetic loadings of 14 and 16 magnetic loadings respectively. Charging rate implied the rate at which MEM gains voltage during the charging process

Table 4-25: Charging Rates Ratio for Neodymium MEM Charging Rate to Ceramic MEM Charging Rate

Item no.	Magnetic Loading	Ceramic, MEM Charging rate	Neodymium MEM Charging rate	Ratio of Neodymium MEM charging rate to Ceramic MEM Charging rate
1	4	1.04	1.25	1.2
2	6	1.08	1.43	1.32
3	8	1.18	1.9	1.61
4	10	1.455	3.85	2.65
5	12	1.52	4.57	3
6	14	1.575	3.85	3.44
7	16	2.1	4.57	2.2

It was further established that the slope for neodymium monopole energizer machine was steeper than that of ceramic magnet monopole energizer design. Figure 4.56 shows the charging rates of the two designs at different levels of magnetic loadings. It was observed that the charging rate for replication design was rapid and steeper than that of original design across all levels of magnetic loadings.

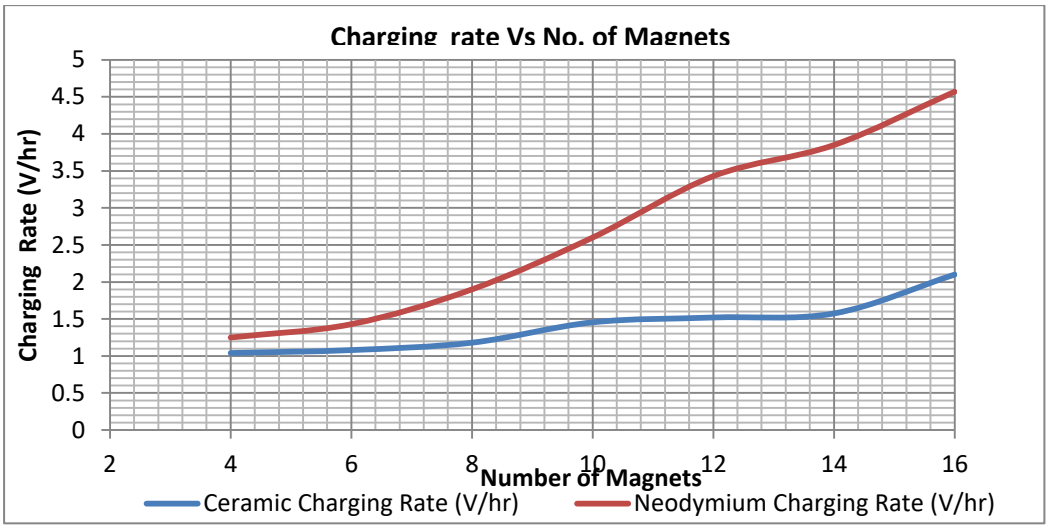

Figure 4-56: Comparison of Charging Rate for Ceramic and Neodymium Magnets Monopole Energizer Model.

4.12 Comparison of Discharging Rates for Ceramic Mem Design and Neodymium MEM Design

The discharging rates of ceramic and neodymium magnets monopole energizer were compared. Figure 4-57shows discharging rates for original and replication designs at various levels of loading. Comparing the discharging rates of the two designs, it was established that the rate of discharging for neodymium magnets was found to be higher than that of Ceramic magnets.

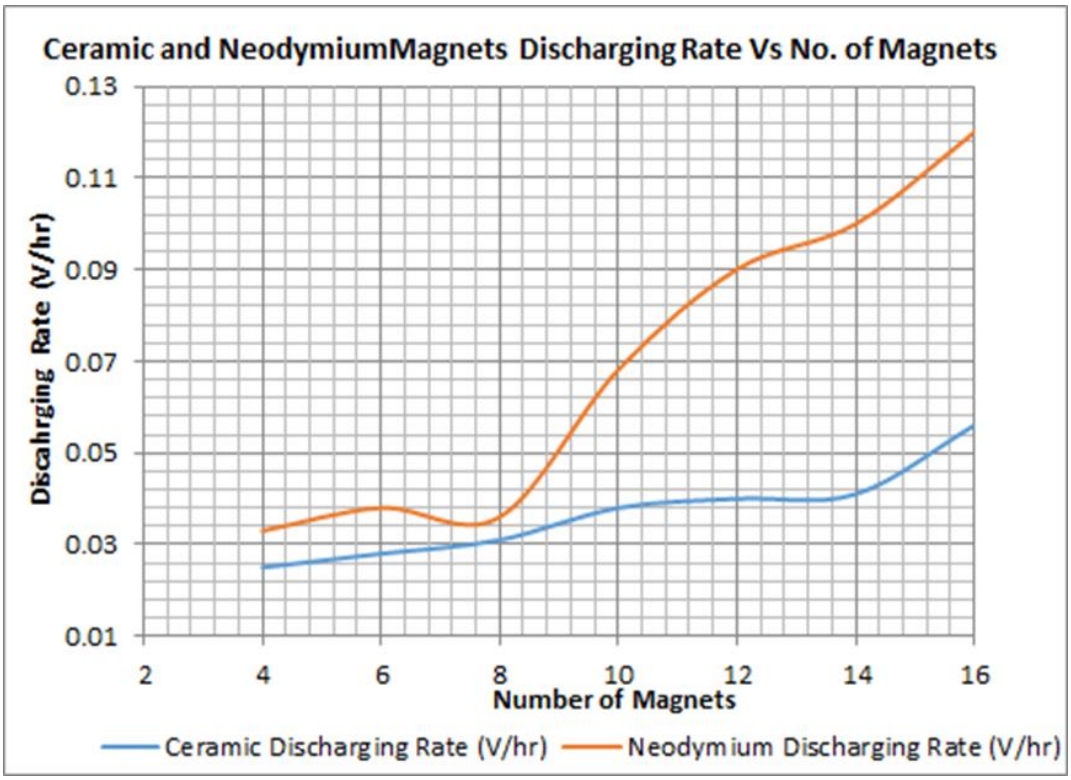

Figure 4-57: Comparison of Discharging Rate for Ceramic and Neodymium Magnets Monopole Energizer Models.

From table 4-26 it was deduced that the discharging rate for Neodymium magnet MEM design was 2.2, 1.4, 1.6, 1.2, 2.2, 2.7 and 2.14 times higher than ceramic magnets MEM designs at magnetic loadings of 4, 6, 8,10,12,14 and 16 magnetic loadings respectively. Figure 4.57 shows the ceramic neodymium magnets discharging rates verses the level of magnetic loadings, whereas table 4.27 shows dis-charging rates ratio for neodymium MEM design to that of dis-Charging rates of ceramic MEM design across all levels of magnetic loadings.

Table 4-26:Dis-Charging Rates Ratios of Neodymium MEM Design to That of Ceramic MEM Design.

Item no.	Magnetic Loading	Ceramic, MEM discharging rate	Neodymium MEM Discharging rate	Ratio of Neodymium MEM discharging rate to Ceramic
1	4	0.0151	0.033	2.2
2	6	0.028	0.038	1.4
3	8	0.031	0.049	1.6
4	10	0.048	0.056	1.2
5	12	0.0214	0.0585	2.7
6	14	0.041	0.11	2.7
7	16	0.056	0.12	2.14

4.13 Comparison of Input and Output Paramaters of Ceramic Mem Design and Neodymium Mem Design

4.13.1 Comparison of Loading and Input Current Rates and Ratios of Ceramic MEM Design and Neodymium MEM Design

This investigation established that when the load current for neodymium MEM design was compared with that of ceramic magnet MEM design, the load current for neodymium was found to be 0.37,0.25 and 0.5 times that of ceramic MEM design for magnetic loadings of 4, 6 and 8 respectively. This investigation further established that the load current for neodymium MEM design was 1.25, 1.14, 1.71 and 2.13 times that of Ceramic Magnet MEM design for magnetic loadings of 10, 12,14 and 16 respectively. Table 4.28 below shows Loading Current rates ratios between neodymium MEM and Ceramic MEM.

Further analysis for the Ratio of Neodymium MEM input current to Ceramic MEM Input current rate showed that with exception of magnetic loadings of 6 and 8 where the ratio was 1.33 and 1, the ratio of all the other levels of magnetic loadings were less than 1. Table 4-27 shows input current rates ratio for neodymium MEM design to ceramic MEM design. Similarly, Table 4-28 shows input current rates ratio for neodymium MEM Current Rate to Ceramic MEM current rate.

Table 4-27: Loading current rates ratio for Neodymium MEM current rate to ceramic MEM current rate

Item no.	Magnetic Loading	Ceramic, MEM Load current rate	Neodymium MEM Load current rate	Ratio of Neodymium MEM load current to Ceramic MEM load current
1	4	0.0128	0.0047	0.37
2	6	0.0142	0.0036	0.25
3	8	0.014	0.0071	0.5
4	10	0.013	0-0162	1.25
5	12	0.015	0.0172	1.14
6	14	0.014	0.024	1.71
7	16	0.016	0.034	2.13

Table 4-28:Input Current Rates Ratio for Neodymium MEM Current Rate to Ceramic MEM current rate

Item no.	Magnetic Loading	Ceramic, MEM Input current rate	Neodymium MEM Input current rate	Ratio of Neodymium MEM input current to Ceramic MEM Input current rate
1	4	0.0055	0.0047	0.85
2	6	0.0054	0.0072	1.33
3	8	0.0097	0.0097	1
4	10	0.0075	0.0014	0.2
5	12	0.0086	0.0043	0.5
6	14	0.091	0.0029	0.03
7	16	0.096	0.0034	0.04

4.13.2 Comparison of Output and Input Power Rates and Ratios of Ceramic MEM Design and Neodymium MEM Design

The analysis for the ratio of neodymium MEM output power to ceramic MEM output power showed that with exception of magnetic loadings of 6 and 12 where the ratio was 0.5. The ratio of power output for Neodymium design to that of Ceramic Magnet MEM design was 1.33 and 1, the ratio of all the other levels of magnetic loadings was greater than or equal to 1.9. The highest ratio was at the magnetic loading level of 8. Table 4-30 shows Output Power Rates Ratio for Neodymium MEM Power rate to ceramic MEM Power rate

The investigation established further that the ratio of Neodymium MEM input power rate to ceramic MEM Input power rate was less than one up to the magnetic loadings of 10.This ratio increased with magnetic loading and the maximum ratio was recorded at the magnetic loading of 14, and the registered ratio was 1.1.After the magnetic loadings of 14 the ratio started dropping. Table 4-29 shows input Power rates ratio for neodymium MEM Power rate to ceramic MEM.

Table 4-29: Output Power Rates Ratio for Neodymium MEM Power Rate to Ceramic MEM Power Rate

Item no.	Magnetic Loading	Ceramic, MEM output power rate	Neodymium MEM output power rate	Ratio of output /input power rate
1	4	0.023	0.181	1.9
2	6	0.342	0.161	0.5
3	8	0.0074	0.214	28.9
4	10	0.04	0.22	5.5
5	12	0.95	0.395	0.5
6	14	0.069	0.44	6.41
7	16	0.168	0.491	2.9

Table 4-30:Input Power Rates Ratio for Neodymium MEM Power Rate to Ceramic MEM Power Rate

Item no.	Magnetic Loading	Ceramic, MEM input power rate	Neodymium MEM input power rate	Ratio of Neodymium MEM input power rate to Ceramic MEM Input power rate
1	4	0.077	0.0093	0.12
2	6	0.077	0.0125	0.16
3	8	0.0544	0.0235	0.43
4	10	0.0673	0.0455	0.73
5	12	0.0705	0.073	1.03
6	14	0.067	0.073	1.1
7	16	0.085	0.074	0.87

4.13.3 Comparison of Instantaneous and Peak Co-efficiencies of Ceramic and Neodymium Magnets Monopole Machine Models.

Figure 4-58 shows the comparison of peak co-efficiencies of both ceramic and neodymium magnets monopole energizer experiments. The investigation showed that the peak co-efficiencies for both ceramic magnets and neodymium magnets increased with the increase in number of magnets used to run the model. It was generally observed that the peak co-efficiency figures for neodymium magnets were generally higher than those of ceramic magnets when co-efficiencies with the same number of magnetic loadings were compared. It was further established that when similar or same number of magnets were compared it generally took relatively shorter time to reach peak co-efficiency with neodymium magnets than ceramic magnets.

The investigations established that when instantaneous co- efficiencies for two types of magnets were compared it was established that the efficiencies for neodymium magnets were found to be higher than those of ceramic magnets at all levels. For

example, in the case of 4 ceramic magnet co-efficiencies ranged from 78% to 93% within a time line of 495 minutes. The peak values were found to be 117.41% for ceramic magnets and 144.44% for four neodymium magnets. Similar trends were observed for 12 magnets where it was found to be 138.57% after 310 minutes for ceramic magnets and for neodymium magnets it was found to be 175.12% after 200 minutes. For 16 ceramic magnets it was found to be 165.29 % and this happened after 240 minutes, whereas for 16 neodymium magnets it was 182.77% after 210 minutes.

This investigation further showed that the instantaneous co-efficiencies for neodymium Energizer models were generally higher than those for Ceramic magnet models with varying margin. For instance, the peak co-efficiency for neodymium magnet model was higher by 4%, whereas those of 16 magnets were higher than 32.3%. It was also observed that time taken to reach peak co-efficiencies was shorter in the case of neodymium magnets than ceramic energizer model with similar number of magnets.

The time interval became much less as the number of magnets increased. It was also observed that the peak co-efficiencies increased with increase in number of magnets in both cases even though the increase for neodymium magnets was more significant than the case of using Ceramic magnets models. The investigation further concluded that the time taken to reach peak co-efficiencies decreased with the increase in number of magnets being used in both cases even though it was higher in the case of Neodymium magnets than the case of Ceramic magnets Monopole Energizer Models. It was shown that the peak co-efficiency for 16 Neodymium magnet model was 182.77% and it took 210 minutes to reach it.

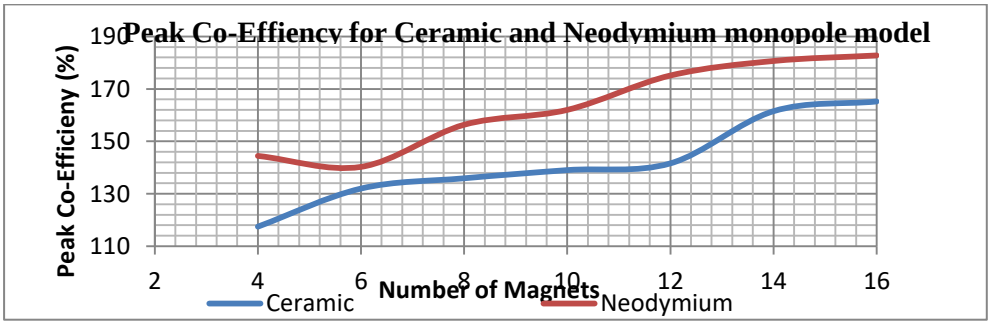

Figure 4-58: Comparison of Peak Co- Efficiencies for Ceramic and Neodymium Magnets for Monopole Energizer Model.

4.13.4 Comparison of Average Co-efficiencies for Ceramic and Neodymium Magnets.

Figures 4-59, and Figure 4-60 shows the comparison of average co-efficiencies of both ceramic and neodymium magnets monopole energizer experiments. The experiments showed that average co-efficiencies for neodymium magnets were higher than those of ceramic magnets across the board. It was also established that the average co-efficiency increased with the number of ceramic magnets and neodymium magnets, but the rate of increase was higher for those of replication designs than for the original design. The graph of co-efficiencies of monopole energizer model fitted with varying numbers of ceramic magnets was plotted.

Table 4-31: Average Co-Efficiencies for Ceramic and Neodymium Magnets.

No. of Magnets	Ceramic Average efficiency	Neodymium Average efficiency
4	94.8	98.8
6	103.9	112.5
8	110.5	129.4
10	116.3	138.9
12	117.4	150.4
14	128.9	162.4
16	135.6	167.9

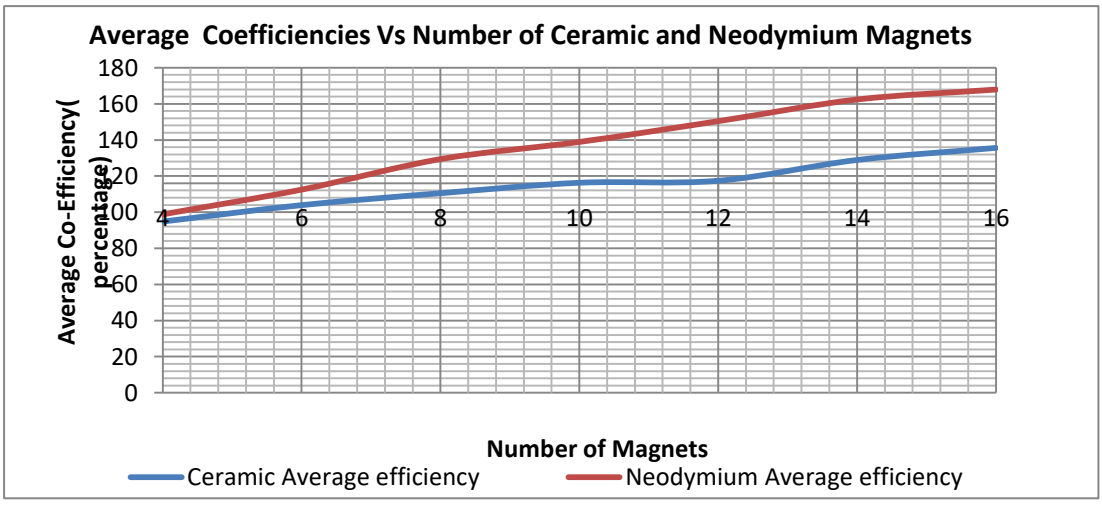

Figure 4-59: Average Co-efficiencies Versus Number of Ceramic Magnets and Neodymium Magnets Monopole Energizer Model.

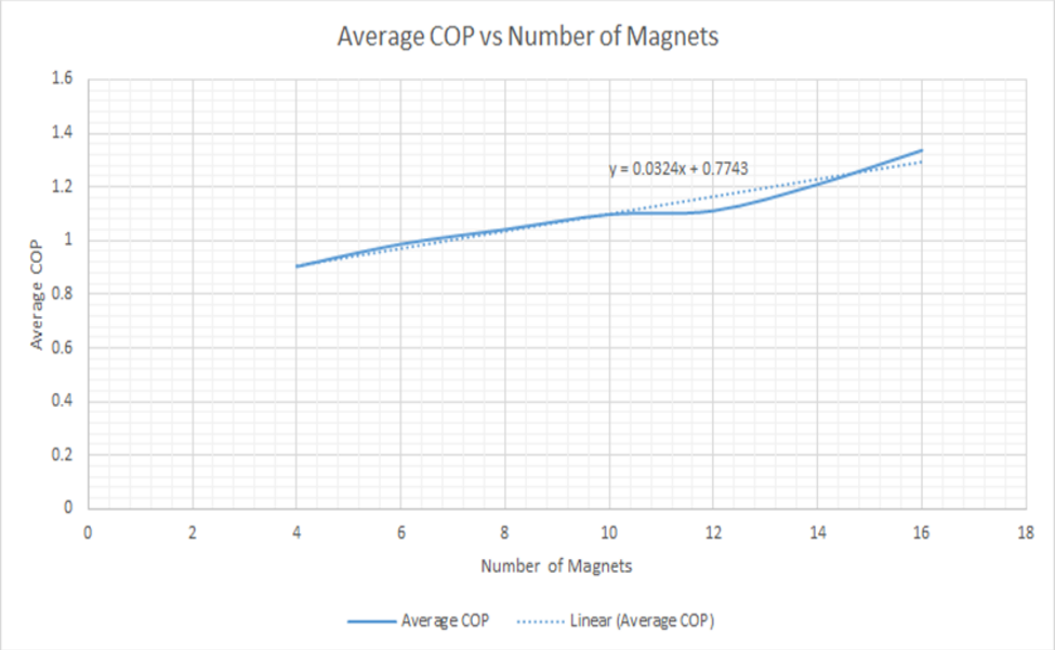

Figure 4-60: Average COP Versus Number of Magnets.

4.14 Comparison of Performance Between Mem with Neodymium Magnets at Different Magnetic Loading Levels

In this section the comparison between Monopole energizer model for Ceramic and Neodymium magnets was done. The performance parameters compared were based on evaluation of performance between two designs or models under consideration. Parameters compared here were mainly input and output current, average voltage, input and output (power) joules, Load current and charge time in seconds as input parameter and discharge time as output parameter. Based on this parameters coefficient of performance based on the two models was computed by using the following formula.

$$Output\ Joules\ (power) = Average\ Voltage(Output) \times output(Amps) \times Time(Seconds)$$

$$Input\ Joules = Average\ Voltage(Input) \times Input(Amps) \times Time(Seconds)$$

$$\boldsymbol{coefficient\ of\ Performance\ (COP) = \frac{Output\ Joules}{Input\ Joules}} \text{---------- (4-2)}$$

Table 4-32 shows the comparison of coefficient of performance of original design and replication design, the results showed that the coefficient of performance

associated with Neodymium magnets design was higher than that of ceramic magnet MEM across all levels of magnetic loadings. The results showed that co-efficiency of performance for replication design was more than 100% across board, whereas in the case of original design the COP was more than 100% for all levels of magnetic loadings except the loading level of 4 magnets. The rate of COP increase was high in both cases a cross all levels of magnetic loadings, but it was higher in the case of replication design.

Table 4-32 :Coefficient of Performance for Replication and Original Design

No of Ceramic Magnets	**Coefficient of Performance COP**	**No of Neodymium Magnets**	**Coefficient of Performance COP**
4	0.96	4	1.01
6	1.05	6	1.13
8	1.07	8	1.3
10	1.15	10	1.39
12	1.25	12	1.5
14	1.28	14	1.62
16	1.35	16	1.7

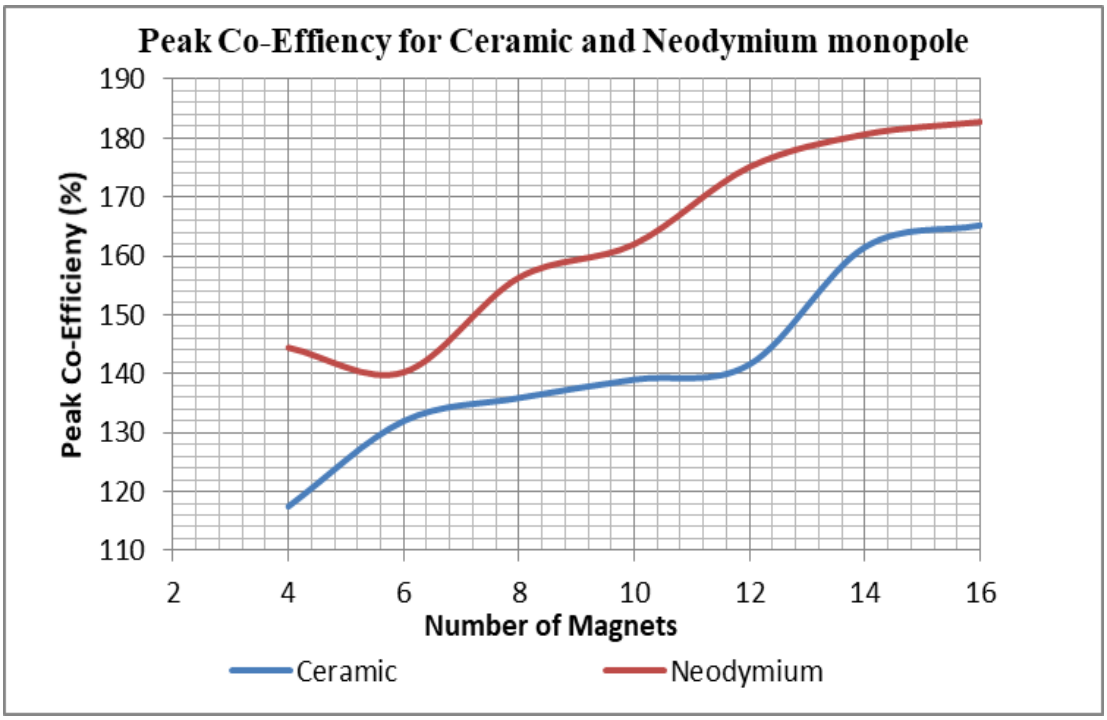

Figure 4-61: Comparison of Peak Co-Efficiency of Number of Ceramic and Neodymium Magnets for Monopole Energizer Model.

CHAPTER FIVE:
PREDICTIVE MATHEMATICAL MODELLING OF MEM SYSTEM AND STEADY STATE ANALYSIS

5. Predictive Mathematical Modelling of Mem System and Steady State Analysis

5.1 Coefficient of Performance Based on Model Equations and Experimental Results

The test procedure was also established to determine the Coefficient of Performance (COP) the original circuit running and charging battery design to compare this with the DC-DC boost converter design. The co-efficient of performance provides a measure of energy transfer, which is defined by the output as a proportion of the operator's input. Co-efficient of performance can be applied in the description of any machine, which derives additional inputs of energy from the surrounding environment. One example would be the use of COP to explain the details of the energy exchange which takes place in solar collectors or in heat pumps. Coefficient of performance contrasts with efficiency in that it can be assigned a value greater than one. Indeed, COP typically exceeds efficiency though would equal efficiency in cases where the input from environmental energy is reduced to zero (Sriphan *et al.*, 2018a).

$$\boldsymbol{CoP = \frac{P_{out}}{P_{in(operator)}}} \text{----------(5-1)}$$

Output equation

$$\boldsymbol{v_{out} = \frac{v_{in} - v_T\Delta - v_D(1-\Delta)}{L}} \text{----------(5-2)}$$

Measured Constants

$\Delta = 7\%$

$R = 4\ \Omega$

$L = 3$ H typical value is 0.3

$V_D = 0.7$ V

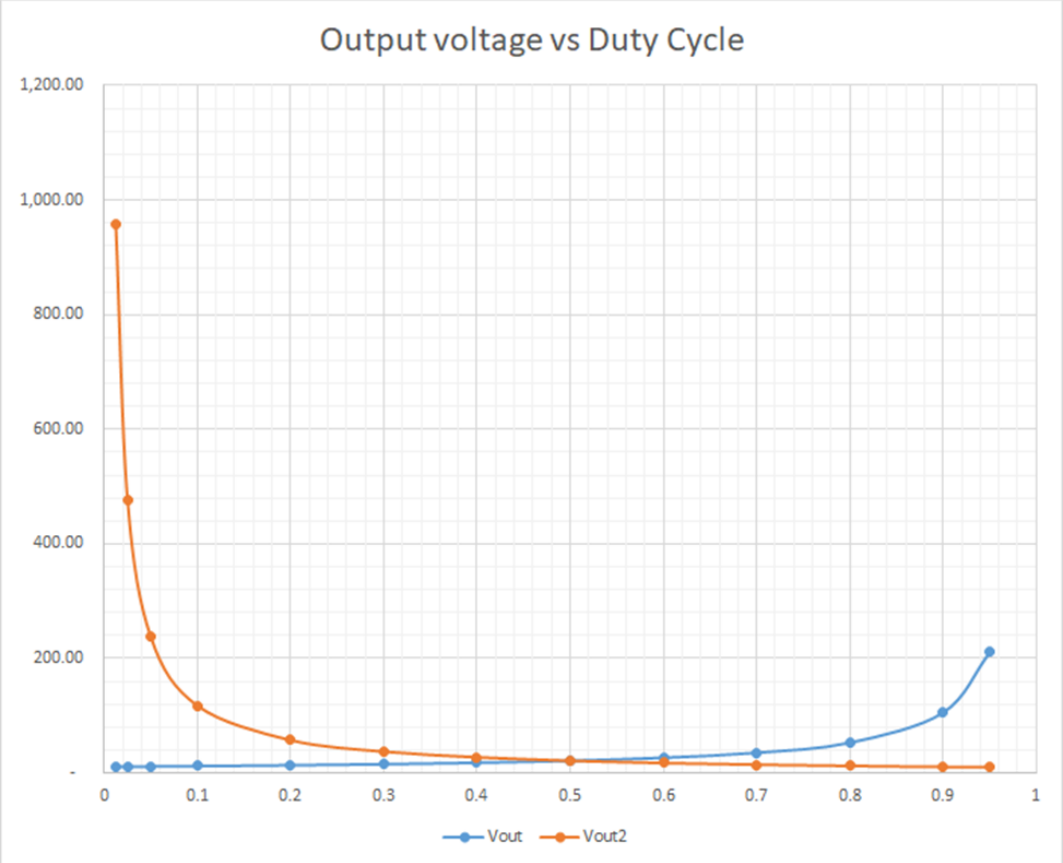

Figure 5-1: Duty Cycle.

$$V_{out} = \left(\frac{V_{in} - V_T \Delta}{(\Delta)}\right) - V_D \text{----------(5-3)}$$

Vout MEM

$$V_{out} = \left(\frac{V_{in} - V_T \Delta}{(\Delta)}\right) - V_D \text{---------- (5-4)}$$

$Vout_2$

Neglecting the voltage drops across the diode and the transistor,

that is, if $V_T = V_D = 0$,…… .(5-5)

then

$$V_{out} = \frac{V_{in} - V_T \Delta}{\Delta} - V_D \text{----------(5-6)}$$

$$\boldsymbol{V_{out}} = \frac{\boldsymbol{V_{in}} - \boldsymbol{0}.\Delta}{\Delta} \text{ ---------- (5-7)}$$

$$\boldsymbol{V_{out}} = \frac{\boldsymbol{V_{in}}}{\Delta} \text{ ---------- (5-8)}$$

$$\boldsymbol{V_{out}}(\Delta) = \boldsymbol{V_{in}} \text{ ---------- (5-9)}$$

$$\boldsymbol{V_{out}}\Delta = \boldsymbol{V_{in}} \text{ ---------- (5-10)}$$

$$\frac{\boldsymbol{V_{in}}}{\boldsymbol{V_{out}}} = \Delta \text{ ---------- (5-11)}$$

$$\Delta = \frac{\boldsymbol{V_{in}}}{\boldsymbol{V_{out}}} \text{ ---------- (5-12)}$$

The $duty$ cycle is defined as $\Delta = \frac{V_{in}}{V_{out}}$ for MEM

Where V_{in} is the input voltage and V_{out} is the load voltage?

The importance of this solution is to demonstrate that what determines the duty cycle for MEM is the ratio of input voltage to output voltage, contrary what happens in the case of generators and motors where the duty cycle is given as $\Delta = 1 - \frac{V_{in}}{V_{out}}$

5.2 Modelling of Mem Original Design Electrical Characteristics

In this section major focus was the development of mathematical model to predict the voltage output and current output of MEM. Since the power output is the product of current and voltage, this component was not modelled. This is because power is a dependent variable on the two electrical characteristics. Similarly, the coefficient of performance and the efficiency of performance as well are ratios and dependency variables, hence mathematical modelling was not developed.

5.2.1 Modeling of Time Function MEM Original Design Voltage Output Characteristics

As a consequence of these findings the model put into consideration the fact that the datum point for charging the battery was 7 volts. This was done to ensure that there was a common basis of recording and analyzing results. This was done to ensure harmony in data recording, monitoring and analysis. Secondly the model equation developed put in consideration experimental behavior in relation to parameters affecting voltage output. Key parameters considered were: - type of magnets, the number of magnets, charging rate or the rate at which the battery gained voltage

with time, all these parameters or variables were considered in formulating model equations.

The table below shows the voltage output equation in relation with the number of ceramic magnets associated with it. In determining the voltage output equation, MEM Ceramic magnet loadings of 4, 6 and 8 were considered.

Table 5-1: Voltage Data for Original Design Based on 4, 6 And 8 Magnetic Loadings.

ITEM	No of Ceramic Magnets	Voltage output equation
1	4	$V = -0.000001t^2 + 0.0151t + 7.1067$
2	6	$V = -0.00001t^2 + 0.0275t + 6.7542$
3	8	$V = -0.00005t^2 + 0.0407t + 6.5603$

Table 5-1 shows set of equations formulated from experimental results/When linearization was done, it was found that, the t^2 term was found to be insignificant. Further linearization and generalization of output voltage for original design was done by considering the three equations. Averaging the above equations and interpolations and eventually testing the equations reached by using the data for magnetic loadings up to level three were used to arrive at the equation below

$$\mathbf{V(t) = 0.028t + 7} \quad \textbf{.....(5-13)}$$

Considering variables that will affect the charging rate in relation to the number of magnets involved at any given time a factor K_C was introduced as an increasing constant associated with the number of magnets at every magnetic loading level. To be able to proceed it was assumed that the four magnets were taken as a datum or a reference point, with K_C assuming the value of 0.64. Proceeding to apply experimental data at magnetic loadings of 6 and 8 magnets, it was established that at every incremental of two magnetic loading on the previous one there was an increment of a constant of 0.08 on the value of K_C **i**mplying for every addition of one magnetic loading on the wheel there was an increment of 0.04 value on the previous value of K and vice versa. These behaviors were observed across the three levels used for modelling. The table below demonstrates this observation.

Table 5-2: Reducing Voltage Ratios Based on 4,6 and 8 Magnetic Loading.

Item	No of Ceramic Magnets	Reducing Ratio
1	4	0.64 ($Taken\ as\ reference\ point.$)
2	6	0.72 (Reference Point + 0.08=0.64+0.08=0.72
3	8	0.8 (Reference point $+ 0.08 + 0.08 = 0.8$

Further analysis showed that, at a reference point where 4 magnets were involved, the following relationship was true

$$\boldsymbol{V(t) = 0.028K_C t + 7} \quad \textbf{.....(5-14)}$$

Further mathematical analysis showed that at the reference point , where the number of magnets were four , the following relationship held good

$$\boldsymbol{V(t) = 0.028(\ 0.64)t + 7} \quad \textbf{.....(5-15)}$$

This implied that at a magnetic loading of four K_C was taken as = 0.64.

The quantity 0.64 was taken as reference point upon which the factor could either reduce or increase depending on the number of ceramic magnets involved in the loading on MEM. This observation guided the formulation of the following equation:-

$$\boldsymbol{V_{out}(t) = 0.028(\ 0.64 \pm 0.04G_C)t + 7} \quad \textbf{---------- (5-16)}$$

$\mathrm{G_C} = \mathrm{N_C} - 4$, Where N is the number of magnets loaded on MEM , G is referred to as gaining constant. If we take $\mathrm{N} = 4$, then above equation reduces to the original equation

$$\boldsymbol{V_{out}(t) = 0.028(\ 0.64)t + 7} \quad \textbf{..... (5-17)}$$

Recalling equation 5.14 then

$$\boldsymbol{V(t) = 0.028K_C t + 7} \quad \textbf{.....(5-18)}$$

Then this implies that ($K_C = (\ 0.64 \pm 0.04G_C)t \quad where\ G_C = N_C - 4$

The datum point of this model , ii taken as 4 magnets , taking G_C as a reference point, then $G_C = N_C - 4$=0.

This equation can then be used to detect the effect of any number of magnetic loading whether less or greater than 4

Where N_C is the number of ceramic magnets, K_C Varied with the rate of loading and $N_C$are constants associated with ceramic magnets?

$V_{out}(t) = 0.028(K_C)t + 7$, this is a time function equation used to generate predicted data depending on the ceramic magnetic loading of MEM. When the predicted data, for MEM ceramic magnet loading of 4,6 and 8 ceramic magnets was generated and compared with experimental data generated by 4, 6 and 8 MEM loadings, it was observed that there was good agreement between the experimental results (pilot testing results) and those predicted by Voltage output mathematical prediction model for MEM. Figures 5.2, 5.3 and 5.4 show the graphical representation of experimental data and predicted data versus time. This research established that experimental and predicted data were in agreement to a very large extend as highlighted in the figures 5.2, 5.3 and 5.4 below.

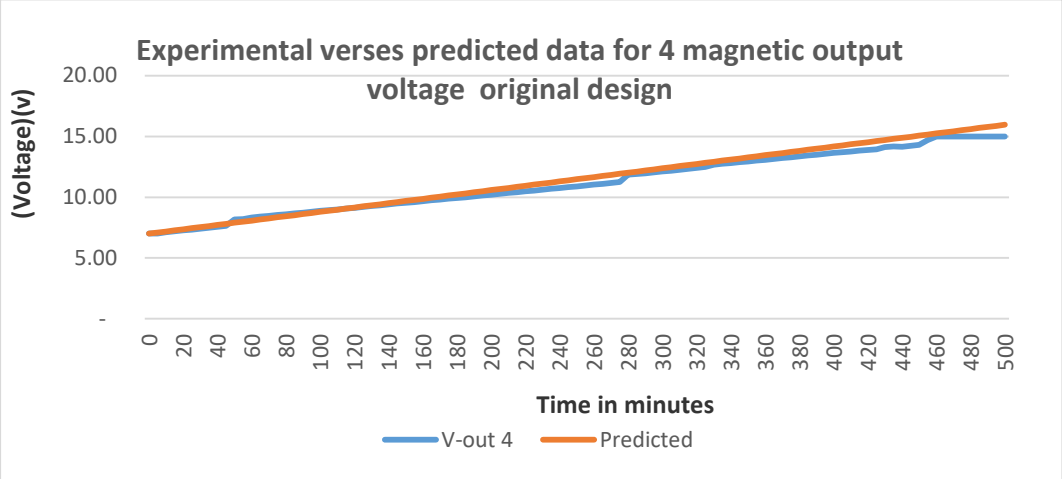

Figure 5-2: Voltage Experimental Data Verses Predicted Data for 4 Magnetic Output Voltage for Original Design.

Similar observation between experimental data and predicted data was observed For magnetic loadings of 6 and 8. It was observed that the experimental data and predicted data were in good agreement of over 98.9 percent.

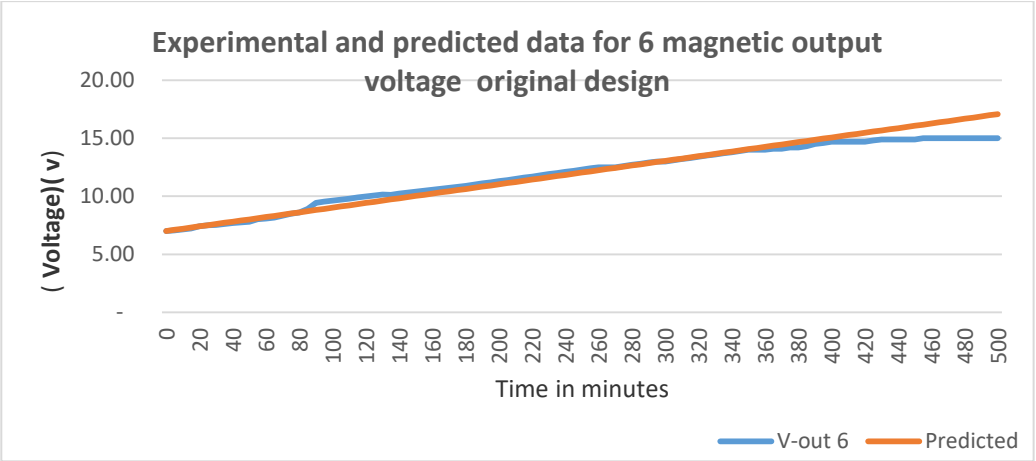

Figure 5-3: Voltage Experimental Data Verses Predicted Data For 6 Magnetic Output Voltage for Original Design.

These findings also presume that if the battery had a larger capacity than 15 volts, then the results of predicted data will equally hold. Figures 5-4, 5-5 and 5.6 shows that the results of experimental runs and predicted data are in agreement and even the time taken to charge the secondary battery to full capacity continued being shortened than the earlier and previous readings of magnetic loadings.

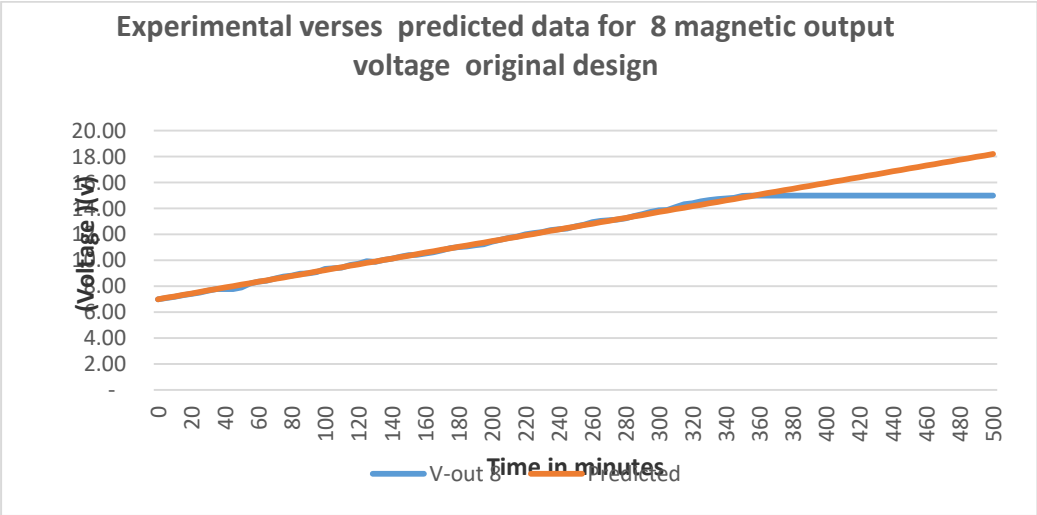

Figure 5-4: Voltage Experimental Data Verses Predicted Data for 8 Magnetic Output Voltage for Original Design.

The Figures 5-5 and 5-6 shows voltage experimental data verses predicted data for 10 and 12 magnetic loading on Monopole Energizer Machine original design respectively. The results further showed that when experimental data was compared

with predicated data, was found to be in agreement to the extent of over 98 %, for 10 and 12 magnetic loadings respectively.

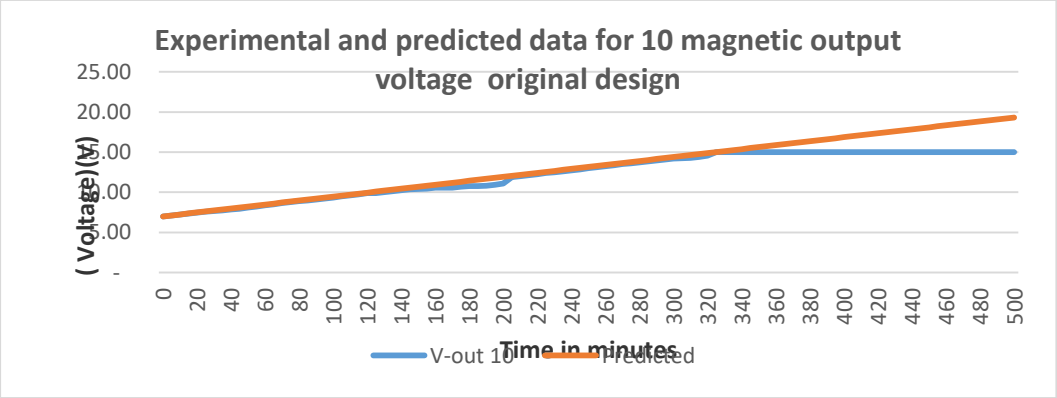

Figure 5-5: Voltage Experimental Data Verses Predicted Data for 10 Magnetic Output Voltage for Original Design.

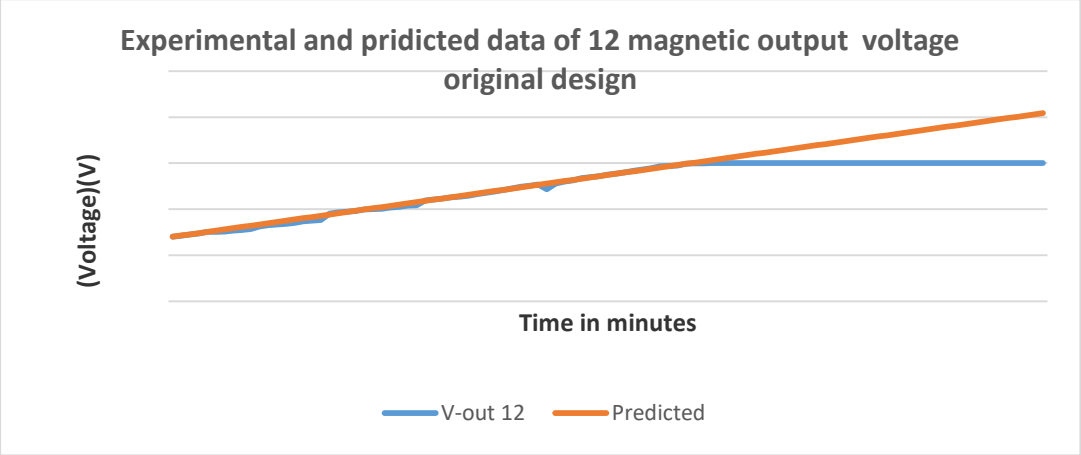

Figure 5-6: Voltage Experimental Data Verses Predicted Data for 12 Magnetic Output Voltage for Original Design.

The model also established that, charging of 14 and 16 magnetic loadings of MEM took a shorter time to charge the secondary battery from seven voltage to full capacity than the 10 and 12 magnetic loadings of MEM of original design, same as what was observed in experimentation at the same magnetic loading level. Figures 5-7 and figure 5-8 showed experimental and predicted data for magnetic loadings of 14 and 16 original designs.

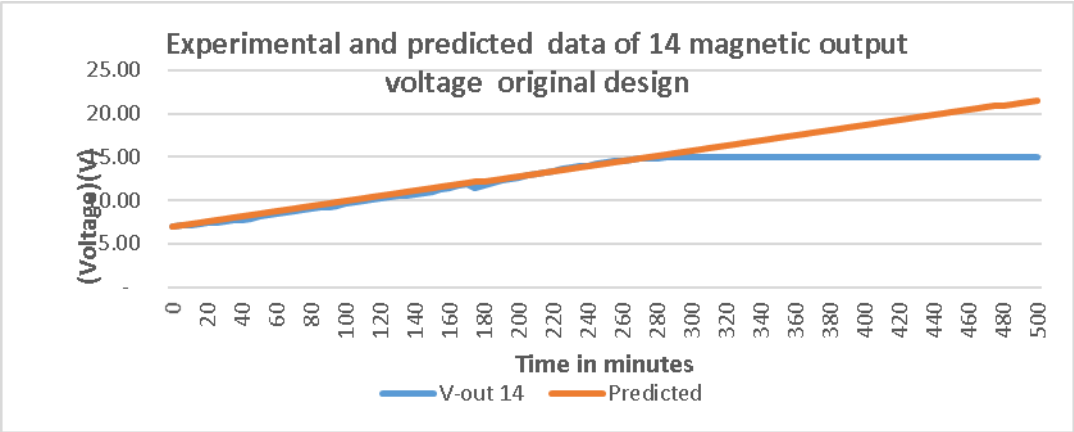

Figure 5-7: Voltage Experimental Data Verses Predicted Data for 14 Magnetic Output Voltage for Original Design

The research further established that it took 290 and 250 minutes respectively to charge the secondary battery from seven volts to full capacity potential of 15 volts by 14 and 16 magnetic loadings of MEM respectively. Figures 5.7 and 5.8 shows graphs of MEM of experimental data and predicted data of 14 and 16 magnetic loadings. The results showed that the experimental data compared with predicted data was in good agreement of over 98%. in both cases of magnetic loadings.

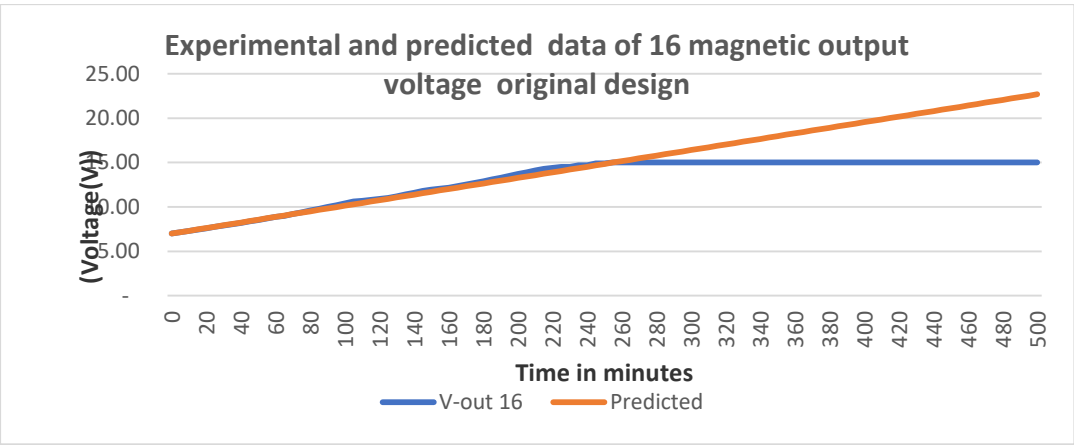

Figure 5-8: Voltage. Experimental Data Verses Predicted Data for 16 Magnetic Output Voltage for Original Design.

5.2.2 Modeling of Time Indepenent Function of MEM Original Design Voltage Output Characteristics.

The time independent function of MEM original design voltage output was modeled from equation 5.19.E below. This was done by removing time function components. The equation reduced to equation 5.18 is time dependence, to get a time independent

function we eliminate the time component from equation 5,18, and hence the equation reduces to equation 5.19

$$\boldsymbol{V = 0.028K_C + 7} \text{..... .....} \qquad \text{.....(5-19)}$$

Where $K_C = (\,0.64 \pm 0.04G) \quad where\ G_C = N_C - 4$

Where N_C is the number of magnets, K_C, G_C and N_C are constants associated with MEM due to Ceramic Magnets?

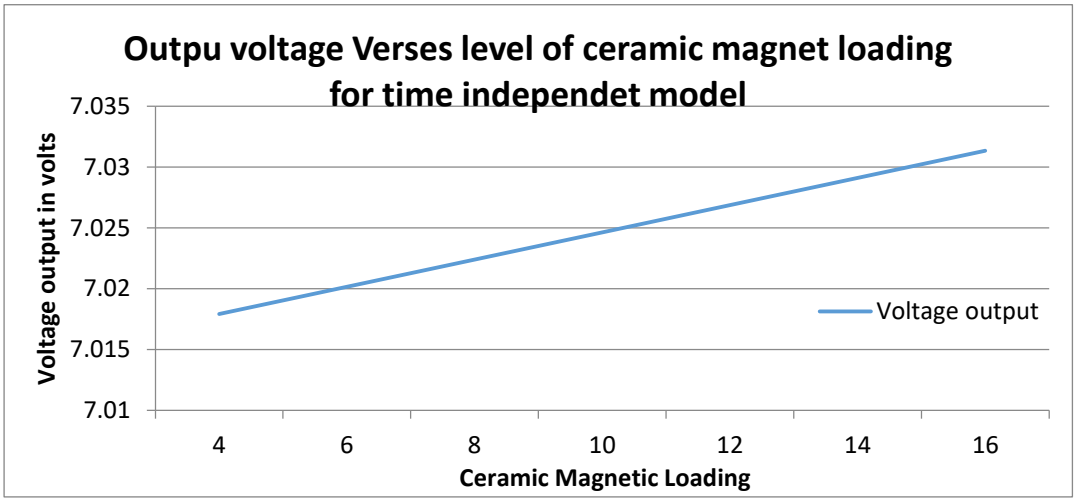

Figure 5-9: Voltage Output Predicted Data for Original Design of MEM at All Levels of Magnetic Loading

The above figure shows that the output voltage increased with magnetic loading. This figure does not consider time component and hence it demonstrates the impact of the magnet alone charging of the battery.

5.2.3 Modeling of MEM Time Function Original Design Current Output Characteristics

Just like in voltage modeling for original design the primary experimental data was used in the modelling of current for original design. The current modelling was characterized by negative slope that is the current amount decreased with increasing number of magnetic loadings. For purposes of developing current output predictive mathematical model, data generated by using four, six and eight MEM ceramic magnets loading were used for model development whereas the data for higher number of ceramic magnets were used for validation and testing of the model. The

table below shows the current output equation in relation with the number of ceramic magnets associated with it.

Table 5-3: Current data for 4, 6 and 8 magnetic loadings of original designs.

ITEM	No of Ceramic Magnets	Current output equation
1	**4**	$\mathrm{I} = -0.0002\mathrm{t} + 0.1637$
2	**6**	$\mathrm{I} = -0.0002\mathrm{t} + 0.1752$
3	**8**	$\mathrm{I} = -0.0002t + 0.1752$

Further linearization and generalization of the above data yielded the following formula.

$$\mathbf{I(t) = -0.0002t + 0.2} \quad \textbf{.....(5-20)}$$

This was the equation based on the loading of four ceramic magnets that

is $I_{out}(t) = -0.0002t + 0{,}2{,}.$

Taking consideration of the effect of magnetic loading in relation to the behavior of current trend the formula below was arrived at.

$$\mathbf{I_{out}(t) = -0.0002L_C t + 0.2} \quad \textbf{.....(5-21)}$$

where L_C is increasing with magnetic loading, to put in consideration the effect of magnetic loadings to the load current

When this model was tried with higher loadings than the loading of four ceramic magnets, it was established that current loading changed with increase in number of magnetic loadings. This implied that the model was to be modified to accommodate the incremental component in relation to magnetic loadings. Just like in the case of voltage output modeling. Further mathematical treatment, including try and error methods with available data up to magnetic loading of 8 showed that, taking the loading of four ceramic magnets as the origin of formulating the equation, the component -0.0002t in the current equation varied with the constant 1.02 to the power G

As the number of magnetic loadings increased, the current reduced at the rate of quantity 1.02 raised to the power of G_C and vice versa. This was found to hold a

cross the three levels of magnetic loadings in relation to experiments ran for original design

The rate of current drop increased with the increase in magnetic loadings. G has been defined as a constant for purposes of this research. This equation was developed further, by putting into consideration the fact that the rate of current drop increased with the number of magnetic loadings. Similarly, through mathematical treatment, including try and error methods with available data up to magnetic loading of 8 showed that, taking the loading of four ceramic magnets as the origin of formulating the equation, the current component of 0.0002 amps reduced by 5% for every loading of two magnets, and 2.5% for every loading of one magnet. Table 5.4 below shows the summary of these behaviors

Table 5-4: Reducing Ratios of Current Based On 4,6 and 8 Original Design Magnetic Loading.

ITEM	No of Ceramic Magnets	Reducing ratio of current
1	4	-0.0002 ($Taken\ as\ reference\ point.$)
2	6	-0.0002×0.95
3	8	$-0.0002 \times 0.95 \times 0.95$

Further optimization, generalization and approximation of this equation yielded the following formula.

$$\mathbf{I_{out}(t) = -0.0002\ (\ [\![1.02]\!]\ \hat{}\ G_C)t + 0.2}$$ **----------(5-22)**

Recalling equation (8.50) , hence L_C= $[\![1.02]\!]\ \hat{}\ G_C$

$$\mathbf{I(t) = -0.0002L_C t + 0.2}$$ **..... ..... (5-23)**

Where

I_{out} (t) output current at any given time,1.02 (2%)was taken as the ratio taken to reduce the gap between experimental data and predicted data (predicted data). it is time in minutes, $\mathbf{G_C}$ is the constant computed as shown below: -

$G_C = N_C - 4$, Where N_C is the number of magnets loaded on MEM , G_C is referred to as a constant. If we take $N_C = 4$, then above equation reduces to the original equation Where $L_C = 1$

$$\mathbf{I(t) = -0.0002t + 0.2} \quad \text{.....(5-24)}$$

The analysis of the above data shows that an increase of two ceramic magnets to MEM loading, was equivalent to the increase of 1.02 to the power G_C.This implied that the current output was constant at 0.2 amps. The rate of drop of this current was -0.0002×(1.02^{G_C}). This implies that the rate of current drop with time increased with the increase in magnetic loadings in the case of original design and vice versa. This equation can be used to generate predicted data in the case of any number of magnetic loadings. It was also assumed that N_C= 4 was taken as reference point upon which the constant could either reduce or increase depending on the number of ceramic magnets involved on the loading on MEM. Based on these facts equation 4.24 was arrived at. This model prediction is in agreement to the fact that both efficiencies and co-efficiencies performance increased with the level of magnetic loading due to the declining trend of current with increase in magnetic loading.

Figures 5-10, 5-11 and 5-12 shows graphs of experimental data and predicted data verses absolute time for MEM loadings of 4, 6 and 8 MEM original design loading current. When the predicted data was compared with experimental data the two sets of data were in an agreement to an extend of over 98% for 4, 6 and 8 magnetic lodgings respectively.

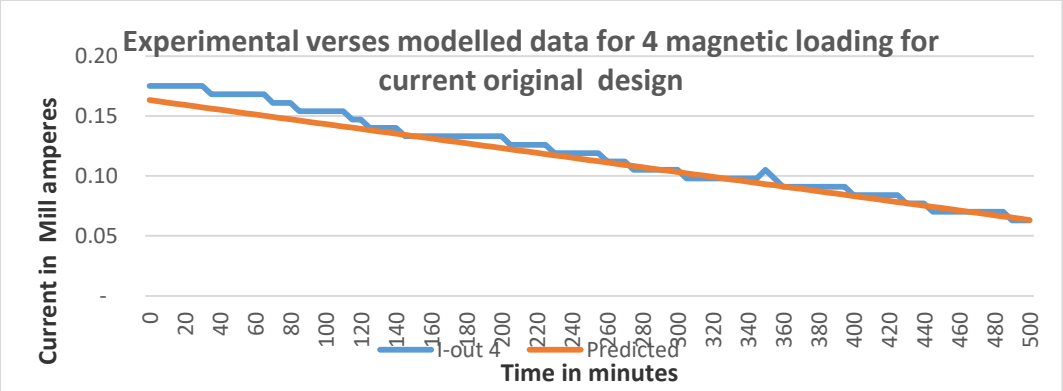

Figure 5-10: Current Experimental Data Verses Predicted Data for 4 Magnetic Loading for Original Design.

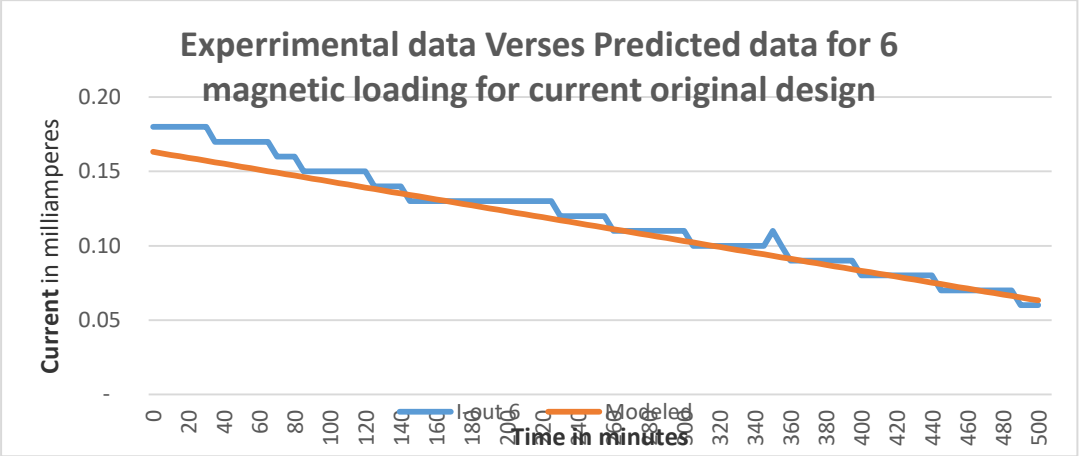

Figure 5-11: Current Experimental Data Verses Predicted Data for 6 Magnetic Loading for Original Design.

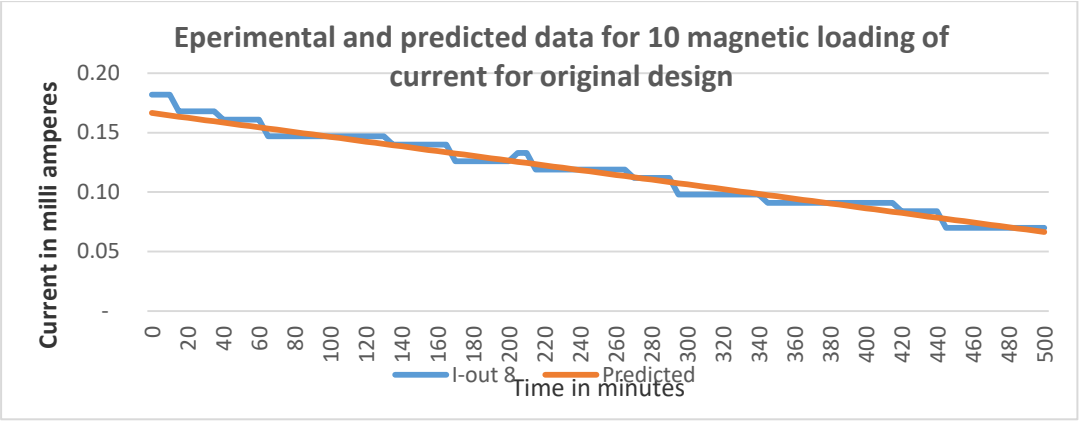

Figure 5-12: Current Experimental Data Verses Predicted Data for 8 Magnetic Loading for Original Design.

Notably, when the graph of original design of current magnetic loadings of 10 and 12 MEM were compared, it was established that the negative slope of experimental data and predicted data became even more steeper than those ones of 4, 6 and 8 magnetic loadings. Figure 5-13 shows Current Experimental data Verses Predicted data for 10 magnetic loading original design.

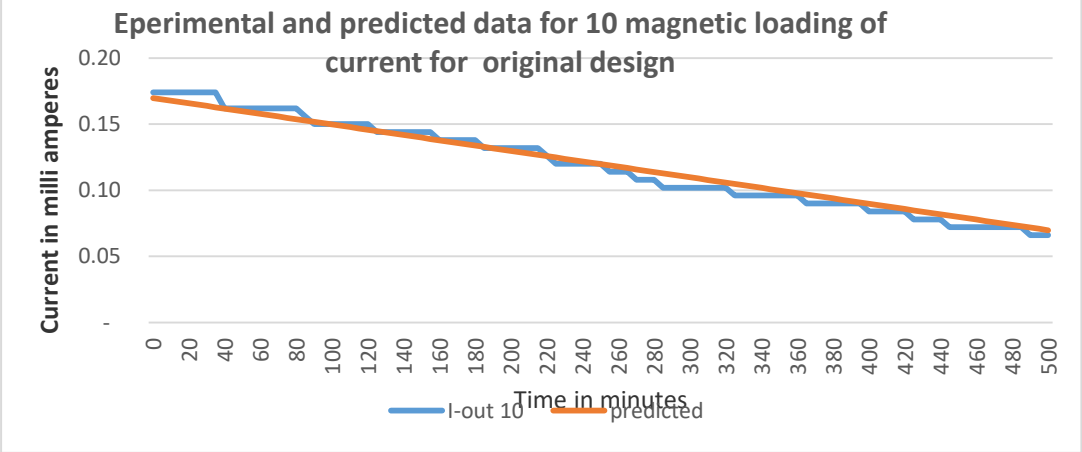

Figure 5-13: Current Experimental Data Verses Predicted Data for 10 Magnetic Loading Original Design.

Further analysis was done by comparing the predicted data and experimental data. The results indicated that the predicted data and experimental data were in agreement to the extent of 99 % in both cases, that is the predicted data and experimental data was found to be fitting perfectly well. This behavior also characterized the behavior of model prediction at the magnetic loading of 12. The model prediction was in agreement with experimental data to the extent of over

99%. Figure 5-14. Below shows the graph of experimental and predicted data versus time of load current at magnetic loading of 12.

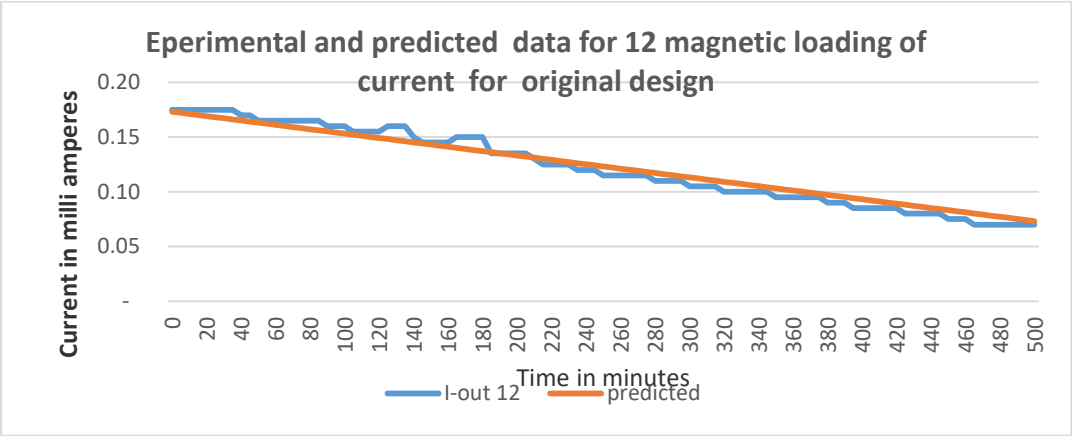

Figure 5-14: Current Experimental Data Verses Predicted Data for 12 Magnetic Loading Current Original Design.

Further analysis was done for 14 and 16 current magnetic loadings, when further analyzed the negative slope became even steeper than those of 10 and 12 current magnetic loadings. This was found to be consistent with the fact that the negative slope for current became steeper with increasing magnetic loadings. Figures 5.15 and 5.16 Shows the graphs of experimental and predicted data for 14 and 16 current magnetic loadings versus time. Similarly, when the predicted data and experimental data was compared for 14 and 16 current magnetic loadings for original design it was found to fit at 99 % and 99.5 % respectively.

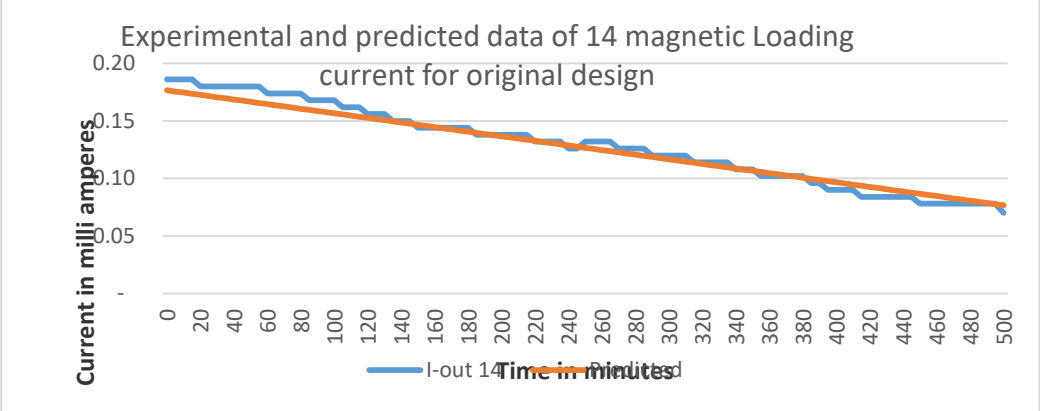

Figure 5-15: Current Experimental Data Verses Predicted Data for 14 Magnetic Loading Original Design.

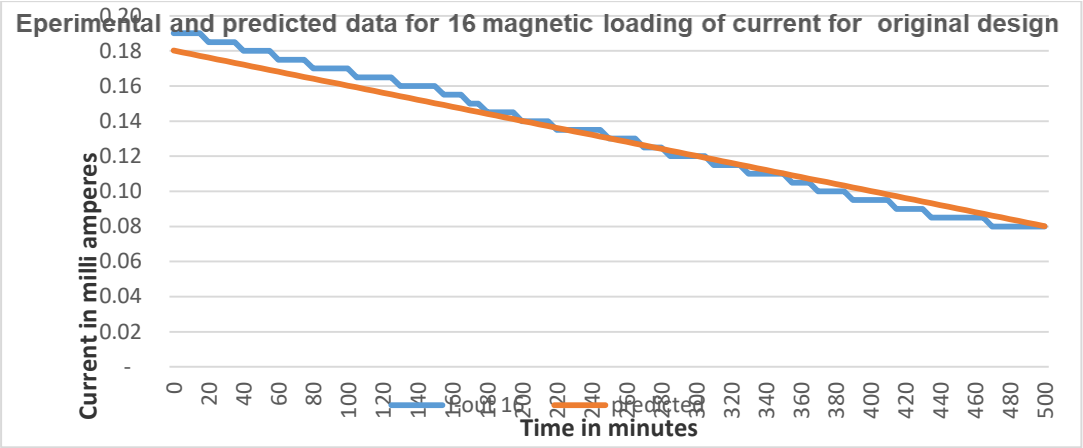

Figure 5-16: Current Experimental Data Verses Predicted Data for 16 Magnetic Loading for Original Design.

5.2.4 Modeling of Time Indepenent Function of MEM Original Design Load Current Characteristics.

The time independent function of MEM original design current output was modeled from equation (4-51) below. This was done by removing time function components from the equation. The equation was then reduced to

Recalling equation (5.23) , hence L_C =1.02^G

$$\mathbf{I(t) = -0.0002L_C t + 0.2} \qquad \textbf{.....(5-25)}$$

Where

I_{out} output current , 1.02 (2%)was taken as the ratio taken to reduce the gap between experimental data and predicted data (predicted data).

G_C is the constant computed as shown below: -

$G_C = N_C - 4$, Where N_C is the number of magnets loaded on MEM , $G_C$is referred to as a constant. If we take$N_C = 4$, then above equation reduces to the original equation

$$\mathbf{I = -0.0002L_C + 0.2} \qquad \textbf{.....(5-26)}$$

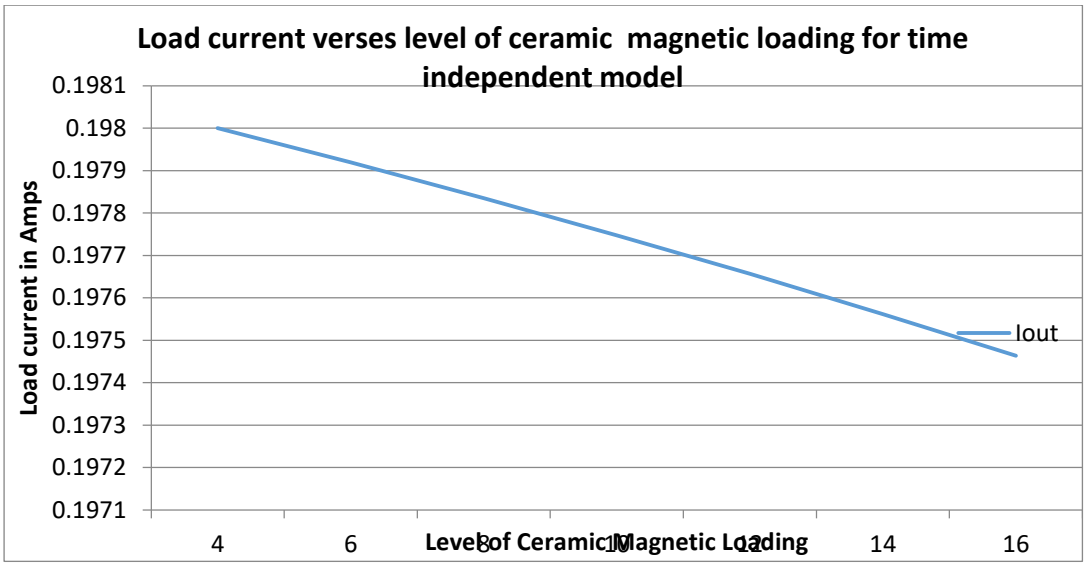

Figure 5-17: Load Current Predicted Data for Original Design of MEM at All Levels of Magnetic Loading

The behavior of load current time independent behavior is closely compared to the case of time function load current modeled behavior, which had a negative gradient that increased with magnetic loading.

5.3 Modelling of Mem Replication Electrical Characteristics

Furthermore, development of mathematical model to predict the voltage output and current output was done for replication design using Neodymium magnets. Likewise, the power output component, the coefficient of performance and the efficiency of performance was not modeled. Similarly, as the case of original design, the first three experimental runs of the loadings of 4, 6 and 8 were used for generation of training data. The other levels of magnetic loadings from ten to sixteen the data generated was used for validation and sensitivity analysis.

5.3.1 Modelling of MEM Replication Voltage Output Time Function Characteristics

The development of the predictive mathematical model for replication design was developed based on Monopole Energizer Machine using Neodymium magnets. Range of experiments were undertaken using neodymium magnets and the rate of charging was monitored at every level of MEM magnetic loading. The experiments showed that the rate of charging increased with the number of magnets. Similarly, the model put into consideration the fact that in all the experiments the charging of

the battery started when the battery voltage was at 7 volts. This was done to ensure harmony in data recording, monitoring and analysis. Secondly the model equation was to put in consideration the increase in charging rate due to the number of magnets involved. The observation made in MEM experiments with Neodymium magnets was similar to that of original design. Hence similar approach was used in formulation of voltage output predictive mathematical model.

Table 5-5 below shows the voltage output equation in relation to the number of Neodymium magnets associated with it. In determining the voltage output equation, MEM Neodymium magnets loadings of 4, 6 and 8 were considered.

Table 5-5: Reducing Voltage Ratios Based on 4, 6 And 8 for Replication Design Magnetic Loading.

ITEM	No of Neodymium Magnets	Voltage output equation
1	4	$V = -0.000001t^2 + 0.0151t + 7.1067$
2	6	$V = -0.00001t^2 + 0.0275t + 6.7542$
3	8	$V = -0.00005t^2 + 0.0407t + 6.5603$

After generalization, the following formula was established. The formula shows a relationship between voltage and time based on the running Monopole Machines. Recalling the approach used in developing equation for voltage output for original design. The behavior of the two designs is similar, hence a similar approach applied in developing model equations for replication design.

Similarly, further linearization and generalization of output voltage for replication design was done by considering the three equations. Averaging the above equations and interpolations and eventually testing the equations reached by using the data for magnetic loadings up to level 8 of magnetic loading

$$\boldsymbol{V(t) = 0.00042t^2 + 0.0441t + 7} \quad \textbf{....(5-27)}$$

Further linearization, factorization and generalization of the above equation showed that the voltage output increased as the number of magnetic loadings with the relationship shown below

. $V_{out}(t) = 0.0441(\ 0.4 \pm 0.023G_N)t + 7 = 0.028(\ 0.64 \pm 0.043G)t + 7$---

(5-28)

Taking $K_N = (\ 0.64 \pm 0.043G_N)$

The above equation reduces to

$$\mathbf{V_{out}(t) = 0.028K_N t + 7}$$ **----------(5-29)**

$G_N = N_N - 4, Where\ N\ is\ the\ number\ of\ magnets,$
$4\ is\ used\ because\ the\ reference\ point\ is\ loading\ of\ 4\ magnets.$ G is defined as constant, because it will determine the increase or decrease of voltage output. Similarly, this equation can be used to generate simulation data depending on the neodymium magnetic loading of MEM. For example, in the case of original design, when the simulation data, for MEM neodymium magnet loading of 4, 6 and 8 was compared with experimental data was found to be in agreement. Figures 5-18 and 5-19 below depicts the behavior of experimental and predicted data versus time for 4 and 6, magnetic loadings of replication designs for voltage output. It was generally observed that voltage output increased with increase in the neodymium magnetic loading on MEM. It was also generally observed that the charging rate was more for replication design than original design at all levels of loadings. These model results were found to be in agreement with experimental at a close range of about 99,5%.

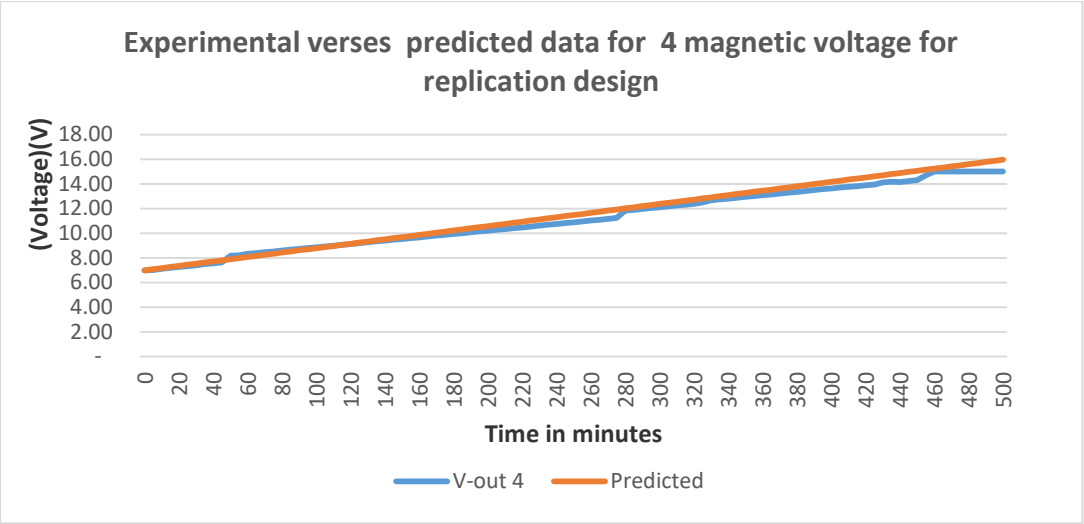

Figure 5-18: Voltage Experimental Data Verses Predicted Data for 4 Magnetic Loading for Replication Design.

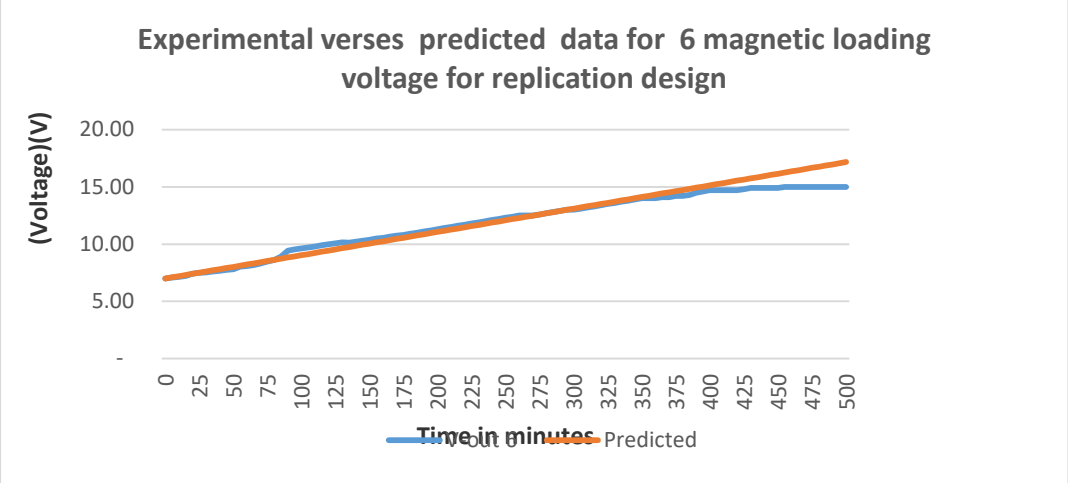

Figure 5-19: Voltage Experimental Data Verses Predicted Data for 6 Magnetic Loading for Replication Design.

Further analysis of modeling results at a magnetic loading of 8 and 10 continued showing high level approbation of the model to experimental data.

Figures 5-20 and 5-21 below demonstrates the behavior of experimental and predicted data versus time for 8 and 10 magnetic loadings of replication designs for voltage output. The model, just like the analysis of experimental results, the model showed that voltage output increased with increase in the neodymium magnetic loading on MEM. Model approximation, just like the case of experimental results presentation, it was demonstrated that the charging rate for replication model was higher than or that of original model at all levels of magnetic loadings. When

experimental and predicted data for the model were compared, it was shown that the two sets of data were in agreement to the extent of 99.9% for both cases of 8 and 10 magnetic loadings.

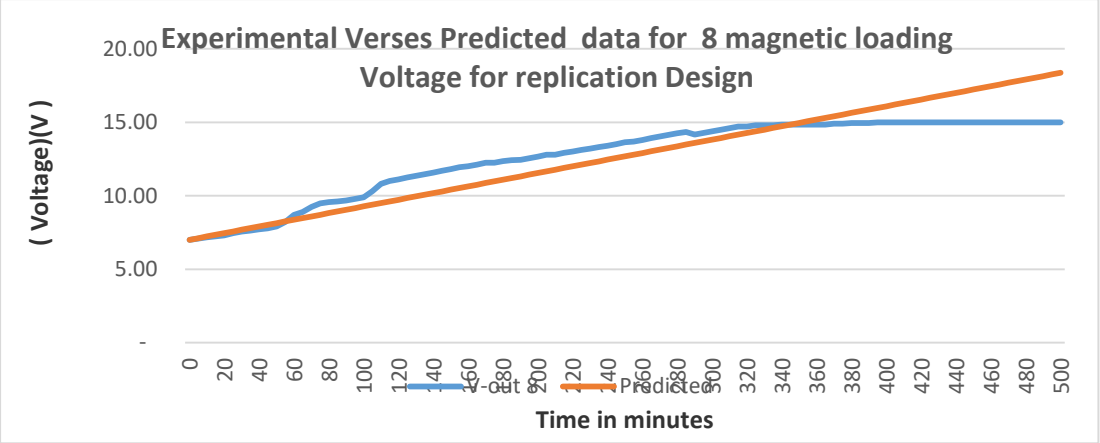

Figure 5-20: Voltage Experimental Data Verses Predicted Data For 8 Magnetic Loading for Replication Design.

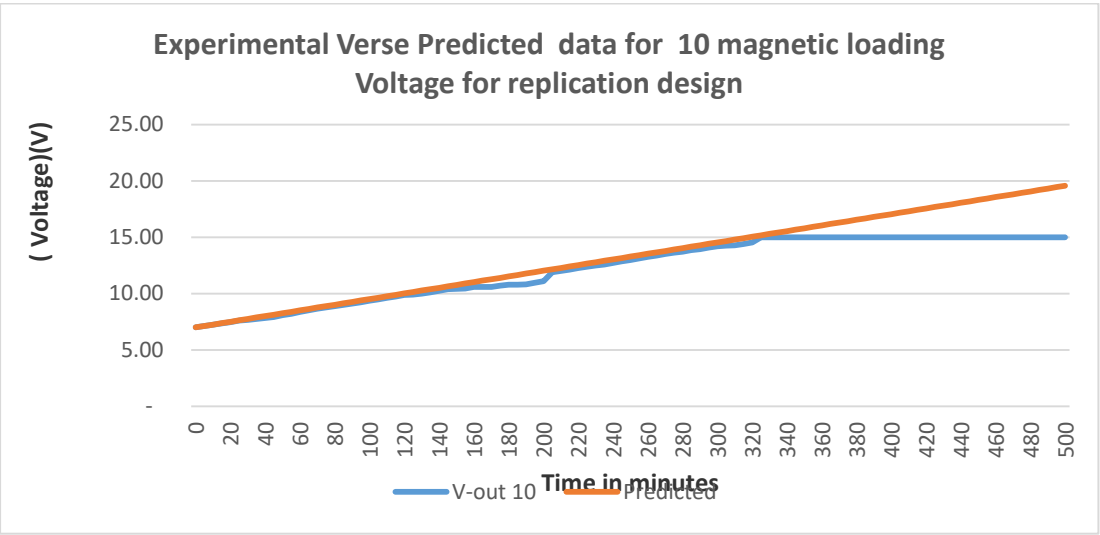

Figure 5-21: Voltage Experimental Data Verses Predicted Data for 10 Magnetic Loading for Replication Design.

Besides the above, model testing was done at a magnetic loading of 12 and14.The results of model data with comparison with experimental data was found to be in agreement to the extent of over 99%. Figures 5.22 and 5.23 shows the graph of voltage experimental and predicted data versus time for replication design of 10 and 12 magnetic loading.

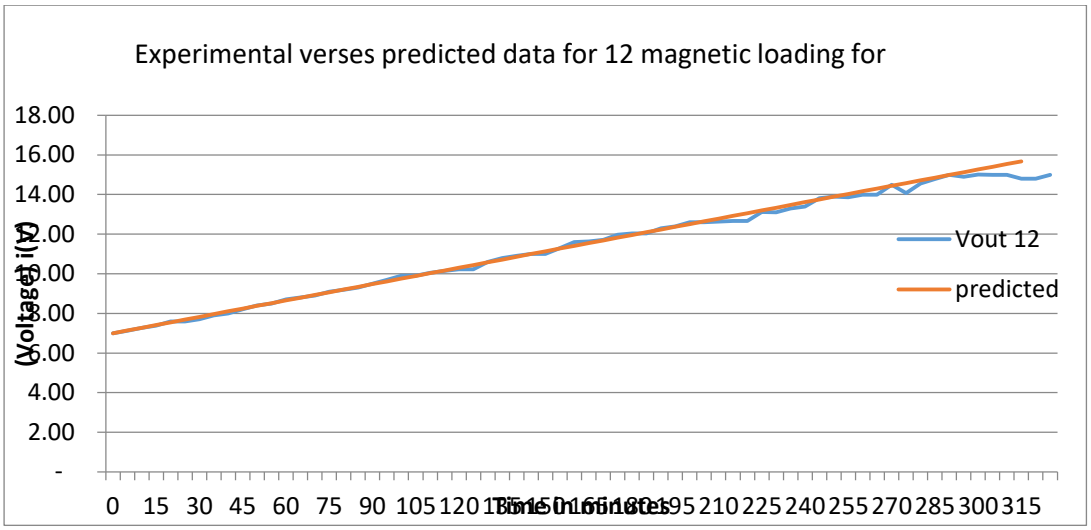

Figure 5-22: Voltage Experimental Data Verses Predicted Data for 12 Magnetic Loading for Replication Design.

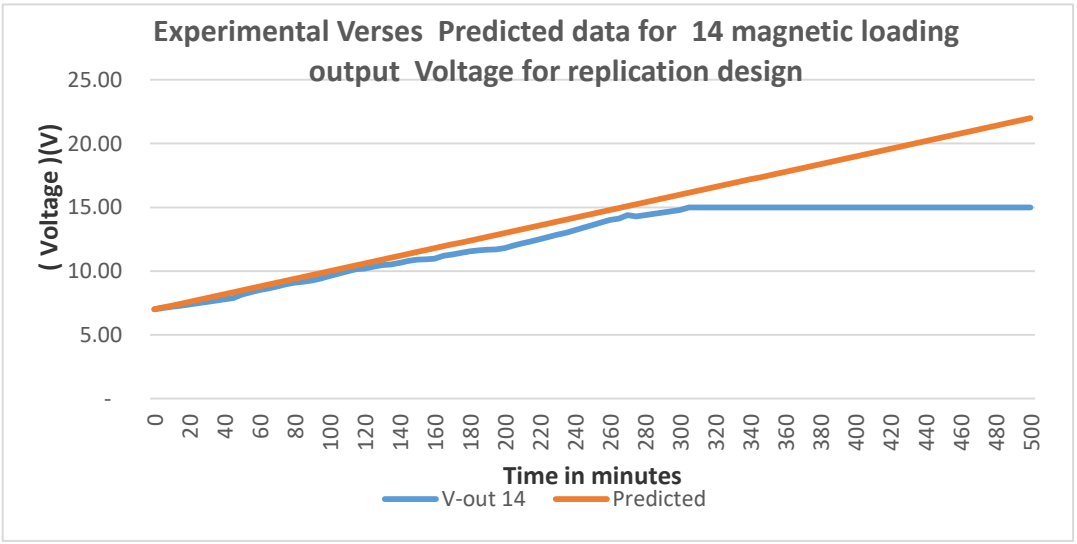

Figure 5-23: Voltage Experimental Data Verses Predicted Data for 14 Magnetic Loading for Replication Design

Figure 5-24 shows the graph of voltage experimental and predicted data versus time for replication design of 16 magnetic loadings. It was established that the rate of charging at these levels was higher than the rate of charging at same level of loading as in the case of original design.

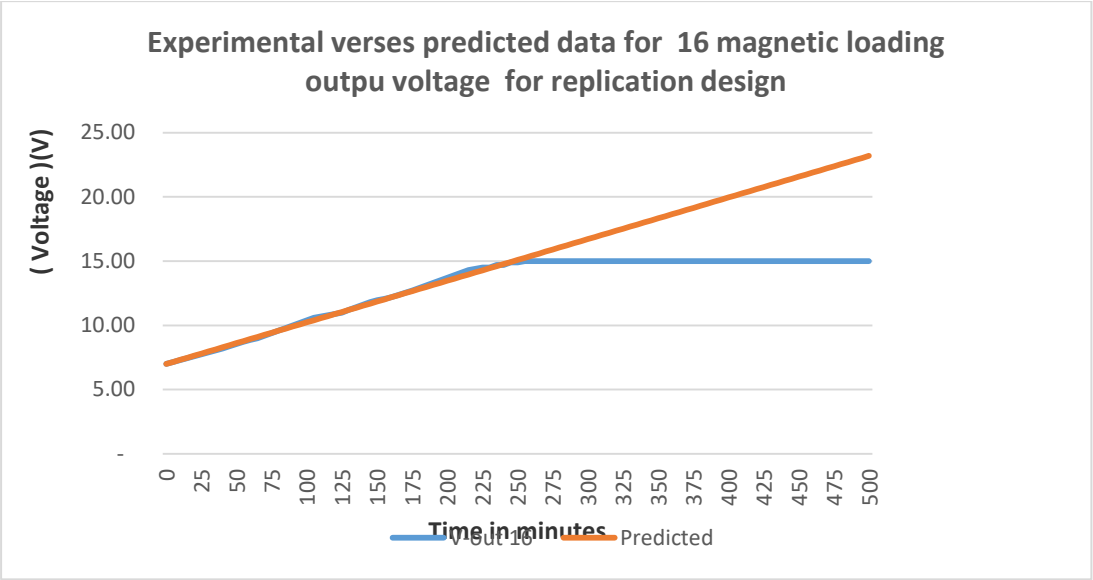

Figure 5-24: Voltage Experimental Data Verses Predicted Data for 16 Magnetic Loading for Replication Design.

Further analysis of predicted data and experimental data showed that, the level of agreement between the two sets of data was 98%, 99%, 100% and 98% at a magnetic loading of 10, 12,14 and 16 magnetic loadings.

5.3.2 Modelling Of MEM Replication Voltage Output Time Independent Characteristics**.**

This was modelled by modifying equation 5.29 as shown below, in this equation the time component was dropped.

$$\boldsymbol{V_{out} = 0.028K_N + 7}\text{----------}\textbf{(5-30)}$$

$G_N = N_N - 4, Where\ N_N\ is\ the\ number\ of\ magnets,$

$4\ is\ used\ because\ the\ reference\ point\ is\ loading\ of\ \ the\ 4\ magnets.\ \ G_N$ is defined as a constant, because it will determine the increase or decrease of voltage output.

The graph below predicts voltage output for time independent model for replication design. The model shows that the voltage output increased with the level of magnetic loading.

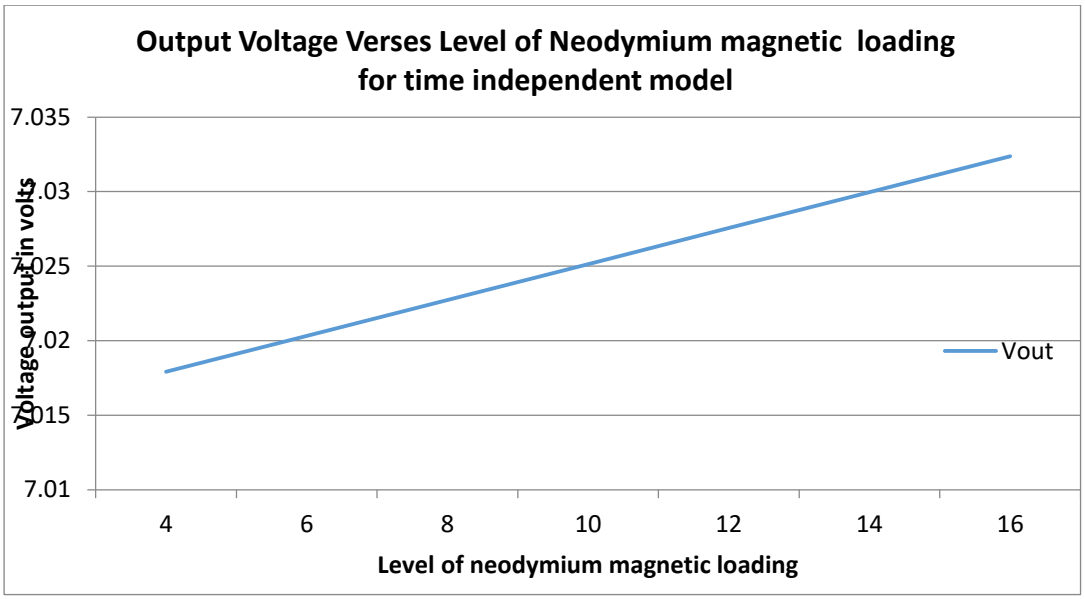

Figure 5-25:Voltage Output Predicted Data for Replication Design of MEM for Time Independent Model at All Levels of Magnetic Loading

5.3.3 Modelling of Time Function MEM Replication Load Current Output Characteristics

Observations was made on current data experimentation results for replication design. Just like the case of current loading for original design, the gradient for the current was a negative slope. It was generally observed that the current slope decreased further and at a higher rate than the case of original design with the increase in number of neodymium magnets. Similarly, for purposes of developing current output predictive mathematical model, data generated by 4, 6 and 8 MEM neodymium magnets loading were used for model development whereas the data for higher number of ceramic magnets was used for validation and testing. The table below shows the current output equation in relation with the number of Neodymium magnets associated with it. In determining the current output equation, MEM Neodymium magnet loadings of 4, 6 and 8 were considered.

Table 5-6: Reducing Current Ratios Based on 4, 6 And 8 Magnetic Loading.

ITEM	No of Neodymium Magnets	Current Output Equation
1	4	$\mathrm{I} = -0.00007\mathrm{t} + 0.1753$
2	6	$\mathrm{I} = -0.00003\mathrm{t} + 0.1536$
3	8	$\mathrm{I} = -0.00007\mathrm{t} + 0.1456$

Reference is made on modeling of current output for original design in section 5.5.3.The above equations were averaged to get a linear and generalized equation to predict the load current for replication design. The initial equation obtained by averaging the above equations was

$I(t) = -\{\, 0.0000563t) \, + 0.16$, Further generalization resulted in the equation below

$\boldsymbol{I(t) = -0.000195t \, + 0.17,}$ t represents time, I (t) current varying with time, this was taken as current for replication design. In considering the incremental factor due to the increasing number of magnetic loadings, it was further linearized to:

$$\mathbf{I_{out}(t) = 0.17 - 0.000195t \times 0.98^{G}} \text{----------} \quad \textbf{(5-31)}$$

Further mathematical treatment was undertaken by using the training data, which was mainly that of the magnetic loading data at level 4, 6 and 8. This was later followed by interpolation, extrapolation including trial and error to ensure that the best possible model equation that is eqn 5.32 is obtained.

$$\mathbf{I_{out}(t) = 0.17 - 0.000195L_N t - -} \text{----------} \quad \textbf{(5-32)}$$

Where $\boldsymbol{L_N}$=0.98^{G}

$I_{out}(t)$ *is component of output current with time,* G_C and N_C are constants, where N_C represents the number of magnets. $G_C$is given by; $G_C = N_C - 4$, where 4 is taken as reference point that I s a point where N_C=4, so that $G_C = N_C - 4$,=0

Figures 5-26 and 5-27 shows the behavior of experimental data and modelled data versus time at magnetic loadings of 4 and 6 of MEM replication design. It was also

generally observed that the experimental data and predicted data were in agreement in the range of over 98 percent in both cases.

the range of over 98 percent in both cases.

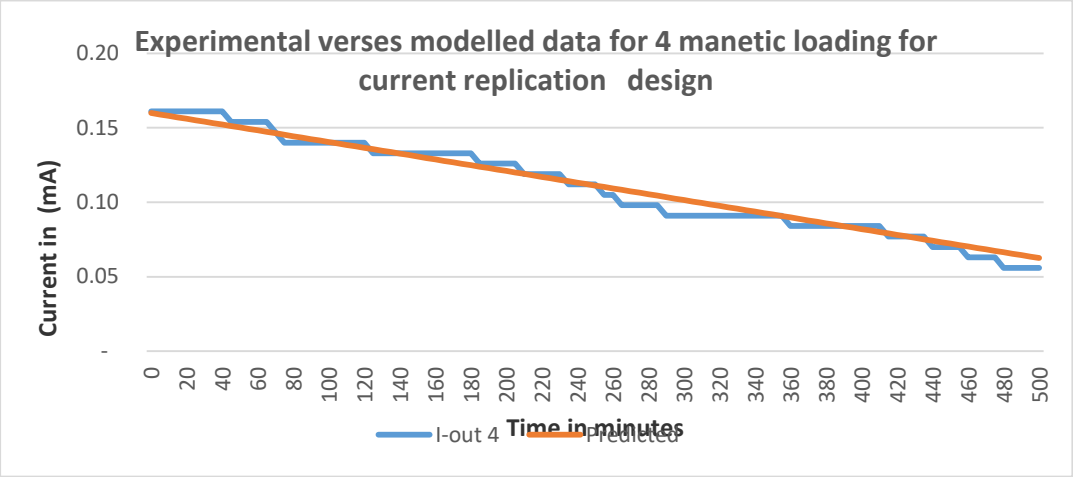

Figure 5-26: Current Experimental Data Verses Predicted Data for 4 Magnetic Loading Replication Design.

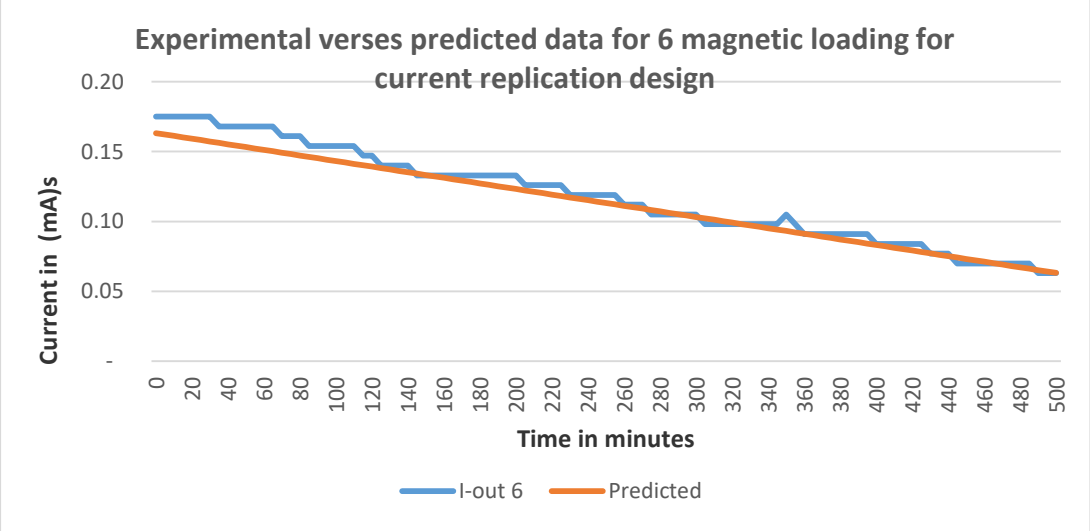

Figure 5-27: Current Experimental Data Verses Predicted Data for 6 Magnetic Loading for Replication Design.

Figures5-27and 5-28 depicts the behavior of experimental data and modelled data versus absolute time at magnetic loadings of 8 and 10 of MEM replication design. In this model, the result showed that the current had a more negative steeper slope at all levels of magnetic loadings when closely compared with that of original design. This mirrored what was seen in experimental data at the same magnetic loading

level. It was also generally observed that the experimental data and predicted data were in agreement in the range of over 99.

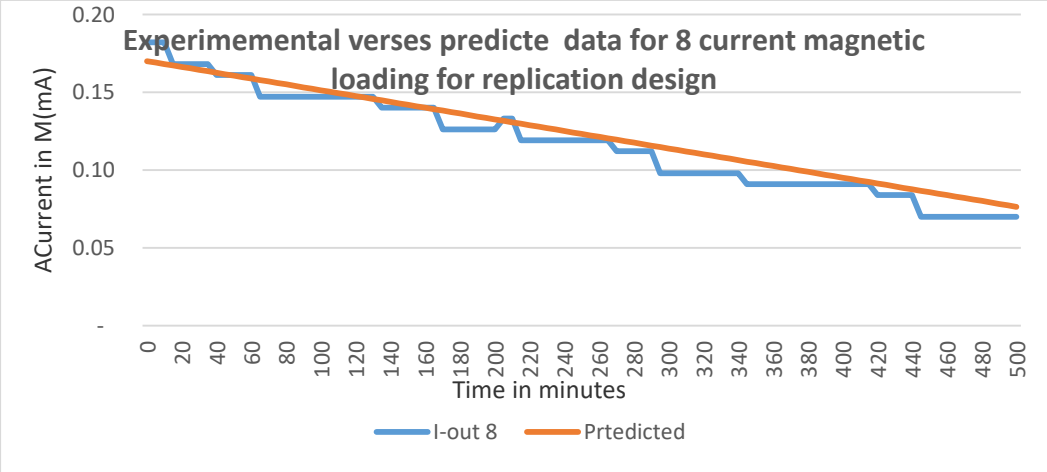

Figure 5-28: Current Experimental Data Verses Predicted Data for 8 Magnetic Loading Replication Design.

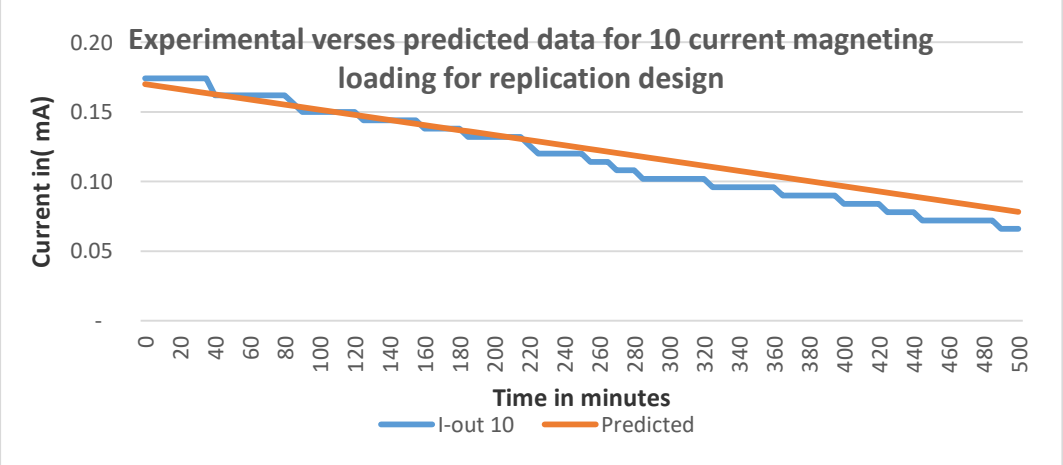

Figure 5-29: Current Experimental Data Verses Predicted Data for 10 Magnetic Loading for Replication Design.

Figures 5-30 and 5-31 shows the behavior of experimental data and modelled data versus absolute time at 12 and 14 levels of magnetic loadings of MEM replication design. It was observed that the graph continued depicting a picture of having a steeper slope than the lower levels of magnetic loadings of replication designs, and were also found to be relatively higher at same levels of loadings of original designs. When experimental and predicted data were compared, it was established that the two sets of data were in agreement at the level of 98%, and 98.5% for12 and 14 magnetic loading respectively.

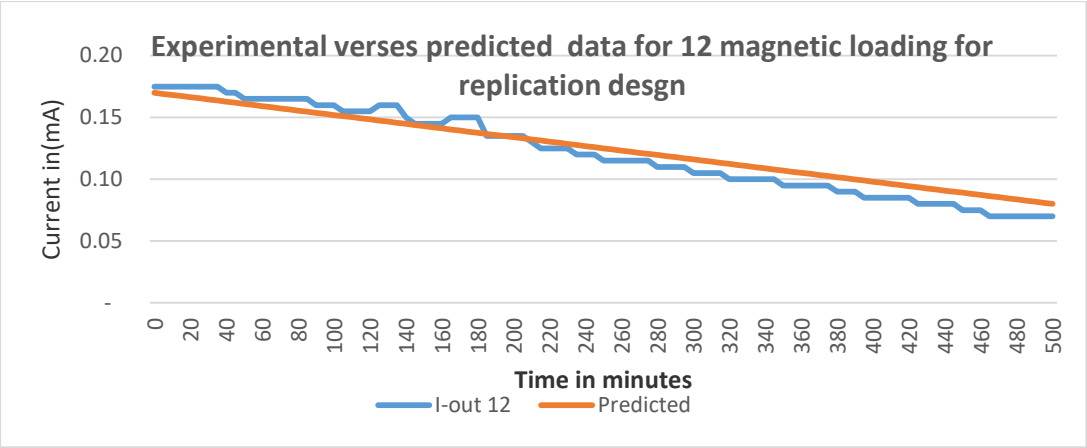

Figure 5-30: Current Experimental Data Verses Predicted Data for 12 Magnetic Loading Replication Design.

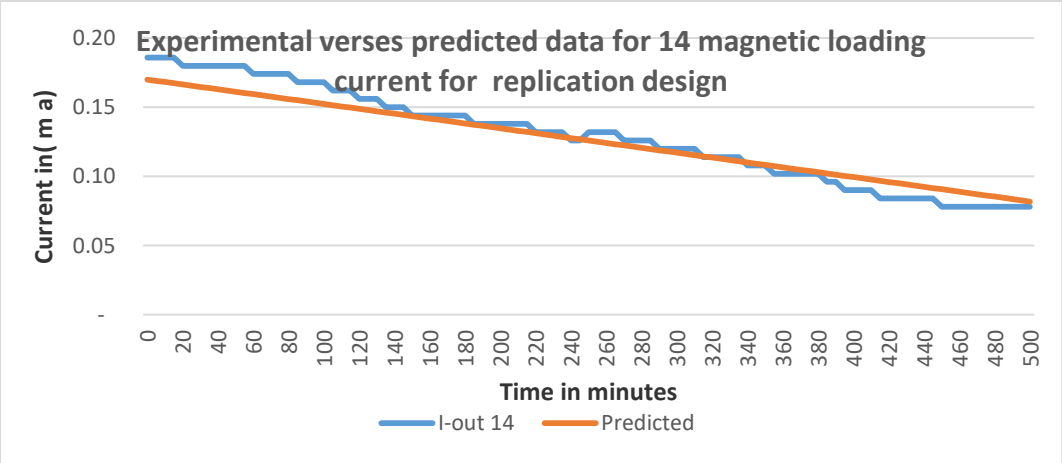

Figure 5-31: Current Experimental Data Verses Predicted Data for 14 Magnetic Loading Replication Design.

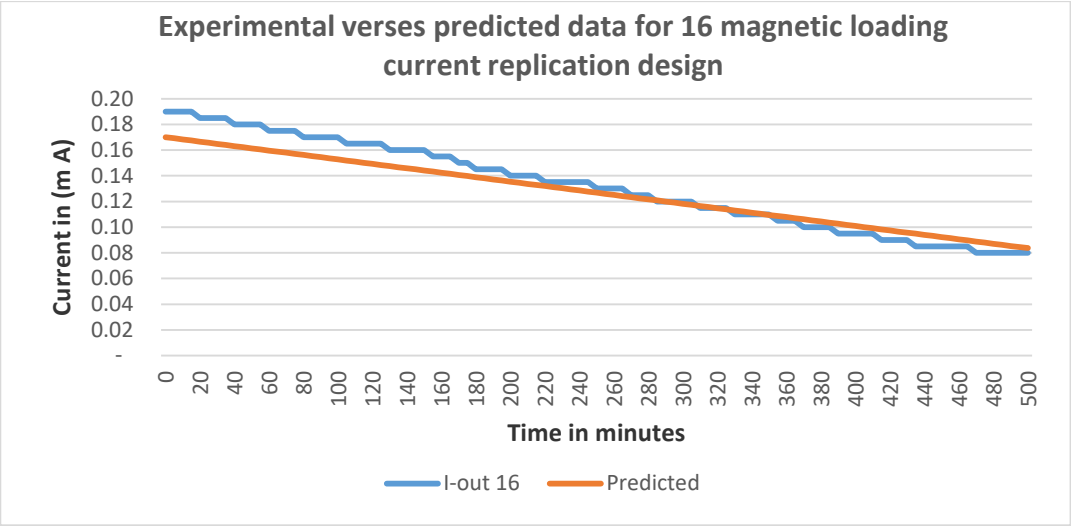

Figure 5-32: Experimental Data and Modelled Data Versus Time at Magnetic Loading of 16 of MEM Replication Design

Figure 5-32 show the behavior of experimental data and modelled data versus time at magnetic loading of 16 of MEM replication design. The results indicated that the gradient was steeper than the lower levels of magnetic loadings of replication designs, and were also found to be relatively higher at same levels of loadings of original designs. When experimental and predicted data were compared, it was established that the two sets of data were in agreement at a level of 99.6% for 10 magnetic. Hence the model approximation accuracy increased with the level of magnetic loadings.

Similarly, when experimental data was compared with predicated data for 12, 14 and 16 for replication current magnetic loadings the two sets of data were found to be in agreement to the extent of 97.7%, 98.3% and 99.2% respectively.

5.3.4 Modelling of Time Independent MEM Replication Current Output Characteristics.

Modelling of time independent function of MEM replication load current characteristics was modelled from time function MEM replication of load current characteristics. This was done by removing time aspect from equation 4.32

$$I_{out} = 0.17 - 0.000195L_N - \text{----------} \quad \textbf{(5-33)}$$

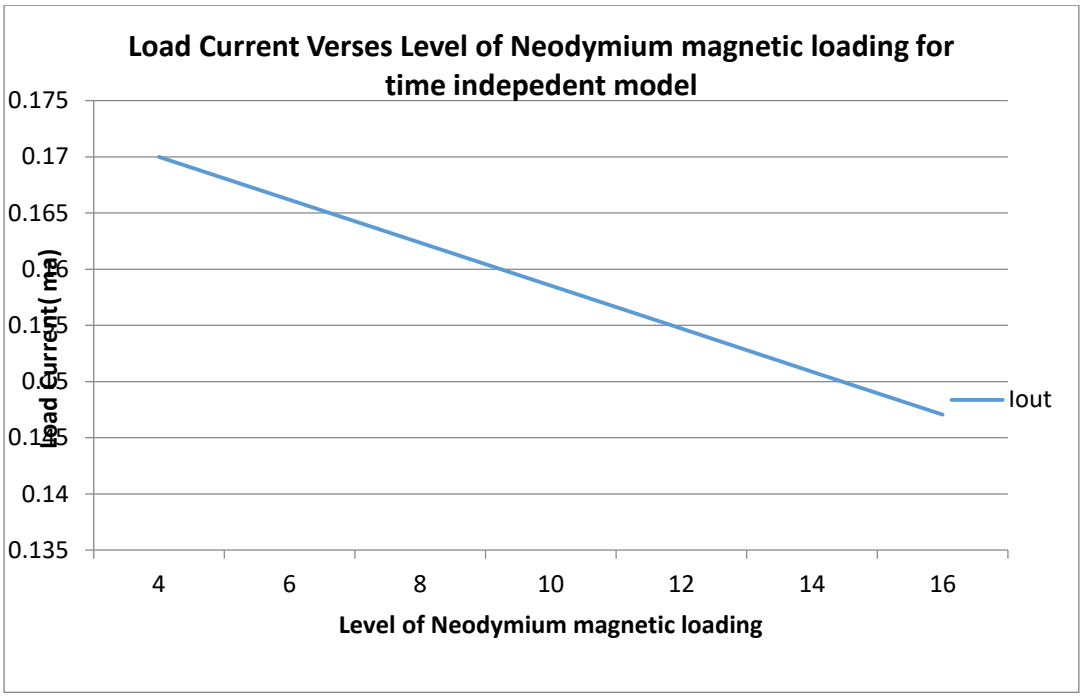

Figure 5-33: Time Independent Load Current Predicted Data for Replication Design of MEM at All Levels of Magnetic Loading

This model approximation is closely compared with that of load current verses the level of neodymium magnetic loading for time function model. The two models are similar to the extent of predicting load current in relation to magnetic loading.

5.4 Model Validation And Sensitivity Analysis

5.4.1 Results for Voltage Output Coefficient of Determination, R^2 , Efficiency and RMSE for Original And Replication Designs

From the model data of predictive voltage output by original design it is shown that there is a relationship between the number of ceramic magnets and the R^2 value of a regression model. The R^2 value represents how well the regression model fits the data, and a higher R^2 value generally indicates a better fit**.** Based on the data, from table 5.7, R^2 value is 1.000 when there are 4 ceramic magnets. This indicates a perfect fit between the regression model and the data, meaning that all of the variability in the dependent variable can be explained by the independent variable(s) included in the mode

Table 5-7: Voltage Output Coefficient of Determination, Efficiency and RMSE

Level of Magnetic Loading	R^2 original design	R^2 replication design	EFF original design	EFF replication design	RMSE original	RMSE replication design
4	1.000	1.000	0.970255401	0.979751361	0.413695062	0.055264366
6	0.997702795	0.998505819	0.988864384	0.942173343	0.6380761	0.073931403
8	0.99030754	0.993305785	0.751882089	0.656142598	1.281704465	0.083822212
10	0.99349841	0.99631017	0.689540459	0.86343985	1.520284692	1.008287561
12	0.991610651	0.995595686	0.446468354	0.854711796	2.071469283	1.061261595
14	0.987677894	0.994375165	0.079309143	0.79463105	2.6096929	1.232536759
16	0.976722542	0.988685297	-0.442585779	0.50453647	3.13964466	1.839990247

In terms of percentages, the R^2 value of 1.000 corresponds to a percentage of 100%, indicating that all of the variation in the dependent variable can be explained by the independent variable(s) included in the regression model. This is the highest possible value for R^2, and suggests that the model is a very good fit for the data when there are 4 ceramic magnets. In this case, the R^2 value appears to marginally decrease as the number of ceramic magnets increases from 4 to 16. The R^2 value is highest (1.000) when there are 4 ceramic magnets and decreases as the number of magnets increases, with the lowest R^2 value at (0.976722542) for 16 ceramic magnets. Based on this observation, the model is reliable and can predict up to more than 97.6 percent ..

Similar deductions were observed from the analysis of the replication design mathematical voltage output model. It was observed that there is a relationship between the number of Neodymium magnets and the R^2 value of a regression model. From table 5.7 it was further deduced that the R^2 value was 1.000 at the magnetic loading of 4 neodymium. This indicated a perfect fit marginally better than the one for original design, between the regression model and the data, meaning that all of the variability in the dependent variable can be explained by the independent variable(s) included in the model. In general, the prediction of voltage output by neodymium magnets was much stronger than that of original design.

In terms of percentages, the R^2 value at magnetic loading of 4 was 1.000 corresponds to a percentage of 100%. Which indicates that all of the variation in the dependent variable can be explained by the independent variable(s) included in the regression model. This is the highest possible value for R^2, and suggests that the model good fit for the data when there are 4 ceramic magnets.

In this case, the R2 value decreased marginally as the number of neodymium magnets increased from 4 to 16. The R^2 value was highest (1.000) when there were 4 neodymium magnets and decreased very marginally as the number of magnets increased, with the lowest R^2 value of 0.988685297 observed when there were 16 neodymium magnets. Based on this observation it was deduced that the model was reliable and can predict up to more than 98.9 percent reliable**.**

In analyzing the efficiency for voltage output for model designs, it was further established that the values for the neodymium magnets were generally higher than

those for the ceramic magnets. For example, with 4 magnets, the neodymium magnets had an efficiency of 0.979751361, while the ceramic magnets had an efficiency of 0.970255401. This trend continues for most of the values in the Table 5-7. Based on this investigation, it was observed that efficiency values for both types of magnets varied significantly depending on the number of magnets used. For example, with 16 magnets, the neodymium magnets had an efficiency of 0.50453647, while the ceramic magnets had an efficiency of -0.442585779, which is actually negative. Based on these results the replication design still stands out as a better approximation

Table 5-7 also shows that, in general, the neodymium magnets have lower RMSE values than the ceramic magnets for most of the values in the table. This suggests that the model using neodymium magnets is more accurate than the model using ceramic magnets. For example, with 4 magnets, the RMSE value for the neodymium magnets was 0.055264366, while the RMSE value for the ceramic magnets was 0.413695062. This means that the predicted values using neodymium magnets are, on average, closer to the actual observed values than the predicted values using the ceramic magnets.

This trend continues for most of the values in the table, with the neodymium magnets generally having lower RMSE values than the ceramic magnets. However, it's worth noting that the RMSE values for both types of magnets vary significantly depending on the number of magnets used. This suggests that the optimal number of magnets for achieving the highest accuracy may be different for each type of magnet.

However, it's worth noting that the RMSE values for both types of magnets vary significantly depending on the number of magnets used. For example, with 10 magnets, the neodymium magnets had an RMSE of 1.008287561, which is higher than the RMSE for the ceramic magnets with the same number of magnets (1.520284692). This suggests that the optimal number of magnets for achieving the highest accuracy may be different for each type of magnet.

It's worth noting that while the correlation coefficient can tell us about the strength and direction of a linear relationship, it does not necessarily imply causation. It's

possible that other factors, beyond just the number and type of magnets used, could be driving the observed relationship with the outcome variable.

5.4.2 Load Current Coefficient of Determination, Efficiency and Root Mean Square Model Analysis

Table 5-8: Load Current Coefficient of Determination, Efficiency and RMSE

Level of magnetic Loading	R^2 original design	Efficiency original design	RMSE original design	R^2 replication design	Efficiency replication design	RMSE replication design
4	0.9916654	-0.62145021	0.040072212	0.996602	0.999999	0.001933
6	0.993857	0.890781014	0.030194137	0.995892	0.999999	0.001516
8	0.996454	0.941989998	0.028960053	0.995855	0.999999	0.001181
10	0.9937908	0.990824207	0.011691637	0.993791	0.990824	0.011692
12	0.9977785	0.975148006	0.01980784	0.991497	0.990019	0.012553
14	0.9992708	0.99326944	0.010843396	0.992838	0.992688	0.012553
16	0.9996608	0.998167597	0.005784149	0.992095	0.9917	0.01231

From Table 5-8 it was observed that the R^2 values for both types of magnets marginally increased as the number of magnets used increased, it was further established that the rate of increase was more for replication design than original design. This suggests that the number of magnets used has a significant impact on the load current, and that the regression models using both types of magnets are able to explain a high proportion of the variation in the load current. For the ceramic magnets, the R^2 values range from 0.992 (with 4 magnets) to 1.000 (with 16 magnets). For the neodymium magnets, the R^2 values range from 0.997 (with4 magnets) to 0.992 (with 16 magnets). This suggests that both types of magnets are able to provide a good fit to the observed data, with the ceramic magnets generally exhibiting slightly higher R^2 values than the neodymium magnets. For the neodymium magnets, the R^2 values range from 0.992, (with 16 magnets) to 0.997 (with 4 magnets), these values are insignificant for discussion which also suggests a very good to excellent fit for the data to the observed.

From Table 5-8, it was deduced that the efficiency values for both types of magnets generally increased as the number of magnets used increased. This suggests that the number of magnets used has a significant impact on the efficiency of the system. For the ceramic magnets, the efficiency values range from -0.62145021 (with 4 magnets) to 1.000 (with 16 magnets). For the neodymium magnets, the efficiency values range from 0.999999089 (with 16 magnets) to 1.000 (with 4 magnets). This suggests that both types of magnets are able to provide high levels of efficiency, with the neodymium magnets generally exhibiting slightly higher efficiency values than the ceramic magnets. For the neodymium magnets, the efficiency values range from 0.999999089 (with 16 magnets) to 1.000 (with 4 magnets). The efficiency values for the neodymium magnets are generally higher than those for the ceramic magnets, with all values being very close to 1.000, which indicates a very high level of efficiency. It was further deduced from the table that the values of RMSE for load current of both original and replication designs were about 0-0. This showed a perfect fit for approximation of the model for both MEMs designs. For original design the value of RMSE ranged from 0.04 at magnetic level of loading of 4 to 0.005 to a magnetic level of loading of 0.05. In the case of replication design, the value of RMSE ranged from 0.001933 to 0.01233 at a magnetic loading of 4 and 16 respectively.

5.4.3 Further Model Validation and Sensitivity Analysis Through Pilot Testing

In validating these results, seven pilot tests at different levels of magnetic loading for original and replication designs were taken. The points taken were both for current output and voltage output. In the case of voltage, plot points were taken from zero time up to the point where the secondary battery had been fully charged. This explains why the plot points for voltage were reducing with the increase in magnetic loadings. In the case of current plots, the experiment was run from zero time and data was recorded at intervals of 5 minutes. In the current plots 100 points were considered. 100 plots corresponded to 500 minutes. The experimental results and predicted data verses time plots were made as indicated in Table 5-9.

In each case the experimental results (here referred to us true values) were compared with predicted results (modelled results). The deviations between the two sets of data were recorded and compared. Based on this approach the percentage sensitivity and reliability of each set of experiment for original and replication designs at every

level of loading were determined. The percentage deviations were also worked out for both original and replication designs. Table 5-9 and 5-10 shows the behavioral characteristics of voltage and current for original design.

Table 5-9: Model Characteristics of Voltage Output Based on the Original Design.

Magnetic loading for original design	**Plotted points**	**Model Points within 98.5% ≤100% Of true values**	%	**Model Points within 95% ≤98.4% Of true value**	%	**Model Points outside range**	%	**Model points within 95% ≤100% Range of true values**	%
4	92	88	96	4	4	0	0	100%	
6	91	88	97	3	3	0	0	100%	
8	72	72	100	0	0	0	0	100%	
10	66	63	95	3	5	0	0	100%	
12	62	62	100	0	0	0	0	100%	
14	61	61	100	0	0	0	0	100%	
16	51	51	100	0	0	0	0	100%	

Table 5-10: Model Characteristics of Current Output Based on the Original Design.

Magnetic loading for original design	**Plotted points**	**Model Points within 98.5% ≤100% Of true values**	%	**Model Points within 95% ≤98.4% Of true value**	%	**Model Points outside range**	%	**Model points within 95% ≤100% *range of of true values***
4	100	95	95	5	5	0	0	100%
6	100	94	94	6	6	0	1	99%
8	100	98	98	2	2	0	0	100%
10	100	100	100	0	0	0	0	100%
12	100	100	100	0	0	0	0	100%
14	100	96	96	4	4	0	0	100%
16	100	98	98	2	2	0	0	100%

The results of magnetic loadings for Replication design for both voltage and current characteristics showed that the charging rate was higher than in the case of original design. This was clearly indicated by voltage output trend at increasing levels of magnetic loadings of replication design. The tables below and above show the sensitivity, reliability of the replication model at different levels of loadings for both sets of designs.

Considering the model behavior of voltage and current output for both original and replication it was observed that the model was 100% reliable at the confident level of 99 %., allowing for the margin of error of 1%, whereas the model was sensitive and reliable at confident level of 98.5% only allowing a margin of error of 1.5%. These characteristics were acceptable across all the levels of original design loadings for both current and voltage characteristics. Tables 5.11 and5.12 depicts these characteristics. In general, it was observed that the sensitivity and reliability of

the model ranged between 98.5% and 99.7 %. This shows that the model is very reliable and it has the margin of error ranging between 0.3% and 1.5 percent.

Table 5-11: Model Characteristics of Voltage Output Based on the Replication Design.

Magnetic loading for original design	**Plotted points**	**Model Points within 98.5% ≤100% Of true values**	%	**Model Points within 95% ≤98.4% Of true value**	%	**Model Points outside range**	%	**Model points within 95% ≤100 %** Range of true values
4	90	85	94	4	4	1	2	98%
6	88	86	98	1	1	1	1	99%
8	75	74	99	0	0	1	1	99%
10	59	56	95	3	5	0	0	100%
12	53	51	96	2	4	0	0	100%
14	47	47	100	0	0	0	0	100%
16	42	41	98	1	2	1	0	100%

Table 5-12:Model Characteristics of Current Output Based on the Original Design.

Magnetic loading for original design	Plotted points	Model Points within 98.5% ≤100% Of true values	%	Model Points within 95% ≤98.4% Of true value	%	Model Points outside range	%	Model points within 95% ≤100 range of true values	%
4	100	95	95	3	3	2	2	98%	
6	100	94	94	4	4	2	2	98%	
8	100	94	94	5	5	1	1	99%	
10	100	96	96	4	4	0	0	100%	
12	100	97	97	2	2	0	0	100%	
14	100	93	93	6	6	1	1	99%	
16	100	92	92	7	7	1	1	99%	

5.5 Weaknesses of The Model

The model assumes the rate of charging to be uniformly distributed throughout the charging process. In practical situation the charging rate was not necessarily linear. There were some cases where the responses were big within a very short time. This was clearly observed in the case of voltage output responses in relation to time accumulation. This behavior was noticed for both original and replication designs. In these cases, the data output indicated irregular output and nonlinear relationship.

Establishing the limit of Model application. This model especially for voltage and current output was concluded as a linear increasing model with increase in magnetic loadings for the voltage output for both original and replication designs. In the case of current behavior, it was observed that, the current decreased linearly with increasing magnetic loading for both original and replication designs. This investigation did not establish the limit of operations for both current and voltage, hence more investigation is required to establish the operating limit of this model. The limit of operation for this model stands at the loading of 16 magnetic loadings

for both original and replication designs. It assumes infinite linear relationship for output voltage and load current.

5.6 Steady State Analysis of Monopole Energizer Machine.

5.6.1 MEM Input and Output Equations

The fourth objective of this research was to perform steady state analysis of Monopole Energizer Machine. MEM was modelled after SRM for input parameters and after BC for output parameters. The main controlling parameter was voltage whereas current, power were dependent variables. The input equation for MEM was established as

$$\boldsymbol{V_{in} = iR + L\phi\frac{di}{dt} + i\omega\frac{dl}{d\theta} + V_D} \text{ ----------(5-34)}$$

The two terms; i$\omega\frac{dl}{d\theta}$ and V_D can be ignored without loss of generality. Therefore

$$\boldsymbol{V_{in} = iR + L\theta\frac{di}{dt}} \text{ .... (5-35)}$$

This investigation also established that the voltage output Monopole Energizer Machine depends on input voltage and duty cycle, that is

$$\boldsymbol{V_{in}\overset{(s)}{\rightarrow}\ \frac{1}{k} \rightarrow V_{out}}) \text{ ---------- (5-36)}$$

when k$> 0,\ then$

$$(\boldsymbol{V_{out} = \frac{1}{constant} \times Voltage} \text{ ,----------(5-37)}$$

when k=1, $(\ minima) then\ (V_{out} = V_{in}\ )$,

$$\boldsymbol{V_{OUT} = \frac{1}{K} \times V_{in}\ ,\ K = duty\ cycle\ 0 \leq K \leq 1} \text{----------(5-38)}$$

MEM has very low back EMF when in operation. Voltage drop across diode $V_D \sim 0.7v$

and

$$\boldsymbol{V_{in} = iR + L\theta\frac{di}{dt}} \text{----------(5-39)}$$

5.6.2 MEM Stability Anaysis

MEM has the following constants $R = 4\Omega \quad L\emptyset = 3$

$V_{in} = 4i + 3\frac{di}{dt}$ as time domain equation, and $V_{in}(s) = 4I(s) + 3\dot{S}\, I(s)$

in frequency domain, $V_{in}(s) = I\,(s)(3\dot{S} + 4)$

$$\frac{\boldsymbol{I(s)}}{\boldsymbol{V_{in}(s)}} = \frac{\mathbf{1}}{\mathbf{3\dot{S}+4}} \quad \text{----------} \qquad \textbf{-(5-40)}$$

$$\boldsymbol{V_{in}} \xrightarrow{(s)} \frac{\mathbf{1}}{\mathbf{3\dot{S}+4}} \rightarrow \boldsymbol{I(s)} \text{----------} \qquad \textbf{------(5-41)}$$

Hence, the Monopole Energizer Machine as a control system has the following transfer function; $\frac{I(s)}{V(s)} = \frac{1}{3\dot{S}+4}$

The transfer function of a control system describes the relationship between the input and the output of the system in the Laplace domain. In this case, the transfer function is given as:

I(s)/V(s)=3s+4

where:

$I(s)$ is the Laplace transform of the output (response) of the system (current, in this case).
$V(s)$ is the Laplace transform of the input (control signal) to the system (voltage, in this case).
s is the complex frequency variable.

To analyze the behavior of the control system described by this transfer function, we look at its poles and zeros. Poles and zeros are important concepts in control systems theory that help us understand the system's stability, transient response, and frequency response. In this transfer function, the denominator $3S^2$ + 4s + 4 represents the characteristic equation of the system. Here, the transfer function's denominator is given, which is a quadratic equation in the variable 's' (representing the Laplace variable). The denominator is also referred to as the characteristic

equation, and it's crucial for analyzing the system's dynamics. In this transfer function, the denominator $3S^2$ + 4S=0

To analyze the behavior of the control system described by this transfer function, we can look at its poles and zeros' find the poles, we set the denominator equal to zero and solve for 's': 3s^2 + 4 = 0. Solving this equation for's' will give us the values of 's' where the denominator becomes zero, representing the poles of the system. s = -4/3, s = -4. These are the solutions for's' that are obtained by solving the quadratic equation from the previous step. They represent the poles of the system. the pole of the system is at s = -4/3, s = -4.

To find the poles, we set the denominator equal to zero and solve for *s*:

's': 3s^2 + 4 = 0."

s = -4/3, s = -4

So, the pole of the system is at s = -4/3, s = -4

The location of the pole in the left-half plane (Re(s) < 0) indicates that the system is stable.

Stable systems have poles with negative real parts. The real part of the pole (-4/3, -4) determines the time response of the system. - This indicates that the real part of the pole influences the time response characteristics of the system. A larger negative real part usually corresponds to faster decay and quicker settling in the system's response. The location of the pole in the left-half plane (Re(s) < 0) indicates that the system is stable. The real part of the pole (-4/3, -4) determines the time response of the system.

5.6.3 Plotting the System on A Pole Zero Map

To plot the system on a pole-zero map, we need to represent the poles and zeros of the transfer function in the complex plane. The pole represents the location of the denominator's roots, while the zero represents the location of the numerator's roots.

To plot the system on a pole-zero map, we need to represent the poles and zeros of the transfer function in the complex plane. This explains the purpose of a pole-zero map and mentions that poles and zeros will be depicted on the map. The pole represents the location of the denominator's roots, while the zero represents the location of the numerator's roots. This distinguishes between poles and zeros in the context of the transfer function. Poles are the roots of the denominator polynomial, while zeros are the roots of the numerator polynomial.

For the given transfer function $(s) = \frac{1}{4+3S^2}$ ----------(5.42)

The transfer function has one pole at and no zero-x s = -4/3, s = -4 os (since the numerator is a constant 1).

The following steps are followed when plotting the system on a pole-zero map:

1. Mark the pole: In the complex plane, mark a point at **s = -4/3**
2. Mark the zero: Since there are no zeros, there is nothing to mark in the numerator.

This pole-zero map indicates that the system has a single pole located at s = -4/3, s = -4 in the left-half plane, which confirms the stability of the system.

5.7 Ploting the Root Locus of the System

This was done by writing a MATLAB code. In this case the **rlocus** function was used This function generates the root locus plot for a given transfer function or state-space representation. The MATLAB code to plot the root locus of the given control system is given in section 9.6. In this code, we first define the numerator and denominator of the transfer function. Then, we create the transfer function using **tf(numerator, denominator)**. The **rlocus** function is then used to generate and plot the root locus. The **grid on** command adds a grid to the plot, and the **title**, **xlabel**, and **ylabel** commands are used to label the plot.

When you run this code, it will display the root locus plot, which shows the variation of the closed-loop poles as a function of a parameter (typically a gain) in

the open-loop transfer function. The root locus plot helps in understanding the system's stability and how the poles move based on the parameter changes.

5.7.1 Matlab Code and Display

```
% Define the transfer function
numerator = 1;
denominator = [3, 4]; % The coefficients of 's' in descending powers.
% Create the transfer function
sys_tf = tf(numerator, denominator);
% Plot the root locus
figure;
rlocus(sys_tf);
grid on;
title('Root Locus Plot');
xlabel('Real Part (Re)');
ylabel('Imaginary Part (Im)');
```

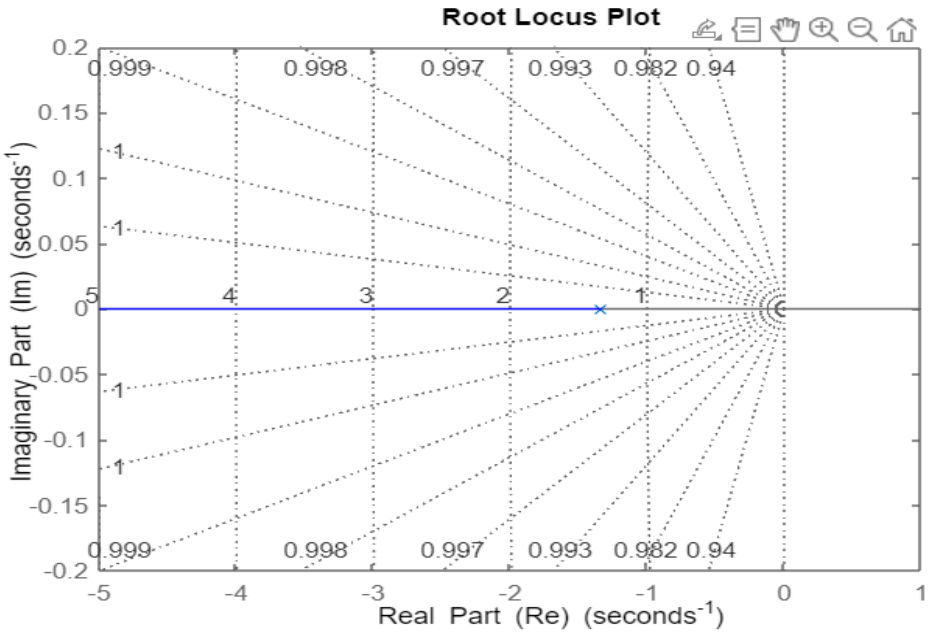

Figure 5-34:Root Locus of Steady State System

5.7.2 Matlab Code to Convert The Transfer Function to State Space Representation

To convert a transfer function to state-space representation in MATLAB, the **tf2ss** function is used . This function takes the numerator and denominator coefficients of

the transfer function as input and returns the corresponding state-space representation. Here's the MATLAB code to convert the given transfer function to state-space representation:

```
% Define the transfer function numerator = 1; denominator = [3, 4];
 % The coefficients of 's' in descending powers.
% Create the transfer function
 sys_tf = tf(numerator, denominator);
% Convert transfer function to state-space representation
 sys_ss = tf2ss(sys_tf);
 % Display the state-space representation disp('State-Space Representation:');
 disp('A =');
disp(sys_ss.A);
disp('B ='); disp(sys_ss.B);
 disp('C ='); disp(sys_ss.C);
disp('D ='); disp(sys_ss.D);
```

In this code, we first define the numerator and denominator of the transfer function. Then, we create the transfer function using **tf(numerator, denominator)**. Next, we use the **tf2ss** function to convert the transfer function to state-space representation. The resulting state-space representation is stored in the variable **sys_ss**, which contains matrices A, B, C, and D representing the state-space system.

The **disp** function is used to display the matrices A, B, C, and D of the state-space representation in the command window.

When you run this code, it will display the state-space representation of the given transfer function in the command window.

```
% Define the transfer function
num = 1;
den = [3, 4]; % The coefficients of 's' in descending powers.
```

```
% Create the transfer function
sys_tf = tf(num, den);
[A,B,C,D]=tf2ss(num,den)
% Convert transfer function to state-space representation
sys_ss = ss(sys_tf)
% Display the state-space representation
disp('State-Space Representation:');
disp('A =');
disp(sys_ss.A);
disp('B =');
disp(sys_ss.B);
disp('C =');
disp(sys_ss.C);
disp('D =');
disp(sys_ss.D);
```

Output

```
A =
        x1
 x1  -1.333

B =
     u1
 x1  0.5

C =
        x1
 y1  0.6667

D =       u1
 y1   0
```

Continuous-time state-space model.

matlab:disp(char('',' A: -1.3333 ',' B: 0.5000 ',' C: 0.6667 ',' D: 0 ',' E: [] ',' Scaled: 0 ',' StateName: %7b''''%7d ',' StatePath: %7b''''%7d ',' StateUnit: %7b''''%7d ',' InternalDelay: [0×1 double] ',' InputDelay: 0 ',' OutputDelay: 0 ',' InputName: %7b''''%7d ',' InputUnit: %7b''''%7d ',' InputGroup: [1×1 struct] ',' OutputName: %7b''''%7d ',' OutputUnit: %7b''''%7d ',' OutputGroup: [1×1 struct] ',' Notes: [0×1 string] ',' UserData: [] ',' Name: '''' ',' Ts: 0 ',' TimeUnit: ''seconds'' ',' SamplingGrid: [1×1 struct] ',' '))

State-Space Representation:

A = -1.3333

B = 0.5000

C = 0.6667

D = 0

5.7.3 Matlab Program To Perform Steady State Stability Analysis

Steady-state stability analysis involves analyzing the stability of a control system in equilibrium condition. For this analysis, we need to check the poles of the transfer function or state-space representation. If all the poles have negative real parts, the system is stable at the steady-state.

Here's a MATLAB program to perform steady-state stability analysis for a given transfer function: matlab Copy code

```
% Define the transfer function numerator = 1;
Denominator = [3, 4];
% The coefficients of 's' in descending powers.
 % Create the transfer function sys_tf = tf(numerator, denominator);
 % Get the poles of the transfer function poles_tf = roots(denominator);
 % Perform steady-state stability analysis if all(real(poles_tf) < 0) fprintf('The system is stable at steady-state.\n');
 else fprintf('The system is not stable at steady-state.\n');
 end
```

In this code, we first define the numerator and denominator of the transfer function. Then, we create the transfer function using **tf(numerator, denominator)**. The **roots**

function is used to find the poles of the transfer function, and the **real** function is used to extract the real parts of the poles.

The **if** statement checks if all the real parts of the poles (**real(poles_tf)**) are less than zero, indicating stability at steady-state. If all the poles have negative real parts, it prints a message indicating that the system is stable. Otherwise, it prints a message indicating that the system is not stable.

When you run this MATLAB program with your specific transfer function coefficients, it will determine if the system is stable at steady-state or not.

a control system has the following transfer function; I(s)/V(s)=1/(3s+4), write a matlab program to perform steady state stability analysis using state space representation

To perform steady-state stability analysis using the state-space representation for the given transfer function H(s) = 1 / (3s^2 + 4) we need to find the state-space matrices **A**, **B**, **C**, and **D** and then check the eigenvalues of the state matrix **A**. If all the eigenvalues have negative real parts, the system is stable at steady-state.

Here's the MATLAB program to perform steady-state stability analysis for the given transfer function:

```
% Define the transfer function coefficients
numerator = 1;
denominator = [3, 4];
% The coefficients of 's' in descending powers.
% Convert transfer function to state-space representation
sys_tf = tf(numerator, denominator);
sys_ss = ss(sys_tf);
% Extract the state-space matrices
A = sys_ss.A
B = sys_ss.B
C = sys_ss.C
```

```
D = sys_ss.D
% Get the eigenvalues (poles) of the state matrix
poles_ss = eig(A);
% Perform steady-state stability analysis
if all(real(poles_ss) < 0)
    fprintf('The system is stable at steady-state.\n');
else
    fprintf('The system is not stable at steady-state.\n');
end
```

Solution

A = -1.3333

B = 0.5000

C = 0.6667

D = 0

poles_ss = -1.3333

The system is stable at steady-state.

In this code, we first define the numerator and denominator of the transfer function. Then, we create the transfer function using **tf(numerator, denominator)** and convert it to the state-space representation using **ss(sys_tf)**.

Next, we extract the state-space matrices **A**, **B**, **C**, and **D** from the state-space system **sys_ss**.

The **eig** function is used to find the eigenvalues (poles) of the state matrix **A**. The **if** statement checks if all the real parts of the eigenvalues (**real(poles_ss)**) are less than zero, indicating stability at steady-state. If all the eigenvalues have negative real parts, it prints a message indicating that the system is stable. Otherwise, it prints a message indicating that the system is not stable.When you run this MATLAB Code, it will determine if the system is stable at steady-state or not for the given transfer function.

CHAPTER SIX:
SUMMARY, CONCLUSIONS AND RECOMMENDATIONS

6. Summary, Conclusions and Recommendations

6.1 Summary of the Findings

6.1.1 Summary of the Findings Based on Objective One

In undertaking experiments with Ceramic based and Neodymium based MEMs, the following was established: - It was generally observed that in the case of voltage electrical characteristics for both designs the output voltage took upward trajectory as the number of magnetic loadings increased across all the seven experiments undertaken**.** This implied that voltage output had a positive gradient slope which increased with magnetic loadings and time. It was further observed that the input voltage took downward trend a cross the seven experiments undertaken**.** The input voltage had negative gradient which decreased with magnetic loading and time.

It was also noted that in both designs, profile of load currents was marginally higher than input current across all levels of magnetic loadings. Both input and load currents were noted to have a negative gradient. Loading currents profile graphs were marginally steeper than input current profile graphs which increased with the level of magnetic loadings. The rate of reducing current was greater for loading current than input current. The load current reduced at a faster rate than input current.

Besides the analysis of voltage and current, the power graphs, when plotted against time across all levels of magnetic loadings of both designs of MEMs, showed the typical bell graphs as expected for power graphs. The research established that the power profile for 4, 6 and 8 original designs with Ceramic magnets showed that the power output increased at the rate of 0.023 watts per hour, 0.342 watts per hour and 0.0074 watts per hour respectively. Likewise, it was noted that the power profile for 4,6 and 8 original designs with Neodymium magnets showed that the power output increased at the rate of 0.182 watts per hour, 0.161 watts per hour and 0.0214 watts per hour respectively.

This investigation also determined that, in both designs it was established that there was generally a declining rate of power input unlike the case of output power which was on increasing trend. Besides these findings the research demonstrated that in

the case of 4,6 and 8 replication design of Monopole Energizer Machines input power reduced at the rate of 0.0093 watts per hour, 0.0125 per hour and 0.0235 watts per hour respectively. It continued to reduce at the rate of 0.0455 watts per hour , 0.077 watts per hour, 0.077 watts per hour and 0,0544 watts per hour 10,12,14 and 16 magnetic loadings respectively. All efficiencies types increased with increase with number of magnets in the both case s of design.

6.1.2 Summary of the Findings Based on Objective Two

The experimental analysis with both designs that is Neodymium Magnet MEM design Ceramic magnets MEM design, showed that the output voltage took upward trajectory as the number of magnetic loadings increased across all the seven experiments undertaken**.** It was further observed that Neodymium MEM design in comparison to Ceramic MEM design maintained a higher trajectory voltage out put a cross all levels of magnetic loadings. In both cases of the designs the voltage output had a positive gradient which increased with magnetic loadings and time. The voltage gradient slope for Neodymium magnet MEM design was steeper than that of Ceramic magnet MEM design a cross all levels of magnetic loadings. It was further noted that the input voltage in both cases of the designs took downward trend a cross the seven experiments undertaken, with the slope of Neodymium magnet MEM design being steeper than that of Ceramic MEM design**.** The investigation also established that the two designs had a negative slope for input voltage with that of Neodymium design with a higher negative gradient. The input voltage had negative slope which decreased with magnetic loading and time in both cases of design.

It was established that profile of load currents was higher than input current across all levels of magnetic loadings. Both input and load currents were noted to have a negative gradient. Loading currents profile graphs were steeper than input current profile graphs which increased with the level of magnetic loading. The rate of reducing current was greater for loading current than input current. The rate of reducing current was greater for loading current than input current in both cases of the designs even though the magnitude was greater for Neodymium MEM design

The study established further that the power output profile for Neodymium Magnet MEM design was higher than that of Ceramic Magnet MEM design. The research

established that the power profile for 4,6 and 8 original designs with Neodymium magnets showed that the power output increased at the rate of 0.182 watts per hour, 0.161 watts per hour and 0.0214 watts per hour respectively. This investigation also determined that, in the case of power input there was generally a declining rate of power input unlike the case of output power which was on increasing trend. It was observed that in the case of 4,6 and 8 original designs with neodymium magnets original design of Monopole Energizer Machines input power reduced at the rate of 0.0093 watts per hour, 0.0125 per hour and 0.0235 watts per hour respectively. This trend was consistent across the board of all the seven experimental runs. It was generally observed and concluded that the power graphs assumed bell form as a common characteristic of power graphs. Most of the power output equations assumed polynomial nature, whereas as those of input power graph mirrored straight lines trend equations. The power output increased at increasing rates with increase in number of magnets of replication designs and vice versa. All co-efficiencies types increased with increase with number of magnets in both cases of the designs. The average Coe-efficiencies of performance, Instantaneous Coe- efficiencies of performance and peak Coe-efficiencies of performance increased with the level of magnetic loadings across board in both cases of the design, even though the increase was more, and the time taken to attain the respective efficiencies was shorter in the case of Neodymium magnet MEM design than the case of Ceramic Magnet MEM designs across all levels of magnetic loading

6.1.3 Summary of the Findings Based on Objective Three

The predictive mathematical model of MEM system was modelled after SRM for input parameters and B.C for output parameters. This is because MEM can be closely compared with SRM for input parameters and BC for output parameters. The model equations for input and output parameters were developed and subsequent solutions were determined. In this investigation, it was established that the duty cycle for MEM was determined as the ratio of input voltage to output voltage. This is contrary to other machines like motors and generators apart from MEM where the duty cycle was given as one minus the ratio of input voltage to output voltage as indicated below :-

The $duty$ cycle is defined as $\Delta = \frac{V_{in}}{V_{out}}$ for MEM, where as other machines $is\ given\ as\ \Delta = 1 - \frac{V_{in}}{V_{out}}$

In this research, using experimental data this research developed predictive mathematical model for Monopole Energizer Machine This model was referred to us Masinde Muliro University of science and Technology Monopole Energizer predictive mathematical model (MMUSTMEPMM). The predictive mathematical model was developed based on the data generated by original design and replication design. The model developed has eight components .Four equations or components are for prediction of voltage output for original and replication designs. Two of the equations are meant to predict voltage output for time function model for the two designs of MEM and time independent model for the two MEM designs. The other four equations are for predicting the load current time function equations for original and replication designs , whereas the remaining two equations are for predicting the load current equations for time independent functions for original and replication designs,

The models developed for voltage output for time function and time independent for original and replication design are :-

i. $\mathrm{V_{out}(t)} = 0.028\mathrm{K_C t} + 7$ for predicting voltage output time function for original design. function n and time independent

ii. $\mathrm{V_{out}} = 0.028\mathrm{K_C} + 7$. *For predicting voltage output time independent function for original design*

$Where$

$K_C = (\ 0.64 \pm 0.04 G_C)t$, G_C is referred to as gaining constant associated with ceramic design MEM,. , K_C and $N_C$are constants associated with ceramic magnets.

$G_C = N_C - 4, N_C\ is\ the\ number\ of\ magnets\ loaded\ on\ MEM$

iii. $V_{out}(\mathrm{t}) = 0.028 K_N \mathrm{t} + 7$ is the time dependent equation to predict the voltage output for Neodymium Magnet MEM design according to the level of magnetic loadings?

iv. $V_{out} = 0.028 K_N + 7$ is the time independent equation to predict the voltage output depending on the level of magnetic loadings associated with MEM replication design , $K_N = (\ 0.64 \pm 0.043\mathrm{G}_N)$,

$G_N = N_N - 4, Where\ N\ is\ the\ number\ of\ magnets,$

$4\ is\ used\ because\ the\ reference\ point\ is\ loading\ of\ 4\ magnets.$ G is defined as constant, because it will determine the increase or decrease of voltage output.

The models developed for load current for time function and time independent for original and replication design are :-

i. $I(t) = -0.0002L_C t + .2\ldots$, L_C=1.02^G this is time function equation for original design load current prediction

ii. $l = -0.0002Lt + 0.2\ldots\ldots$this is time independent function of MEM original load current

Where

$I_{out}(t) and\ I_{out}\ output\ current\ at\ any\ given\ time\ for\ time\ dependent\ and$ time independent functions. t is time in minutes, G_C is the constant computed as shown below:-

$G_C = N_C - 4, Where\ N_C\ is\ the\ number\ of\ magnets\ loaded\ on\ MEM$, G_C is referred to as a constant.

The two model equations developed for replication load current are shown below:-

iii. $I_{out}(t) = 0.17 - 0.000195L_C t$ this is time function equation for replication load current prediction

iv. $I_{out} = 0.17 - 0.000195L_C$ this is time independent equation for replication load current prediction

L_C=0.98^G

$I_{out}(t)\ is\ component\ of\ output\ current\ with\ time$

I_{out} $is\ a\ time\ independent\ component\ of\ output\ current$, N_C is a constant and represents the number of magnets at a reference point

Features of this model was that when the model predictions were compared with experimental data and predicted figures, the model was in agreement with experimental data to more than 98 percent. It also concurred with the behavior of experimental data for both model outputs, load current and co-efficiency of performance

6.1.4 Summary of the Findings Based on Objective Four

The steady state analysis was performed on the MEM, with assistance of MATLAB. The system was found to be stable based on mathematical stability analysis and secondly physical observation also showed that the system was stable when operation.

6.2 Conclusions

6..2.1 Conclusions Based on Objective One

This study has resulted in three main conclusions based on objective one .The conclusions arrived at are as follows :-

This research has established that in both machines of MEMs for original and replication design, output voltage took the upward trajectory across all levels of magnetic loadings. Voltage output –input ratio was greater than one and it increased with the level of magnetic loadings in both cases. This investigation also concluded that in both designs, both load current and input current increased marginally with magnetic loadings even though the increase in load current was marginally greater than that of input current. Both parameters had a negative slope , whose gradient increased with magnetic loadings. Thirdly in both cases of designs it was concluded that across all levels of magnetic loadings, the magnitude and the rate of attainment of all categories of efficiencies of performance increased with magnetic loading. The power output maintained a positive slope whereas the input power graphs maintained a negative slope. The magnitude of the two slopes increased with magnetic loadings,

6.2.2 Conclusions Based on Objective Two

On the second objective this research arrived on two conclusions .First the replication design showed that, voltage, current and power characteristics were in addendum with the characteristics of original design, even though for both voltage and power the input-output ratios of replication designs were higher than those of original designs across all levels of magnetic loadings. Furthermore, this research concluded that the slope of input voltage, input current and load currents had a negative gradient whose magnitude increased with magnetic loadings. Secondly this investigation concluded that across all levels of magnetic loading the Voltage output increased with magnetic loading, even though it was higher for replication design than that original design, this trend continued to increase with increase in

level of magnetic loading. The results further showed that the ratio of charging rate or rate of gaining voltage for replication design to that of original design in charging process was greater than one across board and it increased with magnetic loading, the highest ratio recorded was 3.44 at magnetic loading of 14.

6.2.3 Conclusions Based on Objective Three

From the third objective and specifically on modeling this research drew two major conclusions. First in this investigation it has been deduced that the duty cycle of the monopole energizer machine is given by the ratio of input voltage to output voltage. That is $\Delta = \frac{V_{in}}{V_{out}}$, This is contrary to computation of duty cycle of other machines which is given by $\Delta = 1 - \frac{V_{in}}{V_{out}}$, Secondly **t**his research has further concluded that predictive mathematical model can determine the voltage output and the load current .The investigation concluded that the following models can be used to predict voltage output and load current for original and replication design machines with accuracy level of more than 98 percent. This is confirmed by coefficient of determination, Efficiency analysis and Root Mean Square Error.

6.2.4 Conclusions Based on Objective Four

Objective four of this investigation was to perform Steady state Analysis of Monopole Energizer Machine. Based on the steady state analysis it was concluded that the system is stable.

6.3 Recommendations

6.3.1 Recommendations

There are cases where the RMSE values for neodymium magnets are higher than the RMSE values for ceramic magnets, even when the same number of magnets are used. This suggests that the optimal number of magnets for achieving the highest accuracy may be different for each type of design, and that other factors (such as the specific application requirements) should also be considered when choosing a magnet for a particular application. Furthermore, the R^2 value of neodymium magnets is slightly higher than that of ceramic magnets, suggesting that neodymium magnets may be a slightly better predictor of the outcome variable than ceramic magnets.

Bedini SSG is a great invention that can be relevant in our daily life. Simple example from Bedini SSG concept is to generate a free energy fan. Besides, it also has potential to generate electricity that can be further enhancing for future improvement so that it can give benefit for our next generation. It is recommended that scale up of this system should be undertaken in this area to advance the innovation and its application.

6.3.2 Recommendations on Areas for Further Investigations

The study on effect of stationery coil size on capability of electricity generation of monopole energizer, characteristics of electrical outputs, comparison of electric power generation for different coil sizes can be undertaken was beyond the scope of this study.

1. In this investigation the model predicts output for voltage, current and power output forever. This may also imply that the power output prediction can be on the upward trend forever. Hence further investigation to establish the limits of power, current and voltage output in relation to the magnetic loadings need to be established.
2. The experimental rid is conducted at constant radius and circumference. It will be important to conduct more investigation at different radius and circumference using similar number of magnets for both original and replication design. This will assist in establishing if there is a relationship between voltage output and the radius of the wheel.
3. Undertake an investigation varying the number of coils or turns and the number of poles or magnets for both original and replication designs.
4. COP is greater than 1, extra energy is obtained from the environment making COP greater than 100%. The operation of this model gives that indication indirectly based on its output parameters for voltage and current. The product of these two parameters at different intervals of time and magnetic loadings gives the product of power and energy. There are a number of instances where the output- input ratio is greater than one, implying that the output power is greater than the input power. This model can predict that, but it cannot determine how much energy is utilized from the environment. Establishing the amount of energy obtained from the environment is

complex, and it would also require a complex experimental assembly or set up. Based on these facts further investigation is required to modify the model so as to determine the amount of energy or power obtained from environment. This will help in determining the real efficiency of the system.

6.4 Research Contribution

This research has contributed to the body of knowledge in seven principle ways, as discussed below:-

6.4.1 Development of Predictive Mathematical Model:-

In this research, Masinde Muliro University of Science and Technology Monopole Energizer Machine Physical and Predictive Mathematical Model has been developed (MMUSTMEMPPMM). The physical model was developed in the lab based on ceramic magnets (here referred to as original design) and Neodymium magnets (here referred to as replication design). The predictive mathematical model developed has the following features.

The model developed has eight equations. Four equations are for prediction of voltage output for original and replication designs. Two of the equations are meant to predict voltage output for time function model for the two designs of MEM and time independent model for the two MEM designs. The other four equations are for predicting the load current time function equations for original and replication designs , whereas the remaining two equations are for predicting the load current equations for time independent functions for original and replication designs,

6.4.2 The Strenght of MEM is Associated With Magnetic Type and The Number Of Magnets

This investigation has also established that the rate of charging or speed of charging the battery is determined by the number of magnets fixed on the monopole ,wheel, the more the magnet ,the higher the speed of charging and the shorter the time of charging hence the conclusion the rate of charging (R_C) is directly proportional to type of magnet T_{ype} or magnetic flux density, the number of magnets fixed on the wheel (N_M), the speed of the wheel(S_W) and size of the coil i.e. Diameter of the wheel (D_W) and number of turns (N_T) $R_c \propto M_{type} \times N_M$ x $S_w \times D_w \times R_p \times N_T$(number of turn)x$D_wxR_p$ or magnetic flow. Rate of pulses production or current

Rp hence Re=K(N_W $S_{WCS\ RpLc}$) this leads to creation of the above formula or knowledge as for and also type of magnet.

$$R_c \propto M_{typ} \times N_m \times S_w \times D_w \times R_P$$

$$R_c = KM_{typ} \times N_m \times S_w \times D_w \times R_P$$

Replacing M_{type} by magnetic flux density

Secondly the Rate of charging is also determined by the type of magnet under consideration ,it has been consistently observed that between neodymium magnet and original design replication design was found to be more strong than original design

6.4.3 Development Of Duty Cycle For Use By MEM Design

In this investigation it has been deduced that the duty cycle of the monopole energizer machine is given by the ratio of input voltage to output voltage. That is $\Delta = \frac{V_{in}}{V_{out}}$, This is contrary to computation of duty cycle of other machines which is given by

$\Delta = 1 - \frac{V_{in}}{V_{out}}$, hence the new duty cycle for Monopole Energizer Machines of both types of design.

6.4.4 Effect of Lenz Law on Coefficient of Performance

It was observed that the rate of charging of neodymium magnet was higher than that of ceramic magnet monopole energizer model at the same loading (Diameter of the wire of the wire).In both cases of design the output power profile was higher than input power profile figures. This trend increased with magnetic loading. Further observation showed that both cases of design increased with magnetic loading and it was higher for Neodymium magnet replication design than original design a cross all levels of magnetic loading. It was also demonstrated that the co-efficient of performance of MEM was higher than those of generators, motors and transformers.

This investigation further showed that for both cases of design the input and load current marginally reduced with magnetic loading. In replication design this trend was more than original design. This implied that the rate of current flow reduced with magnetic loading and was more for the case of replication design than original

design. In some cases, it was assumed that input current will tend towards zero as the number of magnets increased regardless as to whether they were original or replication design. It is also true that as the number of magnets increased, the resistance mounted by EMF also reduced remarkably due to substantial reduction in current flow or pulses flow.

Lenz law is a consequence of the law of conservation of energy**.** It is due to a current that induces a counter magnetic field which opposes the magnetic field generating the current. Electrical machines (transformers, motors and generators) in operation are subject to Lenz's law. They develop back emf which is a function of supply current and consequently reduces operation efficiency. Lenz law formula is given by $EMF = -N\left[\frac{\partial\theta}{\partial t}\right]$ Where N-Number of loops,$\partial\theta - is\ change\ in\ magnetic\ flux, \partial t - \ is\ change\ in\ time$

In Monopole Energizer Machine EMF component is minimized or reduced.

$EMF = -N\left[\frac{\partial\theta}{\partial t}\right] = e_b = k_b\frac{\partial\theta}{\partial t} = k_b W$Reduces or is minimized**.**

In the case of Monopole operation, the current is not allowed to flow continuously but instead the current flows as pulses (on-off) .Due to this , the Lenz effect is minimized even more with increased magnetic loading for both designs and more so for replication design. This explains why the current flowing into the Monopole Energizer Machine is very low and subsequently the effect of Lenz law is minimal. The low input current passing through the coil is very small and is sufficient to establish magnetic field in the coil. Once the magnetic field is established the current should be interrupted, consequently magnetic field collapses, introducing inductive kickbacks. Inductive kickback is output of Monopole Energizer Machine used to charge secondary battery. The input current to energizer (MEM) does this over and over again that is the magnetic field is established and collapses that is you don't need much current.

Due to reduced effect of Lenz-law or induced Emf (Electro motive force) . Monopole energizer has low Lenz's effect. In operation the MEM consumes very low supply current and hence develops very low back emf. The rotor of the energizer experiences low drag leading to much better efficiency compared to

typical electrical machines. Monopole energizer overcomes the Lenz law by changing the design geometry of the machine. Whereas generators, motors and transformers allow or furnish continuous current, Monopole current prevents the flow of continuous current, it is forbidden. In generators the aim is to minimize or eliminate the harmonics. Consequently, this confirmed why efficiency and Co-efficient of performance kept on increasing with increase in magnetic loading.

6.4.5 Utilizing Hammonis In Electrical Machines

This investigation has shown that the harmonics can be utilized for a better purpose in the electrical machines unlike in the past where its usage was dismissed. Unlike Monopole Energizer Machines, Generators will furnish continuous current during their operations. Monopole Energizer Machine prevents the flow of continuous current, it is forbidden.

In generators the aim is to minimize or eliminate the harmonics. Problems associated with harmonics are increased heating, higher core losses, short life of the machine, and increased current in the neutral conductor, telecommunication inference etc. These could justify, harnessing harmonics for better use rather than dismissing it. Practical way is we want the current to flow in the shortest time possible by doing this you minimize Lenz law effect that is impulses have a lot of harmonics. Impulses are from inductive kick back of the armature coil due to collapse of magnetic field which is a secondary source of energy in the Monopole system .That is the source from the primary battery. In electronic switching circuits the inductive kickbacks are suppressed through free –wheeling diode connection. In Monopole Energizer Model it is harnessed for charging for a secondary battery.. Another example is in thermodynamics where sharp or steep gradients are known to violate the second law , impulse (kick back) is a steep gradient.. Energy of the collapsing magnetic field is called inductive kickback. It destroys unprotected semiconductor switches using freewheeling diodes.

6.4.6 Location Of Behavior of MEM in Scientific Theory and Frame Work.

One of the research gaps identified was lack of scientific proof that MEM cannot be located in scientific setting or frame work, there has been little or scanty information in locating the working of monopole Energizer machine in scientific setting and frame work. This investigation has shown that the operation of MEM demonstrates

exchange of both matter and energy fluxes with the environment. This investigation has further demonstrated that MEM has exhibited open thermodynamic non-equilibrium steady state system behavior. This investigation has further demonstrated that MEM, is open non equilibrium steady state thermodynamic system and it is also a time function system that exhibits both time independent and time function aspects just like a heat pump and Photoelectric systems, based on this behavior the system satisfies the condition for it to be classified as an open Non-Equilibriums Steady State Thermodynamic Systems.

6.4.7 Vacuum is not inert as Per The Initial Assertion

In the electrodynamics model of Electrical systems, it is assumed that the vacuum is inert. However, the vacuum is not inert in a form that needs to be transformed into electrical form, an example is a charged inductor. It develops a magnetic field which at the moment of being de-energized the magnetic field collapses. It is the collapsing magnetic field that generates the inductive kickback and, in this sense, the charged inductor functions as a transducer of energy to electrical energy. Monopole energizer machine (MEM) utilizes this energy in the form of impulses to charge an output capacitor or battery, hence its COP will be higher than 100%.

This investigation has established and more so based on experimental investigations in addition to other attempts by other authors and researchers suggests that this principle is anchored on particle physics principle which postulates that any bipolarity, including any scalar potential is a broken symmetry in virtual vacuum flow, despite of the, fact that interaction with vacuum is not considered in classical electrodynamics at the stage of electrical systems design. Dipoles asymmetry means that it is collecting disordered energy from the vacuum, ordering part of it and sending it in observable form to all directions. It follows that any dipole and potential in essence is negative resistor and that may be used in real circuits. It has also been shown that scalar potential is a composition, consisting of pairs of longitudinal electromagnetic waves propagating in opposite directions. The potential is ordered reorganization of vacuum energy to the determinate system of bid directional energy flows. To attach increased potential to negative resistance in battery for using bidirectional property of potential it is possible to overexcite heavy ions charging battery and also overexcite electrons which may feed load at the external circuit. The system becomes open, the thermodynamic principle of

equilibrium between electrical system and Surrounding vacuum is violated and possibility to work with COP>1or 100 percent becomes available. A simple DC Bedini motor-generator which using a little amount of energy for controlling purposes, stores energy from vacuum in rotor/flywheel and charging battery or sets of battery in Non-traditional way. Such device works with COP>1 greater than 100 percent

REFERENCES

Abraham, W. T., Fisher, W. G., Smith, A. L., Delurgio, D. B., Leon, A. R., Loh, E., . . . Hayes, D. L. (2002). Cardiac resynchronization in chronic heart failure. *New England Journal of Medicine, 346*(24), 1845-1853.

Abuissa, H., Jones, P., and Marso, S. (2005). Bibliography Current World Literature Vol 15 No 5 September 2006. *Circulation, 112*, 1719-1727.

Agardy, T., Bridgewater, P., Crosby, M. P., Day, J., Dayton, P. K., Kenchington, R., . . . Parks, J. E. (2003). Dangerous targets? Unresolved issues and ideological clashes around marine protected areas. *Aquatic conservation: marine and freshwater ecosystems, 13*(4), 353-367.

Aharonov, Y., and Bohm, D. (1961). Further considerations on electromagnetic potentials in the quantum theory. *Physical Review, 123*(4), 1511.

Ahn, A. C., Tewari, M., Poon, C.-S., and Phillips, R. S. (2006). The limits of reductionism in medicine: could systems biology offer an alternative? *PLoS medicine, 3*(6), e208.

Al-Zareer, M., Dincer, I., and Rosen, M. A. (2019). A novel approach for performance improvement of liquid to vapor based battery cooling systems. *Energy conversion and management, 187*, 191-204.

Ali, B. J., and Anwar, G. (2021). An empirical study of employees' motivation and its influence job satisfaction. *Ali, BJ, & Anwar, G.(2021). An Empirical Study of Employees' Motivation and its Influence Job Satisfaction. International Journal of Engineering, Business and Management, 5*(2), 21-30.

Anwar, F., and Rashid, U. (2007). Physico-chemical characteristics of Moringa oleifera seeds and seed oil from a wild provenance of Pakistan. *Pak. J. Bot, 39*(5), 1443-1453.

Bamisaye, A., and Adeoye, O. (2016). Design of a mobile phone controlled door: a microcontroller based approach. *J Electr Electron Syst, 5*(167), 2332-0796.1000167.

Bass, B., Nishikura, K., Keller, W., Seeburg, P. H., Emeson, R., O'connell, M., . . . Herbert, A. (1997). A standardized nomenclature for adenosine deaminases that act on RNA. *Rna, 3*(9), 947.

Bassily, E., Capolino, G., Henao, H., and Poloujadoff, M. (1995). *Simulation of switched reluctance motor back-emf compensation.* Paper presented at the Proceedings of International conference on power systems transients (JPST'95).

Bauwens, O., Dusart, M., Pierard, P., Faber, J., Prigogine, T., Duysinx, B., . . . Ninane, V. (2008). Endobronchial ultrasound and value of PET for prediction of pathological results of mediastinal hot spots in lung cancer patients. *Lung cancer, 61*(3), 356-361.

Baxter, C. V., Fausch, K. D., and Carl Saunders, W. (2005). Tangled webs: reciprocal flows of invertebrate prey link streams and riparian zones. *Freshwater biology, 50*(2), 201-220.

Baxter, M., and King, R. G. (1993). Fiscal policy in general equilibrium. *The American Economic Review*, 315-334.

Bedini, J. (2003). Patent US 6545444 Device and method for utilizing a monopole motor to create back emf to charge batteries. *April 8th*.

Bedini, J. C. (2003). Device and method for utilizing a monopole motor to create back EMF to charge batteries. In: Google Patents.

Berry, M. V., and Geim, A. K. (1997). Of flying frogs and levitrons. *European Journal of Physics, 18*(4), 307.

Bien, T. H., Miller, W. R., and Tonigan, J. S. (1993). Brief interventions for alcohol problems: a review. *Addiction, 88*(3), 315-336.

Bilyk, O., Sekurova, O. N., Zotchev, S. B., and Luzhetskyy, A. (2016). Cloning and heterologous expression of the grecocycline biosynthetic gene cluster. *PloS one, 11*(7), e0158682.

Bohren, C. F. (1983). How can a particle absorb more than the light incident on it? *American Journal of Physics, 51*(4), 323-327.

Braatz, D., Cherri, M., Tully, M., Dimde, M., Ma, G., Mohammadifar, E., . . . Haag, R. (2022). Chemical approaches to synthetic drug delivery systems for systemic applications. *Angewandte Chemie International Edition, 61*(49), e202203942.

Bridgewater, S., Ratter, J. A., and Felipe Ribeiro, J. (2004). Biogeographic patterns, β-diversity and dominance in the cerrado biome of Brazil. *Biodiversity & Conservation, 13*, 2295-2317.

Büscher, C., and Sumpf, P. (2015). "Trust" and "confidence" as socio-technical problems in the transformation of energy systems. *Energy, sustainability and Society, 5*(1), 1-13.

Cápek, V., and Sheehan, D. P. (2005). *Challenges to the second law of thermodynamics*: Springer.

Cardoza, L., Korir, A., Otto, W., Wurrey, C., and Larive, C. (2004). Applications of NMR spectroscopy in environmental science. *Progress in nuclear magnetic resonance spectroscopy, 45*(3), 209-238.

Carrington, G., and Stephenson, J. (2018). The politics of energy scenarios: Are International Energy Agency and other conservative projections hampering the renewable energy transition? *Energy research & social science, 46*, 103-113.

Çetin, N. S., and Özmen, N. (2003). Studies on lignin-based adhesives for particleboard panels. *Turkish Journal of Agriculture and Forestry, 27*(3), 183-189.

Chen, X.-K., Qian, D., Wang, Y., Kirchartz, T., Tress, W., Yao, H., . . . Zou, Y. (2021). A unified description of non-radiative voltage losses in organic solar cells. *Nature Energy, 6*(8), 799-806.

Cheng, M. L., Zhang, L., Borok, M., Chokunonga, E., Dzamamala, C., Korir, A., . . . Van Loon, K. (2015). The incidence of oesophageal cancer in Eastern Africa: identification of a new geographic hot spot? *Cancer epidemiology, 39*(2), 143-149.

Chiaramonti, D., Oasmaa, A., and Solantausta, Y. (2007). Power generation using fast pyrolysis liquids from biomass. *Renewable and sustainable energy reviews, 11*(6), 1056-1086.

Cieszczyk, P., Krupecki, K., Maciejewska, A., and Sawczuk, M. (2009). The angiotensin converting enzyme gene I/D polymorphism in Polish rowers. *International journal of sports medicine*, 624-627.

Cortés, E., Grzeschik, R., Maier, S. A., and Schlücker, S. (2022). Experimental characterization techniques for plasmon-assisted chemistry. *Nature Reviews Chemistry, 6*(4), 259-274.

Crutchfield, J. P., Ellison, C. J., and Riechers, P. M. (2016). Exact complexity: The spectral decomposition of intrinsic computation. *Physics Letters A, 380*(9-10), 998-1002.

Dangerman, A. J., and Schellnhuber, H. J. (2013). Energy systems transformation. *Proceedings of the National Academy of Sciences, 110*(7), E549-E558.

Das, S. P. (2004). Mode-coupling theory and the glass transition in supercooled liquids. *Reviews of modern physics, 76*(3), 785.

Datta, A., Pietzonka, P., and Barato, A. C. (2022). Second law for active heat engines. *Physical Review X, 12*(3), 031034.

Dudley, B. (2019). BP statistical review of world energy 2016. *British Petroleum Statistical Review of World Energy, Bplc. editor, Pureprint Group Limited, UK*.

Fakhrurrazey, F. S., Munim, W. N. W. A., and Othman, Z. (2014). *Performance comparison of 4-Pole Neodymium Magnet Bedini SSG free energy generator.* Paper presented

at the 2014 IEEE 8th International Power Engineering and Optimization Conference (PEOCO2014).

Faraday, M. (1839). I. Experimental researches in electricity.—fifteenth series. *Philosophical Transactions of the Royal Society of London*(129), 1-12.

Felfli, F. F., Luengo, C. A., Suárez, J. A., and Beatón, P. A. (2005). Wood briquette torrefaction. *Energy for sustainable development, 9*(3), 19-22.

Gallavotti, G., and Cohen, E. G. D. (1995). Dynamical ensembles in nonequilibrium statistical mechanics. *Physical review letters, 74*(14), 2694.

Gommans, M., Krishman, K. S., and Scheffold, K. B. (2001). From brand loyalty to e-loyalty: A conceptual framework. *Journal of Economic & Social Research, 3*(1).

Green, M. A., Emery, K., Hishikawa, Y., and Warta, W. (2010). Solar cell efficiency tables (version 37). *Progress in photovoltaics: research and applications, 1*(19), 84-92.

Green, M. A., Hishikawa, Y., Dunlop, E. D., and Levi, D. H. (2019). J. Hohl? Ebinger, M. Yoshita and AW Ho? Baillie,". *Solar cell efficiency tables (Version 53)," Progress in Photovoltaics, 27*(1), 3-12.

Hashemi, Z., Zohrabi, F., and Mardaneh, M. (2019). A multi-objective optimization of switched reluctance motor using a hybrid analytic-ANFIS model considering the vibrations. *Iranian Journal of Science and Technology, Transactions of Electrical Engineering, 43*(2), 361-371.

Ibanez, L. E., and Uranga, A. M. (2012). *String theory and particle physics: An introduction to string phenomenology*: Cambridge University Press.

Idogwu, S., Onah, T., and Ugwuanyi, B. (2019). Evaluation of A Four Stroke Compression-Ignition Engine with Load (100N). *Evaluation, 9*(8).

Jazdzynski, W., and Majchrowicz, M. (2013). Analytical Model of a Switched Reluctance Motor for its Optimization–Selected Problems. *Electrical Review, 89*(11), 153-158.

Kassebaum, N., Bernabé, E., Dahiya, M., Bhandari, B., Murray, C., and Marcenes, W. (2014). Global burden of severe periodontitis in 1990-2010: a systematic review and meta-regression. *Journal of dental research, 93*(11), 1045-1053.

Kerner, R. A., Xu, Z., Larson, B. W., and Rand, B. P. (2021). The role of halide oxidation in perovskite halide phase separation. *Joule, 5*(9), 2273-2295.

Khan, S., Khan, M., Hanjra, M. A., and Mu, J. (2009). Pathways to reduce the environmental footprints of water and energy inputs in food production. *Food policy, 34*(2), 141-149.

Kodama, Y., Ng, C. S., Wu, T. T., Ayers, G. D., Curley, S. A., Abdalla, E. K., . . . Charnsangavej, C. (2007). Comparison of CT methods for determining the fat content of the liver. *American Journal of Roentgenology, 188*(5), 1307-1312.

Koder, R. L., Haynes, C. A., Rodgers, M. E., Rodgers, D. W., and Miller, A.-F. (2002). Flavin thermodynamics explain the oxygen insensitivity of enteric nitroreductases. *Biochemistry, 41*(48), 14197-14205.

Kondepudi, D. K. (2008). *Introduction to modern thermodynamics* (Vol. 666): Wiley Chichester.

Lahsasni, S., Kouhila, M., Mahrouz, M., and Jaouhari, J. (2004). Drying kinetics of prickly pear fruit (Opuntia ficus indica). *Journal of food engineering, 61*(2), 173-179.

Landon, B. (2015). Entropic fluctuations of XY quantum spin chains. *arXiv preprint arXiv:1503.02331*.

LINDEMANN, P., and MURAKAMI, A. (2012). Bedini SG: The Complete Beginner's Handbook. *Liberty Lake, Washington: A&P Electronic Media*.

Liu, Y., Hayakawa, T., Suzuki, K., Hamakawa, S., Tsunoda, T., Ishii, T., and Kumagai, M. (2002). Highly active copper/ceria catalysts for steam reforming of methanol. *Applied Catalysis A: General, 223*(1-2), 137-145.

Lumley, M. A., Cohen, J. L., Borszcz, G. S., Cano, A., Radcliffe, A. M., Porter, L. S., . . . Keefe, F. J. (2011). Pain and emotion: a biopsychosocial review of recent research. *Journal of clinical psychology, 67*(9), 942-968.

Lutes, O., and Maxwell, E. (1955). Superconducting transitions in tin whiskers. *Physical Review, 97*(6), 1718.

Ma, L. (2006). *Combustion and gasification of chars in oxygen and carbon dioxide at elevated pressure.* Stanford University Stanford,

Majid, A. (2009). *We are all Moors: Ending centuries of crusades against Muslims and other minorities*: U of Minnesota Press.

McDonald, R., Nivre, J., Quirmbach-Brundage, Y., Goldberg, Y., Das, D., Ganchev, K., . . . Täckström, O. (2013). *Universal dependency annotation for multilingual parsing.* Paper presented at the Proceedings of the 51st Annual Meeting of the Association for Computational Linguistics (Volume 2: Short Papers).

Monthus, C. (2019). Large deviations for the density and current in non-equilibrium-steady-states on disordered rings. *Journal of Statistical Mechanics: Theory and Experiment, 2019*(2), 023206.

Moore, K., Stockton, M., and Bearden, T. (2006). Electromagnetic Energy from the Vacuum.

Murakami, K., Aoki, H., Nakamura, S., Nakamura, S.-i., Takikawa, M., Hanzawa, M., . . . Kiyosawa, T. (2010). Hydrogel blends of chitin/chitosan, fucoidan and alginate as healing-impaired wound dressings. *Biomaterials, 31*(1), 83-90.

Nikulov, A. (2001). Quantum force in a superconductor. *Physical Review B, 64*(1), 012505.

Nordhaus, W. (2014). *A question of balance: Weighing the options on global warming policies*: Yale University Press.

Pakulska, T., and Poniatowska-Jaksch, M. (2022). Digitalization in the Renewable Energy Sector—New Market Players. *Energies, 15*(13), 4714.

Pekarek, R. T., Christensen, S. T., Liu, J., and Neale, N. R. (2019). Energetic effects of hybrid organic/inorganic interfacial architecture on nanoporous black silicon photoelectrodes. *Sustainable Energy & Fuels, 3*(7), 1660-1667.

Perkinson, C. F., Tabor, D. P., Einzinger, M., Sheberla, D., Utzat, H., Lin, T.-A., . . . Baldo, M. A. (2019). Discovery of blue singlet exciton fission molecules via a high-throughput virtual screening and experimental approach. *The Journal of chemical physics, 151*(12).

Phurahong, T., Tibeye, T., Sangkaew, C., and Deepala, S. (2019). *Performance Analysis of Six Coils Monopole and Eight Pole Neodymium Magnet Generator.* Paper presented at the International Conference on Applied Electrical and Mechanical Engineering 2019.

Plasson, R., Kondepudi, D. K., Bersini, H., Commeyras, A., and Asakura, K. (2007). Emergence of homochirality in far-from-equilibrium systems: Mechanisms and role in prebiotic chemistry. *Chirality: the Pharmacological, Biological, and Chemical Consequences of Molecular Asymmetry, 19*(8), 589-600.

Raimondi, G., Longo, A., Giannici, F., Merkle, R., Hoedl, M., Chiara, A., . . . Maier, J. (2022). Electronic modifications in (Ba, La)(Fe, Zn, Y) O 3− δ unveiled by oxygen K-edge X-ray Raman scattering. *Journal of Materials Chemistry A, 10*(16), 8866-8876.

Rangan, K., Chase, L. A., and Karim, S. (2012). Why every company needs a CSR strategy and how to build it.

Ried, P., Bucher, E., Preis, W., Sitte, W., and Holtappels, P. (2007). Characterisation of La0. 6Sr0. 4Co0. 2Fe0. 8O3-d and Ba0. 5Sr0. 5Co0. 8Fe0. 2O3-d as Cathode Materials for the Application in Intermediate Temperature Fuel Cells. *ECS Transactions, 7*(1), 1217.

Rodger, M. A., Gris, J.-C., De Vries, J. I., Martinelli, I., Rey, É., Schleussner, E., . . . Ramsay, T. (2016). Low-molecular-weight heparin and recurrent placenta-mediated

pregnancy complications: a meta-analysis of individual patient data from randomised controlled trials. *The Lancet, 388*(10060), 2629-2641.

Saikia, B. K., Benoy, S. M., Bora, M., Tamuly, J., Pandey, M., and Bhattacharya, D. (2020). A brief review on supercapacitor energy storage devices and utilization of natural carbon resources as their electrode materials. *Fuel, 282*, 118796.

Sauer, D. U., and Wenzl, H. (2008). Comparison of different approaches for lifetime prediction of electrochemical systems—Using lead-acid batteries as example. *Journal of Power sources, 176*(2), 534-546.

Şen, A. (2008). The US fashion industry: A supply chain review. *International Journal of Production Economics, 114*(2), 571-593.

Shang, Y., Hu, X., DiRenzo, J., Lazar, M. A., and Brown, M. (2000). Cofactor dynamics and sufficiency in estrogen receptor–regulated transcription. *Cell, 103*(6), 843-852.

Sheehan, D., Garamella, J., Mallin, D., and Sheehan, W. (2012). Steady-state nonequilibrium temperature gradients in hydrogen gas–metal systems: challenging the second law of thermodynamics. *Physica Scripta, 2012*(T151), 014030.

Shih, H.-Y., Hsieh, T.-L., and Goldenfeld, N. (2016). Ecological collapse and the emergence of travelling waves at the onset of shear turbulence. *Nature Physics, 12*(3), 245-248.

Sieberer, L., Chiocchetta, A., Gambassi, A., Täuber, U. C., and Diehl, S. (2015). Thermodynamic equilibrium as a symmetry of the Schwinger-Keldysh action. *Physical Review B, 92*(13), 134307.

Siviero, A., Delunardo, T. A., Haverroth, M., Oliveira, L. C. d., and Mendonça, Â. M. S. (2011). Cultivo de espécies alimentares em quintais urbanos de Rio Branco, Acre, Brasil. *Acta Botanica Brasilica, 25*, 549-556.

Sriphan, U., Kerdchang, P., Prommas, R., and Bunnang, T. (2018a). Coefficient of performance of battery running and charging by magnet generator Bedini. *Journal of Electrochemical Energy Conversion and Storage, 15*(4).

Sriphan, U., Kerdchang, P., Prommas, R., and Bunnang, T. (2018b). Coefficient of performance of battery running and charging by magnet generator Bedini. *Journal of Electrochemical Energy Conversion and Storage, 15*(4), 041002.

Stevenson, F. J., and Cole, M. A. (1999). *Cycles of soils: carbon, nitrogen, phosphorus, sulfur, micronutrients*: John Wiley & Sons.

Sun, X., Dai, Y., Ge, T., Zhao, Y., and Wang, R. (2019). Heat and mass transfer comparisons of desiccant coated microchannel and fin-and-tube heat exchangers. *Applied Thermal Engineering, 150*, 1159-1167.

Svoboda, E., McKinnon, M. C., and Levine, B. (2006). The functional neuroanatomy of autobiographical memory: a meta-analysis. *Neuropsychologia, 44*(12), 2189-2208.

Tseng, M.-L., Chang, C.-H., Lin, C.-W. R., Wu, K.-J., Chen, Q., Xia, L., and Xue, B. (2020). Future trends and guidance for the triple bottom line and sustainability: A data driven bibliometric analysis. *Environmental Science and Pollution Research, 27*, 33543-33567.

Valone, T. J. (2007). From eavesdropping on performance to copying the behavior of others: a review of public information use. *Behavioral ecology and sociobiology, 62*, 1-14.

Van Kampen, N. G. (1992). *Stochastic processes in physics and chemistry* (Vol. 1): Elsevier.

Vilariño-Güell, C., Wider, C., Ross, O. A., Dachsel, J. C., Kachergus, J. M., Lincoln, S. J., . . . Bacon, J. A. (2011). VPS35 mutations in Parkinson disease. *The American Journal of Human Genetics, 89*(1), 162-167.

Vujicic, V., and Vukosavic, S. N. (2000). A simple nonlinear model of the switched reluctance motor. *IEEE Transactions on energy conversion, 15*(4), 395-400.

Wambui, V., Njoka, F., Muguthu, J., and Ndwali, P. (2022). Scenario analysis of electricity pathways in Kenya using Low Emissions Analysis Platform and the Next Energy

Modeling system for optimization. *Renewable and sustainable energy reviews, 168*, 112871.

Warf, B., and Arias, S. (2008). *The spatial turn: Interdisciplinary perspectives*: Routledge.

Wheeler, M. (2019). Cupidine Caeci: The Ethics of Perception in Lucretius' De rerum natura IV.

Xiaoren, S., Maolin, G., Jinwang, W., and Jianjun, L. (2008). *Transformation of World Energy Composition and Future of Solar Energy in the 21st Century.* Paper presented at the Proceedings of ISES World Congress 2007 (Vol. I–Vol. V).

Xue, S., Li, H., Guo, Y., Zhang, B., Li, J., and Zeng, X. (2022). Water lubrication of graphene oxide-based materials. *Friction, 10*(7), 977-1004.

Yang, H., Bahk, J.-H., Day, T., Mohammed, A. M., Snyder, G. J., Shakouri, A., and Wu, Y. (2015). Enhanced thermoelectric properties in bulk nanowire heterostructure-based nanocomposites through minority carrier blocking. *Nano letters, 15*(2), 1349-1355.

Yusaf, T., Fernandes, L., Abu Talib, A. R., Altarazi, Y. S., Alrefae, W., Kadirgama, K., . . . Mamat, R. (2022). Sustainable aviation—Hydrogen is the future. *Sustainability, 14*(1), 548.

Zhang, X., Hasani-Sadrabadi, M. M., Zarubova, J., Dashtimighadam, E., Haghniaz, R., Khademhosseini, A., . . . Li, S. (2022). Immunomodulatory microneedle patch for periodontal tissue regeneration. *Matter, 5*(2), 666-682.

Zhang, X., and Shu, C.-W. (2010). On positivity-preserving high order discontinuous Galerkin schemes for compressible Euler equations on rectangular meshes. *Journal of Computational Physics, 229*(23), 8918-8934.

Zhang, Z., Dong, Y., Li, F., Zhang, Z., Wang, H., Huang, X., . . . Wang, H. (2016). The Shandong Shidao Bay 200 MWe high-temperature gas-cooled reactor pebble-bed module (HTR-PM) demonstration power plant: an engineering and technological innovation. *Engineering, 2*(1), 112-118.

Zheng, J., Lau, C. F. J., Mehrvarz, H., Ma, F.-J., Jiang, Y., Deng, X., . . . Hu, L. (2018). Large area efficient interface layer free monolithic perovskite/homo-junction-silicon tandem solar cell with over 20% efficiency. *Energy & Environmental Science, 11*(9), 2432-2443.

Zhu, W., Zhang, Q., Zhang, C., Chen, D., Zhou, L., Lin, Z., . . . Hao, Y. (2018). A non-equilibrium Ti 4+ doping strategy for an efficient hematite electron transport layer in perovskite solar cells. *Dalton Transactions, 47*(18), 6404-6411.

Zimm, C., Boeder, A., Chell, J., Sternberg, A., Fujita, A., Fujieda, S., and Fukamichi, K. (2006). Design and performance of a permanent-magnet rotary refrigerator. *International journal of refrigeration, 29*(8), 1302-1306.